# BULGARIAN CHEMICAL COMMUNICATIONS

EDITORIAL
Seventh International Conference
"Modern Trends in Science" - FMNS-2017



14 - 18.06.2017, Blagoevgrad, BULGARIA

Dear Reader,

This special issue collects selected papers, presented during the Seventh International Conference „Modern Trends in Science" (FMNS-2017), which held from 14th till 18th June 2017 in Blagoevgrad, Bulgaria. The conference was organized by the Faculty of Mathematics and Natural Sciences at South-West University "Neofit Rilski", Blagoevgrad.

The main objective of FMNS-2017 was to provide a platform for researchers, working in different fields of natural sciences, to report their current research achievements, to exchange new ideas and experiences, to create new contacts and to find global partners for future cooperation.

The Conference was organized in seven sections – Chemistry, Ecology and Environmental Protection, Geography, Mathematics, Informatics, Methodology in Education, Physics and Technical Sciences.

More than 140 researchers from Albania, Austria, Bulgaria, Czech Republic, Greece, Kazakhstan, Poland, Republic of Macedonia, Russia and United Kingdom attended the conference. Four prominent scientists – Acad. Julian Revalski (President of Bulgarian Academy of Sciences), Prof. Armen Sergeev (Vice-President of European Mathematical Society), Prof. John Greenman (University of the West of England, Bristol, UK) and Prof. Erwin Rosenberg (TU-Vienna, Austria), presented attractive plenary lectures, devoted to the interrelations between natural sciences. Most of the reported research during the oral and poster sessions also outlined the interdisciplinarity and multidisciplinarity as major trends of the modern science.

A specialized Workshop "Recent Progress in Bio-electrochemical systems", organized by Innovative Center for Eco Energy Technologies at South-West University "Neofit Rilski" – Blagoevgrad, Bulgaria, in collaboration with Institute of Electrochemistry and Energy Systems "Acad. Evgeni Budevski" – Bulgarian Academy of Sciences and Institute of Engineering Chemistry - Bulgarian Academy of Sciences, was also held in the framework of the conference. The Workshop was chaired by Assoc. Prof. Yolina Hubenova from Institute of Electrochemistry and Energy Systems "Acad. Evgeni Budevski" – Bulgarian Academy of Sciences. This satellite event provided opportunity for researchers working in the field of electrochemical systems as fuel cells, biofuel cells, microbial electrolysis cells, enzyme electrodes, etc., to report their achievements in development of these innovative technologies.

A round table discussion on the current progress of the projects "Sediment-based bioelectrochemical systems – self-powered devices for bioremediation and ecological monitoring" (Contract DFNI E02/14/2014) and "Novel fuel cells based on chemical and microbial processes" (Contract DFNI E02/15/2014) took place during the Workshop.

On behalf of the Organizing committee of the Seventh International Conference FMNS-2017 I would like to express our gratitude to the Ministry of Education and Science and the National Science Fund of Bulgaria for the provided financial support.

We gratefully use the chance to disseminate a part of the reported achievements during the conference among the audience of Bulgarian Chemical Communications journal.

*Prof. Mario Mitov,*
*Chairman of the Organizing*
*Committee of FMNS-2017*

Section

*Chemistry*

# Impact of malt quality parameters on beer filtration optimization process

T. Kamburi[1*], L. Pinguli[2], L. Lici[3]

*[1] University of Korça, Faculty of Natural and Human Sciences, Department of Biochemistry, Nënë Tereza Str., Korçë, Albania*
*[2] University of Tirana, Faculty of Natural Sciences, Department of Industrial Chemistry, Zogu I Blvd, Tiranë, Albania*
*[3] Polytechnic University of Tirana, Faculty of Geology and Mining, Department of Energy Resources Engineering, Nënë Tereza Square, Tiranë, Albania*

Filtration optimization process needs developing a strategy based on observations, empirical determinations, and continuous monitoring in order to ensure efficient filter operation. This objective will be reached by identifying critical malt parameters which will influence filtration efficiency. Yeast and components that came from malt dominate the filtration process. The biggest case of concern, since they are more difficult to remove than yeast, are the non-microbial particles. Malt is also responsible for the major part of enzymes that impact on beer and wort filterability. Experiments were carried out in pilot and industrial scale. Proteins and polyphenols dominate the filtration process, but if we use filter-aids and centrifugation, carbohydrates will dominate the filtration characteristics. More important carbohydrates include: unmodified starch, dextrins, pentosans and β-glucans. Carbohydrates that have a significant impact on filtration were tested using enzymatic techniques for three different beers.

## INTRODUCTION

Mashing is a key step in the beer production process. During mashing, enzymatic degradation of the polysaccharides present in the malt takes place. Fermentable carbohydrates are produced from the degradation of the polysaccharide starch. Such carbohydrates are converted into alcohol in the fermentation step of beer manufacturing.

Nonstarch polysaccharides also degrade during mashing into smaller-chain carbohydrates. Different enzymes catalyze all the involved reactions. Because the activity of the different enzymes is highly dependent on temperature, the manipulation of such variable is the main control mechanism for the mashing process [10]. Proteins are a very important class of organic components in beer. They are long chains or polymers with large molecular weight composed of amino acids, connected to each other *via* peptide bonds. Quality and sustainability of beer depends on its protein content. Proteins play a very important role in many stages of the brewing process. They are essential in malt and wort production, and also have a direct impact on the consistency and the formation of beer foam. Presence of proteins and their derivatives in wort can be associated with several factors that affect the nutritional value of the liquor, turbidity and colloidal stability, microbial nutrition, formation of by-products during fermentation and foam stability. A special class of proteins is called enzymes. Enzymes are catalysts that accelerate chemical reactions without any changes in character or structure, which play a decisive role in malting and wort production. In beer production, the most important spectrum of enzymes includes amylases, proteases and beta-glucanases [16]. Starch fraction that is not properly liquefied (such as beta-glucans and other soluble gums extracted during malting) has poor filtering characteristics as a result of thicker mash. Also there may be problems of turbidity in the finished beer. At the same time, insoluble gum or hemicelluloses, which can hold up to 20 times their weight, are present in wort in variable amounts. This will increase the filter mass resistance. The boiler is intended to reduce the viscosity of beer and wort, as well as to reduce the filter mass resistance in order to improve the time of circulation during boiling process. The most important enzyme responsible for filtration is beta-glucanase. The purpose of filtration is to preserve the beer so that no visible changes occur in the long run and the beer keeps its original appearance. Generally, the filtration steps fulfill two roles: to remove suspended materials from the green beer (the real filtration) and to unhinge potential turbidity formers (stabilization) [3]. Beta-glucanase acts on maltose rubber substances to improve the viscosity (liquefied wort) and the clarity of the beer. The rubber character of beta-glucan increases the viscosity of the wort and results in poor filtration and poor clarity of wort.

---

* To whom all correspondence should be sent.
 E-mail: tanjakamburi@yahoo.com

Beta-glucans tend to dissolve in hot water but are insoluble in cold beer thus contributing to cold turbidity. Consequently, it is necessary to ensure the continued activity of beta-glucanase during mashing, since the release of beta-glucan will continue through the activity of beta-glucan solubilase which is more heat-stable than the malt beta-glucanase which breaks down the beta-glucan structure. The high molecular weight beta-glucans released by beta-glucan solubilase contribute to wort viscosity and poorer extract recovery. Most brewers are very careful in selecting malt with low beta-glucan levels, and beta-glucan degradation occurs during malting. However, most initial mash temperatures are at or above the maximum stability temperature of the malt beta- glucanase enzymes, and it is common practice in many breweries to add exogenous beta-glucanase to decrease wort and beer viscosity and to improve filterability [16]. The objective of this paper is to provide information for identification of potential critical parameters of malt that have a significant impact on beer filterability. Wort production is the most significant process related with the amount of NMP in beer. An understanding of how milling, mashing, mash filtration, boiling and cooling (whirlpool) affect particle formation and removal will allow us to more easily control the process and to achieve a consistent and optimum level of beer particles in wort and beer.

## EXPERIMENTAL

This work was performed on "Stefani & Co" brewery (Albania), in pilot (Fig. 1.) and industrial scale. Testing methods were taken from Analytica EBC and Analytica-EBC Microbiologica [7]. The results were statistically analyzed according to Analytica-EBC, Section 14, Statistics, Method 14.1. The minimum number of experimental trials was eight and each trial was performed in duplicate. In a pilot plant built in the laboratory was measured the maximum filtration volume, the viscosity, the time of filtration of the wort produced from two different types of malt. Low-quality malt and high-quality malt were used and differences were noticed between them. The performance of malt enzymes used in industrial scale for brewery has been studied in 2013, 2014, 2015.

## RESULTS AND DISCUSSION

Carbohydrates that have a significant impact on filtration were tested using enzymatic techniques for two different beers (Beer A) 100% bad malt beer, (Beer B) 100% good malt beer. The filterability of a beer was represented by the maximal filtrate volume, $V_{max}$ at a given differential pressure (Table 1). All the worts for these trials were produced by infusion and the enzymes were used one by one [6].

**Table 1**. Impact of enzymes on beer filterability (n = 8)

| Enzymes used in wort production | Carbohydrate attacked | Vmax | |
|---|---|---|---|
| | | Beer A | Beer B |
| No enzymes used | - | 80 | 120 |
| Alpha-amylase | Starch, oligosaccharides. | 100 | 150 |
| Amyloglucosidase | Dextrins | 100 | 150 |
| Xylanase | Pentosans | 130 | 150 |
| β-glucanase | β-glucans, cellulose, hemicelluloses | 180 | 190 |
| All enzymes | Many carbohydrates | 260 | 290 |



**Fig. 1.** Pilot scale apparatus and centrifuge used for beer filterability monitoring in experimental scale
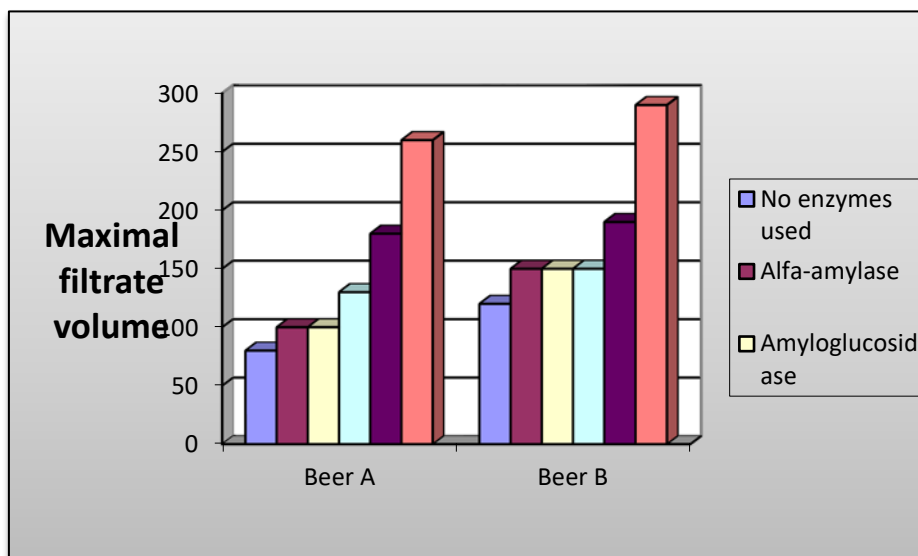
**Fig. 2.** Impact of enzyme on beer filterability

If we compare the performance in beer A and beer B, from Figure 2 we notice that in all cases the beer produced from malt with good quality presents a maximal filtrate volume higher than the beer B. In both types of beer the highest maximal filtrate volume is obtained when they are treated with all enzymes and the lowest values - if they are not treated with enzymes. If we compare the impact of each enzyme on beer filterability we see that beta-glucanase presents a maximum filtrate higher than other enzymes in both beers A and B. The most important enzyme responsible for filtration is beta-glucanase, which breaks down the beta-glucan structure. If the large viscous beta-glucan molecules are not broken down during malting or mashing other process problems can also occur: reduced extract recovery, high wort viscosity, poor run off performance, beer filtration problems and beer haze problems.

β-Glucanase enzyme was used in wort and beer during maturation. There were no significant differences between filterability of these beers, but the most important fact was that β-glucanase enzyme used in breweries also shortens the mash filtration time in the lauter tun filter (Figure 3).

In Figure 4 are given the values of the amount of β-glucanases and amylases in the samples. We notice that there is an oscillation of the amount of β-glucanases. None of the samples exceeds the limit value of 15 to 200 mg/l. β-glucanase acts on maltose rubber substances to improve viscosity and clarity of beer, however, should not exceed 200mg/l because it causes problems in the production process. Amylases decompose strach into simpler sugars, and the samples we have studied have values that provide a satisfactory transformation of amide.
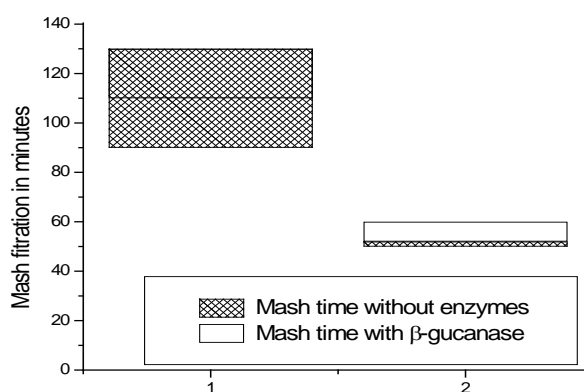


**Fig. 3.** Impact of  enzyme β-glucanase  on wort filtration time (n = 18)
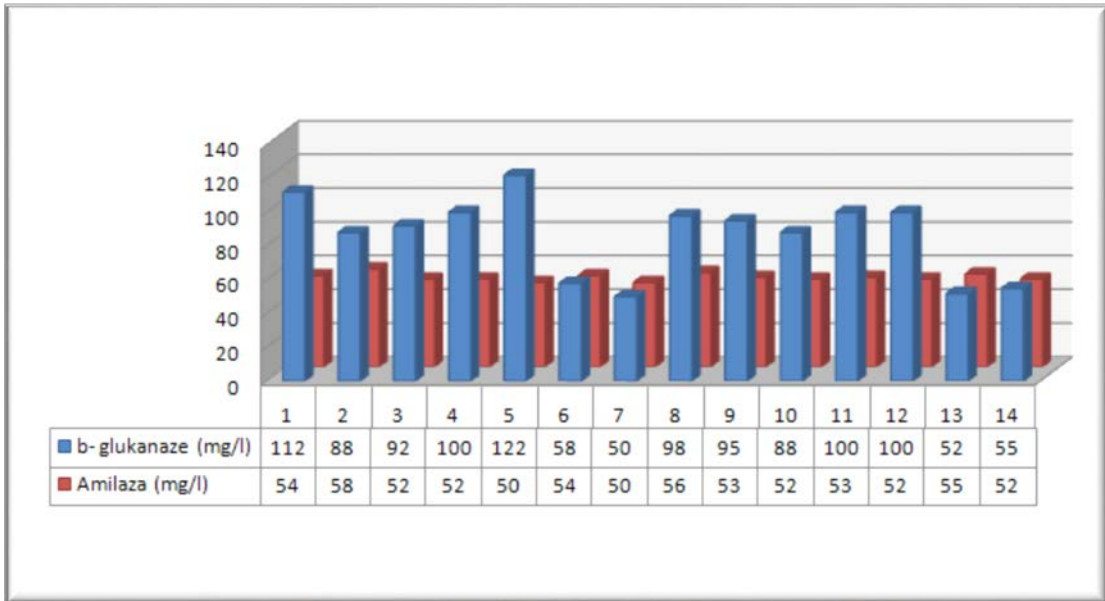
**Fig. 4.** Values of β-gluconazole and amylase in industrial mash
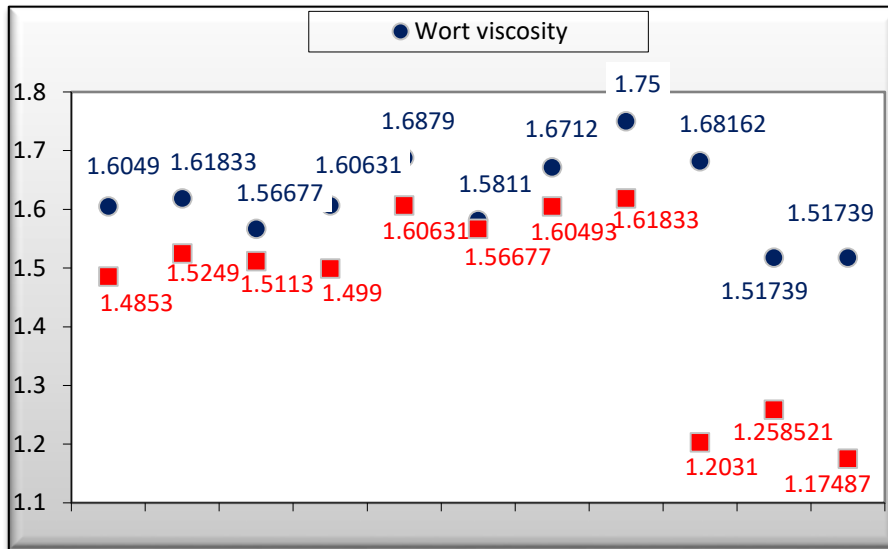


**Fig. 5.** Dynamic viscosity (mPa s) monitoring in wort and beer (100% bad malt beer)
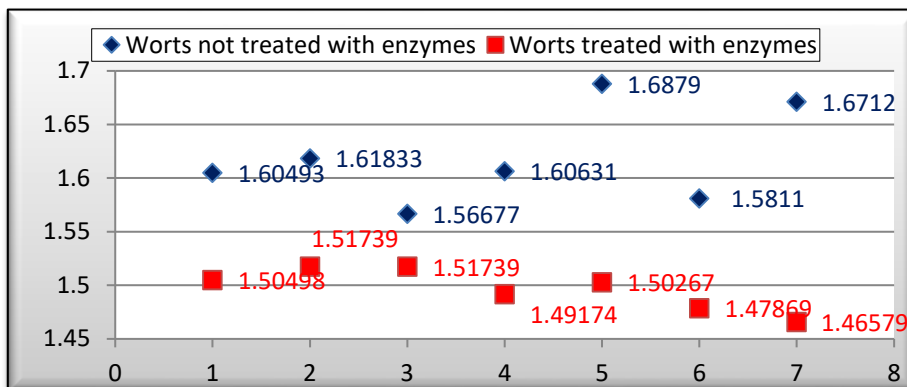


**Fig. 6.** Dynamic viscosity (mPa s) in worts treated and not treated with enzymes
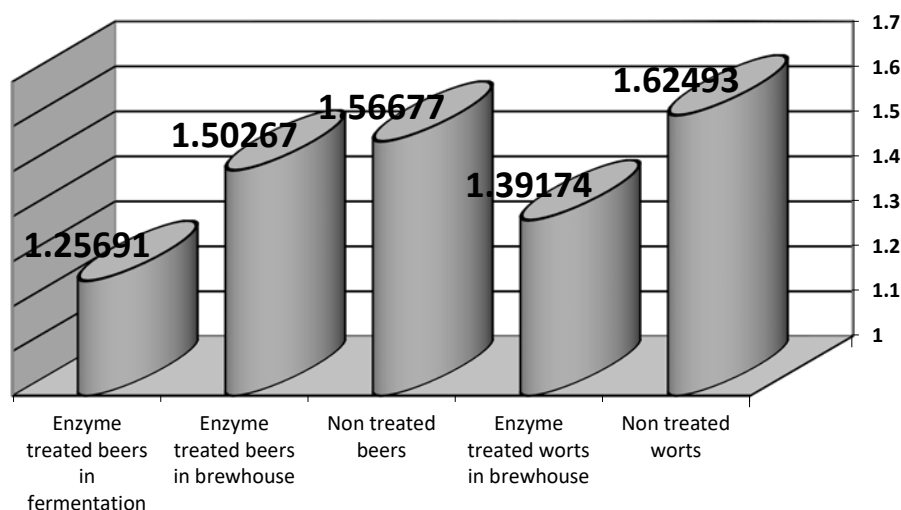
**Fig. 7.** Viscosity in worts and beer treated in different manner with enzymes

Viscosity was determined in wort and beers. We see in Figure 5 that in all samples studied the wort has a higher viscosity than the final product, beer. Sample 8 of wort has a viscosity of 1.75 that presents difficulties in filtering. So in this case the addition of β-glucanase in the mashing process is necessary.

In Figure 6 are given the viscosity values measured in the wort treated with enzyme and in wort not treated with enzyme. The lowest values of viscosity are obtained in the case of wort treated with enzyme. Although the wort not treated with enzyme does not exceed 1.75 viscosity, enzyme treatment is needed to avoid filtering problems

CONCLUSIONS

Filtration optimization process needs developing a strategy based on observations, empirical determinations and continuous monitoring in order to ensure efficient filter operation. This objective will be reached by identifying critical factors which will influence filtration efficiency, by monitoring and recording all parameters surrounding these factors, determining any transgression from the norm, for whatever reason.

Beer filterability strongly depends on malt quality, especially β-glucans and gomma content. If worts are characterized by high viscosity and a gomma structure, it is strongly recommended to use enzymes to control carbohydrates that dominate filtration characteristics such as unmodified starch, dextrins, pentosans, and β-glucans.

When dynamic viscosity is higher than 1.55, poor beer filterability is noticed. Beer filterability was

improved using β-glucanase enzyme in brewery or in fermentation. Using this enzyme in the brewery is more efficient because it simultaneously improves wort filterability, protein coagulation and it needs less energy for wort boiling.

REFERENCES

1. C. Bamforth, J. *Amer. Soc. Brewing Chem.*, **57**, 81 (1999)
2. D.E. Briggs, C.A. Boulton, P.A. Brookes, R. Stevens. Brewing Science and Practice. Woodhead Publishing Lid, Abington Hall, K.Abington, H. Erdal, B.Outtrup, B. Ahrenst-Larsen (eds.), 2004.
3. H.M. Eblinger, Handbook of Brewing. Processes, Technology, Markets, Weinheim, p. 437, 2009.
4. European Brewery Convention, Proceedings of the 20th Congress, Helsinki, p. 459, 1985.
5. European Brewery Convention. Manual of Good Practice. Beer Filtration, Stabilization and Sterilization, p. 156, 1999.
6. European Brewery Convention. Manual of Good Practice. Fermentation & Maturation, 187, 2000.
7. European Brewing Chemists: Analytica EBC; Methods of Analysis, 1992.
8. European Brewing Chemists: Analytica-EBC Microbiologica , https://www.analytica-ebc.com/
9. M. Gupta, N. Abu-Ghannam, E. Gallaghar, Barley for Brewing: Characteristic Change during Malting, Brewing and Applications of its By-Products. School of Food Science and Enviromental Health, p. 318, 2010.
10. W.A. Hardwick, Handbook of Brewing, New York, Marcel Dekker Inc., 1995.
11. L.I, Ward, Wort and Beer Clarification Manual,, p. 53, Brewers Supply Group (2008).

12. Y.-L. Jin, R.A. Speers, Effect of environmental conditions on the flocculation of *Saccharomyces cerevisiae. J. Am. Soc. Chem.,* **58**, 108 (2000)

13. W. Kunze, Technology Malting and Brewing. (Internat. ed., T.Wainwright, transl.). VLB, Berlin. p. 726, 1996.

14. R.V. Leather, C.J. Dale, Proceedings of the 6th International Brewing Technology Conference, Harrogate, (1996)

15. R.V. Leather, The Cambridge Prize Lecture 1996: From Field to Firkin an integrated approach to beer clarification and quality, *J. Inst. Brew*., 104, 9 (1998).

16. T. O'Rourke, The function of enzyme in brewing. *The Brewer International, Technical Summary,* **9** (2), 14 (2002).

17. R.A. Speers, M.A. Tung, T.D. Durance, G.G. Stewart, Colloidal aspects of yeast flocculation: a review. *J. Inst. Brew.*, **98**, 525 (1992).

18. M. Stratford, A.T. Carter, Yeast flocculation: Lectin synthesis and activation. *Yeast*, **9**, 371 (1993).

19. M.H. Straver, J.W. Kijne, G. Smit, Cause and control of flocculation in yeast, *Trends Biotechnol.*, **11**, 228 (1993).

20. The Brewers' Society and The Brewing Research Foundation, A Manual of Good Practice for the Production of Cask Conditioned Beer, p. 30, 1985.

# Computer modelling of the CB1 receptor by Molecular Operating Environment

F. I. Sapundzhi[1*], T. A. Dzimbova[1,2]

[1]*South-West University Neofit Rilski, 2790 Blagoevgrad, Bulgaria*
[2]*Institute of Molecular Biology, Bulgarian Academy of Sciences, 1113 Sofia, Bulgaria*

Thus far two classes of G-protein-coupled receptors (GPCRs) have been discovered and validated as the main therapeutic targets of this system: the cannabinoid receptor type 1 (CB1), which is most widely expressed in the brain and the cannabinoid receptor type 2 (CB2), predominantly found in the immune system. These receptors have been intensively studied for drug development and for their role in the signalling pathway. The computer modelling and homology modelling approaches can be used in the design and discovery of cannabinoid analogues, because the computational structure prediction methods provide a cost-effective alternative in the absence of experimental structures. This study aims to present an attempt to construct a homology model of the cannabinoid receptor using Molecular Operating Environment. The present investigation provides a consistent framework for further investigation of the ligand-receptor interactions.

**Keywords:** Cannabinoid receptors, CB1, Molecular Operating Environment, G protein–coupled receptors, Homology modelling, Ligand-receptor interactions

## INTRODUCTION

Homology modelling, also known as comparative modelling of protein is a computational technique, within structural biology, to determine the 3D structure of proteins [1,2]. More detailed information about homology modelling is available in recently published reviews [3-8].

Gaoni and Mechoulam identified Δ-9-tetrahydrocannabinol (THC) as the principal psychoactive molecule present in cannabis [9]. The pharmacological effects of cannabinoids are mediated through at least two cannabinoid receptors-CB1 and CB2. Regarding their distribution and functionality, CB1 receptors are located in the central nervous system, and they are responsible for most of the pharmacological effects of cannabinoids [10-13]. The CB2 receptor is found in peripheral tissues [14]. The CB1 and CB2 are seven transmembrane receptors that belong to the rhodopsin-like family Class A of G protein coupled receptors (GPCRs).

When the X-ray structure of a ligand-bound receptor is not available, homology models of the target protein can be used to obtain the ligand-receptor interactions. A knowledge of the three-dimensional structure of CB1 receptors could be helpful in the task of understanding their function and in the rational design of specific ligands. For this reason, many biochemical, pharmacological, and computational studies have been carried out on CB1 receptors. Different theoretical models were proposed in the literature but they are not available for the investigators in that field, because theoretical models have not been published in the data base (Table 1).

The objective of this research is to construct and refine a three-dimensional model of the human CB1 receptors in their activated forms by Molecular Operating Environment (MOE).

## MATERIALS AND METHODS

### Receptor

The protein sequence for the human cannabinoid receptor 1 was obtained from the Swiss Prot database (accession number P21554).

**Table 1.** Number of protein and protein/nucleic acid complex structures obtained by various experimental methods, available in the PDB as of 15 June 2017 (modified from www.rcsb.org/pdb/statistics/holdings.do).

| Experimental method | Proteins | Nucleic Acids | Protein/NA complexes | Other | Total |
|---|---|---|---|---|---|
| X-RAY | 110584 | 1866 | 5630 | 4 | 118084 |
| NMR | 10426 | 1217 | 244 | 8 | 11895 |
| El. microscopy | 1159 | 30 | 412 | 0 | 1601 |
| HYBRID | 102 | 3 | 2 | 1 | 108 |
| Other | 194 | 4 | 6 | 13 | 217 |
| Total | 122465 | 3120 | 6294 | 26 | 131905 |

* To whom all correspondence should be sent.
E-mail: sapundzhi@swu.bg

For homology models based on multiple templates, the template search was done with sequence search option of RCSB [15].

*Computational tools*

In order to perform computational studies a different software was used in the present work. The protein sequence of CB1 receptor was obtained from UNIPROT (http://www.uniprot.org/).

Homology modelling studies and ligands preparation were carried out using MOE (http://www.chemcomp.com/). The software MOE is a chemical computing and molecular modelling tool, which is a very widely used program in scientific applications. In the present investigation the MOE's Protein Modelling applications: MOE-SearchPDB, MOE-Align, Homology Model, and Protein Geometry were used. As the search progresses, pre-aligned families appear in the software with their calculated E-values. All docking calculations were performed with the software GOLD (Genetic Optimisation for Ligand Docking) 5.2 using the scoring functions available in the tool: ChemPLP, GoldScore, ChemScore and ASP (Astex Statistical Potential) scoring functions, [16-19]. Molegro Molecular Viewer was used for generating the figures (http://molegro.com/ index.php).

The correlation between the affinity of cannabinoid ligands from the literature [20] and the docking results for the obtained model by homology modelling was carried out in software GraphPad Prism 3.0 (http://www.graphpad.com/ scientific-software/prism). The Pearson's correlation coefficient was used, which is a measure of the correlation between normally distributed variables.

The structural similarity between the obtained model by homology modelling and the real structure of the human CB1 receptor from the PDB was assessed from the root mean square deviation (RMSD) values [21]. In general, a RMSD value,

which is less than 3Å, implies a fairly good similarity between the structures.

## RESULTS AND DISCUSSION

In our case, the search identifies members of rhodopsin as homologues of our target sequence. The displayed code represents the PDB structure from within the family that scored the highest against the target sequence.

Homology modelling starts with template identification that defines appropriate homologue(s) of known protein structure, called template(s), which are sufficiently similar to the target sequence to be modelled. Using MOE a simple search was performed by submitting the sequence of the human cannabinoid receptor 1 (CB1) obtained from Swiss Prot database (accession number P21554, Fig. 1). It was found that the conformation of the crystal structure of squid rhodopsin (PDBid:2z73) [22], the structure of bovine rhodopsin (dark adapted) (PDBid:1jfp) [23] and the structure of bovine rhodopsin (Metarhodopsin II) (PDBid:1ln6) [24] have high similarity with CB1 sequence.

In order to build a homology model, we aligned the target sequence to the protein family and after that decided which chain is to be the template for our model, and then built the model. This process goes through the following steps: Performing a Homology Search, Building a Homology Model and Evaluating the Homology Model.

The second step of the homology modelling procedure in MOE involves creating an alignment of the target sequence of CB1 receptor with some similar structures (Fig. 2). It was found in sequence alignment that there was a sequence similarity greater than 50% in almost all transmembrane regions. Thus, it could be expected that homology models built with this alignment would be accurate.

```
>sp|P21554|CNR1_HUMAN Cannabinoid receptor 1 OS=Homo sapiens GN=CNR1 PE=1 SV=1
MKSILDGLADTTFRTITTDLLYVGSNDIQYEDIKGDMASKLGYFPQKFPLTSFRGSPFQE
KMTAGDNPQLVPADQVNITEFYNKSLSSFKENEENIQCGENFMDIECFMVLNPSQQLAIA
VLSLTLGTFTVLENLLVLCVILHSRSLRCRPSYHFIGSLAVADLLGSVIFVYSFIDFHVF
HRKDSRNVFLFKLGGVTASFTASVGSLFLTAIDRYISIHRPLAYKRIVTRPKAVVAFCLM
WTIAIVIAVLPLLGWNCEKLQSVCSDIFPHIDETYLMFWIGVTSVLLLFIVYAYMYILWK
AHSHAVRMIQRGTQKSIIIHTSEDGKVQVTRPDQARMDIRLAKTLVLILVVLIICWGPLL
AIMVYDVFGKMNKLIKTVFAFCSMLCLLNSTVNPIIYALRSKDLRHAFRSMFPSCEGTAQ
PLDNSMGDSDCLHKHANNAASVHRAAESCIKSTVKIAKVTMSVSTDTSAEAL
```

**Fig. 1.** Sequence alignment of the human CB1 obtained from Uniprot database (P21554).
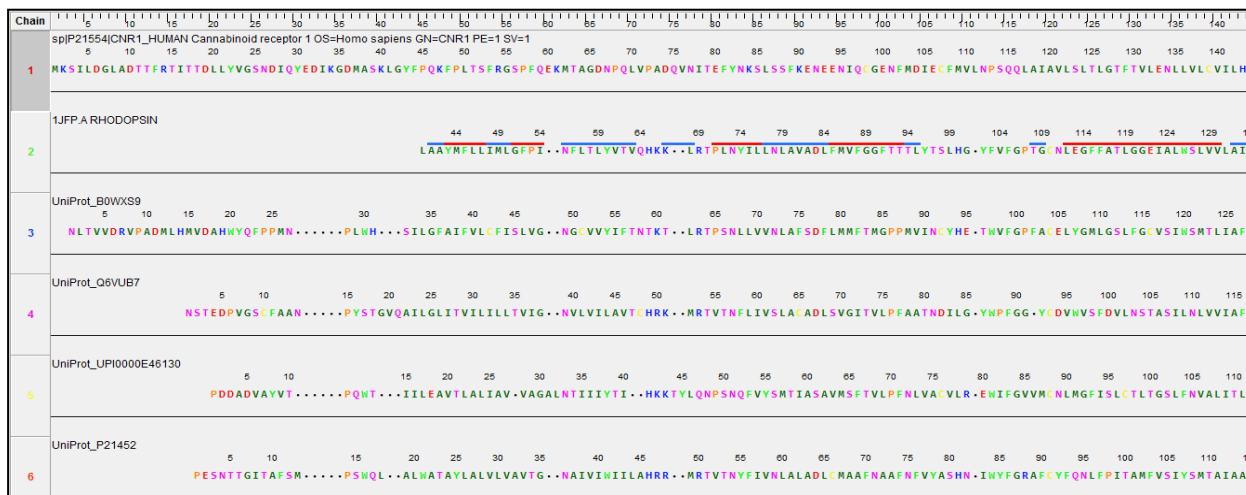
**Fig. 2.** Sequence alignment of CB1 receptor with some similar structures obtained from MOE.

Next step is building of homology models in MOE. The standard molecular mechanics AMBER 99 forcefield was used. Of the forcefields supported in MOE, Amber99 or Charmm27 are specifically designed to support protein simulations. The Amber99 forcefield for protein homology applications has been recommended [25].

The backbone fragments from a high-resolution structural database were collected and alternative side chain conformations for non-identical residues were assembled from an extensive rotamer library during data collection. During model building in software MOE, 10 independent models were created based upon loop and side chain placements scored by a contact energy function (Fig. 3). The final, refined model was loaded in MOE after the calculation was finished, (Fig. 4). After that the stereochemistry of homology models for unusual or geometrically unreasonable features was examined.

Our model has RMSD 0.6230 < 3Å, which means that the generated model is built correctly.

The model with the best contact energy was chosen (-175.4267) and it was validated directly in MOE. The stereochemical quality of the modelled proteins was assessed from Ramachandran validation score for favoured regions and allowed regions (Fig. 5). In general, a score close to 100% implies good stereochemical quality of the models.

The molecular docking experiments with the obtained model of CB1 receptor by homology modelling in MOE and the ligands from literature [20] were carried out with software GOLD 5.2 and all four scoring functions embedded in the program: GoldScore, ChemScore, ASP and ChemPLP. According to Shim *et al.* [26] there exists a hydrophobic binding pocket that interacts with the alkyl chain of the cannabinoids.

| | mol | name | RMSD to Mean | CA RMSD to Mean | Contact Energy | Packing Score | GB/VI | U | E sol | E ele | E vdw | E bond |
|---|---|---|---|---|---|---|---|---|---|---|---|---|
| 1 | | Model #1(1) | 0.5321 | 0.4335 | -170.5224 | 2.5773 | -11979.084 | 44.0562 | -5489.7065 | -3670.9124 | -1578.8199 | 4192.5435 |
| 2 | | Model #2(1) | 0.5999 | 0.4840 | -171.1597 | 2.5411 | -11946.157 | 55.1725 | -5077.1636 | -3709.1528 | -1350.6154 | 4050.9197 |
| 3 | | Model #3(1) | 0.6230 | 0.4680 | -175.4267 | 2.4970 | -12384.922 | -465.5206 | -4022.0649 | -4885.0430 | -1470.7916 | 4672.6147 |
| 4 | | Model #4(1) | 0.5001 | 0.4120 | -170.9495 | 2.5883 | -12226.305 | -642.7585 | -4680.9507 | -4376.6196 | -1501.2986 | 4089.6438 |
| 5 | | Model #5(1) | 0.5971 | 0.5120 | -167.9658 | 2.4401 | -12483.975 | -689.5169 | -3515.0066 | -5215.2861 | -1420.5818 | 4648.6338 |
| 6 | | Model #6(1) | 0.5601 | 0.4499 | -166.6386 | 2.5825 | -11415.081 | 341.8376 | -5764.7217 | -2798.6863 | -1600.3688 | 3804.0024 |
| 7 | | Model #7(1) | 0.6687 | 0.5838 | -161.2423 | 2.4580 | -12526.668 | -1077.5608 | -3243.3823 | -5334.0039 | -1420.6730 | 4385.4292 |
| 8 | | Model #8(1) | 0.6448 | 0.5364 | -172.5911 | 2.4157 | -12503.752 | -760.5984 | -3513.8774 | -5252.4111 | -1415.8101 | 4643.9072 |
| 9 | | Model #9(1) | 0.5660 | 0.4784 | -168.1365 | 2.4765 | -12431.845 | -901.6127 | -4003.0608 | -4989.3452 | -1459.3658 | 4308.2290 |
| 10 | | Model #10(1) | 0.5322 | 0.4337 | -168.3179 | 2.5163 | -11409.416 | 519.5591 | -5675.1157 | -2803.8230 | -1589.4479 | 3975.6216 |

**Fig. 3.** Screenshot of database obtain after modelling by MOE.

The docking is effective when the polar residue from the receptor sequence was chosen - Asp366 and the investigated ligands bind near to it.
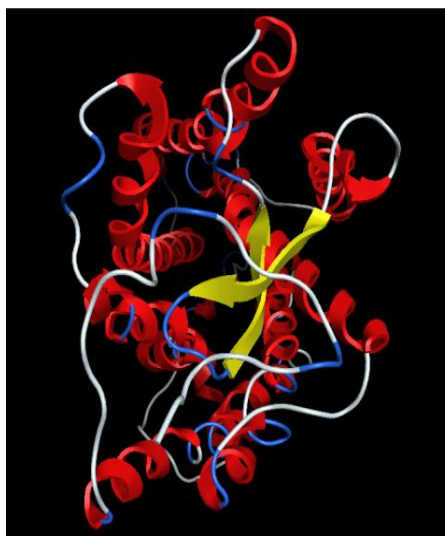


**Figure 4.** Refined model after the calculation was finished.
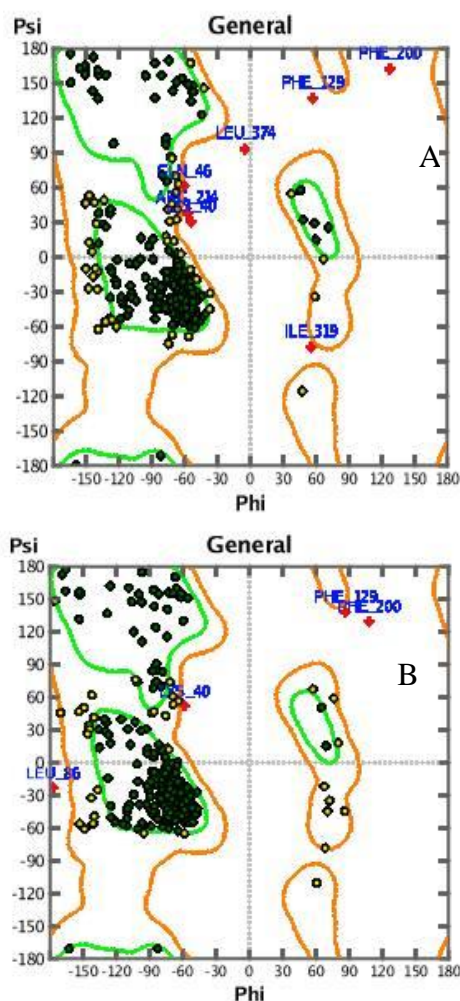




**Figure 5.** Ramachandran plot generated by MOE: A - before optimization of the structure; B - after optimization of the structure.

Correlations between the data of molecular docking and the affinity of ligands were performed with GraphPad Prism 3.0. The correlation between the data was assessed by the Pearson's correlation coefficient.

Significant correlation is established between the values of ASP scoring function and the values of affinity of cannabinoid ligands [20], (Pearson R=0.9594) for obtained model by homology modelling of human CB1 receptor [27-35].

The established correlation between these parameters shows that the model of CB1 receptor developed by homology modelling in MOE allows to optimally determining the binding affinity by ASP scoring function. For some work along these lines, see [36-42].



**Figure 6.** Graphical representation of the obtained model of homology modelling of CB1 receptor by the software MOE. The diagram was generated with the MMV.

The generated model of the human CB1 receptor obtained by homology modelling in MOE could be used in further investigations (Fig. 6). It could serve as a target in docking studies for design of new selective and effective cannabinoid ligands.

REFERENCES

1. R. Sanchez, A. Sali, *Curr. Opin. Struct. Biol.*, **7**, 206 (1997).
2. J. Bujnicki, A. Elofsson, D. Fischer, L. Rychlewski, *Protein Sci.,* **10**, 352 (2001).
3. A. Hillisch, L. Pineda, R. Hilgenfeld, *Drug Discov. Today,* **9**, 659 (2004).
4. T. Blundell, B.Sibanda, R.Montalvão, S. Brewerton, V.Chelliah, C.Worth, N.Harmer, O.Davies, D.Burke, *Phil. Trans. R. Soc. B,* **361**, 413 (2006).
5. R. Lapatto, T.Blundell, A.Hemmings, J.Overington, A.Wilderspin, S.Wood, J.Merson, P.Whittle, D.Danley, K.Geoghegan, *Nature,* **342**, 299 (1989).
6. M. Miller, J. Schneider, B. Sathyanarayana, M.Toth, G.Marshall, L.Clawson, L.Selk, S.Kent, A.Wlodawer, *Science* **246**, 1149 (1989).
7. N. Eswar, B.John, N.Mirkovich, A.Fiser, V.Ilyin, U.Pieper,A.Stuart,M.Marti-Renom,M. Madhusudhan, B.Yerkovich, A.Sali, *Nucl. Acids Res.,* **31**, 3375 (2003).
8. R. Dunbrack, *Curr. Opin. Struct. Biol.* **16**, 374 (2006).
9. Y. Gaoni, R. Mechoulam, *J. Am. Chem. Soc.*, **86**, 1646 (1964).
10. L. Matsuda, S. Lolait, M.Brownstein, A.Young, T. Bonner, *Nature*, **346**, 561 (1990).
11. J. Huffman, J. Lainton, *Curr. Med. Chem*, **3**, 101 (1996).
12. M. Herkenham, A.Lynn, M.Little, M.Johnson, L. Melvin, B. de Costa, K. Rice, *Proc. Natl. Acad. Sci. U.S.A.,* **87**, 1932 (1990).
13. R. Pertwee, *Curr. Med. Chem.*, **6**, 635 (1999).
14. S. Galiegue, S. Mary, J. Marchand, D. Dussossoy, D. Carrière, P. Carayon, M. Bouaboula, D. Shire, G. Le Fur, P.Casellas, *Eur. J. Biochem.*, **232**, 54 (1995).
15. RCSB Protein Data Base, www.rcsb.org
16. http://www.chemcomp.com/
17. G. Jones, P. Wilett, R. Glen, A. Leach, R. Taylor. *J Mol Biol*, **267**, 727 (1997).
18. GOLD, version 5.2 UserGuide, *CCDC Software Ltd. Cambridge*, UK, 2010.
19. M. Verdonk, J. Cole, M. Hartshorn, C. Murray, R. Taylor, *Proteins*, **52**, 609 (2003).
20. R. Reinscheid, H. Nothacker, A. Bourson, A. Ardati, R. Henningsen, J. Bunzow, D. Grandy, H. Langen, F. Monsma, O. Civelli, *Science*, **270**, 792 (1995).
21. https://en.wikipedia.org/wiki/Cannabinoid_receptor
22. O. Carugo, S. Pongor, *Protein Sci*. **10**, 1470 (2001).
23. M. Murakami, T. Kouyama, *Nature,* **453**, 363 (2008).
24. P. Yeagle, G. Choi, A. Albert, *Biochemistry,* **40(39)**, 11932 (2001).
25. G. Choi, J. Landin, J.Galan, R. Birge, A. Albert, P.Yeagle, *Biochemistry*, **41(23)**, 7318 (2002).
26. C. Summa, M. Levitt, *PNAS,* **104**, 3177 (2007).
27. Joong-Youn Shim, A. Bertalovitz, D. Kendall. *Journal of Biological Chemistry*, **286 (38)**, 33422 (2011).
28. T. Schwede, J. Kopp, N. Guex, M. Peitsch, *Nucleic Acids Res.*, **31**, 3381 (2003).
29. V. Kralev, *IJASEIT,* **7** (5), 1685 (2017).
30. V. Kralev, R. Kraleva, *IJACR,* **7** (28), 1 (2017).
31. T. Dzimbova, F. Sapundzhi, N. Pencheva, P. Milanov, *Journal of Peptide Science*, **18** (S1), S84, P072, (2012).
32. F. Sapundzhi, T. Dzimbova, N. Pencheva, P. Milanov, *Journal of Peptide Science*, **20** (S1), S294 (2014).
33. T. Dzimbova, F. Sapundzhi, N. Pencheva, P. Milanov, *Int. J. Bioautomation,* **17**, 5-16, (2013).
34. F. Sapundzhi, T. Dzimbova, N. Pencheva, P. Milanov, *Bulgarian Chemical Communications*, **47**(2), 613 (2015).
35. F. Sapundzhi, T. Dzimbova, N. Pencheva, P. Milanov, *Der Pharma Chemica*, **8**, 118 (2016).
36. F. Sapundzhi, T. Dzimbova, N. Pencheva, P. Milanov, *Bulgarian Chemical Communications*, **49** (4), 768 (2017).
37. F. Sapundzhi, T. Dzimbova, N. Pencheva, P. Milanov, *Bulgarian Chemical Communications*, **49** (4), 23 (2017).
38. F. Sapundzhi, T. Dzimbova, N. Pencheva, P. Milanov, *ITM Web of Conferences, AMCSE 2017*, **16**, 02008 (2018).
39. F. Sapundzhi, T. Dzimbova, N. Pencheva, P. Milanov, *Proceedings of Biomath Communications Supplement, 25-30 June 2017, Skukuza Camp, South Africa*, **4(1)**, (2017).
40. G. Koroleva, *Proceedings of Seventh International Conference of FMNS* 2017, 14-18 June 2017, Blagoevgrad, Bulgaria, **1**, p.166 (2017).
41. F. Sapundzhi, T. Dzimbova, N. Pencheva, P. Milanov, *Proceedings of Seventh International Conference of FMNS* 2017, 14-18 June 2017, Blagoevgrad, Bulgaria, **1**, p.167 (2017).
42. F. Sapundzhi, M. Popstoilov, N. Nikolova, M. Bozhinova, *Proceedings of Seventh International Conference of FMNS* 2017, 14-18 June 2017, Blagoevgrad, Bulgaria, **1**, p.181 (2017).

# Amino acid functionalized silica gel as a selective sorbent for enrichment of Pt (II)

P. Petrova[1*], M. Chochkova[1], I. Karadjova[2], I. Dakova[2], M. Karadjov[3]

[1] *South-West University Neofit Rilski, Faculty of Mathematics and Natural Sciences, Department of Chemistry, 66, Ivan Mihailov Str, 2700 Blagoevgrad, Bulgaria*

[2] *Sofia University St. Kliment Ohridski, Faculty of Chemistry and Pharmacy, 1, Blvd. J. Bourchier, 1164 Sofia, Bulgaria*

[3] *Geological Institute, Bulgarian Academy of Science, Acad. G. Bonchev Str. Bl.24, 1113 Sofia, Bulgaria*

In this study we report on the synthesis and applicability of 3 new sorbents based on silica gel impregnated with amino acids or with amino acid derivatives, namely *L*-cystine modified silica gel (SiO$_2$-Cys-Cys), silica gel modified with *L*-cysteine amide of 4-aminoantypirine (SiO$_2$–Cys) and silica gel modified with *N*-benzyloxycarbonyl-*L*-methionine (SiO$_2$-Met) as an efficient sorbent for solid-phase extraction of Pt from hydrochloric acid solutions. Extraction efficiency and selectivity of the sorbents toward Pt(II)/Pt(IV) were studied by batch procedure. The influence of analytical parameters such as acidity of the sample solution, eluent type and volume, effects of foreign ions on the sorption/desorption behavior of Pt(II)/Pt(IV) were investigated. The results obtained demonstrate that SiO$_2$-Cys and SiO$_2$-Met showed high sorption activity toward Pt(II) while SiO$_2$-Cys-Cys is not able to extract quantitatively neither Pt(II) nor Pt(IV). The experiments revealed that the new sorbents SiO$_2$–Cys and SiO$_2$-Met are highly selective toward Pt(II) extracted as Pt(Cl)$_4^{2-}$ complex while sorption of Pt(IV) is negligible at the same HCl concentration. Analytical procedure was developed for total Pt determination in cosmetic cream samples, based on solid-phase extraction using SiO$_2$-Met as an effective sorbent combined with ICP-OES measurements. Under optimised conditions, the limit of quantification achieved for total Pt in cosmetic creams was 0.2 μg g$^{-1}$, the RSD value varied between 6-16 % for Pt content between 0.2-1 μg g$^{-1}$. The accuracy of the proposed method was confirmed by the added/found method and by comparative analysis using direct ICP-MS measurements.

*Keywords:* Solid phase extraction, Noble metal determination, Amino acid modified sorbent

## INTRODUCTION

Quantification of Pt in environmental samples is an analytical challenge, even by using highly sensitive ICP-MS spectrometry because of its extremely low environmental concentrations, as well as observed interferences from matrix constituents. In the literature many analytical procedures have been described for noble metals determination in different types of samples, such as road dust [1], airborne particulate matter [2-4], soil [5], sediments [6], water [7,8], biological [9] and geological samples [10]. In most of these procedures an additional separation/enrichment step was included for preliminary Pt enrichment prior to instrumental measurement. Solid-phase extraction is a method frequently utilized for matrix elimination and enrichment of noble metals using various types of sorbents [11], many of them based on silica gel modified with different chelating agents [12-16]. Sorbents based on silica matrix are often applied because of their high mechanical and thermal stability and good chemical resistance in organic solvents and mineral acids. The sorption selectivity is regulated using suitable functional groups fixed on the sorbent surface. Complexing agents containing N- and S- donor groups are employed in enrichment of PGE *via* solid phase extraction [17,18]. Incorporation of chelating functional groups on the support can be accomplished by covalent grafting or by impregnation and physical adsorption of the organic reagent achieved by inclusion in the pores of the support material, by adhesion process or by electrostatic interaction [18,19].

In the present work, we focused our attention on: (i) the synthesis of amino acid derivatives as modifiers for silica gel and preparation of new sorbents for effective separation and enrichment of Pt(II) and (ii) the applicability of the newly synthesized sorbents for the determination of total Pt in cosmetics.

## EXPERIMENTAL

### Reagents

The stock standard solution for platinum ions (1000 mg L$^{-1}$) was Sigma–Aldrich (Germany) in 5% HCl. Silica gel for column chromatography ≤0.063 mm, ≥230 mesh ASTM, the amino acids *L*-cisteine, *L*-cystine, *L*-methionine and *N*-(benzyloxycarbonyloxy) succinimide were purchased from Sigma-Aldrich Ltd. Tin (II) chloride (SnCl$_2$) was from Merck, Germany.

---

* To whom all correspondence should be sent.
 E-mail: petya_dukova@yahoo.com

*Apparatus*

ICP-OES measurements were performed on an ICP-OES spectrometer Ultima 2, Jobin Yvon under optimized instrumental parameters using the wavelength 203.646 nm for Pt II.

A microwave oven Milestone Ethos 900-Mega II was employed for cream sample digestion.

A centrifuge NEYA 8 Giorgio Bormac was used for separation of silica sorbent from the supernatant solutions in the batch experiments.

*Synthesis of amino acid derivatives*

*Synthesis of N-benzyloxycarbonyl-L-methionine:* *N*-Benzyloxycarbonyl-*L*-methionine (Z-Met-OH) (Fig. 1) was synthesized according to a previously published method [20].
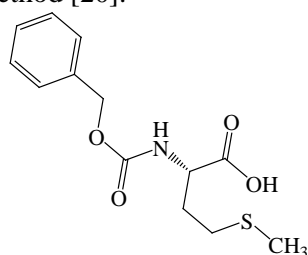


**Fig. 1.** Structure of *N*-benzyloxycarbonyl-*L*-methionine (Z-Met-OH)

*Synthesis of Boc-S-benzyl-L-cysteine amide of 4-aminoantipyrine (Boc-Cys(Bzl)-4-AAP):* The synthesis of the target amide Boc-Cys(Bzl)-4-AAP (Fig. 2) was performed according to the EDC/ HOBt method [21].
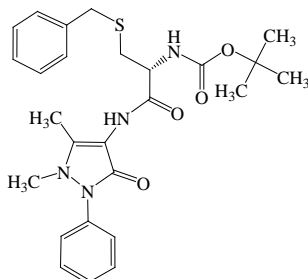


**Fig. 2.** Structure of Boc-S-benzyl-L-cysteine amide of 4-aminoantipyrine

To a cold solution of Boc-Cys(Bzl)-OH (1.0 g, 3.2 mmol), 1-[3-(dimethylamino)propyl]-3-ethylcarbodiimide hydrochloride (0.61 g, 3.2 mmol) and 1-hydroxybenzotriazole (0.43 g, 3.2 mmol) in $CH_2Cl_2$ (10 ml) was added 4-methylmorpholine (0.35 mL, 3.2 mmol). After 10 min, 4-aminoantipyrine (0.65 g, 3.2 mmol) in 5 ml $CH_2Cl_2$ was added, and the resultant reaction mixture was stirred for 24 h at room temperature.

The mixture was diluted with $CH_2Cl_2$ and then washed consequently with 5% $NaHCO_3$ (3 × 30 mL), 10 % Citric acid (3 × 30 ml) and water (3 × 50 mL), dried over $Na_2SO_4$, and concentrated *in vacuo*. The residue was purified by crystallization from hexane-

EtOAc to afford 1.1 g (69%) of Boc-Cys(Bzl)-4-AAP amide as pale yellow crystals.

*Preparation of modified silica gels: silica gel modified with Z-methionine, silica gel modified with cystine and silica gel modified with Boc-S-benzyl-L-cysteine amide of 4-aminoantipyrine*

The physical modification of silica gel with *Z*-methionine-OH (Fig. 1), cysteine amide of 4-aminoantipyrine (Fig. 2) and cystine (Fig. 3.) was performed by the procedure proposed by Bartyzel *et al*. [22] and further optimized by Petrova *et al*. [20].
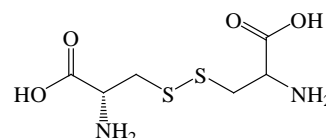


**Fig. 3.** Structure of the amino acid cystine

*Analytical procedures for sorption/desorption studies*

To a sample aliquot of 10 ml containing 100 μg Pt(II)/Pt(IV) in HCl, 50 mg sorbent was added. After shaking for 5 – 60 min, the mixture was centrifuged and the supernatant solution was removed and analyzed by ICP-OES as effluate. The sorbent was washed with doubly distilled water and the metal complexes retained on the sorbent were eluted with a solution of thiourea in HCl. In order to investigate the degree of elution, metal ions content in eluate was determined by ICP-OES.

The degree of sorption was calculated using the following equation:

$S,\% = [(C_i - C_{ef})/C_i] × 100$

where S is the degree of sorption (%), $C_i$ is the total cation concentration in the initial solution and $C_{ef}$ is the final concentration of metal ion in the effluate solution after extraction.

The degree of elution from the sorbent was obtained by the equation:

$E, \% = (C_{el}/C_s) × 100$

where $C_{el}$ is the amount of metal ion in the eluate after extraction, $C_s$ is the amount loaded on the sorbent.

*Analytical procedure for the determination of Pt in cream samples*

*Microwave digestion of cream samples:* About 0.3 g of the sample was weighed into a closed vessel to prevent the evaporation of the volatile fractions in the cream. Then 10.0 mL of HCl (37%) and 3.5 mL of $HNO_3$ (68%) were added and the mixture was left at room temperature for 24 h. The MW digestion was conducted using the following program: 10 min at 250 W; 5 min at 400 W; 5 min at 500 W; 5 min at

600 W. After cooling, the solution was quantitatively transferred to a volumetric flask and diluted up to 25 mL with 0.02 mol L$^{-1}$ HCl [23].

*Determination of Pt(II):* 50 mg SiO$_2$-Met sorbent and 20 mL solution of digested cream sample to which 1 ml 1 M SnCl$_2$ was added were transferred to a 50 mL centrifuge tube and shaken for 30 min. After centrifugation the sorbent was washed with deionized water and Pt(II) was eluted with 2 mL of thiourea solution in 2 mol L$^{-1}$ HCl. The concentration of Pt(II) in the eluate was measured by ICP-OES.

## RESULTS AND DISCUSSION

It is well known that the extraction efficiency of sorbents for noble metals is enhanced by their modification with sulfur-containing compounds [24]. In the present study we chose as modifiers sulfur containing amino acids *L*-cystein, *L*-methionine and *L*-cystin with different S-containing functional groups such as thioether (-SR) and disulfide (-S-S). In order to increase the sorption ability, we furthermore additionally functionalized some of the amino acids introducing one more chelating group. After the synthesis of the amino acid derivatives they were impregnated on the silica gel by physical adsorption and further investigated as efficient sorbents for Pt.

### *Optimization of the experimental conditions for solid phase extraction (SPE) of Pt (II)*

*Influence of HCl concentration:* The protonation/deprotonation of N- and S- containing functional groups which is related to their pKa, strongly depends on the pH of the solution. On the other hand, in HCl media noble metals form anionic chloro complexes which compositions and charges vary with the HCl concentration. Consequently, the degree of Pt sorption on amino acid modified silica gel sorbent should be strongly influenced simultaneously by pH value and HCl concentration

in the sample solution, hence sorption experiments for optimization of the hydrochloric acid concentration were performed.

The results obtained for the degree of sorption of Pt(II) and Pt(IV) in 0.01 - 3 mol L$^{-1}$ HCl for the newly synthesized sorbents in presence and absence of SnCl$_2$ as a reducing agent are shown in Table 1.

The silica gel sorbents containing cysteine and methionine as modifiers, SiO$_2$-Cys and SiO$_2$-Met, ensured high degree of sorption between 93-95% in the presence of 0.1-1 mol L$^{-1}$ HCl for Pt(II) and Pt(IV) after reduction with SnCl$_2$, whereas the degree of sorption for SiO$_2$-Cys-Cys was less than 20 % for the same HCl concentration for both Pt species.

It can be concluded that SiO$_2$-Cys and SiO$_2$-Met ensured very good separation of Pt(II) from Pt(IV) at low HCl concentration around 0.1 mol L$^{-1}$, which might be used for their selective determination. Total Pt in the sample should be determined in the presence of SnCl$_2$ as reducing agent for Pt(IV).

The electrostatic attraction between anionic chlorocomplexes [PtCl$_4$]$^{2-}$ and positively charged amino- and S- thioether groups on the sorbent surface is one of the possible reasons for the quantitative Pt(II) sorption in HCl media. Complex formation is another possible mechanism of Pt binding on the amino acids derivatives as it was confirmed by V. Joshi [25] who found that the amino acids *L*-cysteine and *DL*-homocysteine behave as bidentate ligands, bonded to Pt(II) *via* ionized sulfur and amino nitrogen while carboxylate groups remain un-coordinated and protonated. However, although SiO$_2$-Cys-Cys contains an S-group it does not ensure satisfactory extraction which may be attributed to a difference in disulfide (-S-S-) moieties chelating properties or to some steric, geometrical or kinetic factors. The most probable explanation for the low extraction efficiency of SiO$_2$-Cys and SiO$_2$-Met toward Pt(IV) is the fact that Pt(IV) complexes in an octahedral geometry are said to be substitution-inert.

**Table 1**. Influence of HCl concentration on the degree of sorption of Pt(II) and Pt(IV). Data represent an average of three independent experiments.

| Sorbent | Metal ion | Degree of sorption, % | | | | |
|---|---|---|---|---|---|---|
| | | 0.01 mol L$^{-1}$ HCl | 0.1 mol L$^{-1}$ HCl | 1 mol L$^{-1}$ HCl | 2 mol L$^{-1}$ HCl | 3 mol L$^{-1}$ HCl |
| SiO$_2$-Met | Pt(II) | 85±6 | 94±3 | 96±4 | 85±7 | 87±5 |
| | Pt(IV) | < 1 | < 1 | 35±4 | 40±8 | 38±9 |
| | Pt(IV)/SnCl$_2$ | 87±8 | 94±7 | 95±6 | 87±6 | 86±4 |
| SiO$_2$-Cys | Pt(II) | 86±3 | 91±5 | 94±5 | 90±4 | 95±6 |
| | Pt(IV) | < 1 | <1 | 23±4 | 33±4 | 35±4 |
| | Pt(IV)/SnCl$_2$ | 88±6 | 90±7 | 93±4 | 92±5 | 94±6 |
| SiO$_2$-Cys-Cys | Pt(II) | 14±4 | 18±6 | 19±6 | 11±4 | 3±1 |
| | Pt(IV) | <1 | <1 | <1 | 3±1 | 2±1 |
| | Pt(IV)/SnCl$_2$ | 11±4 | 20±7 | 15±2 | 10±4 | 2±1 |

Summarizing the results obtained for Pt(II), acidity in the range 0.5 - 1 mol L$^{-1}$ HCl was accepted as optimal for quantitative and selective sorption of Pt(II). Total Pt content can be found under the same acidity range after reduction of Pt(IV) with SnCl$_2$ using both sorbents SiO$_2$-Cys and SiO$_2$-Met.

The optimization procedure was further continued by carrying out Pt(II) desorption experiments with different types of eluents. Results obtained revealed that 0.7 mol L$^{-1}$ thiourea in 2 mol L$^{-1}$ HCl is the optimal eluent ensuring fast and quantitative elution of Pt(II) sorbed on both SiO$_2$-Cys and SiO$_2$-Met. The effect of the eluent volume on the metal desorption was investigated in the range of 1–5 mL. The complete Pt(II) desorption was reached with 2 ml of 0.7 mol L$^{-1}$ thiourea in 2 mol L$^{-1}$ HCl.

### Kinetic studies

Kinetic characteristics of the sorption/ desorption process are very important features for sorbents practical application and are connected with their nature and surface properties. Sorbents based on impregnated silica gel are usually characterized by good kinetic properties ensured by the large surface area and easy accessibility of the functional groups [26]. In our study the time for establishing the sorption equilibrium for the investigated sorbents was varied from a few minutes to one hour. The kinetics of the sorption process of Pt(II) was examined in a batch system with 50 mg of SiO$_2$-Cys and SiO$_2$-Met particles in 1 mol L$^{-1}$ HCl for 5–60 min. The kinetics of desorption was studied for both sorbents, for the same time interval using the optimal eluent. Results revealed quantitative Pt(II) sorption on SiO$_2$-Cys and SiO$_2$-Met within 30 min, and quantitative desorption with the optimal eluent for 15 min.

### Selectivity of the sorbents

The selectivity of the newly synthesized sorbents towards Pt(II) was tested using model solutions containing Pt(II) and non-noble metals in a batch mode under optimized chemical conditions for sorption. The results presented in Table 2 show that at optimal HCl concentration the degree of sorption for the non-noble cations is almost negligible, demonstrating high selectivity of the SiO$_2$-Cys and SiO$_2$-Met sorbents towards Pt(II).

### Analytical application

Recovery experiments were performed to assess the applicability of the SiO$_2$-Met sorbent for separation and concentration of Pt(II) in real samples. Our attention was turned to the cosmetic samples where Pt is recently being added as the newest ingredient in anti-aging creams. A cream sample (without Pt) was mineralized using MW digestion procedure and known amounts of Pt(IV) were added before mineralization.

**Table 2.** Matrix interferences of some metal ions on the recovery of Pt(II) by SPE using SiO$_2$-Met and SiO$_2$-Cys sorbents (10 mL sample solution, 1 mol L$^{-1}$ HCl, 30 min sorption time; three parallel determinations).

| Metal ions | Added (mg L$^{-1}$) | Recovery, % | |
|---|---|---|---|
| | | SiO$_2$-Cys | SiO$_2$-Met |
| Al (III) | 1000 | < 1 | < 1 |
| Zn (II) | 1000 | < 1 | < 1 |
| Ni (II) | 1000 | <1 | < 1 |
| Mn (II) | 1000 | <1 | < 1 |
| Cu (II) | 2000 | <1 | < 1 |
| Fe (III) | 1000 | <1 | < 1 |
| Pt(II) | 50 | 94.0 ± 5 | 94.9 ± 4 |

After digestion SnCl$_2$ was added to the sample solution and stirred with 50 mg SiO$_2$-Met for 30 min. After centrifugation the sorbent was washed with distilled water and the retained Pt was eluted with 2 mL of 0.7 mol L$^{-1}$ thiourea in 2 mol L$^{-1}$ HCl and measured by ICP-OES. Recoveries for the investigated element in spiked cream samples varied in the range 93–104 % demonstrating the applicability of the proposed analytical procedure (Table 3).

**Table 3.** Recovery studies for the determination of Pt(II) by SPE and ICP-OES measurements, using SiO$_2$-Met (20 mL sample solution, 1 mol L$^{-1}$ HCl, 30 minutes sorption time; three parallel determinations).

| Added, µg g$^{-1}$ | Found, (mean±sd) µg g$^{-1}$ | RSD, % | Recovery, % |
|---|---|---|---|
| 0 | BDL* | - | - |
| 0.2 | 0.19±0.03 | 16 | 93 |
| 0.5 | 0.51±0.04 | 8 | 103 |
| 1.0 | 1.02±0.06 | 6 | 104 |

*BDL – below detection limits

The reached limits of quantification (LOQ), calculated as ten time the standard deviation of the blank, are 0.2 µg g$^{-1}$ Pt in the cosmetic cream sample. Relative standard deviations for the concentration range 0.2–1.0 µg g$^{-1}$ Pt in the cream sample varied between 6-16 % (Table 3).

The developed SPE-ICP-OES procedure was applied for the determination of Pt in Pt-containing cream, purchased from the market and the results were compared with those obtained by direct ICP-MS measurements of the same sample after MW digestion.

Results (0.25 ±0.05) µg g$^{-1}$ found by SPE-ICP-OES and (0.21±0.05) µg g$^{-1}$ found by direct ICP-MS (performed in an external lab) agreed very well

(Student's t-test, 95% confidence limit) thus demonstrating that there are no statistically significant differences between the results obtained by the two methods and confirming the accuracy of the developed SPE-ICP-OES method for Pt determination in cosmetic creams.

CONCLUSION

Sorbents $SiO_2$-Met and $SiO_2$-Cys based on newly synthesized derivatives of cysteine and methionine, respectively, impregnated on silica gel surface were prepared and studied for the separation and enrichment of Pt. The chemical conditions for quantitative sorption of Pt(II) were defined and the sorbent $SiO_2$-Met was applied for the determination of total Pt in cosmetic cream.

REFERENCES

1. P. Kovacheva, R. Djingova, *Analytica Chimica Acta,* **464**, 7 (2002).
2. H. Mukai, Y. Ambe, M. Morita, *J. Anal. At. Spectrom.*, **5**, 75 (1990).
3. K. Akatsuka, S. Hoshi, J. McLaren, S. Berman, *Bunseki Kagaku,* **43**, 67 (1994).
4. H. Mukai, Y. Ambe, M. Morita, *J. Anal. At. Spectrom.,* **5,** 75 (1990).
5. H. Bayrak, V. Bulut, M. Tufekci, H. Bayrak, C. Duran, M. Soylak, *Toxicological & Environmental Chemistry,* **99,** 590 (2017).
6. R. Sutherland, D. Pearson, C. Ottley, *Applied Geochemistry,* **22,** 1485 (2007)
7. A. Cantarero, M. Gomez, C. Camara, M. Palacios, *Anal. Chim. Acta,* **296**, 205 (1994).
8. B. Qu, *Analyst*, **121,** 139 (1996).
9. V. Otruba, M. Strnadová, B. Skalníková, *Talanta*, **40**, 22 (1993).
10. K. Jankowski, A. Jackowska, P. Łukasiak, *Analytica Chimica Acta,* **540**, 197 (2005).
11. K. Pyrzyńska, *Talanta,* **47**, 841 (1998).
12. B. Godlewska-Żyłkiewicz, *Microchim. Acta,* **147**, 189 (2004).
13. E. Mladenova, I. Dakova, I. Karadjova, M. Karadjov, *Microchemical Journal*, **101**, 59 (2012).
14. M. Osman, S. Kholeif, N. Abou-Almaaty, M. Mahmoud, *Anal Sci,* **20**, 847 (2004).
15. X. Wu, P. Liu, Q. Pu, Q. Sun, Z. Su, *Talanta,* **62**, 918 (2004).
16. Y. Yamini, M. Chaloosi, H. Ebrahimzadeh, *Talanta,* **56**, 797, (2002).
17. R. Vlašánkova, V. Otruba, J. Bendl, M. Fišera, V. Kanický, *Talanta*, **48,** 839 (1999).
18. P. Jal, S. Patel, B. Mishra, *Talanta,* **62,** 1005 (2004).
19. D. Bilba, D. Bejan, L. Tofan, *Croatica Chemica Acta,* **71**, 155 (1998).
20. P. Petrova, I. Karadjova, M. Chochkova, I. Dakova, M. Karadjov, *Bulgarian Chemical Communications*, Special Issue E, **95** (2017).
21. J. Sheehan, G. Hess, *J. Am. Chem. Soc.*, **77**, 1067 (1955).
22. A. Bartyzel, E. Cukrowska, *Analytica Chimica Acta*, **707**, 204 (2011).
23. A. Bocca, G. Forte, F. Petrucci, A. Cristaudo, *Journal of Pharmaceutical and Biomedical Analysis*, **44**, 1197 (2007).
24. E. Guibal, N. Von Offenberg Sweeney, T. Vincent, J. Tobin, *Reactive and Functional Polymers*, **50**, 149 (2002).
25. V. Joshi, *Indian Natn. Sci. Acad.*, **54,** 664 (1988).
26. D. Vermeulen, F. Cantwell, *Anal. Chem.,* **65,** 1360 (1993).

# Optimization of biogas production from lignocellulosic materials by different methods of substrate treatment

## I. Angelov*, V. Beschkov

*Institute of Chemical Engineering, Bulgarian Academy of Sciences, Sofia 1113, Bulgaria*

Biogas is considered a possible alternative to the conventional fuels. It is produced by anaerobic digestion of different organic materials. Generally those materials include mostly manure and municipality waste. Our research focuses on the possibility to utilize new types of organic materials (e.g. ground coffee residue, coniferous vegetation) in combination with the traditional ones. We believe that adding new materials will enhance the process of biogas production and will contribute to higher range of waste treatment. The final product is biogas with higher methane content which makes it useful for heat and power generation. Therefore we focused on utilizing of coniferous material mixed with other organic materials in anaerobic digestion reactor.

## INTRODUCTION

Biofuels play an important role in our efforts to reduce $CO_2$ emissions and keep the environment cleaner. As we depend more and more on fuels to power our economies (by generating electricity, producing chemical products, as fuel for planes, ships and vehicles), it becomes more difficult to reduce the pollution of the environment.

Biogas is a widely used fuel in economically developed countries, as well as in the countries from the 3rd world. It has many applications. Among the most important ones are as a fuel for thermal power plants, addition to the national gas grid and as a fuel in various types of vehicles, including passenger cars, trucks, small and midsize boats and aircrafts. The main source to produce biogas is manure. Some of the disadvantages of producing biogas are the low content of methane (50% – 60%) and the presence of sulfuric compounds. In the current case, our aim is to investigate the possibilities of optimizing the methods and conditions for biogas production from vegetal waste.

During the experiments, we used a coniferous material from the type *Picea excelsa L.* The first part of treatment focused on the lignocellulosic material. The branches and leaves were shredded and then collected in a beaker. After that, their weight was measured. In the next step, the material was mixed with water or acid. Then, the material was autoclaved for 20 min at 121 °C. In the meantime, the second part of the treatment was carried out. A specific amount of organic waste (cattle manure) was taken, and was mixed with water. After that, the slightly liquefied manure was treated in various ways. One of them included passing electrical current through the mixture for some time. After that, the lignocellulosic material and the organic waste were mixed. Then the mixture was poured in air- insulated glass vessels. The vessels were installed in a water bath, where the temperature was kept at 32 to 35 °C. Each experiment included different ways of treatment, mixing and autoclaved material.

Three series of experiments were conducted. They are all part of a long-term scientific research which focuses on producing biogas by utilizing coniferous material mixed with other waste organic materials. Each of the experimental series included 2 samples.

## MATERIALS AND METHODS
### Experiment 1

Experiment 1 (which included samples A1 and B1) used coniferous material treated with 1% $H_2SO_4$. Then the material was mixed with residues of ground coffee waste (sample A1) and manure. The mixture was poured into a glass bottle tank and kept at 32°C in a water bath. The bottle was connected to a gas holder which collected the produced biogas. Then the biogas was analyzed. Sample B1 was treated in the same way, with one difference, that instead of coffee, the coniferous material was mixed with waste glycerol. The substrate compositions are shown in Table 1. Some results for the biogas yield of this experiment are shown in Figs 1 and 2. It is obvious that glycerol is more efficient as addition to the coniferous material. It is because of the high stoichiometric methane yield.

---

* To whom all correspondence should be sent.
E-mail: yeraodos@abv.bg; vbeschkov@yahoo.com
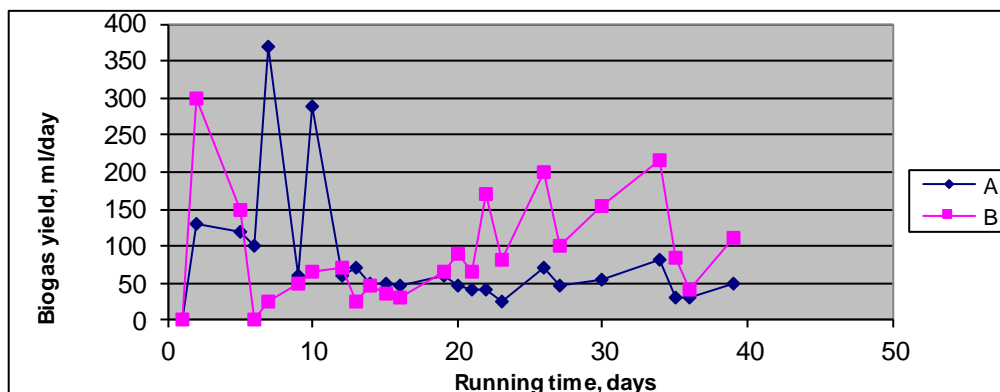
**Fig. 1.** Daily biogas yield. Samples A1 and B1
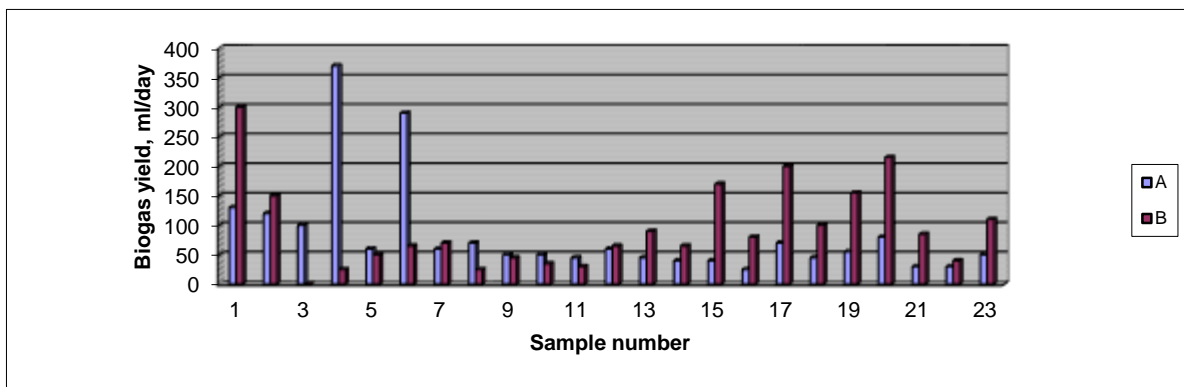


**Fig. 2**. Biogas yield for longer period of time (experiment 1).

**Table 1.** Biogas yield. Combustion test results. A1: 8 g con. matter (100 ml 1% $H_2SO_4$ ) + ground coffee waste (4 g) + manure (317 g). B1: 8 g con. matter (100 ml 1% $H_2SO_4$) + glycerol (4 g) + manure (304 g)

| Total volume of biogas | Sample A1 = 1915 ml | Sample B1 = 2170 ml |
|---|---|---|
| % Burning of biogas | 47 % | 79.26 % |
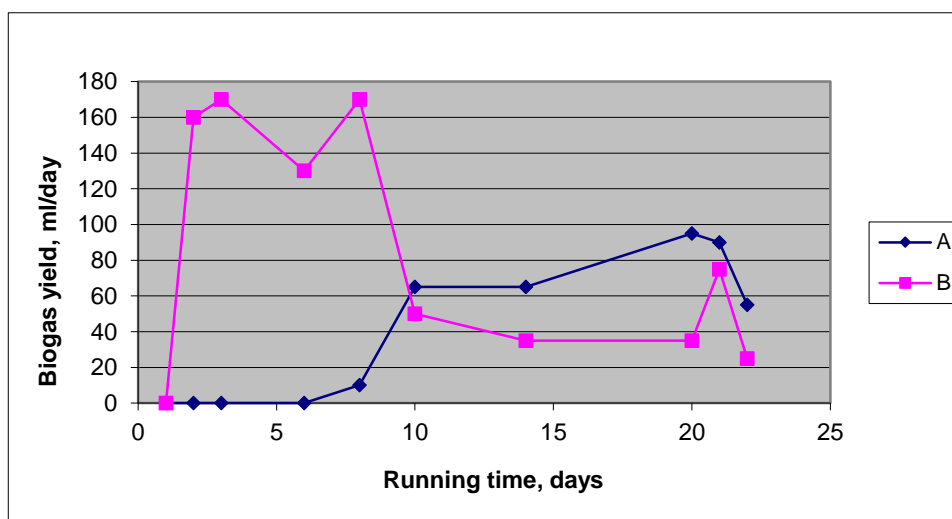


**Fig. 3**. Biogas yield. Samples A2 and B2

*Experiment 2*

Experiment 2 (samples A2 and B2) contained coniferous materials treated with 1% $H_2SO_4$ acid. Coffee residues were added in sample A2 and wasted glycerol was added in sample B2. Then cow manure was treated with constant voltage for 30 min. After the treatment it was added to the reaction vessels. There is also better effect of glycerol on the combustion capacity of the produced biogas, being additionally enhanced by manure after the electrical treatment.
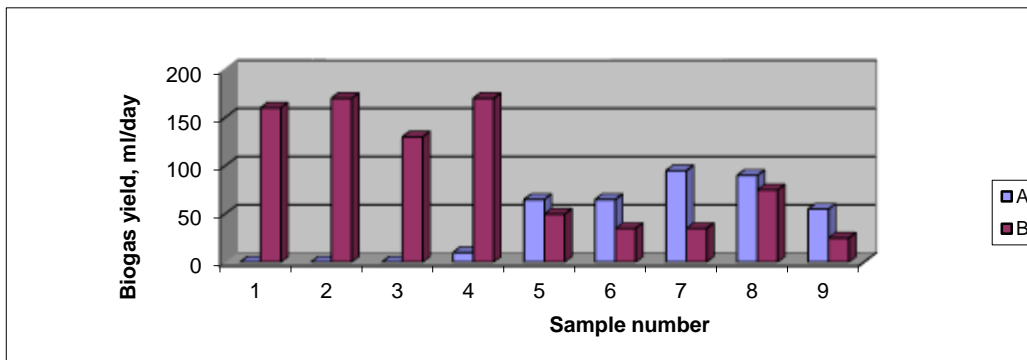


**Fig. 4**. Biogas yield for experiment 2

**Table 2.** Biogas yield. Combustion test results. A2: 8 g con. mat. (100 ml 1% $H_2SO_4$ ) + coffee (4 g) + manure (300 g, electric field for ½ h). B2: 8 g con. mat. (100 ml 1% $H_2SO_4$) + glycerol (4 g) + manure (300 g, electric field for ½ h)

| Total volume of biogas | Sample A2 = 380 ml | Sample B2 = 850 ml |
|---|---|---|
| % Burning of biogas | 0 % | 81.17 % |
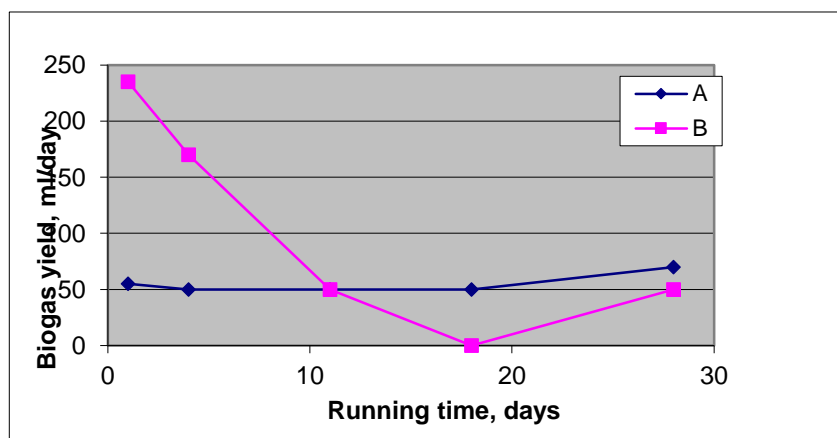


**Fig. 5.** Biogas yield. Samples A3 and B3
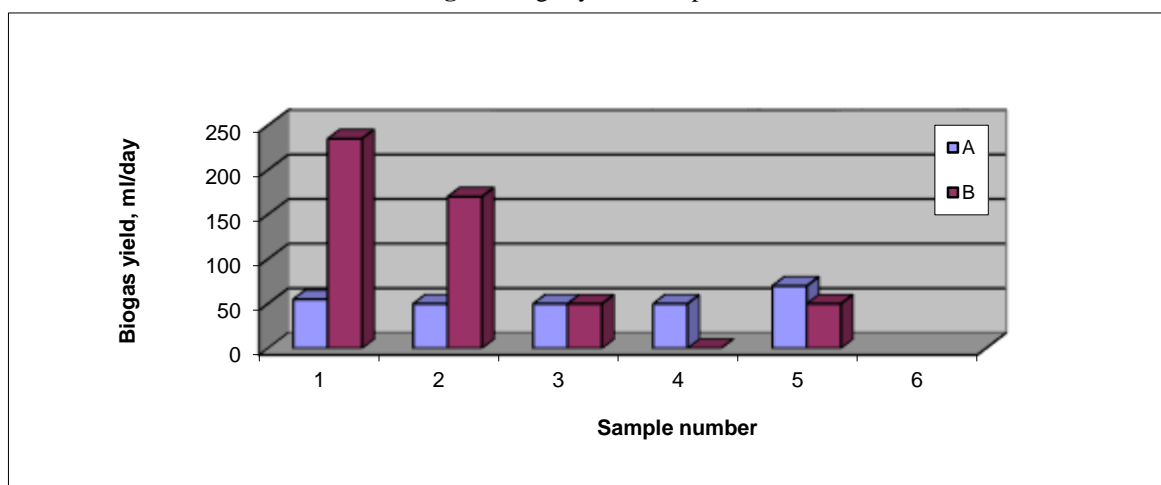


**Fig.6.** Biogas yield for experiment 3

**Table 3.** Biogas yield. Combustion test results. A3: 8 g con. mat. (100 ml 1% $H_2SO_4$ ) + coffee (4 g) + manure (300 g, electricity for 1 h), B3: 8g con. mat. (100 ml 1% $H_2SO_4$) + glycerol (4 g) + manure (300 g, electricity for 1 h)

| Total volume of biogas | Sample A3 = 275 ml | Sample B3 = 505 ml |
|---|---|---|
| % Burning of biogas | 43.6 % | 90 % |

### *Experiment 3*

Experiment 3 (samples A3 and B3) contained coniferous materials treated with 1% $H_2SO_4$ acid. Coffee residues were added in sample A3 and wasted glycerol was added in sample B3. Then the manure was treated with electricity for 1 h. After the treatment, it was added to the reaction vessels.

### RESULTS AND DISCUSSION

Throughout the series of experiments, the aim of our research was to investigate different types of substrate combinations (as mixing with food waste) and the influence of electricity charge in the complex biochemical reactions of anaerobic digestion. For that purpose, the electricity applied in experiment 2 was ½ h and in experiment 3, it was 1 h. As a conclusion, according to the results we obtained from our experiments, we have noticed that coniferous material can be used as a substrate for biogas production if mixed with cattle manure, as well as the treatment of manure with electricity improved the quantity and methane content of the collected biogas. We have also noticed that the used food waste (which in our case was ground coffee waste), was hardly used by the microorganisms in the bioreactor. On the other hand, the addition of waste glycerol gives better effect on biogas yield and combustibility. In all cases, the treatment of manure by DC enhances the methane content and the biogas combustibility.

### REFERENCES

1. T. Al Seadi, D. Rutz, H. Prassl, M. Köttner, T. Finsterwalder, S. Volk, R. Janssen, Biogas Handbook, University of Southern Denmark Esbjerg, Niels Bohrs Vej 9-10, DK-6700 Esbjerg, Denmark, 2008. ISBN: 978-87-992962-0-0
2. Directive 2009/28/EC of the European Parliament and of the Council of 23 April 2009 on the promotion of the use of energy from renewable sources and amending and subsequently repealing Directives 2001/77/EC and 2003/30/EC. https://eur-lex.europa.eu/legal-content/EN/ALL/?uri=celex%3A32009L0028
3. K. Ostrem, N. J. Themelis, Greening waste: anaerobic digestion for treating the organic fraction of municipal solid wastes, Department of Earth and Environmental Engineering Foundation of School of Engineering and Applied Science, Columbia University, May 2004.

# Electrohydraulic ragging of metallurgical silicon

B.R. Nussupbekov[1], A.K. Khassenov[1*], D.Zh. Karabekova[1], M. Stoev[2],
A.Zh. Beysenbek[1], B.I. Kazankap[1]

*[1] E. A. Buketov Karaganda State University, Kazakhstan*
*[2]Neofit Rilski South-West University, Blagoevgrad, Bulgaria*

The article presents a crushing technology of metallurgical silicon. The proposed ore crushing method is based on the use of the energy of an impulse shock wave resulting from an electrical spark discharge in a liquid. Electro-hydraulic technology is one of the most acceptable in production environment because it provides intensive ragging and crushing of the test material.

## INTRODUCTION

Currently, on account of the high content of metal impurities in metallurgical silicon it is not used to produce photo cells, since the purity of the silicon should be at least 99.99% [1, 2]. Material of this purity is currently supplied to the world market by about 10 companies (from USA, Japan, Germany and Italy), and the number of manufacturers does not actually increase. This is due primarily to the fact that metallurgical silicon refinement technology is very complex and expensive, so the required manufacturing investments exceed several billion dollars [2].

Electrical properties of silicon crystals substantially depend on the amount of impurities. Besides, ferrous metals including iron, chromium, manganese, heavy non-ferrous metals such as copper, nickel and alkali metals such as sodium and potassium are unnecessary impurities; so to produce photoelectric current converters it is necessary to reduce the number and contents of the elements [3].

However, metallurgical silicon containing more than 98.8% of silicon in the form of powder having a particle size greater than $6 \cdot 10^{-7}$ m is used in manufacturing organic silicon compounds and trichlorosilane as a source raw material to produce semiconductor silicon [3].

In connection with the above, the objective of this work is to break up metallurgical silicon by electro-hydraulic pulsed discharge, and to match the basic electrical and energy parameters of an electric hydropulse plant [4].

## Materials and routine of the experiment

To investigate breaking and ragging of metallurgic silicon, an electric hydropulse plant with a crushing unit was developed and assembled in the Laboratory of electrohydrodynamics at the E.A. Buketov Karaganda State University [5].

In the crushing unit there is a cylindrical chamber where a linear system of electrodes is installed. The positive electrode is set vertically, while the negative electrode is the bottom of a hemispherical metal chamber. When a high power pulse passes through a liquid medium, which is a wet mass, an electrical breakdown occurs there, accompanied by a hydraulic shock of high destructive power.

The aqueous medium, in which the high-voltage electric discharge occurs, is a transformer of the energy released in the discharge channel, and due to low compressibility it leads to a sharp increase in pressure.

Due to electrohydropulse effect, a hydrodynamic fluid flow and an acoustic wave arise in the processed medium; and cavitation results from local pressure reduction in the fluid. At the same time a cavitation bubble, entrained by the fluid flow to a greater pressure area, collapses and causes a shock wave. After the bubble collapse, microshocks of cumulative jets are formed. The mixture, accelerated by the discharge channel broadening at a high rate, moves away in all directions.

At the start of the process, the discharge channel dilates at a maximum rate; on completion of the current flow due to the inertia of the medium, the space of the discharge channel continues to extend, it reaches the maximum size and then falls into contraction. When the space extends, the

* To whom all correspondence should be sent.
 E-mail: ayanbergen@mail.ru

temperature and pressure in the discharge channel fall, and at its contraction they rise, i.e. damped pulsation of the space occurs.

When solid substances are exposed to electrohydraulic action in aqueous solution, the intensity of the crushing process grows by the impact of the additional pressure due to cavitation. Indeed, at each solid particle a cavitation microcavity occurs; when collapsing, the latter increases its mechanical action [4-7].

During testing, the initial diameter of the metallurgical silicon particles averaged $3 \cdot 10^{-3} \div 15 \cdot 10^{-3} \textit{ì}$ .

Tests at the electrohydraulic plant were carried out at various values of discharge energy $(W = 65 \div 245 \textit{Äæ})$, capacitor bank capacity $\left(\tilde{N} =: 0,25; 0,4; 0,8; 1 \cdot 10^{-6} F\right)$, interelectrode gap at a commutation switch $\left(l_p =: 6; 8; 10; 12 \cdot 10 \textit{ìì}\right)$ and a pulse repetition rate of 5 to 15 Hz. The value of the applied voltage to the switching device was adjusted from $15 \cdot 10^3$ to $40 \cdot 10^3 \textit{Â}$.

## RESULTS AND DISCUSSION

During the experiment, the best value of the interelectrode gap at the commutation switch was 10 mm and the diameter of the fractions undergoing the most intense breakup was $d_{\hat{o}\partial} = 7 \cdot 10^{-3} \textit{ì}$ . The fineness number increases with increase in the specific energy supplied to the discharge channel. This can be explained by the fact that on the shockwave way a microcrack network is first formed in the substance structure and it causes a complete stress state. The results of the laboratory tests carried out at different values of capacitance of the capacitor bank are shown in Figure 1.
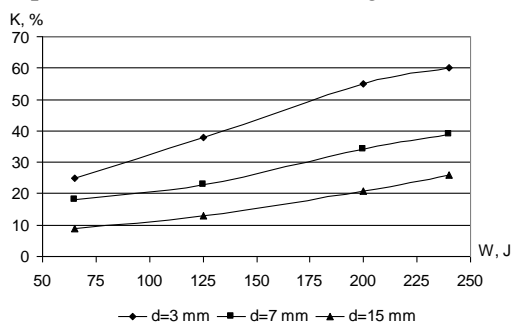


**Fig. 1.** Dependence of silicon fineness number on the discharge energy at the commutation switch

As the figure shows, the fineness number of metallurgical silicon crushed to 0.5 mm is rather low at the discharge energy value of 65 J, and when the discharge energy increases from 125 J to 250 J the fineness number of the material increases at

about the same rate. By the impact of a series of pulses of $10^{-5} \div 10^{-4} \tilde{n}$ width on solid fractions, they initially cumulate plastic strain, which on the one hand increases its strength to some extent, but in the defect structure areas voltage arises which destroys materials.

The analysis of the qualitative and quantitative elemental composition of materials before and after processing at the electropulse plant was performed on a scanning electron microscope Philips SEM 515 in accordance with the standard technique of "The testing procedure of the structure of a solid body surface using scanning electron microscopy," at the Tomsk State University. The chemical analysis and elemental composition of the metallurgical silicon processed at the electropulse plant were compared with the samples crushed by a gyratory mill. The analysis of the element composition after mechanical operation and electric pulse machining shows different changes in the processed samples (Table 1).

**Table 1.** Elemental composition of metallurgical silicon

| Element | Cone mill | Electropulse installation |
|---|---|---|
| Silicon (%) | 99.78 | 99.96 |
| Aluminum (ppm) | 79 | 55 |
| Sulfur (ppm) | 74 | 12 |
| Magnesium (ppm) | 152 | 53 |
| Potassium (ppm) | 18 | -5 |
| Vanadium (ppm) | 14 | -8 |
| Phosphorus (ppm) | 19 | 29 |
| Calcium (ppm) | 301 | 76 |
| Iron (ppm) | 1264 | 507 |
| Nickel (ppm) | 40 | 12 |
| Chromium (ppm) | 83 | 16 |
| Copper (ppm) | 428 | 23 |
| Titanium (ppm) | 56 | 19 |
| Boron (ppm) | 463 | 142 |
| Sodium (ppm) | 57 | 0 |

After the electro-hydraulic processing, the content of ferrous metals decreased: iron from 1264 ppm to 507 ppm, chromium from 83 ppm to 16 ppm. The content of heavy non-ferrous metals decreased too. Particularly the copper content decreased from 428 ppm to 23 ppm, the content of nickel from 40 ppm to 12 ppm, and of alkali metals the content of sodium fell from 57 ppm to 0 ppm, and the potassium content from 18 ppm to -5 ppm. Reduction in inclusions may be due to the fact that during the treatment process taking place in a liquid medium, silicon lumps are cleaned by pulses.

30

## CONCLUSION

This is the first experimental study of the effect of underwater electrical explosion on the selectivity of ragging and crushing of metallurgical silicon. In accordance with the fineness number of the material under examination, the best optimal parameter for the discharge energy is 200 J. By the electro-hydraulic technology metallurgical silicon is crushed to fractions of preset parameters.

## REFERENCES

1. E.S. Filkevich, Semiconductor silicon technology, M., Metalurgiya, p. 408, 1992.
2. O.M. Katkov, Smelting of silicon, Irkutsk, Publishing house IPU, p. 243, 1997.
3. N.V. Nemchinova, S. S. Belsky, B. A. Krasin, High-purity metallurgical silicon as a basic element for solar energy, Success of modern natural science. - M., № 4. p. 56, 2006.
4. L.A. Yutkin, Electrohydraulic effect and its application in industry. A: Engineering, Leningrad Branch, p. 253, 1986.
5. B.R. Nusupbekov, G. M. Shaimerdenova, D. K. Kusainova, Dynamics of destruction and formation of structures in the process of electroimpulse processing of silicium minerals, *Eurasian Physical Technical Journal,* **5**, 24 (2008).
6. B.R. Nussupbekov, M. Stoev, A. K. Khasenov, A. Zh. Beisenbek, Electric pulse method of rock crushing, Mathematics and natural science: Proceedings of the Fifth International Scientific Conference FMNS2013 – Blagoevgrad, **3**, 45, 2013.
7. B.R. Nusupbekov, K. Kussaiynov, S. E. Sakipova, A. K. Khassenov, A. Zh. Beisenbek, On improvement of technology of complex extraction of rare and trace metals by electropulse method, *Metallofizika i Noveishie Tekhnologii– Kyiv,* **36**(2), 275 (2014).

# Correlation between Cambisols soil characteristics and lead content in wild edible mushrooms (*Cantharellus cibarius, Tricholoma equestre, Craterellus cornucopioides*)

L. Dospatliev[1*], M. Ivanova[2], K. Gavazov[3,4]

[1]*Department of Pharmacology, Animal Physiology and Physiological Chemistry, Trakia University, Stara Zagora, Bulgaria;*
[2]*Department of Informatics and Mathematics, Trakia University, Stara Zagora, Bulgaria;*
[3]*Faculty of Chemistry, University of Plovdiv Paisii Hilendarski, Plovdiv, Bulgaria;*
[4]*Faculty of Pharmacy, Medical University of Plovdiv, Plovdiv, Bulgaria*

The study was conducted on Cambisols soils and wild edible mushrooms from the Batak Mountain, Bulgaria. The total lead content in the soils was determined after their decomposition with HF, $HClO_4$, and $HNO_3$ acids. The mushroom samples were prepared by dry ashing and subsequent dissolution in 3 M HCl. All lead analyses were performed by inductively coupled plasma atomic emission spectroscopy (ICP-OES) at a wavelength of 220.353 nm. Certified reference materials (three soils and tobacco leaves) were also analysed for verification of the accuracy of Pb determination. A correlation/regression analysis was carried out to reveal possible associations between pH, humus content, and total lead content of the soils and the concentration of this element in the mushroom samples.

## INTRODUCTION

Environmental pollution is one of the most serious problems in industrialized countries. Emissions of heavy metals from anthropogenic sources have been constantly increasing in recent decades. Heavy metals are very persistent in the environment and, due to the ability of accumulation, threat to living organisms [1-3]. Mushrooms are known to accumulate high concentrations of toxic metallic elements, metalloids, and radionuclides [4,5].

Lead is a naturally occurring heavy metal with an average content in the Earth's crust of 14 ppm. Its widespread use in various industrial processes has resulted in extensive environmental contamination, human exposure and significant public health problems in many parts of the world [6]. Important sources of environmental contamination include mining, smelting, recycling activities, metal plating, effluents from storage batteries, and, in some countries, the continued use of leaded paint, leaded gasoline and aviation fuel [6,7].

When Pb enters the body, it distributes throughout the organs such as brain, kidneys, liver, and bones. It is particularly harmful to young organisms and can cause irreversible health effects [6,8,9].

Although a number of investigations have been carried out on heavy metal accumulation by mushrooms, to the best of our knowledge there is no clearness concerning the correlation between soil characteristics and lead content in mushrooms.

The purpose of this study is to provide information on the relationship between pH, humus, and total content of lead in Cambisols soils from one hand, and the concentration of this element in wild-grown edible mushroom species (*Cantharellus cibarius, Tricholoma equestre, Craterellus cornucopioides)* from the other hand.

## EXPERIMENTAL

Fifteen Cambisols soil samples (from Batak mountain, Bulgaria) were taken from a depth of 0 – 20 cm. The following soil characteristics were determined: pH in water, humus according to Turin [9], total content of lead through decomposition by HF, $HClO_4$, and $HNO_3$ acids, following ISO (International Organization for Standardization) 14869-1 standard [11].

Forty five mushroom samples (found in the regions of the soil sampling sites) were collected in 2014 and 2015 by the authors themselves. All samples were washed so as to remove any adhering soil particles and rinsed with distilled water, after which they were dried at 105°C for 24 h and ground. The further processing of the samples included dry ashing and dissolution in 3 M HCl.

An inductively coupled plasma atomic emission (ICP-OES) system HORIBA Jobin Yvon ULTIMA 2 (Jobin Yvon, Longjumeau, France) was

* To whom all correspondence should be sent.
 E-mail: lkd@abv.bg

used for determination of Pb content in the Cambisols soil and mushroom samples. The operating wavelength was 220.353 nm.

*Accuracy and precision*

Soil and plant materials used for accuracy and precision tests included three certified soil samples corresponding to two main soil types in Bulgaria and one certified reference material of tobacco leaves as follows:

i) Light Alluvial–deluvial Meadow Soil PS-1,SOOMET No. 0001-1999 BG, SOD No. 310[a]-98.

ii) Light Meadow Cinnamonic Soil PS-2,SOOMET No. 0002-1999 BG, SOD No. 311[a]-98.

iii) Light Alluvial–deluvial Meadow Soil PS-3,SOOMET No. 0003-1999 BG, SOD No. 312[a]-98.

iv) Polish reference material CTA-VTL-2 (Virginia tobacco leaves).

For evaluation of the correctness of the results (Table 1), three generally accepted criteria were used as follows:

1. $D = X - X_{CRM}$, where $X$ is the measured value and $X_{CRM}$ is the certified value. When $D$ is within the borders of $\pm 2\sigma$, where $\sigma$ is the standard deviation from the certified value, the result is considered to be good; when it is $-3\sigma \leq D \leq 3\sigma$ - satisfactory, and beyond these limits the result is unsatisfactory.

2. $D\% = D / X_{CRM} \cdot 100$ - percentage difference. When the values of $D\%$ are in the limits $\pm 200\sigma / X_{CRM}$, the result is considered to be good; when the value is in the limits $\pm 200\sigma / X_{CRM}$ and $\pm 300\sigma / X_{CRM}$ - satisfactory; and when it is out of the limits $\pm 300\sigma / X_{CRM}$, the result is unsatisfactory.

3. $Z = X - X_{CRM} / \sigma$. When $Z \leq 2$, the result is considered to be good; when $2 \leq Z \leq 3$ – satisfactory; when $Z > 3$ – unsatisfactory.

For evaluation of the accuracy of the digestion and measuring procedures, we have used R criterion showing the extent of extraction of the element in percent from the certified value. When the measured value $X$ is within the borders of $X_{CRM} \pm U_{CRM}$, where $U_{CRM}$ is the indefiniteness of the certified value, we accept an extent of extraction to be 100%. In all the remaining cases, the extent of extraction is equal to $X / X_{CRM} \cdot 100$.

*Statistical processing*

SPSS (Statistical Package for Social Science) program for Windows was used for statistical data processing.

RESULTS AND DISCUSSION

*Soils*

Table 2 presents the pH values for the tested Cambisols soils. As evident from the table, the Cambisols soil reaction is medium acid.

**Table 1.** Analytical results of the certified materials for Pb

| Element | Sample | Certified value | $X \pm \sigma_x$ mg kg$^{-1}$ | $D$ | $D$, % | $Z$ | $R$ |
|---|---|---|---|---|---|---|---|
| Pb | PS-1 | 120.48 ± 5.20 | 117.39 ± 3.04 | - 3.09[b] | - 2.57[b] | 0.59[b] | 100 |
| | PS-2 | 51.21 ± 5.09 | 52.40 ± 3.71 | - 1.87[b] | 2.32[b] | 0.23[b] | 100 |
| | PS-3 | 87.50 ± 11.68 | 88.65 ± 5.46 | 1.15[b] | 1.32[b] | 0.1[b] | 100 |
| | CTA-VTL-2 | 22.1 ± 1.2 | 21.7 ± 7.6 | - 0.4[b] | - 1.81[b] | 0.33[b] | 100 |

[a]"Satisfactory" result
[b]"Good" result

**Table 2.** Soil properties and content of Pb in Cambisols soil and mushrooms (n = 15)

| Statistical index | pH | Humus | Content of Pb in soil, mg kg$^{-1}$ Total | Content of Pb in *Cantharellus cibarius*, mg kg$^{-1}$ | Content of Pb in *Tricholoma equestre*, mg kg$^{-1}$ | Content of Pb in *Craterellus cornucopioides*, mg kg$^{-1}$ |
|---|---|---|---|---|---|---|
| Mean | 5.76 | 2.60 | 17.10 | 0.27 | 1.16 | 0.41 |
| Standard Error | 0.17 | 0.14 | 0.46 | 0.03 | 0.04 | 0.01 |
| Median | 5.85 | 2.68 | 16.45 | 0.27 | 1.12 | 0.42 |
| Mode | 5.45 | 3.15 | #N/A | #N/A | #N/A | #N/A |
| Standard Deviation | 0.65 | 0.56 | 1.80 | 0.11 | 0.16 | 0.06 |
| Sample Variance | 0.42 | 0.31 | 3.23 | 0.01 | 0.03 | 0.00 |
| Kurtosis | -1.52 | -1.38 | -0.66 | -1.38 | -1.47 | -1.28 |
| Skewness | -0.15 | -0.16 | 0.78 | 0.23 | 0.36 | 0.19 |
| Range | 1.84 | 1.70 | 5.17 | 0.32 | 0.43 | 0.15 |
| Minimum | 4.81 | 1.75 | 15.15 | 0.13 | 0.96 | 0.34 |
| Maximum | 6.65 | 3.45 | 20.33 | 0.44 | 1.40 | 0.50 |
| Sum | 86.41 | 39.06 | 256.55 | 4.09 | 17.36 | 6.19 |
| Count | 15.00 | 15.00 | 15.00 | 15.00 | 15.00 | 15.00 |
| Con. Level (95.0%) | 0.36 | 0.31 | 1.00 | 0.06 | 0.09 | 0.03 |
| CV. % | 11.28 | 21.54 | 10.53 | 40.74 | 13.79 | 14.63 |

The average arithmetic value is 5.76, as pH of most of the Cambisols soils is close to this value, i.e., they are very suitable for mushrooms growing. The humus content is within the limits from 1.75 to 3.45 (low to medium), as most of the soils have low humus content and they are suitable for the mushroom variety group [12].

The total lead content in Cambisols soil ranges from 15.15 to 20.33 mg kg$^{-1}$. According to the requirements of the Bulgarian standards for allowable lead content in the Cambisols soil depending on the active soil reaction (pH) is below the limit concentration (90 mg kg$^{-1}$). The arithmetic mean is $\bar{X}$ = 17.10 mg kg$^{-1}$, as its value is greater than the median (*Me* = 16.45), therefore there is a right-tail distribution. This is proved by the positive coefficient of skewness (*Sk* = 0.78). The coefficient of kurtosis is negative (*Kr* = − 0.66), i.e. observed low peak height of the distribution. Not greater dispersion of the values of Pb, the mean value leads to no higher values of standard deviation (σ = 1.80) and coefficient of variation, which reaches 10.53% (Table 2).

*Mushrooms*

Heavy metal contents in mushrooms are largely dependent on their trophic pattern, hysiology of mushroom species, area of sample collection, mushroom accumulation of other metals, and the distance from the pollution sources. Moreover, the age of mycelium and lag between fructification seem to be further factors affecting metals content [13].

Toxicity of lead is enhanced by its ability to bio-concentrate and bio-transform in the tissues [14, 15]. Lead ions produce physiological poisoning by becoming attached or absorbed on the cellular enzymes, causing inhibition of enzymatic control of respiration, photosynthesis and poor respiration [14, 15]. Lead is primarily absorbed via respiration and ingestion, circulated through the bloodstream and thereafter enters all tissues of the body [13]. Lead can displace calcium from the bones causing them to be brittle [14-16]. Bioaccumulation in the liver or kidney can occur leading to liver or kidney malfunction, disruption of the central nervous system (encephalopathy) resulting in uncoordinated muscular control and poor eyesight has also been reported [15-19]. However, these symptoms do not become noticeable until the level in a particular organism exceeds its tolerance limit for the metal. Every organism has a different limit for each toxic substance for example lead can be tolerated in plants at a higher concentration than mercury [15].

The total lead content in the samples of the three investigated mushrooms species (*Cantharellus cibarius, Tricholoma equestre, Craterellus cornucopioides*) varied in the range from 0.13 to 1.40 mg kg$^{-1}$. These values are several times lower than those specified in The Annex to Regulation (EC) No 1881/2006 [20] (0.3 mg kg$^{-1}$ wet weight), having in mind that the average water content in our samples was 90%. These results comply with the data published by other authors [21-33].

*Correlation dependencies among pH, humus, and total quantities of Pb in cambisols soil and in the mushrooms.*

Correlation coefficients among soil parameters and concentration of lead in mushroom are summarized in Table 3 and Figures 1 – 3.

The results of the conducted correlation/regression analysis show that there are statistically significant dependencies determined between the humus content, total forms and Cambisols soil pH and lead concentration in the mushrooms.

Lead concentration in mushrooms increases linearly with the increase of the total element content in the Cambisols soil. The observed level of significance has a lower value than the critical level of significance of 0.01; the correlation coefficients are high and statistically significant. Determination coefficients show that nearly 85 – 97% of the lead concentration in mushrooms depend on the total lead content in the Cambisols soils.

**Table 3.** Correlation at the 0.05 level between the soil parameters and concentration of lead in the mushrooms (*n* = 15)

| Element | Soil parameters | *Cantharellus cibarius* | *Tricholoma equestre* | *Craterellus cornucopioides* |
|---------|-----------------|-------------------------|-----------------------|------------------------------|
| Pb | pH | 0.95[**] | 0.96[**] | 0.81[**] |
| | Humus | 0.86[**] | 0.82[**] | 0.67[**] |
| | Total | 0.97[**] | 0.90[**] | 0.85[**] |

*ns* no significant correlation; [**] Correlation is significant at the 0.05 level; [*]Correlation is significant at the 0.01 level
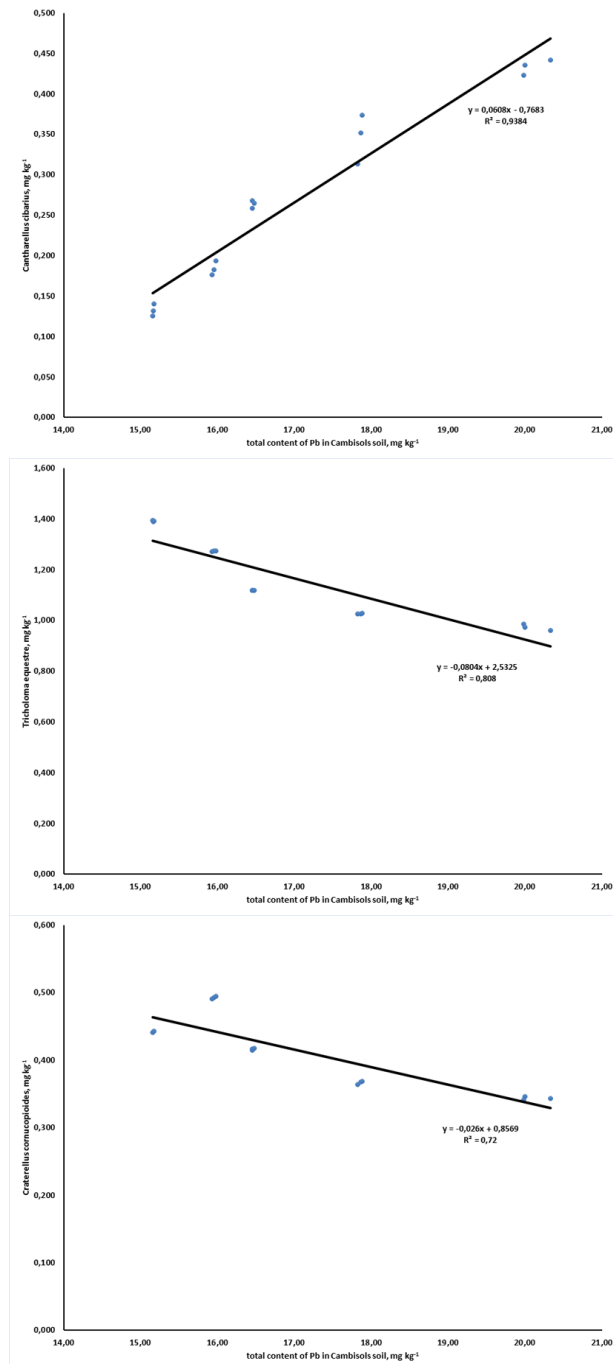
**Fig. 1.** Correlation between the total Pb content in Cambisols soil and Pb content in mushrooms
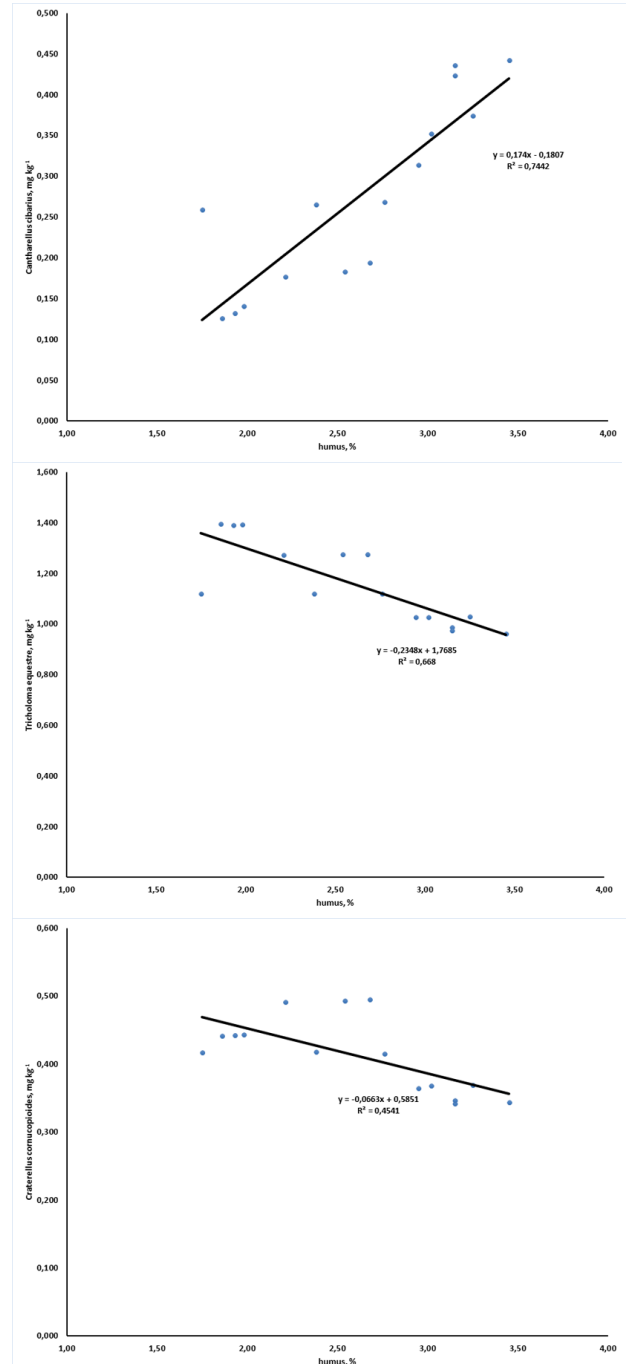


**Fig. 2.** Correlation between the Cambisols soil humus and Pb content in mushrooms
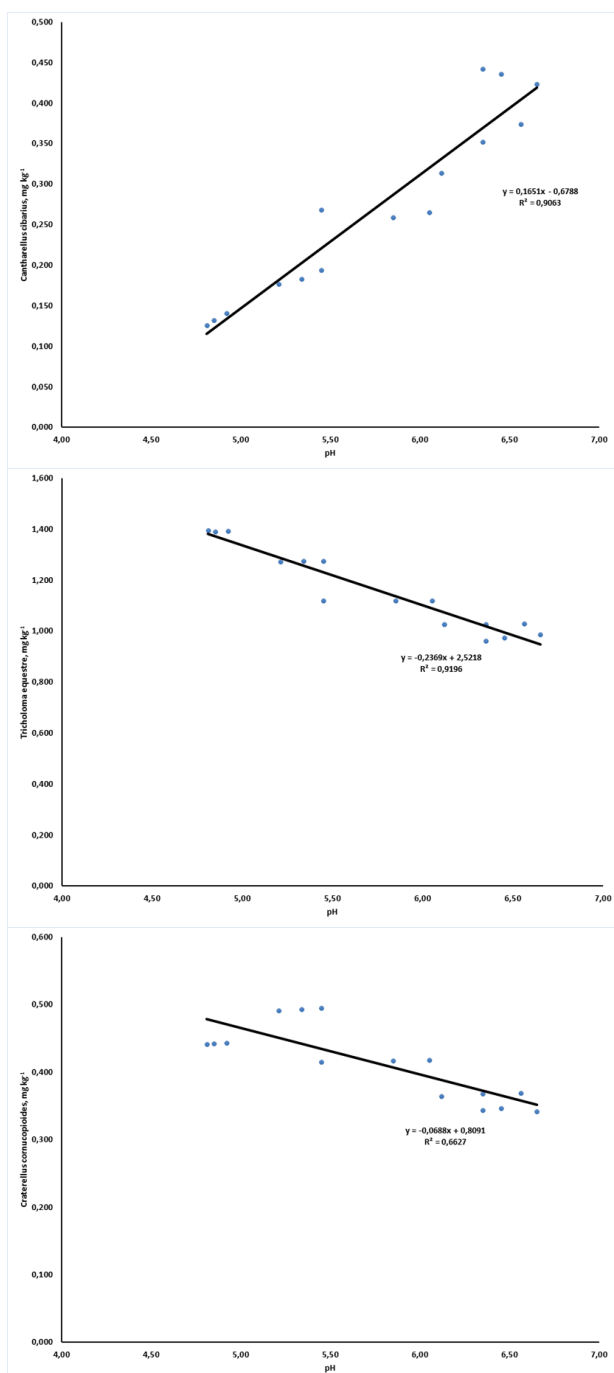
**Fig. 3.** Correlation between the Cambisols soil pH and Pb content in mushrooms

## CONCLUSION

A correlation/regression analysis was conducted between pH, humus, total content of lead in the Cambisols soil, and the concentration of these elements in the mushrooms. The results obtained show that:

• There are statistically significant dependencies determined between the Cambisols soil pH and lead concentration in the mushrooms. Pb concentration in the Cantharellus cibarius mushrooms increase linearly with the increase of the pH in the Cambisols soils. Pb concentration in the Tricholoma equestre and Craterellus cornucopioides mushrooms decrease linearly with the increase of the pH in the Cambisols soils.

• Pb concentration in the Cantharellus cibarius mushrooms increase linearly with the increase of the total element content in the Cambisols soils. Pb concentration in the Tricholoma equestre and Craterellus cornucopioides mushrooms decrease linearly with the increase of the total element content in the Cambisols soils.

• There are statistically significant dependencies determined between the Cambisols soil humus and lead concentration in the mushrooms. Pb concentration in the Cantharellus cibarius mushrooms increase linearly with the increase of the humus in the Cambisols soils. Pb concentration in the Tricholoma equestre and Craterellus cornucopioides mushrooms decrease linearly with the increase of the humus in the Cambisols soils.

From the obtained concentrations of heavy metals one can say that the locality Batak mauntain is ecologically clean area and very suitable for collecting wild edible mushrooms that we can use in our daily menu.

## REFERENCES

1. P. Kalač, *Food Chem*., **75**, 29 (2001).
2. P. Zaprjanova, L. Dospatliev, V. Angelova, K. Ivanov, *Environ Monit Assess*., **163**, 253 (2010).
3. L. Dospatliev, P. Zaprjanova, K. Ivanov, V. Angelova, *Bulg. J. Agric. Sci*., **20**, 1380 (2014).
4. J. Vetter, *Eur. Food Res. Technol*., **219**, 71 (2004).
5. L. Svoboda, B. Havlickova, P. Kalač, *Food Chem*., **96**, 580 (2006).
6. World Health Organization (WHO). Lead poisoning and health, 2014. http://www.who.int/mediacentre/factsheets/fs379/en/
7. P. Sharma, R.S. Dubey, *Braz. J. Plant. Physiol*., **17**, 35 (2005).
8. L. Dospatliev, M. Ivanova, *CR Acad Bulg Sci*, **70**, 795 (2017).
9. G. Flora, D. Gupta, A. Tiwari, *Interdiscip. Toxicol*., **5**, 47 (2012).
10. T. Totev, P. Gribachev, H. Nechev, N. Artinova, Soil science, Zemizdat, Sofia, 1987.
11. ISO 14869-1. Quality of the soils. Mineralization for determining the total content of elements. Part 1: Mineralization with fluoride hydrogen and perchloric acid. (2002).
12. E. Tanov, K. Lukanov, I. Miljanchev, P. Penchev, A. Andonov, A. Konarev, District-division, concentration and specialisation of tobacco-cultivation and tobacco-processing in Bulgaria, Hristo G. Danov, Plovdiv, 1978.
13. O. Isildak, I. Tukekul, M. Elmastas, H.Y. Aboulenein, *Anal. Lett*., **40**, 1099 (2007).

14. O. Adriana, B. Hudson, *J. of Environ. Monit.*, **6**, 36 (2004).
15. N. Evert, G.G. Fisher, Y. Thomassen, *J. of Environ. Monit.*, **1**, 1 (1999).
16. B.A. Brown, A.A. Brown, G.C. Lalor, *Environ. Geochem. Health*, **17**, 51 (1995).
17. A.M. Moir, I. Thornton, *Environ. Geochem. Health*, **11**, 113 (1989).
18. J.E. Ferguson, The Heavy Elements, Chemistry, Environmental Impact and Health Effects, London: Pergamon Press, 1990, p. 614.
19. L. Dospatliev, M. Ivanova, *Bulg. Chem. Commun.*, **49**, G, 5 (2017).
20. Commission Regulation (EC) 1881/2006. Setting maximum levels for certain contaminants in foodstuffs.
21. A. Brzostowski, J. Falandysz, G. Jarzynska, Z. Dan, *J. Environ. Sci. Health*. A, **46**, 378 (2012).
22. A. Chojnacka, M. Drewnowska, G. Jarzynska, I.C. Nnorom, J. Falandysz, *J. Environ. Sci. Health*. A, **47**, 2094 (2012).
23. J. Falandysz, A. Mazur, A.K. Kojta, G. Jarzynska, M. Drewnowska, A. Dryzalowska, I.C. Nnorom, *J. Sci. Food Agric.*, **93**, 853 (2012).
24. M. Aloupi, G. Koutrotsios, M. Koulousaris, N. Kalogeropoulos, *Ecotoxicol. Environ. Saf.*, **78**, 184 (2012).
25. M. Gucia, G. Jarzynska, A. Kojta, J. Falandysz, *J. Environ. Sci. Health*. B, **47**, 81, (2012).
26. M.A. Garcia, J. Alonso, M.J. Melgar, *Food Chem. Toxicol.*, **58**, 249 (2013).
27. S.S. Petkovšek, B. Pokorny, *Sci. Total Environ.*, **443**, 944 (2013).
28. I. Širić, I. Kos, D. Bedeković, A. Kaić, A. Kasap, *Period. Boil.*, **116**, 319 (2014).
29. J. Falandysz, M. Drewnowska, *J. Environ. Sci. Health*. B, **50**, 374 (2015).
30. G. Toncheva, K. Gavazov, Z. Georgieva, L. Dospatliev, A. Peltekov, B. Boyanov, *Bull. Chem. Soc. Ethiop.*, **30**, 325 (2016).
31. M. Saba, J. Falandysz, I.C. Nnorom, *Environ. Sci. Pollut. Res.*, **23**, 2749 (2016).
32. V. Stefanović, J. Trifković, J. Mutić, Ž. Tešić, *Environ. Sci. Pollut. Res.*, **23**, 13178 (2016).
33. L. Dospatliev, M. Ivanova, *Oxid. Commun.*, **40**, 993 (2017).

# A cloud-point extraction-chromogenic system for copper(II) based on 1-(2-thiazolylazo)-2-naphthol

T. S. Stefanova-Bahchevanska[1], R. S. Ahmedov[1], S. Zaruba[2], V. Andruch[3],
V. B. Delchev[1], L. K. Dospatliev[4], K. B. Gavazov[1,5*]

*[1]University of Plovdiv Paisii Hilendarski, Plovdiv, Bulgaria;*
*[2]Oles Honchar Dnipropetrovsk National University, Dnipro, Ukraine;*
*[3]Pavol Jozef Šafárik University in Košice, Košice, Slovak Republic;*
*[4]Trakia University, Stara Zagora, Bulgaria; [5]Medical University of Plovdiv, Plovdiv, Bulgaria*

A cloud point extraction-chromogenic system, containing Cu$^{II}$, 1-(2-thiazolylazo)-2-naphthol (TAN), and Triton X-100 (TX) was investigated. The optimum conditions for Cu$^{II}$ extraction and spectrophotometric determination were found: absorption maximum (565 nm), concentration of TAN ($4 \times 10^{-5}$ M), mass fraction of TX (2.5%), pH (6.0), and incubation time (65 min). The molar absorptivity, limit of detection, linear working range, and fraction extracted were $2.9 \times 10^5$ dm$^3$ mol$^{-1}$ cm$^{-1}$, 2.2 ng cm$^{-3}$, 7.2 – 380 ng cm$^{-3}$ and 91%, respectively. The composition of the extracted complex is 1:2 (Cu:TAN). Its structure was optimized at the BLYP/aug-cc-pVDZ level of theory. The electron spectrum of the compound was simulated using Lorentzian band shape and compared with the experimental one.

**Keywords:** Cloud Point Extraction, Copper(II), Azo Dye, Spectrophotometry, TDDFT calculations, CPE

## INTRODUCTION

Copper is a first row transition element from Group 11 with average content in the Earth's crust of 50 ppm [1]. It is a soft, malleable, and ductile metal with high electrical and thermal conductivity. Two early periods of the human history – Copper Age and Bronze Age – are closely related to this element. Nowadays, copper is considered as one of the most widely produced metals [2]. It is broadly used in electrical equipment and appliances, electrical transmission and communication wires, roofing and plumbing, industrial machinery, coins, pigments, micronutrients, etc. [1, 2].

Copper is an essential trace element to living organisms that performs a number of fundamental physiological functions. In humans, copper is the third most abundant trace element (after iron and zinc). Copper deficiency can cause anaemia, neutropenia, osteoporosis, hypopigmentation, increased incidence of infections, hyperthyroidism, and abnormalities in glucose and cholesterol metabolism. Because of difficulties in establishing the recommended dietary intake of copper, the National Research Council [3] has published a safe range in adults of 1.5–3 mg day$^{-1}$. At higher levels copper can be toxic [4].

Various methods have been used for copper determination. Sample preparation approaches which can improve significantly the characteristics of the determination are the extraction and microextraction techniques, such as liquid-liquid extraction (LLE) [5-7], solid phase extraction (SPE) [8-10], suspended droplet solvent microextraction (SDSME) [11], homogeneous liquid-liquid microextraction (HLLME) [12], dispersive liquid-liquid microextraction (DLLME) [13,14], and cloud point extraction (CPE) [15-23].

CPE is a modern alternative of LLE [24] which is consistent with the principles of "Green Analytical Chemistry" [25, 26]. It was introduced for the first time by Watanabe and Tanaka in 1978 [27] and a lot of scientists are oriented today towards its application for copper analysis [24]. A prerequisite for successful implementation of CPE is relatively high hydrophobicity of the analyte. That is why it is necessary to convert it into hydrophobic form, e.g. by complexation with chelating organic ligands. When using azo dyes as chelating reagents [24, 28], it is possible CPE to be combined with spectrophotometry – a simple and sensitive analytical method, which does not require expensive equipment and is therefore preferred in many laboratories [6].

The aim of this work was to investigate the CPE-chromogenic system for copper(II) containing 1-(2-thiazolylazo)-2-naphthol (TAN), acetate buffer, and Triton X-100 – a non-ionic surfactant with higher and more convenient in some aspects cloud-point temperature than the most utilized Triton X-114 [24, 29]. In addition, we used TD DFT calculations to optimise the structure of the extracted complex, to find its vertical excitation energies and simulate an electron spectrum for

---

direct comparison with the experimental one. Such calculations can be of help to better understand the system behaviour. Moreover, they have the potential to allow researchers to reduce the number of experiments on the selection of dyes and to predict in which direction the synthesis of new analytical reagents should be moved.

## EXPERIMENTAL

### *Reagents and chemicals*

A stock solution containing $2 \times 10^{-2}$ M of $Cu^{II}$ was prepared by dissolving $CuSO_4 \cdot 5H_2O$ (Sigma-Aldrich, Schnelldorf, Germany, purum p.a.) in water and standardizing by EDTA titration [7]. The working $Cu^{II}$ solution ($2 \times 10^{-4}$ M) was prepared by suitably diluting with water. The ligand TAN (Fluka AG, Buchs, Switzerland, puriss. p.a.) was dissolved in ethanol, $c_{TAN} = 2 \times 10^{-3}$ M. Acetate buffer solutions were prepared by mixing 0.1 M aqueous solutions of $CH_3COONa$ and $CH_3COOH$ at appropriate ratios. Triton X-100 (electrophoresis grade) was purchased from Fisher Scientific, USA; 14% intermediate aqueous solutions of this reagent were prepared. Doubly distilled water was used through the work.

### *Instrumentation*

A Camspec M508 spectrophotometer (United Kingdom), equipped with 0.5 and 1.0 cm path-length cells, was used for the spectrophotometric measurements. CPE was carried out in a home-made thermostated water bath heated on a ceramic heater Diplomat DPL CS-H20A9 (Bulgaria). The weighing was made with an electronic analytical balance (Kern, ABJ, Germany). A HANNA HI-83141 pH meter (Romania) was used for pH measurements.

### *Procedure for establishing the optimum CPE-spectrophotometric conditions*

Various amounts of Triton X-100 solution (14%; 2 – 14 g), $Cu^{II}$ working solution (0.1 – 2.5 cm³), buffer solution (3.0 cm³; pH ranging from 3.8 to 6.7), and TAN solution (0.05 – 1.8 cm³) were placed into 50 cm³ centrifuge test tubes. The solution volume was made to 50 cm³ with water. Then the test tubes were heated above the cloud point temperature (*ca.* 65°C) in 85°C water bath for 15-105 min. After the heating, the samples were

cooled in a freezer for 45 min (at −20°C) and the upper aqueous layers were decanted by inverting the tubes [30, 31]. Water was added to the viscous surfactant-rich phases to a total mass of 5 g and the mixtures were carefully heated for homogenization. Aliquot of the obtained solutions was transferred into the spectrophotometer cell and the absorbance was read against corresponding blank test.

### *Calculations*

The ground-state equilibrium geometry of the copper complex was optimized at the BLYP level of theory and cc-pVDZ basis functions with no symmetry and geometry restrictions. Subsequently at the same level the vertical excitation energies of the compound were calculated. GAUSSIAN 03 program package [32] was used. Visualization of the optimized structure was done with the ChemCraft software [33].

## RESULTS AND DISCUSSION

### *CPE-spectrophotometric optimisation*

Wada and Nakagawa [34] investigated some o-(2-thiazolylazo)-phenol derivatives as metal indicators for copper. They found that TAN forms $CuL^+$ chelate with an absorption maximum at 578 nm and a stability constant of $10^{11.9}$. However, our CPE experiments showed that the absorption maximum position depends on the TAN concentration in the aqueous phase. At low TAN concentrations, the maximum is close to that previously reported [34] (Fig. 1, curve 2). On the other hand, at $c_{TAN} > c_{Cu(II)}$ there is a tendency the maximum to be shifted hypsochromically (by 10-20 nm) and split by a narrow minimum (at *ca.* 562 nm; Fig. 1, curve 1) which could be attributed to a change in the complex composition. This gave us an idea to examine this phenomenon in more detail.

Our further optimisation experiments included the following steps: (i) choice of the TAN concentration; (ii) choice of pH of the aqueous phase; (iii) choice of the Triton X-100 mass fraction; and (iv) choice of the incubation time. To achieve reliable optimisation, these steps were repeated. The final step optimisation results are shown in Figs. 1 – 3 and the recommended optimum conditions are summarized in the Table 1.

**Table 1.** CPE-spectrophotometric optimization of the $Cu^{II}$ – TAN – Triton X-100 system

| Parameter | Optimization range | Optimal value | Figure |
|---|---|---|---|
| Wavelength, nm | Visible region | 565 | Fig. 1 |
| Concentration of TAN, M | $(0.2 - 7.2) \times 10^{-5}$ | $4.0 \times 10^{-5}$ | Fig. 2 |
| pH of the aqueous phase | 3.8 – 6.7 | 6.0 | Fig. 3 |
| Incubation time, min. | 15 – 105 | 65 | – |
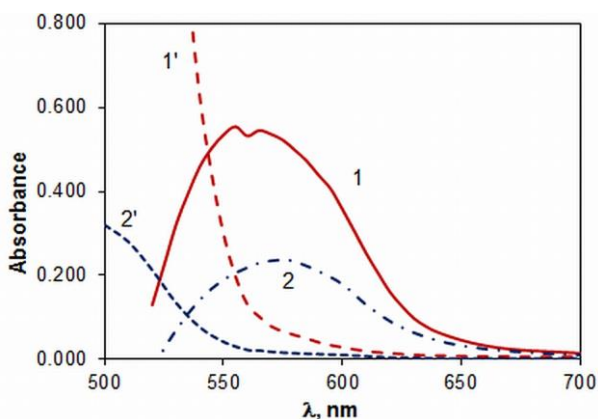
**Fig. 1.** Absorption spectra: (1 and 2) Cu-TAN against blank; and (1' and 2') corresponding blanks against water. Conditions: $c_{Cu(II)} = 4 \times 10^{-6}$ M, pH = 6.0, $w_{triton} = 2.5\%$, $l = 0.5$ cm. $c_{TAN} = 4.0 \times 10^{-5}$ M (1 and 1') or $4.0 \times 10^{-6}$ M (2 and 2').
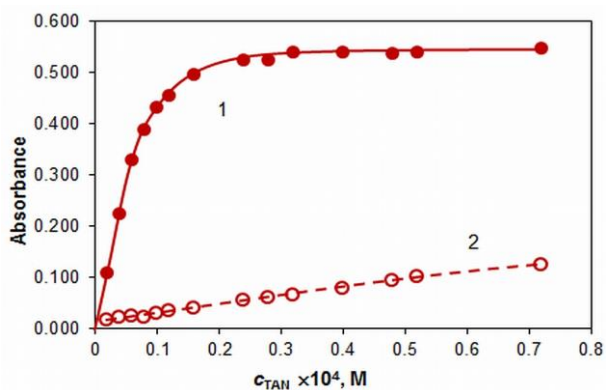


**Fig. 2.** Absorbance of the extracted complex (1) and blank (2) vs concentration of TAN. $c_{Cu(II)} = 4 \times 10^{-6}$ M, pH = 6.0, $w_{triton} = 2.5\%$, $\lambda = 565$ nm, $l = 0.5$ cm.
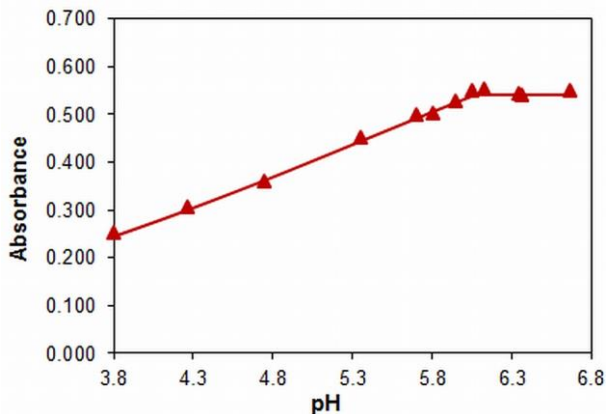


**Fig. 3.** Absorbance of the extracted complex vs pH. $c_{Cu(II)} = 4 \times 10^{-6}$ M, $c_{TAN} = 4 \times 10^{-5}$ M, $w_{triton} = 2.5\%$, $\lambda = 565$ nm, $l = 0.5$ cm.

*Complex composition*

The molar TAN:$Cu^{II}$ ratio was determined by several methods [35] based on the saturation curve presented in Fig. 2, namely the equilibrium shift method (Fig. 4, line 2), Bent-French method (Fig. 4, line 1), straight-line method of Asmus (Fig. 5), and molar ratio method (Fig. 6). Based on the

40

obtained results, we can make the following conclusions: i) 2:1 (TAN:$Cu^{II}$) complex is extracted when $c_{TAN} > c_{Cu(II)}$; and ii) 1:1 complex is co-extracted when TAN concentration is very low ($c_{TAN} < c_{Cu(II)}$).
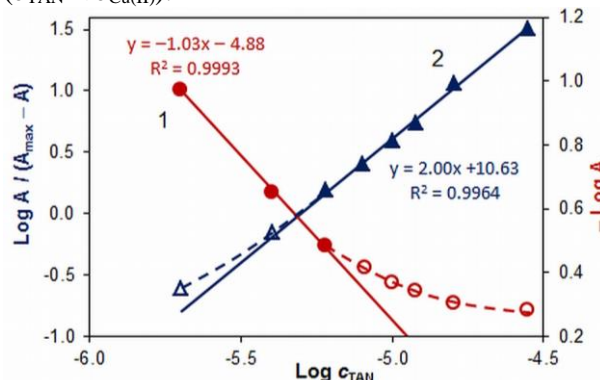


**Fig. 4.** Determination of TAN-to-$Cu^{II}$ molar ratio by the Bent-French method (straight line 1; right ordinate) and the equilibrium shift method (straight line 2; left ordinate).
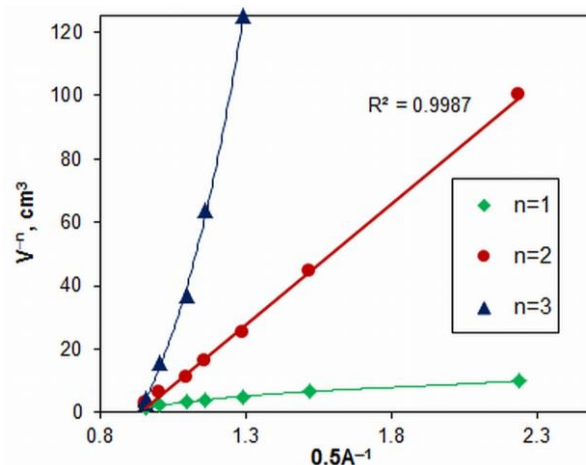


**Fig. 5.** Determination of TAN-to-$Cu^{II}$ molar ratio by the straight-line method of Asmus.
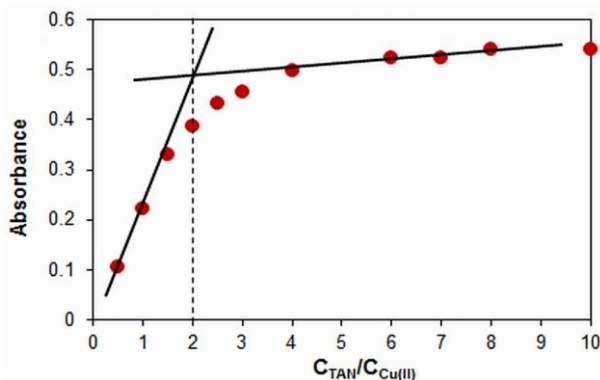


**Fig. 6.** Determination of TAN-to-$Cu^{II}$ molar ratio by the molar ratio method.

Consequently there is a difference in the complex composition in aqueous medium (1:1, reported by Wada and Nakagawa [34]) and in surfactant-rich phase (2:1, at the optimum

conditions reported in this work). Similar differences have been reported by our group for the liquid-liquid extraction of coordination compounds containing azo dyes [31]. However, there are still not enough comparisons from this type (aqueous phase – surfactant-rich phase) for CPE. Generally speaking, authors aimed at developing analytical methodologies often neglect the possible change in the complex composition after CPE.

### Extraction equation and equilibrium constant

The following equation could be proposed for the CPE process under the optimum conditions.

$$Cu^{II}_{(aq)} + 2HTAN_{(aq)} \Leftrightarrow [Cu^{II}(TAN^-)_2]_{(srp)} + 2H^+_{(aq)}$$

In this equation aq means aqueous phase, srp means surfactant rich phase, and HTAN is the protonated form of TAN (which dominates at $pH_{opt}$ [24]). The equilibrium constant characterizing this equation was calculated by two methods: Holme-Langmyhr method [36] (Log $K$ = 11.6 ± 0.4; N = 9) and Harvey-Manning method [37] (Log $K$ = 11.7 ± 0.2; N = 3). As can be seen, the results are statistically indistinguishable.

### Analytical characteristics

A calibration graph was constructed to estimate the applicability of the investigated CPE-chromogenic system for determination of $Cu^{II}$. Table 2 summarizes the obtained analytical characteristics. The fraction extracted (*E*) was calculated by comparing the absorbance values at the optimum conditions for single and triple extractions. The relatively high value for this type of extraction (*E*% = 91 ± 1; N = 3) could be attributed to (i) high stability of the resulting complex; and (ii) high hydrophobicity due to the incorporation of two moles of the reagent in the coordination entity.

**Table 2.** Statistical analysis of the calibration graph

| Parameter | Value |
|---|---|
| Apparent molar absorptivity ($\varepsilon$), dm$^3$ mol$^{-1}$ cm$^{-1}$ | $2.9 \times 10^5$ |
| Linear calibration range, ng cm$^{-3}$ | up to 380 |
| Slope ± Standard deviation, $A$ $\mu$g$^{-1}$ cm$^3$ | 2.13±0.02 |
| Intercept ± Standard deviation, $A$ | 0.010±0.005 |
| Correlation coefficient | 0.9995 [a] |
| Limit of detection (LOD), ng cm$^{-3}$ | 2.2 [b] |
| Limit of quantification (LOQ), ng cm$^{-3}$ | 7.2 [b] |

[a] nine standards used

[b] Defined as $3\sigma_{blank}$/b (LOD) or $10\sigma_{blank}$/b (LOQ), where b is the slope of the calibration plot

### Optimized ground-state equilibrium geometry

The optimized structure of the copper complex is shown in Fig. 7. It shows two almost perpendicular one to other planar TAN$^-$ anions: <C4N1CuN6 = C17N4CuN3 = 90.6°. They are bonded with the oxygen and nitrogen (N1, N3, N4, and N6) atoms to the central Cu$^{II}$ ion. The bonding leads to the formation of a coordination compound with a structure of non-regular octahedron. Due to the structural characteristics of the ligand and the strong repulsion of the lone electron pairs of the oxygen and nitrogen atoms, two of the coordination bonds are longer than the remaining: N6-Cu = 2.321 Å and N3-Cu = 2.313 Å. The angles N1CuN4, O2CuN6, and O1CuN3 are as follows: 177.2°, 153.8°, and 153.9°.
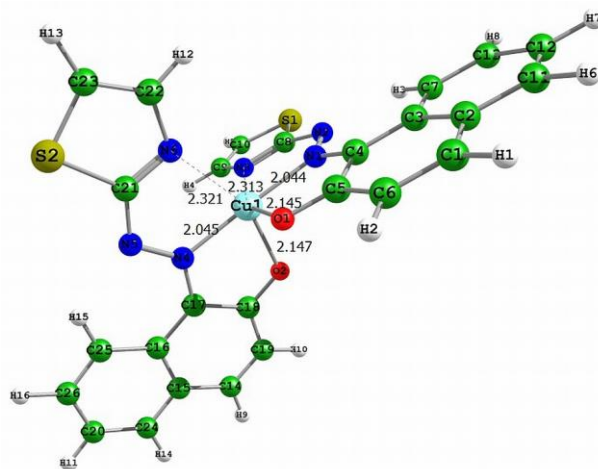


**Fig. 7.** Optimized structure of the copper complex at the BLYP/cc-pVDZ level of theory.

### Theoretical spectrum

A theoretical spectrum of the complex in the visible range was modeled by the calculated electron transition lines and a Lorentzian broadening of the bands. When comparing it with the experimental spectrum one must take into account the following points: (i) the comparison makes sense only in the spectral range over *ca.* 520 nm as TAN (which is taken in excess under the experimental conditions) absorbs significantly at lower wavelengths; (ii) this effect cannot be compensated by reducing the concentration of ligand in the solution because the complex composition will be different (1:1); (iii) the experimental spectrum is registered in the solution (srf), while the theoretical one refers to the gas phase.

In Fig. 8 are compared the experimental spectrum (dotted line) and the theoretical spectrum (full line) of the compound normalized by unity. No scaling factor is required and it can be assumed that the overlap is satisfactory. The calculated main

absorption maximum involves the MOs shown in Fig. 9.

The molecular orbitals involved in the second most intensive peak at 486 nm are 139β and the one illustrated in Fig. 10. As seen, this molecular orbital is of π* type. In other words the electron transition 139β → 147β is a typical ligand field transition. The electron density shifts from the central metal ion towards the ligands.
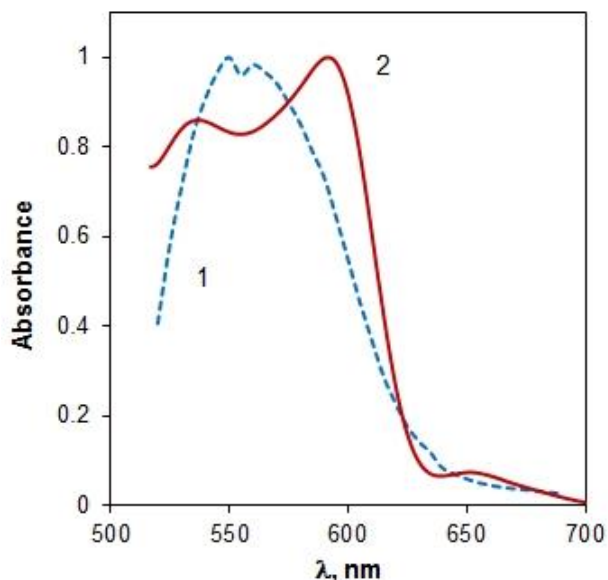


**Fig. 8.** Experimental (curve 1) and theoretical (curve 2) absorption spectra.



139β MO



146β MO
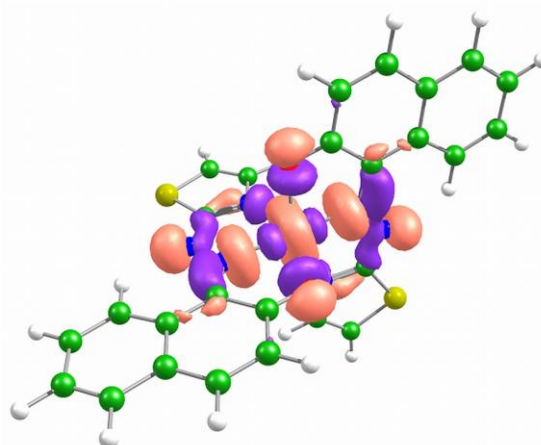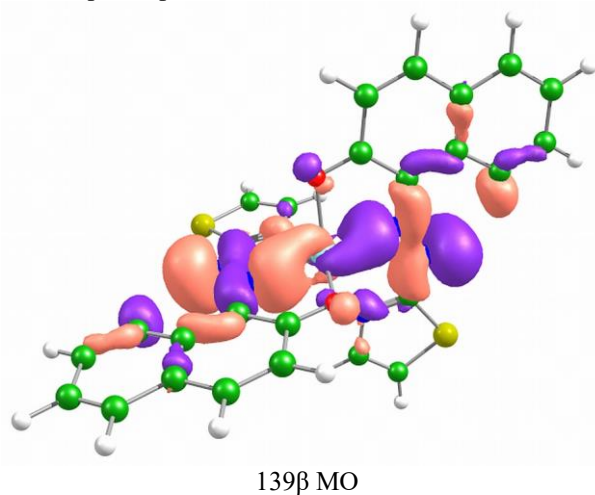
**Fig. 9.** MOs involved in the electron transition responsible for the theoretically main absorption peak (oscillator strength f=0.1388).



147β MO
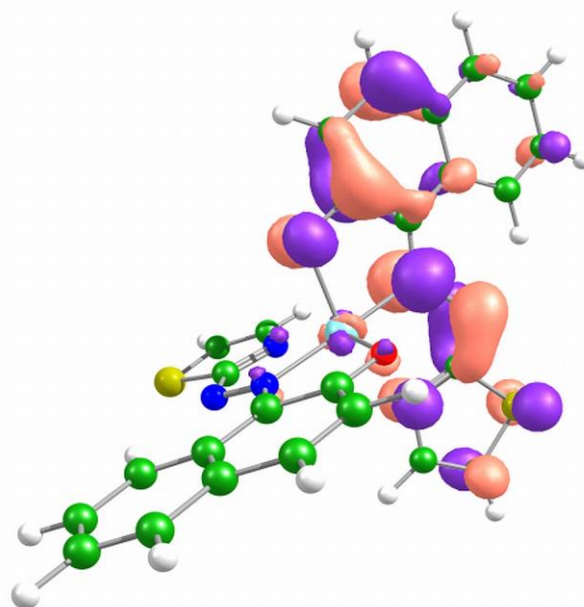
**Fig. 10.** MO involved in the electron transition 139β → 147β (oscillator strength f = 0.1202).

CONCLUSION

The cloud point extraction-chromogenic system $Cu^{II}$ –TAN – TX was investigated in details and the optimum experimental conditions and analytical characteristics were found. The composition of the extracted complex was determined to be Cu:TAN = 1:2. Its structure was optimized and analyzed using the TD DFT method. An electron spectrum of the complex was simulated. The satisfactory fit between this spectrum and the experimental one is an indication for the correctness of the proposed structure.

## REFERENCES

1. J. Emsley, Nature's building blocks: an AZ guide to the elements, Oxford University Press, New York, 2011.
2. A. Potysz, E. D. van Hullebusch, J. Kierczak, M. Grybos, P. N. L. Lens, G. Guibaud, *Crit. Rev. Environ. Sci. Technol.* **45**, 2424 (2015).
3. https://www.nap.edu/read/1349/chapter/11#227.
4. M. Araya, M. C. McGoldrick, L. M. Klevay, J. Strain, P. Robson, F. Nielsen, M. Olivares, F. Pizarro, L. Johnson, K. A. Poirier, *Reg. Toxicol. Pharmacol.* **34**, 137 (2001).
5. M. Thakur, M. K. Deb, *Talanta*, **49**, 561 (1999).
6. Z. Marczenko, M. Balcerzak, Metod'y spektrofotometrii v UF i vidimoj oblastyakh v neorganicheskom analize, Binom. Laboratoriya znanij, Moscow, 2007.
7. I. S. Balogh, M. Ruschak, V. Andruch, Y. Bazeľ, *Talanta*, **76**, 111 (2008).
8. A. Tobiasz, S. Walas, *Trends Anal. Chem.*, **62**, 106 (2014).
9. Ş. Tokalioğlu, V. Yilmaz, Ş. Kartal, *Environ. Monit. Assess.* **152**, 369 (2009).
10. A. Samadi, M. Amjadi, *Microchim. Acta*, **182**, 257 (2015).
11. N. Goudarzi, M. A. Chamjangali, E. Vatankhahan, A. Amin, *J. Anal. Chem.*, **69**, 1061 (2014).
12. N. Khorshidi, A. Niazi, *Separ. Sci. Technol.*, **51**, 1675 (2016).
13. A. Niazi, S. Habibi, M. Ramezani, *Arab. J. Chem.*, **8**, 706 (2015).
14. Z. Li, G. Yu, J. Song, Q. Wang, M. Liu, Y. Yang, *Water Sci. Technol.*, **67**, 247 (2013).
15. H. S. Ferreira, A. C. Santos, L. A. Portugal, A. C. Costa, M. Miró, S. L. Ferreira, *Talanta*, **77**, 73 (2008).
16. A. Pérez-Gramatges, A. Chatt, *J. Radioanal. Nucl. Chem.*, **294**, 163 (2012).
17. A.-N. Tang, D.-Q. Jiang, X.-P. Yan, *Anal. Chim. Acta*, **507**, 199 (2004).
18. E. L. Silva, P. dos Santos Roldan, M. F. Giné, *J. Hazard. Mater.*, **171**, 1133 (2009).
19. V. A. Lemos, M. S. Santos, G. T. David, M. V. Maciel, M. de Almeida Bezerra, J. Hazard. Mater., **159**, 245 (2008).
20. V. A. Lemos, M. S. Santos, M. J. S. dos Santos, D. R. Vieira, C. G. Novaes, *Microchim. Acta*, **157**, 215 (2007).
21. J. Chen, T. Khay Chuan, *Anal. Chim. Acta*, **450**, 215 (2001).
22. S. G. Silva, P. V. Oliveira, F. R. Rocha, *J. Brazil. Chem. Soc.* **21**, 234 (2010).
23. E. K. Yetimoğlu, O. A. Urucu, Z. Y. Gündüz, H. Filik, *Anal. Lett.*, **43**, 1846 (2010).
24. K. Pytlakowska, V. Kozik, M. Dabioch, *Talanta*, **110**, 202 (2013).
25. L. H. Keith, L. U. Gron, J. L. Young, *Chem. Rev.*, **107**, 2695 (2007).
26. P. T. Anastas, *Crit. Rev. Anal. Chem.* **29**, 167 (1999).
27. H. Watanabe, H. Tanaka, *Talanta*, **25**, 585 (1978).
28. V. A. Lemos, E. S. Santos, M. S. Santos, R. T. Yamaki, *Microchim. Acta*, **158**, 189 (2007).
29. W. L. Hinze, E. Pramauro, *Crit. Rev. Anal. Chem.*, **24**, 133 (1993).
30. K. Simitchiev, V. Stefanova, V. Kmetov, G. Andreev, N. Kovachev, A. Canals. *J. Anal. At. Spectrom.*, **23**, 717 (2008).
31. T. S. Stefanova, K. K. Simitchiev, K. B. Gavazov, *Chem. Pap.*, **69**, 495 (2015).
32. M. J. Frisch, et al., Gaussian 03; Gaussian, Inc.: Wallingford CT, 2004.
33. G. A. Zhurko, D. A. Zhurko, Chemcraft, ver.1.7 (build 382).
34. H. Wada, G. Nakagawa, *Bunseki Kagaku*, **14**, 28 (1965).
35. M. I. Bulatov, I. P. Kalinkin, Prakticheskoe rukovodstvo po fotokolorimetricheskim i spektrofotometricheskim metodam analiza, Khimiya, Leningrad, 1986.
36. A. Holme, F. J. Langmyhr, *Anal. Chim. Acta*, **36**, 383 (1966).
37. A. E. Harvey, D. L. Manning, *J. Am. Chem. Soc.*, **72**, 4488 (1950).

# Molecular docking experiments of cannabinoid receptor

F. I. Sapundzhi[1*], T. A. Dzimbova[2], N. S. Pencheva[1], P. B. Milanov[1,3]

*[1]South-West University Neofit Rilski, 2790 Blagoevgrad, Bulgaria*
*[2]Institute of Molecular Biology, Bulgarian Academy of Sciences, 1113 Sofia, Bulgaria,*
*[3]Institute of Mathematics and Informatics, Bulgarian Academy of Sciences, 1113 Sofia, Bulgaria*

The cannabinoid receptor is a part of the endocannabinoid signaling system. CB1 is a therapeutic drug target, and its structure and conformational changes after ligand binding are of great interest. The present study aimed to investigate the interaction between the crystal structure of the human cannabinoid (CB1) receptor (PDB id:5TGZ) and several known cannabinoid ligands in order to determine the structure-activity relationship by using molecular docking with software GOLD 5.2. Four scoring functions provided with GOLD 5.2 were used for molecular docking between the crystal structure of CB1 receptor and the cannabinoid ligands. The obtained results could be used further for *in silico* experiments of the cannabinoid receptor-ligand interactions.

**Keywords:** Cannabinoid receptors, CB1, Molecular docking experiments, Ligand-receptor interactions, Structure-activity relationship

## INTRODUCTION

Human cannabinoid receptor type 1 (CB1) is a part of the class G-protein coupled receptors (GPCRs) that represent the largest membrane protein family and are of great pharmacological importance. It is a therapeutically useful target involved in a different physiological process such as pain, metabolic regulation, craving, anxiety, etc. [1,2]. The drugs target cannabinoid receptors for the treatment of chemotherapy-induced nausea and vomiting, relieving neuropathic pain, etc. [3]. Nowadays, drugs targeting CB1 receptor are constantly being developed [4-6].

The agonists of the cannabinoid receptor can be divided into four structurally distinct classes of compounds. These include classical cannabinoids (like $\Delta$-[9]-THC), non-classical cannabinoids, represented by CP55940, aminoalkylindoles, such as WIN55212-2, and endogenous cannabinoids such as anandamide (AEA) [7]. In the present study we use known cannabinoid ligands with established binding affinity and selectivity from literature [8].

The knowledge of the 3D structure of the cannabinoid receptors could be useful in the task of understanding their function and in the design of specific ligands. Therefore, many biochemical, pharmacological, and computational studies have been carried out on cannabinoid receptors.

The crystal structure of the CB1 receptor was determined in RCSB (PDBid: 5TGZ) [9,10]. This is very helpful for the computational modeling of structure-activity relationships between the receptor and its ligands.

The present research aimed to study the interaction between the CB1 receptor (PDB id:5TGZ) [10] and several known cannabinoid ligands in order to determine the structure-activity relationship by using molecular docking with software GOLD 5.2 [11]. Four scoring functions provided in the software were used for molecular docking experiments [11-14].

## MATERIALS AND METHODS

### *Cannabinoids used in the present work*

### *Receptor*

The crystal structure of the CB1 receptor published in RCSB Protein Data Base (PDB id: 5TGZ, www.rcsb.org) was used [9,10]. It was obtained by X-ray diffraction with 2.8 Å resolution. Length: 452 amino acids.

The CB1 receptor belongs to the Class A of rhodopsin class GPCRs. It has been proposed that there exists a hydrophobic binding pocket that interacts with the alkyl chain of classical and non-classical cannabinoids. One of the important points is Asp 366 residue where the polar parts of the ligands bind [15].

### *Computational tools*

Ligand preparation was done with software Avogadro (an open-source molecular builder and visualization tool - Version 1.0.3) [16]. Image generation and interaction studies were done after docking with Molegro Molecular Viewer (MMV) [17]. A GraphPad Prism 3.0 was used for the correlations [18-25].

---

* To whom all correspondence should be sent.
E-mail: sapundzhi@swu.bg

**Table 1**. Structure, affinity and efficacy of the ligands of CB1

| Structure | Ligands | Efficacy towards CB1 |
|---|---|---|
|  | Anandamide | Full agonist |
|  | N-Arachidonoyl dopamine | Agonist |
|  | 2-Arachidonoylglycerol | Full Agonist |
|  | Δ-$^9$-Tetrahydrocannabinol | Partial Agonist |
|  | EGCG (Epigallocatechin gallate) | Agonist |
|  | Yangonin | - |
|  | UR-144 | Full Agonist |
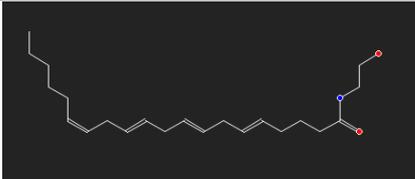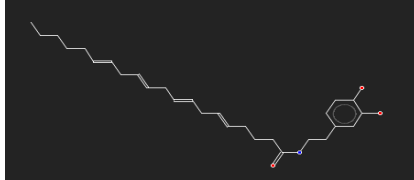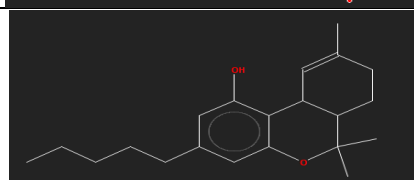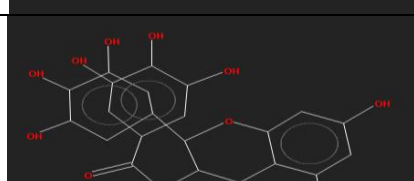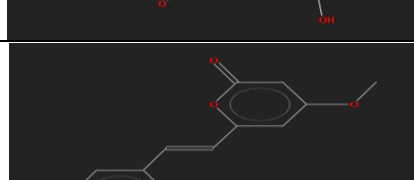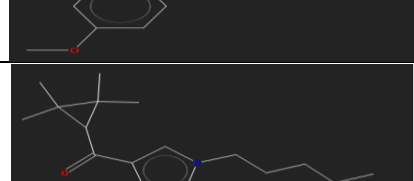
### *Docking of the cannabinoids*

Docking studies were performed by using GOLD 5.2 (Genetic Optimization for Ligand Docking) [11], run on Scientific LINUX 5.5 operating system. It uses a genetic algorithm and considers full ligand conformational flexibility and partial protein flexibility. The active center of the receptor was determined using substrate position in the crystal structure obtained from RCSB [9,10]. Four scoring functions of GOLD 5.2 (ChemScore, ChemPLP, GoldScore, and ASP) were used in order to determine the best algorithm for docking of this class of compounds [11-14]. The conformations of the compounds with the best values of the scoring functions were selected.

### RESULTS AND DISCUSSION

Molecular docking was performed with the CB1 receptor (PDB id: 5TGZ) and the ligands from literature [8] (Table 1). The scoring functions embedded in GOLD 5.2 were used. The obtained results of the molecular docking are presented in the Table 2.

**Table 2.** CB1 receptor affinity and scoring functions values of the ligands.

| Ligands | Affinity, CB$_1$ | ASP score | Goldscore | ChemPLP | ChemScore |
|---|---|---|---|---|---|
| Anandamide | 78 nM | 20.28 | 49.82 | 56.92 | 20.43 |
| N-Arachidonyl dopamine | - | 21.62 | 55.64 | 64.8 | 22.76 |
| 2-Arachidonylglycerol | - | 18.74 | 56.54 | 59.34 | 16.4 |
| Δ-9-Tetrahydrocannabinol | 10 nM | 25.9 | 41.61 | 44.48 | 9.16 |
| EGCG (Epigallocatechin gallate) | 33.6 μM | 22.27 | 39.30 | 53.88 | 25.82 |
| Yangonin | 0.72 μM | 19.06 | 38.63 | 47.03 | 19.23 |
| UR-144 | 150 nM | 20.56 | 32.29 | 44.56 | 19.82 |

Correlations of data from molecular docking and affinity of the cannabinoid ligands were performed with GraphPad Prism 3.0 [18]. When the results were analysed we found correlation between the docking results (the values of all four scoring functions available in GOLD 5.2) and the values of affinity of cannabinoid ligands. The correlation between these data was assessed by the Pearson's correlation coefficient [18] (Table 3).The correlation coefficients for ASP and ChemScore scoring functions are with higher values, but for ASP scoring function it is positive and for ChemScore scoring function it is negative.When the correlation coefficient of Pearson is positive higher affinity corresponds to higher scoring function value, when the Pearson's correlation coefficient is negative

higher affinity corresponds to lower scoring function value. Only the first correlation has biological meaning because the value of the scoring function shows how the ligand binds to the crystal structure of the CB1 receptor. As higher is that value the binding is better.

Shim *et al.* [15] proposed that there exists a hydrophobic binding pocket that interacts with the alkyl chain of the classical and non-classical cannabinoids. He showed that docking is more effective when the polar residue from the receptor sequence was chosen. In our case this residue is Asp366. All of the ligands bind near this residue mainly interacting with the nonpolar residues around but forming hidrogen bonds with their hydroxyl groups and Lys370 from the receptor sequence.

**Table 3.** Pearson's correlation coefficients for the crystal structure of CB1 and different scoring functions of GOLD 5.2.

| Scoring functions | Values of Pearson's correlation coefficient |
|---|---|
| ASP score | Pearson R = 0,8815, $P_{value}$ =0,0202 |
| ChemPLP | Pearson R = -0,5056, $P_{value}$ = 0,3063 |
| ChemScore | Pearson R = -0,8313, $P_{value}$ = 0,0403 |
| GoldScore | Pearson R = -0,09325, $P_{value}$ = 0,8605 |
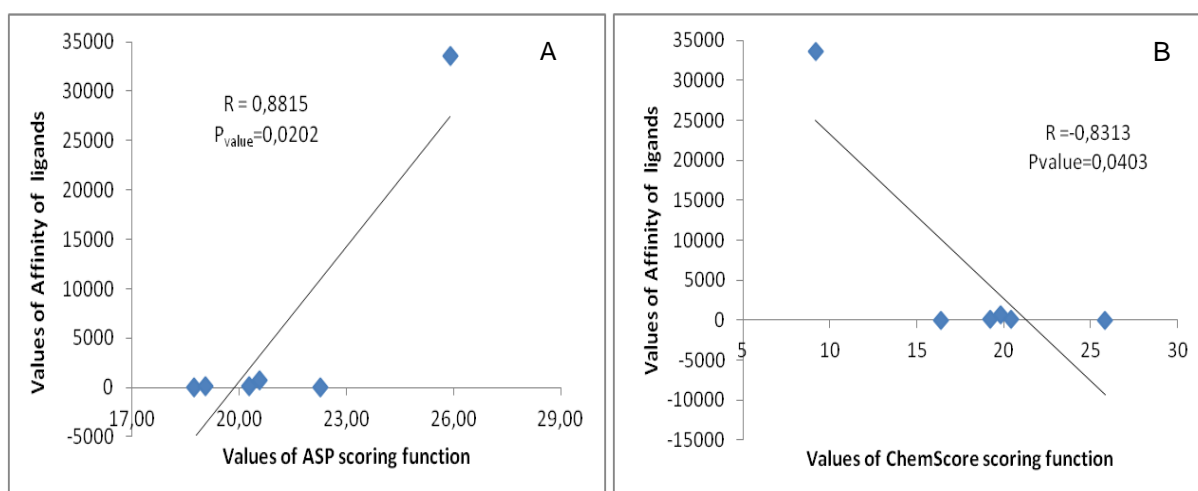


**Fig. 1.** Pearson's correlation between: A - the values of *affinity* of cannabinoid ligands and the values of ASP scoring function; B - the values of *affinity* of cannabinoid ligands of ChemSore scoring function.
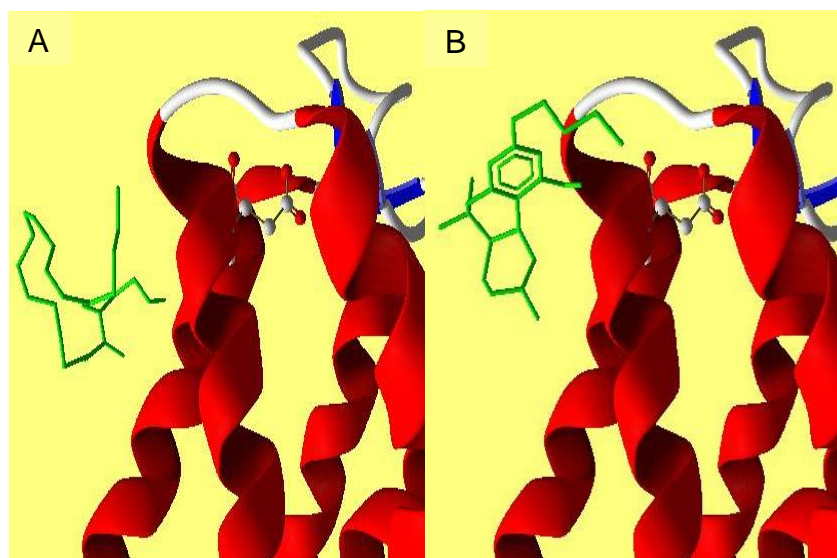
**Fig. 2.** Schematic diagram of the ligand-receptor complex between: A - CB1 receptor (PDBid:5tgz) and ligand anandamide; B - CB1 receptor (PDBid:5tgz) and ligand Δ-$^9$-tetrahydrocannabinol. The receptor is presented in ribbons and helixes. The ligands are presented in green. These diagrams were generated with the MMV.

Given a protein target – in our case model of the CB1 receptor, molecular docking with software GOLD 5.2 generates several probable ligand binding conformations at the active site - Asp366 around the receptor. The ASP scoring function from the program was used to rank the ligand conformations by evaluating the binding density of each of the probable complexes.

As a conclusion we found that the molecular docking between the cannabinoid ligands and the model of the CB1 with crystal structure should be performed using ASP scoring function of GOLD 5.2 as the correlations with the biological results are the best. These data indicate that the software GOLD 5.2 gives reliable results in the docking of cannabinoid ligands with the crystal structure of human cannabinoid receptor (PDBid:5tgz). For some work along these lines, see [25-31].

REFERENCES

1. K. Mackie, *Annual Review of Pharmacology and Toxicology*, **46,** 101 (2006).
2. P. Pacher, S. Batkai, G. Kunos, *Pharmacological Reviews,* **58 (3),** 389 (2006).
3. R. Pertwee, *British Journal of Pharmacology* **156 (3)**, 397 (2009).
4. S. Ben-Shabat, L.Hanus, G. Katzavian, R. Gallily, *Journal of Medicinal Chemistry,* **49 (3)**, 1113 (2006).
5. C. Bourne, S. Roy, J. Wiley, B .Martin, B.Thomas, A. Mahadevan, R. Razdan, *Bioorganic & Medicinal Chemistry,* **15 (24)**, 7850 (2007).
6. P. Reggio, *Current Medicinal Chemistry*, **17 (14),** 1468 (2010).
7. P. Reggio, *Curr. Pharm. Des*., **9**, 1607 (2003).
8. https://en.wikipedia.org/wiki/cannabinoid_receptor
9. http://www.rcsb.org/pdb/home/home.do
10. T. Hua, K. Vemuri, M. Pu, L. Qu, G. Han, Y. Wu et.al.,*Cell*, **167(3)**, 750 (2016).
11. G. Jones, P. Wilett, R. Glen, A. Leach, R. Taylor. *J Mol. Biol.*, **267**, 727 (1997).
12. GOLD, version 5.2 UserGuide, *CCDC Software Ltd.: Cambridge*, UK, 2010**.**
13. M. Verdonk, J. Cole, M. Hartshorn, C. Murray, R. Taylor. *Proteins*, **52,** 609 (2003).
14. R. Reinscheid, H. Nothacker, A. Bourson, A. Ardati, R. Henningsen, J. Bunzow, D. Grandy, H. Langen, F. Monsma, O. Civelli, *Science*, **270**, 792 (1995).
15. Joong-Youn Shim, A. Bertalovitz, D. Kendall, *Journal of Biological Chemistry*, **286 (38)**, 33422 (2011).
16. http://avogadro.openmolecules.net/
17. http://molegro.com/index.php
18. D. Sun, A. Whitty, J. Papadatos, M. Newman, J. Donnelly, S. Bowes, S. Josiah, *J. Biomol. Screen*. **10**, 508 (2005).
19. V. Kralev, *IJASEIT,* **7** (5), 1685 (2017).
20. V. Kralev, R. Kraleva, *IJACR,* **7** (28), 1 (2017)T. Dzimbova, F. Sapundzhi, N. Pencheva, P. Milanov, *Journal of Peptide Science*, **18** (S1), S84, P072, (2012).
21. F. Sapundzhi, T. Dzimbova, N. Pencheva, P. Milanov, *Journal of Peptide Science*, **20** (S1), S294 (2014).
22. T. Dzimbova, F. Sapundzhi, N. Pencheva, P. Milanov, *Int. J. Bioautomation,* **17**, 5-16, (2013).

23. F. Sapundzhi, T. Dzimbova, N. Pencheva, P. Milanov, *Bulgarian Chemical Communications*, **47**(2), 613 (2015).
24. F. Sapundzhi, T. Dzimbova, N. Pencheva, P. Milanov, *Der Pharma Chemica*, **8**, 118 (2016).
25. F. Sapundzhi, T. Dzimbova, N. Pencheva, P. Milanov, *Bulgarian Chemical Communications*, **49** (4), 768 (2017).
26. F. Sapundzhi, T. Dzimbova, N. Pencheva, P. Milanov, *Bulgarian Chemical Communications*, **49** (4), 23 (2017).
27. F. Sapundzhi, T. Dzimbova, N. Pencheva, P. Milanov, *ITM Web of Conferences, AMCSE 2017*, **16**, 02008 (2018).
28. F.Sapundzhi, T. Dzimbova, N. Pencheva, P. Milanov, *Journal of Computational Methods in Molecular Design*, **5(1)**, 98 (2015).
29. F. Sapundzhi, T. Dzimbova, N. Pencheva, P. Milanov, *Proceedings of 7th Bulgarian Peptide Symposium*, 10-12 June 2016, Blagoevgrad, Bulgaria, **1**, p. 89, 2016.
30. F. Sapundzhi, T. Dzimbova, N. Pencheva, P. Milanov, *Proceedings of Biomath Communications Supplement, 25-30 June 2017, Skukuza Camp, South Africa*, **4(1)**, 2017.
31. F. Sapundzhi, T. Dzimbova, N. Pencheva, P. Milanov, *Proceedings of Seventh International Conference of FMNS* 2017, 14-18 June 2017, Blagoevgrad, Bulgaria, **1**, 2017.

# Adamantane-1-carboxamides: synthesis and antimicrobial activity

B. Stoykova[1], M. Chochkova[1]*, G. Ivanova[2], I. Tsvetkova[3], H. Najdenski[3], M. Štícha[4], Ts. Milkova[1]

*[1] Department of Chemistry, South-West University Neofit Rilski, 66 Ivan Mihailov Str., 2700 Blagoevgrad, Bulgaria*

*[2] LAQV-REQUIMTE, Faculdade de Ciências, Universidade do Porto, Rua do Campo Alegre s/n, 4169-007 Porto, Portugal*

*[3] Stephan Angeloff Institute of Microbiology, Bulgarian Academy of Sciences, 26 Georgi Bonchev Str., 1113 Sofia Bulgaria*

*[4] Department of Chemistry, Faculty of Science, Charles University, Hlavova 2030/8, 12843 Prague 2, Czech Republic*

The rapid emergence of resistant bacteria highlights the urgent demand for new effective drugs. In view of the importance of adamantane skeleton in various antimicrobial drugs, herein the synthesis of *N*-adamantane-1-carboxamides of polyamine derivatives is described. The *in vitro* antibacterial activity of the new synthesized compounds against two Gram-positive (*Staphylococcus aureus, Bacillus subtilis*) and two Gram-negative (*Escherichia coli, Pseudomonas aeruginosa*) bacteria, as well as the antifungal activity against *Candida albicans* was assessed. The results revealed that amongst the new synthesized bisamides, *N,N'*-bis-adamantane-1-carboxamide of 1,6-diaminohexane was the most effective one and inhibited both Gram-negative and Gram-positive strains with MIC of 125 µg.ml$^{-1}$. Moreover, the same amide showed the highest antifungal activity (MIC of 63 µg.ml$^{-1}$) against *Candida albicans*.

## INTRODUCTION

The global emergence of infectious diseases caused by viruses, bacteria, fungi and protozoa represents a particularly worrying trend. The high rate of morbidity and mortality is a direct result of these infections. According to the World Health Organization (WHO) lethal outcomes from common infectious diseases (measles, tuberculosis, malaria, AIDS, respiratory and diarrheal diseases, etc.) account for more than 85 % [1].

In this regard, drug resistance has been recognized as a major health concern. A leading strategy to fight against resistant pathogens is the development of new effective antimicrobials.

Adamantane analogues have long been known for their manifold pharmacological activities. Since the discovery of 1-aminoadamantane (amantadine) and its methyl analogue (rimantadine) as effective M2 inhibitors against influenza virus type A [2], more attention has been paid to the adamantane scaffold. Despite the rapidly acquired resistance to M2-blockers and later to the second approved class of drugs (neuraminidase inhibitors-oseltamivir, zanamivir), the combination therapy of both class of inhibitors represents a good option for the control of resistant influenza viral infections [3]

In addition to the antiviral activity, several newly adamantyl analogues have been found to possess bactericidal or fungicidal activities [4-9].

Nowadays, the role of the adamantyl moiety as an essential pharmacophore in biologically active molecules is well known. The incorporation of adamantyl nucleus in molecules could substantially affect their lipophilicity, pharmacological properties and biological activity. Hence, adamantane could positively modulate the therapeutic index of the parent molecule and has been widely used in designing of agents with potential antimicrobial activity.

Other group of compounds that are considered in designing of invaluable chemotherapeutics are polyamines. Biogenic polyamines such as putrescine, spermidine, spermine and cadaverine are the most widely distributed and indispensable components of the living cells [10]. These linear aliphatic molecules possess: two primary (terminal) amino groups, in most cases – with one or more imino groups. Consequently, their basic groups are fully protonated under physiological pH 7 and could further interact with anions and negatively charged sites in cell components [11]. Moreover, these nitrogen containing organic constituents are also known to be involved in cell metabolism, division and differentiation [12].

On the other hand, being endogenous modulators of porin channel function, polyamines influence outer membrane permeability of bacteria [13]. Thus, they induce resistance to different antibiotics (e.g. cationic peptide, aminoglycoside, and quinolone antibiotics) [14]. Several studies

---

* To whom all correspondence should be sent.
E-mail: mayabg2002@yahoo.com

have clearly indicated that some polyamines (cadaverine or spermine) can reduce bacterial susceptibility to antibiotic treatments [15-17] by decreasing outer membrane permeability.

Interestingly, Kwon *et al.* have shown that exogenous natural polyamines at millimolar levels can enhance the susceptibility of *P. aeruginosa* [14]. However, contradictory results have been obtained by Vaara *et al.*, who concluded that polyamines had neither bactericidal nor sensitizing activity at sub-millimolar concentration [18].

It was recently reported that certain molecules including polyamine scaffold can serve as an efficient alternative mechanism to reduce the development of resistance by affecting membrane depolarization/or integrity membrane disruption [19]. In the same context, the importance of lipophilic functionalized polyamines for permeabilisation of an outer membrane of Gram-negative bacteria have been published by Katsu *et al.* [20]. Moreover, significant antimicrobial activities have been reported for polyamines conjugated to cholesterol, cholenic acid and bile acids [21-26].

Considering the potential impact of the hydrophobicity of the adamantane skeleton and polyamine chain as critical factors for the antimicrobial activity, herein we report the synthesis and *in vitro* antibacterial and antifungal activities of novel hybrid molecules consisting of these two fragments.

## EXPERIMENTAL

### General information

All chemicals used in this study were purchased from Sigma-Aldrich (FOT, Bulgaria). Synthesized compounds were purified by column chromatography using silica gel (Acros Organics, mesh 35-70) and identified by TLC, IR, NMR, and MS analysis. TLC was carried out on silica gel $60F_{254}$ (Merck) precoated aluminium plates. Melting points were determined using an apparatus „Stuart SMP10" and are uncorrected. Attenuated total reflectance infrared spectroscopy (ATR-IR) measurements were performed using Thermo Scientific Nicolet iS10 FT-IR device with ID5 ATR accessory (diamond crystal). NMR spectra were recorded on a Bruker Avance III 400 spectrometer in dimethyl sulfoxide-$d_6$ (DMSO-$d_6$) solution and referenced to the solvent resonance peak at 2.49 ppm. One-dimensional (1D: $^1$H, $^{13}$C) and two-dimensional (2D: $^1$H/$^1$H COSY, $^1$H/$^{13}$C HSQC) NMR spectra were acquired using standard pulse sequences and experimental conditions. The

spectra were recorded at a temperature of 25 °C and spectral width of 5000 Hz and 20000 Hz for $^1$H and $^{13}$C, respectively. The ESI mass spectra were recorded on an Esquire3000 plus instrument.

### General procedure for synthesis of amides

The amide bond formation in the target carboxamides (**1–3**) was carried out under mild conditions by means of the coupling method EDC/HOBt, as described previously by us [27].

The physico-chemical parameters and the IR, NMR and MS spectral data of the compounds **1-3** and **1a** are as follows:

### $N^1$-Adamantanoyl-$N^6$-(t-buthyloxycarbonyl)--1,6-diaminohexane

**AdA-NH-(CH$_2$)$_6$-NH-Boc** *(compound 1);* Yield: 35 %; mp~127-129°C; IR (ATR)u$_{max}$: 3320, 2965, 2902, 1681, 1628, 1533, 1450, 1388, 1363, 732 cm$^{-1}$; $^1$H-NMR (DMSO-$d_6$, ppm): δ 1.23 (br. s, 4H, 2 x -CH$_2$-), 1.31 (s, 9H, 3 x –C(CH$_3$)$_3$), 1.38 (br. s, 4H, 2 x -CH$_2$-), 1.69 (12H, 6 x -CH$_2$-), 1.89 (br. s, 3H, 3 x >CH-), 3.11 (br. s, 4H, 2 x >NCH$_2$-), 7.24 (2H, 2 x >NH).

### $N^1$,$N^6$–bis-Adamantanoyl-1,6-diaminohexane

**AdA-NH-(CH$_2$)$_6$-NH-AdA** *(compound 2);* Yield: 22 %; mp ~ 206-208°C; IR (ATR)u$_{max}$: 3318, 2900, 2848, 1710, 1630, 1547, 1447, 724 cm$^{-1}$; $^1$H-NMR (DMSO-$d_6$, ppm): δ 1.20 (br. s, 4H, 2 x -CH$_2$-), 1.35 (br. s, 4H, 2 x -CH$_2$-), 1.64 (12H, 6 x -CH$_2$-), 1.73 (12H, 6 x -CH$_2$-), 1.94 (br. s, 6H, 6 x >CH-), 3.00 (br. s, 4H, 2 x >NCH$_2$-), 7.20 (2 x >NH); $^{13}$C-NMR (DMSO-$d_6$, ppm): δ 25.8 (2 x -CH$_2$-), 27.6 (6 x >CH-), 29.02 (2 x -CH$_2$-), 36.1 (6 x -CH$_2$-), 38.2 (2 x >NCH$_2$-), 38.7 (6 x -CH$_2$-), 176.9 (-C(O)NH-); ESI-MS: 441.5 [M+H]$^+$, 463.4 [M+Na]$^+$, 479.4 [M+K]$^+$.

### Boc-Oseltamivir Carboxamide of $N^1$-adamantoyl-1,6-diaminohexane

**Boc-Os-NH-(CH$_2$)$_6$-NH-AdA** *(compound 3);* Yield: 24 %; m p ~ 144-146°C; IR (ATR)u$_{max}$: 3294, 3079, 2906, 2851, 1686, 1626, 1525, 1453, 1390, 1366, cm$^{-1}$; $^1$H-NMR (DMSO-$d_6$, ppm): δ 0.87 (t, J= 7.52 Hz, 3H, -CH$_2$CH$_3$), 0.93 (t, J= 7.34 Hz, 3H, -CH$_2$CH$_3$), 1.32 (m, 4H, 2 x -CH$_2$CH$_3$), 1.46 (br. s, 4H, 2 x -CH$_2$-), 1.49 (br. s, 4H, 2 x -CH$_2$-), 1.74 (s, 9H, -C(CH$_3$)$_3$), 1.84 (s, 3H, -C(O)CH$_3$), 1.87 (12H, 6 x -CH$_2$-), 2.04 (br. s, 3H, 3 x >CH-), ), 2.31 (m, 1H, =CCH$_{2a}$-), 2.58 (dd, J=17.7, 5.0 Hz, 1H,=CCH$_{2b}$-), 3.11 (m, 1H, -NH-CH<), 3.16 (m, 1H, -NH-CH<), 3.42 (br. s, 4H, 2 x >NCH$_2$-), 3.46 (m, 1H, -OCHC=), 4.11 (m, 1H, -

OCH<), 6.37 (d, J=8.70 Hz, 1H, $H_3CC(O)NH-$), 6.54 (br.s, 1H, =CH-), 7.39 (d, J=9.17 Hz, 1H, -C(O)NH-), 7.86 (m, 1H,-C(O)NH-), 7.99 (m, 1H,-C(O)NH-); ESI-MS: 545.6 [M+H-Boc+H]$^+$, 645.6 [M+H]$^+$, 667.7 [M+Na]$^+$, 683.7 [M+K]$^+$.

### *Removal of the tert-butyloxycarbonyl (Boc) protecting group* [28]

Deprotection of **AdA-NH-(CH₂)₆-NH-Boc** (compound **1**) to **AdA-NH-(CH₂)₆-NH₂.TFA** (compound **1a**) was readily achieved by 50% (v/v) TFA in $CH_2Cl_2$.

### *N¹-Adamantanoyl-1,6-diaminohexane.TFA salt*

**AdA-NH-(CH₂)₆-NH₂.TFA** *(compound 1a);* Yield: 69%. ESI-MS: 279.5 [M+H]$^+$.

### *Microbiology*

The antibacterial activity was tested against *Staphylococcus aureus 209* (G+), *Bacillus subtilis 1A95* (G+)*, Pseudomonas aeruginosa 5749* (G-), *Escherichia coli WF+* (G-); the antifungal activity was tested against the pathogenic fungus *Candida albicans 562*. All microorganisms were obtained from the Bulgarian National Collection for Microorganisms and Cell Cultures (NBIMCC).

The minimal inhibitory concentration (MIC) of all samples was determined by the microdilution method described by Andrews [29]. Briefly, 50 µl of twofold diluted serial dilutions of the examined samples were added to 50 µl of microbial suspension adjusted to yield approximately $1.0 \times 10^5$ CFU ml$^{-1}$. MIC was determined as the lowest concentration of the examined sample that inhibits the visible microbial growth after 24 h incubation at 37°C. For positive controls commercially available antibiotics tobramycin and ketoconazole were used. The solvent DMSO was tested as negative control. Three replicates were done for each compound.

In the course of our program directed towards the design and development of novel adamantane derivatives with a potential antimicrobial and antiviral activity and better therapeutic index, we synthesized adamantane analogues, comprising hydrophobic (adamantane) and cationic (1,6-diaminohexane) components. 1,6-Diaminohexane was used considering the early reported properties of polyamines to inhibit the growth of various microorganisms [30 ] and their effect on antibiotic susceptibility in bacteria [19, 31].

Despite a wide range of different peptide methods are used for the amide bond formation, for the preparation of the new adamantane carboxamides we have chosen the method employing *N*-ethyl-*N*'-dimethylaminopropyl carbodiimide (EDC) as a coupling reagent [32]. The advantage of this coupling reagent in the peptide chemistry is well known and is due mainly to the formation of water-soluble urea, which facilitates the isolation of the reaction products. For acceleration of the reaction an efficient additive as HOBt was added.

However, the derivatization of polyamines often encounters problems with respect to the selective protection of amino functionalities. Therefore, herein we used commercial available mono-Boc (*tert*-butyloxycarbonyl) protected diaminohexane. It is well known that this urethane group can be easily removed under strong acid conditions.

The synthetic strategy towards preparing the target adamantane-1-carboxamides **2** and **3** is presented in Scheme 1. The three-stage synthetic procedure was based on a method recently reported by us for formation of amide bond under mild experimental conditions [27] and following coupling of the obtained amides with 1-adamantane caboxylic acid (AdA) or *N*-Boc-oseltamivir carboxylic acid (Boc-Os-OH). The reactions at all stages were monitored by TLC and the products were purified by column chromatography using silica gel using mobile phase composed of $CH_2Cl_2$:$CH_3OH$. The structures of the targeted compounds **1-3** were confirmed by melting points, NMR, IR and MS analysis.
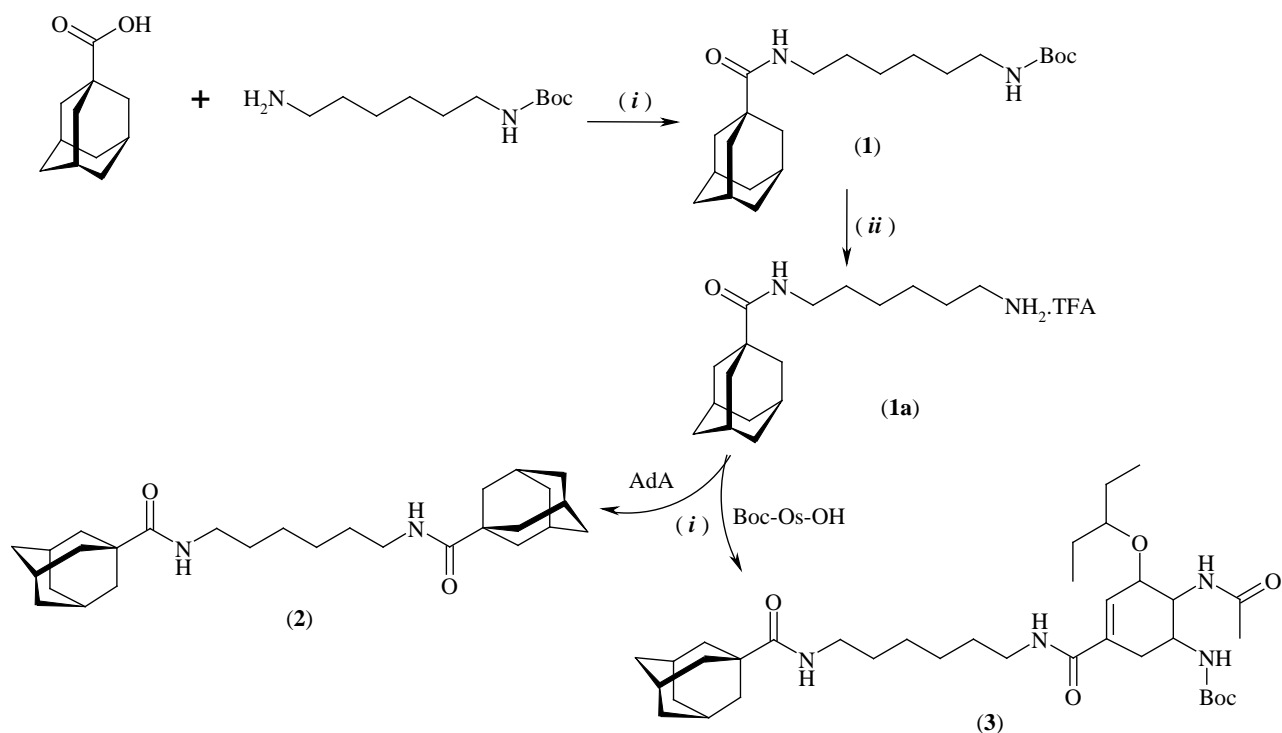
**Scheme 1.** (*i*) EDC/HOBt, CH$_2$Cl$_2$; (*ii*) 50% TFA/CH$_2$Cl$_2$; **AdA**: 1-adamantane carboxylic acid; **Boc-Os-OH**: *N*-Boc-oseltamivir carboxylic acid

The first stage implies solution phase (EDC/HOBt) coupling of 1-adamantane carboxylic acid with *N-tert*-butyloxycarbonyl-1,6-hexanediamine.

As a result, the *N*-(Boc-aminohexyl) adamantane-1-carboxamide (**1**) after purification by column chromatography was obtained in a good yield.

The formation of the amide **1** was confirmed by the presence of characteristic resonance signals for the amide and urethane NH protons (7.24 ppm, 2H, >NH) and methyl-, methyne- and methylene protons (3.11 to 1.23 ppm) in the $^1$H NMR spectra.

IR spectroscopy further confirmed the formation of amide bond by means of very strong absorption (C=O str.) at 1628 cm$^{-1}$ (amide I) and amide II band caused by N-H bending at 1533 cm$^{-1}$.

The next stage involved deprotection of **1** (cleavage of the Boc group) by TFA in CH$_2$Cl$_2$, which allowed the isolation of the semi-product **1a** as TFA salt. Accordingly, the latter was further linked with 1-adamantane carboxylic acid (AdA) or *N*-Boc-oseltamivir carboxylic acid (Boc-Os-OH) through the use of the same coupling reagent EDC/HOBt, which afforded the corresponding symmetrical (**2**) and unsymmetrical (**3**) diamides.

Besides the common infrared characteristic amide group frequencies and characteristic absorption of hydrocarbons derived from adamantyl and diaminohexyl moieties (amides **2, 3**), the IR spectrum of compound **3** shows the specific frequency of the double-bond stretching vibration of a cyclohexenyl skeleton at 1686 cm$^{-1}$.

The structures of the targeted compounds **2** and **3** were confirmed by $^1$H and $^{13}$C NMR analysis. The complete assignment of the resonance signals in the spectra is presented in the Experimental part. The chemical shift and integral intensity of the observed resonance signals in the $^1$H NMR spectra unambiguously demonstrated the formation of amide bond and incorporation of two adamantyl (AdA) moieties in **2** and adamantyl- and *N*-Boc-oseltamivir moieties (Boc-Os-OH) in **3**. The results from the analysis of the $^{13}$C NMR spectra were consistent with those from $^1$H NMR.

Additional information was gained from mass spectral data. The positive-ion ESI-MS of both compounds **2** (Mw=440.6) and **3** (Mw=644.8) displayed the corresponding intense [M+Na]$^+$ peaks at *m/z* 463.4 and *m/z* 667.7, accompanied by smaller signals for the [M+H]$^+$ and [M+K]$^+$ peaks. In the spectrum of compound **3** Boc-characteristic ion at *m/z* 545.6 [M+H-Boc+H]$^+$ was also observed.

*Evaluation of antimicrobial activity in vitro*

Inspired by 'Lipophilic bullet' of adamantane skeleton for providing novel antimicrobials, herein the synthesized adamantane-based diamino derivatives were estimated for their antimicrobial activity *in vitro*.

The antibiotic tobramycin and the antifungal drug ketoconazole were used as positive controls. The minimum inhibitory concentrations (MIC) of the tested compounds are summarized in Table 1. The results of antimicrobial screening indicate that compounds have demonstrated low to moderate antibacterial activity.

Surprisingly, amongst the tested amides, compound **2** has shown to be the most active (MIC = 125 µg/ml) against all tested Gram-positive and Gram-negative bacterial strains. The incorporation of two adamantyl residues in the molecule most probably affects its lipophilicity and enhances its penetration within the cellular membrane. The modification of 1,6-diaminohexane with two adamantyl residues (molecule **2**) suggests that an optimum hydrophobic interaction may be essential for the established activity. On the other hand, the results from the *in vitro* biological test (Table 1) show that the amides **1**, **1a** and **3** exhibit almost the same activity against different bacterial strains and fungus tested, which is significantly lower than that of compound **2**.

Moreover, the terminal free amino group in the amide **1a** seems to be not crucial for the antimicrobial activity (except for *S. aureus*) as compared with its *N*-Boc protected analogue (**1**).

Regarding the antifungal activity, compounds **1**, **1a** and **3** can be considered not to be so active against the pathogenic fungus *C. albicans* (with MIC of 313 µg/ml). Exception is bis-adamantyl carboxamide **2**, which shows MIC of 63 µg/ml. Considering the apparent antifungal activity of compound **2** amongst the other synthetic ones, it could be attributed to the presence of an additional lipophilic motif in its structure.

Finally, the activity of molecule **2** was 8-fold lower than that of the used antifungal drug ketoconazole.

CONCLUSIONS

In conclusion, two novel adamantane-1-carboxamides (**2**, **3**) were obtained, comprising a diamine linker. The antimicrobial activity of the covalently bonded hybrid structures was evaluated *in vitro*. The most active was the *N,N'*-bis-adamantane-1-carboxamide of 1,6-diaminohexane (compound **2**) with regard to the structure cell wall peculiarities of G+, G- bacteria and the fungus *Candida albicans*. All others compounds demonstrated low to moderate antibacterial activity with moderate antifungal activity.

**Table 1**. *In vitro* antimicrobial activity of synthetic adamantane-1-carboxamides

| Compound | | X | MIC (µg/ml) | | | | |
| --- | --- | --- | --- | --- | --- | --- | --- |
| | | | *S. aureus* | *E. coli* | *P. aerug.* | *B. subt.* | *C. albicans* |
| | **1)** | -Boc | 625 | 625 | 313 | 625 | 313 |
| | **1a)** | H | 156 | 625 | 313 | 625 | 313 |
| | **2)** | | 125 | 125 | 125 | 125 | 63 |
| | **3)** | | 625 | 313 | 625 | 625 | 313 |
| Tobramycin | | | 15.6 | 19.5 | NT | 1.0 | NT |
| Ketoconazole | | | NT | NT | NT | NT | 7.8 |
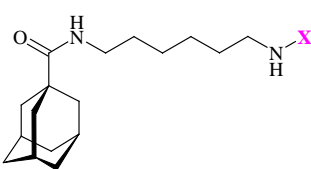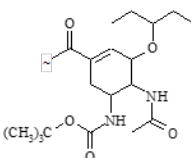
## REFERENCES

1. http://www.who.int/mediacentre/factsheets/fs310/en/index2.html
2. W. L. Davies, R. R. Grunert, R. F. Haff, J. W. McGahen, E. M. Neumayer, M. Paulshock, J. C. Watts, J. C. Wood, T. R. Hermann, E. C. Hoffman, *Science*, **144**, 862 (1964).
3. N. A. Ilyushina, N. V. Bovin, R. G. Webster, E. A. Govorkova, *Antiviral Res.*, **70**, 121 (2006).
4. B. Orzeszko, Z. Kazimierczuk, J. K. Maurine, A. E. Laudy, B. J. Starościak, J. Vilpo, L. Vilpo, J. Balzarini, A. Orzeszko, *Il Farmaco*, **59**, 929 (2004)
5. O. A. Al-Deeb, M.A. Al-Omar, N.R. El-Brollosy, E.E. Habib, T.M. Ibrahim, A.A. El-Emam, *Arzneim.-Forsch./Drug Res.,* **56**, 40 (2006).
6. A. A. Kadi, N.R. El-Brollosy, O.A. Al-Deeb, E.E. Habib, T.M. Ibrahim, A.A. El-Emam, *Eur. J. Med. Chem.*, **42**, 235 (2007).
7. A. A. Kadi, E.S. Al-Abdullah, I.A. Shehata, E.E. Habib, T.M. Ibrahim, A.A. El-Emam, *Eur. J. Med. Chem.,* **45**, 5006 (2010).
8. E. S. Al-Abdullah, H.H. Asiri, S. Lahsasni, E.E. Habib, T.M. Ibrahim, A.A. El-Emam, *Drug Des. Dev. Ther.,* **8**, 505 (2014).
9. C. P. Krimmel, *N*-(Dialkylaminoalkyl)adamantine carboxamides, U.S. Patent 3,374,244 (1968); *Chem. Abstr.*, **69**, 35575t (1968).
10. S. S. Cohen, A guide to polyamines, Oxford University, Press, Oxford, United Kingdom, 1997.
11. Y. Takeda, K. Samejima, K. Nagano, M. Watanabe, H. Sugeta, Y. Kyogoku, *Eur. J. Biochem.,* **130**, 383 (1983).
12. O. Heby, *Differentiation*, **19**, 1 (1980).
13. A. L. Dela Vega, A. H. Delcour, *J. Bacteriol.*, **178**, 3715 (1996).
14. D. H. Kwon, C. D. Lu, *Antimicrob. Agents Chemother.,* **50**, 1615 (2006).
15. R. Chaturvedi, M. Asim, D. P. Barry, J. W. Frye, R. A. Casero, K. T. Wilson, *Amino acids*, **46**, 531 (2014).
16. L. Johnson, H. Mulcahy, U. Kanevets, Y. Shi, S. Lewenza, *J. Bacteriol.,* **194**, 813 (2012).
17. M. Goytia, W. M. Shafer, *Infect. Immun.,* **78**, 3187 (2010).
18. M. Vaara, T. Vaara, *Antimicrob. Agents Chemother.,* **24**, 107 (1983).
19. M. Blanchet, D. Borselli, J.M. Brunel, *Future Med. Chem.,* **8**, 963 (2016).
20. K. Yasuda, C Ohmizo, and T Katsu, *Int J of Antimicrob. Agents,* 24, 67 (2004).
21. H. S. Kim, B. S. Choi, K. C. Kwon, S. O. Lee, H. J. Kwak, C. H. Lee., *Bioorg Med Chem.*, **8**, 2059 (2000).
22. K. Kikuchi, E.M. Bernard, A. Sadownik, S.L. Regen, D. Armstrong, *Antimicrob. Agents Chemother.,* **41**, 1433–1438 (1997).
23. S. R. Jones, W.A. Kinney, X. Zhang, L.M. Jones, B. S. Selinsky, *Steroids,* **61**, 565 (1996).
24. A. Sadownik, G. Deng, V. Janout, S. L. Regen, E. M. Bernard, K. Kikuchi, D. Armstrong, *J. Am. Chem. Soc.,* **117**, 6138 (1995).
25. S. Khabnadideh, C. L. Tan, S. L. Croft, H. Kendrick, V. Yardley, I. H. Gilbert, *Bioorg. Med. Chem. Lett.,* **10**, 1237 (2000).
26. C. Salmi, C. Loncle, N. Vidal, M. Laget, Y. Letourneux, J. M. Brunel, *J Enzyme Inhib. Med. Chem..,* **23**, 860 (2008).
27. M. Spasova, V. Kortenska-Kancheva, I. Totseva, G. Ivanova, L. Georgiev, Ts. Milkova, *J. Pept. Sci.*, **12**, 369 (2006).
28. M. Bodanszky, A. Bodanszky, The Practice of Peptide Synthesis. (Reactivity and structure: concepts in organic chemistry), K. Hafner, Ch.W. Rees, B. M. Trost, l.-M. Lehn, P. von R. Schleyer, R. Zahradnik (eds.), 1ˢᵗ ed., Springer-Verlag, Berlin-Heidelberg GmbH, vol. 21, 1984, 10.1007/978-3-642-96835-8
29. J. M. Andrews, *J. Antimicrob.Chemother.,* **48**, 5 (2001).
30. U. Bachrach, A. Weinstein, *J. Gen. Microbiol.*, **60**, 159-165 (1970).
31. D. H. Kwon, C. D. Lu, *Antimicrob. Agents Chemother.,* **51**, 2070 (2007).
32. J. C. Sheehan, G. P. Hess*., J. Am. Chem. Soc.*, **77**, 1067 (1955).

Section

*Methodology in Education*

# Didactic methods of teaching physics at "Fan S. Noli" University in Korca

L. Kelo[1*], M. Dede[2], S. Marko[1], E. Guliqani[1]

[1]*Department of Mathematics-Informatics-Physics, Faculty of Natural and Human Sciences, University of Korca, Blvd. Rilindasit 11, Korca, Albania*

[2]*Department of Physics, Faculty of Natural Science, University of Tirana, Blvd. Zogu I, Tirana, Albania*

Didactics, once valued as the art of a teacher, is today an established science with properly defined laws, regulations and methods. Considering the actual needs of our schools, the studies concerning the scientific approach of the didactic methods of physics take central priority. The pedagogue at the "Fan S. Noli" University of Korca has put himself up to the selection of the most efficient forms and methods of conveying the concepts of physics to students with different backgrounds, who study the subject of physics for one semester. This article examines the factual aspects of applying *just in time teaching method (Peer Instruction),* using *ConcepTest* and solving *strategy/scheme* for problems, intertwined these with *group studying method* regarding the subject of physics (this includes lectures, seminars and lab work). The results derived, demonstrate an increased efficiency of the new teaching practices, compared to the traditional ones from two years ago. This is clearly manifested in the increased collaboration between students and teachers when discussing about the subject of physics. Finally, an increased conceptual scale is being evidenced, along with higher results/evaluations than two years ago.

**Keywords:** Just in time teaching, Peer Instruction, ConcepTest, Solving scheme, Group studying.

## METHODOLOGY

It includes two basic steps of the teaching process [1]:

- *Transfer of information* - an indispensable step in the classroom, where information is passed to the student through the lecturer.
- *Logical assimilation of information* - an even more important and indispensable step for the sake of truth. It is realized outside the classroom. Some of the students achieve this step in an autodidactic way, while others do not do it at all.

Based on the degree of difficulty in the realization of these two steps, efforts have been made to realize the transfer of out-of-class information and the assimilation of information within the classroom. In this way, we are disconnected from the traditional way of teaching to give way to the modern method (JiTT, Peer Instruction).

### The tactics of organizing cooperative lectures

Students are assigned to read in advance the material to be handled in the next lesson (transferring information to them is done out of the class not through the lecturer but through the book).

*Example:* After the initial reading that the students made to the chapter on the Conservation Laws in the lecture, it is discussed (*ConcepTest*):

- A cube slides without initial velocity in the corrugated and polished gutter as in Figure 1 [2].
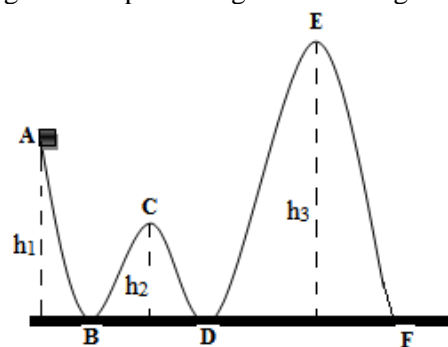


**Fig. 1.** The corrugated and polished gutter

1) The cube passes the C and E obstacles and reaches point F;

2) The cube passes the C but not the E obstacle;

3) The cube fails to pass even the C obstacle.

- How is the cube velocity at the lowest culvert?

1) The cube velocity at points B, D, F is the same;

2) The cube velocity at points B and D is different;

3) The cube velocity at points B and D is the same.

This is the most appropriate phase to apply Peer instruction, which includes students and lecturer in the cycle below as shown in Figure 2.
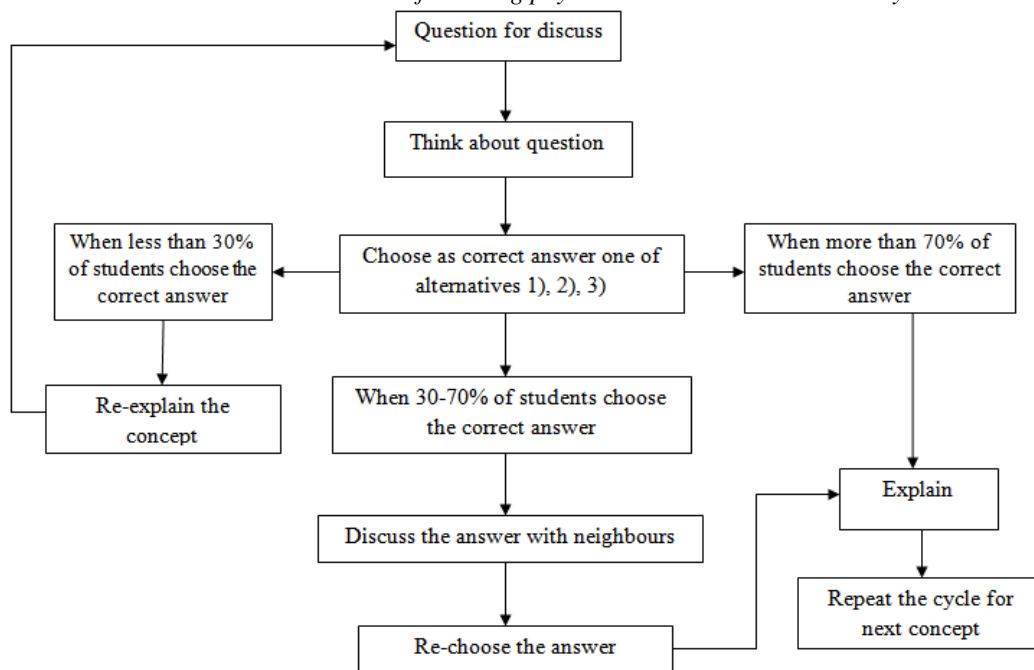
**Fig. 2.** The cycle of Peer Instruction

*Problem solving tactics (seminars)*

Problem solving cannot be independent of the concepts and principles taught. It is important when solving problems to form the kind of knowledge to the student so that he can apply it in a new context. To achieve this goal, the lecturer himself pursues a model procedure for solving a particular problem. Schematically summarized, the scheme / solution strategy [3,4] of the problem is given below in Figure 3:
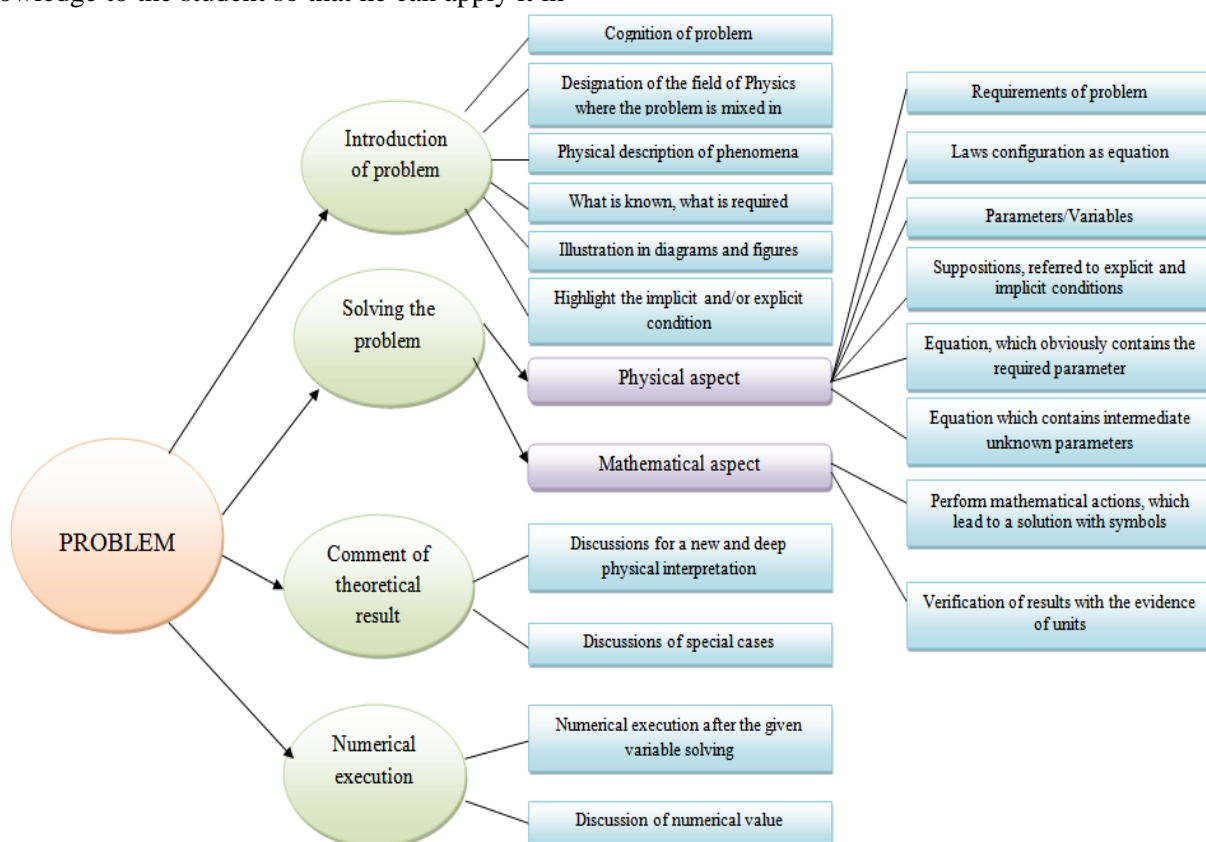


**Fig. 3.** Strategy/scheme of solving problems

Having solved a problem by following the model described above, the lecturer gives another problem to be solved. Classes are organized in small workgroups with 3-4 members each and are encouraged to give ideas (within the group) to solve the problem. The choice of each group is considered, checked and evaluated which of the groups has the most structured solution (according to the model scheme) and the opportunity is given to the members of that group to discuss with others on the blackboard their way of solving the problem.

*Example:* A parachutist, the first 45 m after launch, without initial velocity, from a bridge, did not open the parachute. After its opening, his motion became evenly changed with acceleration, 2.5 m/s$^2$ until he reached the ground with velocity of 2 m/s. Assuming that all his motion is in a straight line, it must be calculated:

- How long did the parachutist stay in the air?
- From what height did he jump?

### Introduction of problem

✓ *Cognition of problem*

1. Parachutist crosses $h_1 = 45\ m$ of height without opening the parachute.

2. After 45 m he steps up the parachute and his motion begins to slow down with acceleration $a$.

3. He keeps this motion until he reaches the ground with velocity $v_T$.

> Is required to calculate the total flight time of parachutist $t_p$.
>
> Is required to calculate the height from which the parachutist jumped $H$.

✓ *Designation of the field/s of physics where the problem is mixed in*

- free falling
- linear motion
- velocity
- acceleration/free falling acceleration
- velocity and height equation
- vertical axis

✓ *Illustration figure*
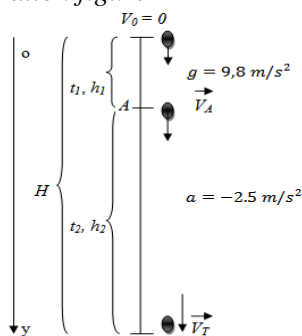


oy - Is chosen as positive axis of motion

✓ *Approaches*

The motion from the moment he jumped till he reaches the ground, is considered as linear motion.

### Solving of problem

<u>Is required</u>: total flight time of parachutist $t_p$.

<u>Condition</u>: $h_1$ is crossed with free falling without initial velocity and $h_2$ is crossed with negative acceleration.

<u>Known variables</u>: $h_1, a, g, v_T$.

(1) $\quad t_p = t_1 + t_2 \qquad (t_1, t_2)$ intermediate unknowns, where $t_1$ is found from the equation of that part of height which the parachutist makes with free falling.

$$(2)\quad h_1 = v_0 t_1 + \frac{g t_1^2}{2} = \frac{g t_1^2}{2} \Rightarrow t_1 = \sqrt{\frac{2h_1}{g}}$$

because of $v_0 = 0$. The equation that contains the intermediate unknown $t_2$ is the velocity equation for that part of height that the parachutist crosses with acceleration $\vec{a}$.

(3) $\quad v_T = v_A + a t_2$ ($v_A$ - the velocity that the parachutist has achieved at the end of $h_1 = 45\ m$ which serves as initial velocity for the second part of height $h_2$) intermediate unknowns.

(4) $\quad v_A = v_0 + g t_1 = g t_1$ because of $v_0 = 0$. Now we have no more intermediate unknowns. Making substitutions we obtain:

$$t_p = \sqrt{\frac{2h_1}{g}} + \frac{v_T - \sqrt{\frac{2h_1}{g}}}{a}$$

<u>Is required</u>: $H$

<u>Condition</u>: He crosses $h_1$ with free falling without initial velocity and $h_2$ with negative acceleration.

<u>Known variables</u>: $h_1, a, g, v_T$. From the first part of solving are known: $t_1, t_2$ and $v_A$

(1) $H = h_1 + h_2$ ($h_2$) intermediate unknown, we can find it from the height equation:

$$(2)\quad h_2 = v_A t_2 + \frac{a t_2^2}{2}$$

There are no more intermediate unknowns, after substitutions we achieve:

$$H = h_1 + v_A t_2 + \frac{a t_2^2}{2}$$

*Executing numerical value*

$$t_p = \sqrt{\frac{2x45m}{9.8\frac{m}{s^2}}} + \frac{2\frac{m}{s} - 9.8\frac{m}{s^2}\sqrt{\frac{2x45m}{9.8\frac{m}{s^2}}}}{-2.5\frac{m}{s^2}} \approx 14.3s$$

The parachutist stood about 14.3 sec in air.

$$H = 45m + 30\frac{m}{s}x11.3s + \frac{(-2.5\frac{m}{s^2})x11.3s^2}{2} = 370m$$

The height of the bridge from which he jumped is about 370 m. Dimensional analysis convinced us for the correct solution of the problem.

### *Laboratory development tactics*

Groups of 3-4 students each get acquainted with the specifics (construction of equipment, operation) of the lab's work that they will develop and prepare to measure.

Also, group members have theoretically prepared the lab work assigned to them and by Peer technique are encouraged to discuss what is required to measure and the variables they expect to derive.

Students cooperate in performing measurements by sharing tasks and discussing measurement compliance with what they are expecting to derive.

They argue their work and results in the classroom [5].

*Example:* Work No. 5. Energy Conservation Law. Maxwell's wheel

Maxwell's wheel (Figure 4), is located at *h* height from the potential zero energy level. It is released without initial speed. The end-of-turn velocity is expected to be:

1) greater;
2) smaller;
3) equal

to the velocity, when it is released from the same height without initial velocity, only under the force of gravity (air resistance forces are not taken into consideration).



**Fig. 4.** Maxwell's wheel

## RESULTS AND DISCUSSION

### *Lectures*

The number of students who underwent the concept test in the lecture example (Figure 1) was 29. The results of their responses are given in Table 1, Figures 5, 6 and 7:

**Table 1.** Distribution of the number of students according to respective responses before and after discussion. Confidence levels for the chosen responses.

| BEFORE DISCUSSION | | | | | |
|---|---|---|---|---|---|
| Answers | No. of std for corresponding answers | Students pretty sure for the answer | Percentage | Students not quite sure for the answer | Percentage |
| 1 | 6 | 3 | | 3 | |
| 2 | 13 | 10 | 65.5 % | 3 | 34.5% |
| 3 | 10 | 6 | | 4 | |
| AFTER DISCUSSION | | | | | |
| Answers | No. of std for corresponding answers | Students pretty sure for the answer | Percentage | Students not quite sure for the answer | Percentage |
| 1 | 3 | 2 | | 1 | |
| 2 | 20 | 17 | 79.3% | 3 | 20.7% |
| 3 | 6 | 4 | | 2 | |

**Fig. 5.** Data analysis of responses to the question of Figure 1. Correct answer is 2.
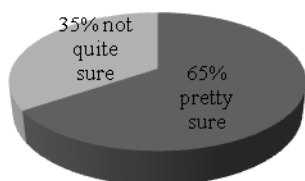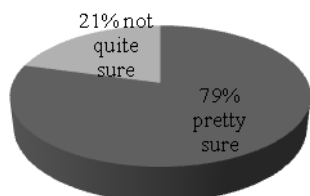


**Fig. 6.** Confidence levels that characterized students' responses before and after the discussion.
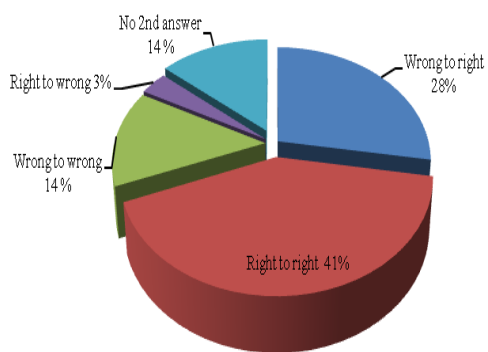


**Fig. 7.** How answers were revised after convincing the neighbours through discussion.

The systematic effort to persuade their neighbours with the help of discussion increases the percentage of correct answers and student security for the chosen response. Usually, the improvement is greater when the initial response rate is about 50%. This is because the auditorium has more students able to convince others of the correct answer. Figure 6 shows how students have revised their responses after discussion. About 28% of them have reconsidered the wrong answer correctly, while only 3% of them have revised the answer from the correct one, in the wrong. Apparently, students are more efficient than the

lecturer, to explain the concepts to each other. Also, it is easier to change the mind of a student who has chosen the wrong answer than the one who has chosen the correct answer.

Half of the course was subjected to Peer technique, while the rest continued the lecture in the traditional way. In the middle of the semester, all course students underwent the Concept Test. The summarized results are given in Table 2 and Figure 8.

**Table 2.** Evaluation in scores for the part of students where we used and did not use *Peer Instruction*.

| Corresponding scores (max. 30 scores) | No. of students for corresponding scores. The part where Peer instruction was used | No. of students for corresponding scores. Traditional method |
|---|---|---|
| 1 | 0 | 0 |
| 2 | 0 | 0 |
| 3 | 0 | 0 |
| 4 | 0 | 0 |
| 5 | 0 | 1 |
| 6 | 0 | 2 |
| 7 | 0 | 2 |
| 8 | 1 | 1 |
| 9 | 2 | 1 |
| 10 | 1 | 3 |
| 11 | 1 | 1 |
| 12 | 1 | 1 |
| 13 | 1 | 1 |
| 14 | 0 | 2 |
| 15 | 1 | 2 |
| 16 | 2 | 1 |
| 17 | 3 | 1 |
| 18 | 3 | 1 |
| 19 | 2 | 1 |
| 20 | 1 | 0 |
| 21 | 0 | 2 |
| 22 | 1 | 2 |
| 23 | 2 | 1 |
| 24 | 1 | 1 |
| 25 | 0 | 1 |
| 26 | 1 | 0 |
| 27 | 1 | 0 |
| 28 | 2 | 0 |
| 29 | 0 | 0 |
| 30 | 2 | 0 |

What is noted is a shift of the average score per student from 14.1 points for (a) to 18.7 points for (b). The change is most noticeable for a large number of students [6-8]. Anyhow, under our conditions, it is very enjoyable.

*Seminars*

The results of the students, as the first part, where we applied the problem-solving scheme, and the second part, where we did not apply it, are summarized in Table 3.

**Table 3.** Percentage of students with structured solutions for two problem-solving methods (solution scheme vs. traditional approach)

| % of students / Methods | Percentage of students with well-structured and well-argued solutions | Percentage of students with a moderately structured and argued solution | Percentage of students with no structured and argued solutions |
|---|---|---|---|
| Problem solving with a scheme | 51.7% | 31% | 17.3% |
| Problem solving using the traditional method | 25% | 32.1% | 42.9% |
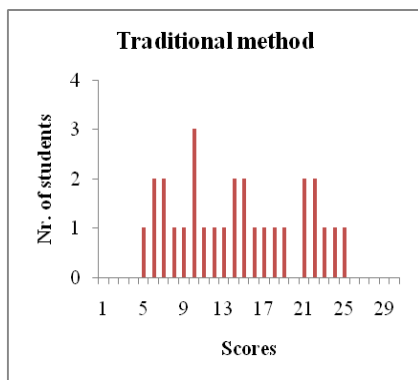


a)
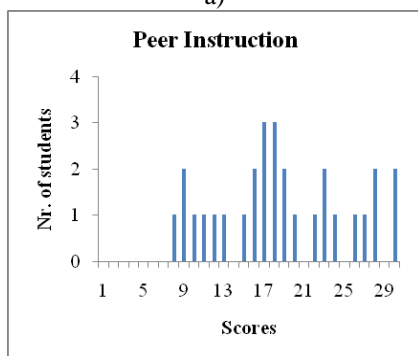


b)

**Fig. 8.** ConcepTest evaluation based on scores of students for traditional method vs. those taken from Peer Instruction.

The results show a higher percentage of students with structured and well-balanced solutions from a conceptual point of view when applying a problem-solving scheme.

### *Laboratories*

The results obtained in laboratories are summarized in Table 4.

Peer technique tracking significantly improves student performance in labs by 7.8% higher than the average of the group's estimation, which is not only lacking in traditional methods, but there is a decrease in the group's average of 4% from the initial estimate.

### CONCLUSIONS

- The active participation of students in discussions with each other spoiled the inevitable monotony of passive lectures. It significantly improved their performance.

- Assimilation of information increased significantly compared to traditional methods.

- Immediate feedback is given to the conceptual understanding of students.

- Troubleshooting with the help of the scheme helps the conceptual learning process. Also, the logical organization of problem-solving stages expanded students' knowledge and made them applicable in new contexts.

**Table 4.** Evaluation at the end of semester for the two laboratory groups working and not working with the Peer Instruction

| PEER INSTRUCTION | | | TRADITIONAL METHOD | | |
|---|---|---|---|---|---|
| Students | Evaluation at the beginning of semester | Evaluation at the end of semester | Students | Evaluation at the beginning of semester | Evaluation at the end of semester |
| Stud. 1 | 9 | 10 | Stud. 1 | 5 | 5 |
| Stud. 2 | 7 | 9 | Stud. 2 | 10 | 9 |
| Stud. 3 | 7 | 7 | Stud. 3 | 7 | 7 |
| Stud. 4 | 8 | 9 | Stud. 4 | 6 | 6 |
| Stud. 5 | 10 | 10 | Stud. 5 | 8 | 7 |
| Stud. 6 | 5 | 6 | Stud. 6 | 9 | 9 |
| Stud. 7 | 7 | 8 | Stud. 7 | 7 | 7 |
| Stud. 8 | 8 | 8 | Stud. 8 | 8 | 7 |
| Stud. 9 | 9 | 9 | Stud. 9 | 8 | 8 |
| Stud. 10 | 9 | 9 | Stud. 10 | 5 | 5 |
| Stud. 11 | 6 | 6 | Stud. 11 | 10 | 9 |
| Stud. 12 | 7 | 7 | - | - | - |
| Mean | 7.6 | 8.2 | Mean | 7.5 | 7.2 |
| Standard deviation | | 1.34 | Standard deviation | | 1.4 |

REFERENCES

1. E. Mazur, Peer instruction: A user's manual, 1st ed., Pearson Education Limited, p. 10, 101, 1997.
2. I. Prifti, A. Prifti, Practical theoretical course of Physics, Erik, Tirane, **1**, p. 139, 2001.
3. M. Dede, F. Vila, , Complex problems in Physics stimulate the independent work of students (2nd National conf. of Physics, Science Academy, Tirane, 1989.
4. M. Dede, F. Vila, On the conception and logical scheme of the complex physics problem's solution, Proc. 1st General Conf. of BPU, Thessaloniki, Greece, 1, 26 (1991).
5. J.D. Wilson, C.A. Hernàndez-Hall, Physics Laboratory Experiments, 8th ed. p. 173, 2014.
6. S. Tobbias, Revitalizing Undergraduate Science Education: Why Some Things Work and Most Don't, Tucson, AZ: Research Corporation, 1992.
7. D. Hestenes, M. Wells, G. Swackhamer, *Phys. Teach.* **30,** 141 (1992).
8. D. Hestenes, M. Wells, G. Swackhamer, *Phys. Teach.* **30,** 159 (1992).

# The problem solving method and the research needed to transmit the new sets of knowledge in physics

S. Marko\*, L. Kelo, E. Guliqani

*[1]Department of Mathematics-Informatics-Physics, Faculty of Natural and Human Sciences, University of Korça, Blvd. Rilindasit 11, Korça, Albania*

If the basic principle defining that "Science gets valued from organized knowledge" is properly respected, then the levels of a whole set of student work outcomes like motivation, interest, differentiated work and effectiveness regarding physics classwork, will increase significantly. From this point of view the results achieved by each student, cultivated during the learning process, will arise to a whole new degree. Cultivating the will to study natural sciences, especially physics, means organizing class work throughout independent student work, stimulating a sense of discovery for each student, not an inventorial one. The traditional type of lectures transmits only basic knowledge, without evaluating the real life situations. Also, it doesn't take into consideration a full scale analysis of the elements presented by a specific model, as well as extracting the needed equations for calculating the quantitative aspect of physical phenomena and their place in the laws of physics. Averaging doesn't count when evidencing knowledge. The use of interactive methods is supported by presenting a problematic or experimental case and its solution. The teacher, as a moderator, and the student, as an explorer, interact to discover the analysis of a specific problem, along with its ways of solving. This also includes hypothesis formulation, raising arguments and verifying them. Finally, a balanced report is created between the work of the student and that of a teacher. This report helps the student transform, from a simple listener, to an analyzer and determinant of the correct knowledge. The texts used in this branch of science should allow the use of such teaching methods. Such a method shapes consistent and connected knowledge to students by preparing the underlying foundation on which to develop in-depth studies in areas where physics has a priority role.

**Keywords**: Motivation, Differentiated work, Independent work, Problematic situation, Research, Knowledge.

## INTRODUCTION

Around us there is a reality that exists regardless of us. Physics is a human effort whose ideas were discovered and developed by people really engaged in a battle of real life issues.

The case that needs to be studied is determined by observing natural phenomena, through senses or instruments, followed by curiosity and re-examining the underlying observations. A simple description allows us to build models through which the nature laws, conditions and boundaries of their application are discovered and experimentally verified to the configuration of a sophisticated yet elegant reality model.

Under these conditions, building up hypotheses and certifying them allows us to build an independent theory that summarizes many observations in the general laws of physics. No method, no matter how perfect it is, can produce a qualitative result if the content of the material studied in the subject of physics is not treated organically and with all the necessary elements as it has been developed.

But what is really happening today with the teaching material that the students of the general secondary schools in Albania have to prepare?

Does this material meet the need for qualitative and sustainable learning of students after finishing high school? Does this material meet in the 3-year high school cycle, a continuation for the in-depth study of applied physics and theoretical knowledge in further undergraduate studies?

For our modest opinion, but based on a real analysis, we can painfully affirm that this teaching material provided by the governing bodies of Education in Albania leaves much to be desired. From 2009 until today, it has been operated with an old text that was implemented for the first time in the 2009-2010 academic year and continues to be in use today and onwards. This teaching material in physics in general secondary schools is more characterized by demand-supply market trends rather than by the content and the quality necessary for treating knowledge in physics. With the revision of the very large range and very low scientific quality of the articles in the market, in 2013-2014 only three texts were presented in English, with a non-appropriate language standard, for the content, quality and need of Learners to gain steady learning, to form habits and skills, to apply the

---

\* To whom all correspondence should be sent.
 E-mail: sotiraqmarko@gmail.com

learning knowledge in experimental practice, or applications in everyday life in the subject of physics. One of them is the text "Fizika 10-11, Prof. Dr. Zenun Mulaj, Dr. Bledar Myrtaj, "Erik" printing company, based on the original title: Complete Physics for IGCSE Student Book, Stephen Pople, 2014 (Part: 1,2).

In a general comparison we conclude that the quality of scientific, methodological and content treatment is lacking, evaluated in the possibility of scientific formation of a student at secondary school. The teaching material is not completely clear, to allow the preparation of a methodical structure planned to increase the effectiveness of the treatment of scientific knowledge in the classroom. The facts, concepts, rules, laws, theories, formulas, basic physical principles, to be elaborated to develop skills and concrete skills acquired by students are lacking. There is no logical connection between new and previous knowledge. In the working conditions with all students, a differentiated lesson cannot be organized.

There is no possibility of preparing a physics teacher to build a scientific and methodical teaching lesson whereby the logical connection of experimental facts, laws, principles and applications is realized that would enable the analysis of a problematic situation where the focus is action, conversation, differentiated work, accurate and correct presentation on the white board of all stages of the learning process.

*Just read the note at the bottom of the entry that says:*

When you are using this book, keep a look out for these marks:

A line down the side of the text means that the material is only required for Extended level. For simplicity, lines like this have *not* been put next for related diagrams or panels in the margin [1].

*Our assessment is based on:*

1. The syllabus and textbooks that have been developed in the subject of general physics in high school until 2006, [2-5] which:

Increase interest and motivate students;

Increase the effectiveness of each teaching lesson in physics in function of the purpose and objective of teaching;

Enable the implementation of differentiated work in addressing new knowledge and solving problematic situations with implementing character;

Provide an hour to encourage, satisfy, focus and evaluate the achievements of each student during the learning process;

Provide a satisfactory and qualitative assessment of students based on the merit-preference principle.

2. In the analysis of the results of the elective examination in physics, at the end of the senior year [6].

The data to analyze the results of the students in the subject of physics, at the end of the high school, on the State Matura exam, were taken referring to the first year of this procedure and the last three years. This choice is based on the fact that the teaching structure has undergone the changes listed below:
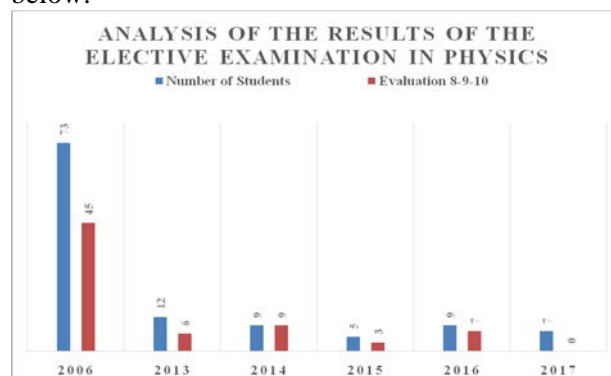


✓ For the academic year 2005-2006, the examination procedure was changed in the subject of physics without changing the curriculum. (*From 1988-1989 until 2004-2005 academic year, the appraisal of the graduates was done in written and oral examination in front of a school-based commission*).

✓ From the academic year 2007-2009, the assessment was done by the State Matura Exam but with the change of the teaching structure by dividing the students into classes directed towards social sciences and classes directed towards natural sciences.

✓ From 2009 to 2013, there was a curriculum for physics but many alternative texts with different content.

✓ From 2013 until now there are only three alternative texts, of which two are often chosen to be studied.

✓ Year after year, fewer students are choosing to pass the state exam in physics. This is due to fears of poor preparation in this subject, conditional preparation from the inappropriate text and the low amount of teaching hours dictated by the curriculum for this subject.

3. In the experience of teaching and learning by the authors of the preparation of this paper.

In the curriculum in accordance with the specific teaching material being considered, the presentation of the problematic situation, the discovery of contradiction, the formulation of the hypothesis, the determination of the ways of solution and the solution and control of the results, can be done by the teacher with a minimal activation of the students, creating an almost equal ratio between the work of the teacher and the work of the students or by the students themselves.

In modern didactics, a learning model is understood as a certain mode of action, which attempts to put the learner in a study situation, more or less as a recipe of accurate and scientific knowledge, observing all the steps of scientific research, up to finalizing implementation in practice. Physics should be treated as a science where the student gets full, intelligent, logical and attractive knowledge.

Without pretending that we will define the key points regarding the application of teaching and learning methods in the subject of physics, we would first point out the undisputed role of those methods that rely on:

a. Processing of material and technique of drafting and conducting questions;

b. Teaching Discussion;

c. Exploration Teaching, etc.

Naturally the question arises: Do these methods apply to all component elements, independent of each other, or combine their particular elements to run and organize a more effective and quality learning lesson?

To answer, we will try to analyze the lessons developed or prepared in practical form and elements of the methods described above:

*Topic: The Uniform Circular Motion, Centripetal Acceleration [7]*

1. After creating a working situation that has crowned the discussion of the concepts discussed in the previous topic and the application of knowledge gained in it, the teacher presents a very significant motive before the audience:

You know how to calculate (measure experimentally) the rate of free fall of a body on the Earth's surface. Can we determine the acceleration of the moon movement around the Earth?

2. After this, a problematic situation is created, coupled with the procedures to be pursued by the student.

We need to determine the acceleration value $|\vec{a}|$ of a material point that performs uniform circular motion.

For this you build a radius of $r$. Determine the location of a material point moving by the circular trajectory at $t_0 = 0$ at point A and point B at time t, recognizing that the time interval of the body's location during the arc development of the (AB) circle is infinitely small. By accepting the movement of the material point as a uniform circular motion, construct the vectors $\vec{v_1}$ and $\vec{v_2}$, respectively points A and B.

3. The student works independently by being checked by the teacher and at the same time the teacher reflects this situation in the table.

a) What do you think about acceleration?

b) What should we determine to find the numerical value of acceleration?

4. After receiving the answers and escalating the questions, for the student asked by the teacher, a new situation is created.

5. Determine the difference $\vec{v_2} - \vec{v_1}$, present the vector $\vec{v_2} - \vec{v_1}$ and its module. To find the module compare the triangles $\Delta OAB$, $\Delta BCD$ (in the figure). What is the result achieved?
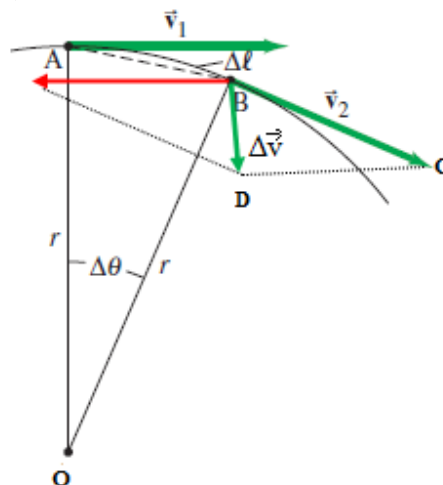


**Fig. 1**

6. After receiving and analyzing the result, the teacher compiles the questions:

7. Acceleration as physical size, how is it characterized?

8. What should we determine after getting the numeric value?

The situation flows freely without strain, with the student's activation led by the teacher with patience and creating situations.

9. Based on the figure, compare the angles formed by $\left( \vec{\Delta v} \overset{\wedge}{} \vec{r} \right)$ and the central angle. What will happen if $\Delta t <<<$? Where will B go? What

about the central angle? What about its half? What about $\overrightarrow{\Delta v}$-s direction?

*After a long-term discussion and timing of what is required, the conclusion is drawn and formulated.*

10. A new situation is followed by the teacher.

Present the vectors $\overrightarrow{v}_1$ and $\overrightarrow{v}_2$ for a rectilinear motion and then build $\overrightarrow{\Delta v}$. What can be said about the direction of the $\overrightarrow{\Delta v}$ during full motion. Can you derive a classification criterion for motion based on $\overrightarrow{\Delta v}$? A very valuable discussion is being started.

11. Then we build the vector $\overrightarrow{a}_{qs}$ for curved movements, as well as the solution to the example, so the motivation for this class and its respective objectives find a good answer.

Naturally, the answer is: In this class, all the elements of the methods described below are distinguished:

• Encouraging the curiosity and thinking of the student.

• Build a clear, comprehensible situation with cognitive and implementing elements. (Exploration Teaching); (2-5, 6)

• Rotate around the classroom, observe independent work, communicate individually, make sure students focus on their tasks, and check their work independently with relevant notes (Exploration Teaching).

• "If you want a smart answer, ask the right question."

✓ The response mode should be specified (not in the chorus). Use question, pause, call technique, and allow students time to respond, escalate the question according to the level of knowledge and according to the students.

✓ Do not judge the answer given by the student (do not give the correct answer to your question).

✓ Ask for a summary of the conclusions reached to help the active hearing:

♦ Please, can you generalize X's response?

♦ Freely seek the student's opinion.

♦ Allow and stimulate students to ask themselves questions (Processing of material and technique of drafting and conducting questions).

• Stimulating creative situations, raising interest, creating student leadership situations, student learning to protect the conclusion or discuss it, student learning to evaluate others' responses (Teaching Discussion).

• The teacher intervenes:

- when the next question is needed according to the specific situation and the purpose sought;

- when generalization is needed; when certain thoughts need to be interpreted without the judgment and discontinuation of students who are unable to give the right answer (Teaching Discussion);

• Designing and conducting challenging questions and situations (not "yes", "no" but "why" and "how many") (Processing of material and technique of drafting and conducting questions, Teaching Discussion).

*In conclusion:*

✓ The deeply scientific content organically associated with all the steps of scientific formation of students from the texts used in this branch of science;

✓ Uniformity and distribution of load and degree of difficulty without creating burdens on teaching and learning;

The structure of scientific material treated in Physics 1, 2, 3, 4 [2-5] which was used in four courses of "Raqi Qirinxhi" high school during 2002-2006, is matched with the most successful models such as: Frish, General Physics, Vol.1-2-3, I. V. Savelyev: A general Course Mechanics Molecular Physics I, Electricity and Magnetism Waves Optics II, Quantum Optics, Atomic Physics, Solid State Physics, Physics of the Atomic Nucleus and Elementary Particles, III, Mir Publishers Moscow.

This structure allowed the creation of sustainable knowledge of the students and this is evident in the results shown in Table 1.

**Table 1**. The number of students who have chosen, the State Matura exam, the science of physics from the two compulsory elective exams.

| Student Book | School year | No. of Students. | General Physics | Core Physics | Class C Total students. | Evaluation 8-9-10 |
|---|---|---|---|---|---|---|
| F1-F2-F3-F4 | 2006 | 73 | 73 | 0 | 17 | 45 |
| F1-F2-F3-F4 | 2013 | 12 | 0 | 12 | 0 | 6 |
| 3 - Student Book (Translating) | 2014 | 9 | 0 | 9 | 0 | 9 |
| 3-Student Book (Translating) | 2015 | 5 | 0 | 5 | 0 | 3 |
| 3-Student Book (Translating) | 2016 | 9 | 0 | 9 | 0 | 7 |
| The Complete Physics for Cambridge IGCSE Student Book | 2017 | 7 | 0 | 7 | - | - |

This results show that out of 73 students who opted for the exam physics that year, 17 are top grade students (converted to grade) nationwide. Yes, with the same dedication, a considerable part of them continue their studies at the best Universities in Europe such as the University of Rome-La Sapienza, Russia and so on.

What happens in the coming years? The results show a drastic drop in students choosing to give physics as an exam and a drastic drop in their structured knowledge also.

## CONCLUSIONS

Physics is not about "facts", not that the facts are irrelevant, but physics is more focused on discovering relationships and models than teaching the facts for their own sake.

Physics allows teacher independence in choosing the method that would unify:

- Postponing a problematic situation, clearly defining the objectives to be addressed in the lesson;

- The way of solving this situation in the contradiction between the knowledgeable and the unknown, which necessarily requires a combination of the student's independent work and the one led by the teacher;

- The way of discussion and conclusion, by stimulating the speech and the argument that the student gives;

- The practical application of physical knowledge in certain situations in solving the problems posed by the respective calculations and the interpretation of quantitative values found;

- Physical reasoning of the data (conditions) and results obtained (conclusions).

Creating a unique system in controlling students' knowledge, skills and habits as an important and necessary element of the physical teaching process.

Training to solve any task in physics, whether theoretical or practical, as a miniaturized scientific research process, a modest creative act, cultivating thinking and reasoning.

The ability to interpret knowledge in physics comes from practice, repetition, and effort until we "master" them, apply them in new situations. Often during the physics study the student will be confused, surprised to experience difficulties, but when success is achieved, excitement will be revealed with the joy of discovery.

Physics, as a technical body of knowledge, is important to many professions, but also physics is an exciting adventure of the human mind [8].

## REFERENCES

1. S. Pople, Complete Physics for IGCSE- Student Book, Preface (Part:1), 2014.
2. R. Mejdani, K. Qendro, N. Xhepa, Fizika 1, Tiranë, 1996.
3. R. Bezhani, P. Velaj, R. Mejdani, A. Dhimo, N. Thomo, N, Xhepa, Fizika 2, Naim Frashëri, Tiranë, 2002.
4. I. Prifti, K. Piti, Fizika 3, Tiranë, 1996.
5. R. Mejdani, K. Qendro, S. Çaushi, P. Skënde, Fizika 4, Tiranë, 1996.
6. Statistics Sector, at the Regional Educational Directorate (DAR), Korçë.
7. R. Mejdani, K. Qendro, N. Xhepa, Fizika 1, Tiranë, p. 63, 1996.
8. R. Knight, Physics for scientists and engineers with Modern Physics, Pearson Education, 2017.

# Non-formal education of physics including making devices for demonstration

G. Malchev

*Peyo Kracholov Yavorov High School, Petrich, Bulgaria*

The article views non-formal education of physics as an opportunity for upgrading knowledge, acquiring new skills and improving the personal and social qualities of students during their high-school education. The article offers an alternative form of education in the course of which students make their own devices for demonstrating harmonic oscillation in the 9th grade. It summarizes the importance of non-formal education namely as a way of enlarging the scope of students' intellectual properties and increasing their interest in science and engineering, which, in its turn, makes the learning process a desirable challenge.

## INTRODUCTION

In contemporary pedagogical reality education is efficient provided it is carried out in accordance with the interests of our present-day generation. The last few years have marked an alarming tendency for students to study less. This has become one of the basic problems of Bulgarian education, which rests on the shoulders of every teacher to solve the best way they can think of. That is why, he/she should refer to new and a bit more motivating means and methods to apply at school, so as to boost students' interest and develop their skills. A method which has firmly established itself as fruitful and efficient is incorporating students into the school subject matter through some extracurricular activities, which are part of the so-called non-formal education.

## WHAT IS NON-FORMAL EDUCATION ALL ABOUT?

Personally, education is related to the accumulation of knowledge and the development of certain skills, as well as to the acquisition of competences, and socially it has to do with the establishment of the person as a part of society. Education has three forms [1]:

a) The first one known as *formal education* has a levelled structure functioning from primary to university educational institutions. A student who has completed one level or has got qualification in accordance with this educational system gets a certifying document.

b) The second form known as *informal education* centers round education on the basis of life experience and with the participation of people, media, institutions which we happen to come across in our personal bubbles.

c) Particularly innovative has become lately the third form known as *non-formal education* in which, unlike the traditional formal system, activities are outside the structure framework. Non-formal education is achieved in clubs and courses, during seminars, at work, even through sport because of which it has become the object of much deserved interest. R. Valchev *et al*. point out several important characteristics of this education [2]:

- meets the needs of disadvantaged groups;
- sets target groups which include certain categories of people;
- is directed to a strictly defined goal;
- is rather flexible as regards the organization and the methods that are applied.

V. Gyurova dwells on the way non-formal and informal education relate to each other [3]:

a) *non-formal education* has to do primarily with the choice of activities and subjects. It is offered by schools (clubs, study circles, etc.), as well as by other institutions like foundations, associations, societies…;

b) *informal education*, also called parallel, has to do with the development of mass media as a relevant source of information and knowledge, which one way or another, influences the formation of beliefs and values depending on the intellectual properties and culture of different people.

In non-formal education, creative and innovative approaches are applied, together with familiar classical methods, to actively involve trainees in non-formal activities but with an important learning element. From the point of view of the learner, this is conscious learning, considers V. Bozhilova [4].

M. Eraut argues that non-formal education improves some personal qualities like critical thinking, inquisitiveness, creativity, leader skills, etc. They can be successfully combined with some social skills like capacity for communication,

---

* To whom all correspondence should be sent.
 E-mail: gmalchev@abv.bg

solidarity, justice, responsibility, etc. The combination of these two types of qualities contributes to the formation of a person of social intelligence capable of coping easily with his/her future educational and other activities [5].

D. Livingston thinks that, alongside formal, non-formal education is increasingly being structured – curricula are being developed, training is being developed within training modules, training is being certified and evaluated. Although these tendencies are different in both systems, they are the two sides of a common movement – integrating formal and informal education into a highly applicable hybrid [6].

In pedagogical practice during the last few years one can see blurring of the boundaries between formal and non-formal education. Nevertheless, G. Straka defines three criteria to differentiate formal from non-formal education [7]:

1) degree of educational planning of external conditions – i.e. to what degree these conditions contribute to the achievement of certain educational goals;

2) certifying – getting a certificate (or a document certifying a degree of education);

3) legalization of certificate.

These criteria manage to overcome the ambiguity of the standards used so far in Europe for differentiating and measuring formal, informal and non-formal learning.

In 2008 the first survey of non-formal education was published in Bulgaria. In it S. Nikolaeva on the one hand differentiates this education in terms of theory and practice, and states her reasons for her differentiation on the other. Non-formal education can hardly be defined only as the ideal, procedural or social anti-thesis of formal education. Actually, it is not so much a matter of anti-theses as of parallel elements, processes and sub-systems of the social system of "education", which all complete one mission and achieve common global aims often using the same means but in an alternative context [8].

To put it in a nutshell, non-formal education has its peculiarities in a systematic, contentional, organizational, technological, subject-oriented, result-driven plan. It lays an emphasis on volunteer work and choice, flexibility and adaptability, multifunctionalism and openness. That is a good enough premise for increasing students' motivation as well as for developing their organizational, creative, communicative among other skills.

Through informal learning, hard-to-learn science can become surprisingly accessible. For example, creative cognitive tasks develop the ability to better

understand physical phenomena and laws. By "seeing" the practical side of physics, they can clearly realize that it is not only a "dry" matter, but a fundamental and readily understandable science. In this way, students' desire to study nature, technology and space increases, and this has a positive effect on their motivation for future learning and practical realization.

## NON-FORMAL EDUCATION OF PHYSICS WITH MAKING DEVICES FOR DEMONSTRATION OF HARMONIC OSCILLATION

A form of non-formal education of physics was implemented in Peyo Yavorov High School, Petrich, in 2012. Four students in the 11th grade, divided into two groups constructed and made two devices for demonstration on the topic of Harmonic Oscillation, part of chapter Mechanical oscillation and waves, which is studied in the 9th grade. All the activities on the project took place in the classroom of physics after regular classes whereas the practice was realized in a carpentry workshop and an automotive repair shop again outside regular school hours. From the very start right to the end of the enterprise both groups worked with enthusiasm sharing ideas, offering constructive ideas. All four students had studied harmonious oscillation in their 9th grade, that is two years previously, and knew what exactly to show and how to do it by making the devices.

*The first device*, made by one of the groups has a main body unit, which consists of one horizontal basic plank and two other planks mounted vertically on the sides (fig.1). A graduated wooden scale is attached to them; above it a metal stick with a threaded ball is installed; it is fixed to the spring, which in its turn is fixed to the main body unit. With the stretching of the spring the ball starts moving under the force of elasticity, which is proportional to the deviation from its equilibrium point. Thus the device demonstrates harmonic oscillation. Besides, the scale can also measure the deviation of the ball so as the strength of the force and the acceleration typical for that movement to be estimated.

*The second device* made by the other team is of a wooden body unit and a side wooden plank (fig.2). A metal crank is installed in it with a cardboard disc attached to the front side; a table tennis ball is fixed onto the disc. An L-shaped plate is installed on the vertical plank right above the disc with a tiny lamp powered by battery. The crank makes the disc move steadily with a constant speed. Since the lamp illuminates it from above its shadow starts moving gradually along the horizontal plank. One full circle of the ball round the axis of the disc corresponds to

one full harmonic oscillation. Thus the device demonstrates that the projection of a body that rotates steadily performs harmonic oscillation.



**Fig. 1.** A device for demonstrating harmonic oscillation and for measuring the deviation of an oscillating body.



**Fig. 2.** A device establishing the analogy between harmonic oscillation and moving in a circle.

Both devices were displayed in section Demonstration and lab devices and machines for physics classrooms at the student contest **Devices for the classroom of physics**, organized by the Sofia branch of the Union of physicists in Bulgaria at the beginning of April, 2012 (fig. 3). The panel of judges awarded Donika Angelova and Stoyan Yankov **first prize in the category 9-12 class** for the making of the device for establishing the analogy between harmonic oscillations and moving in a circle.

CONCLUSION

Non-formal education is a preferred form of education by students, since it easily changes their attitude towards the educational contents studied at school. It is an object of interest because practically

it can be realized everywhere, it can cover different fields and make use of various means, as well as lead to a targeted motivation.

The basic conclusion the non-formal education of physics leads to is that this type of education enriches students intellectually, develops their skills and boosts their interest in science and technology. Thus studying becomes a yearned for challenge. In pedagogical practice the teacher of physics should deftly combine formal and non-formal education so that students can acquire knowledge better and for longer and give meaning to the studied physical processes and phenomena.



**Fig. 3.** Students of Peyo Yavorov High School, Petrich, presenting their devices in the foyer of the Faculty of Physics at St. Kliment Ohridski University of Sofia.

REFERENCES

1. V. Gyurova, Education in the World: Problems and Perspectives, Education and Qualification, Sofia, 1994.
2. R. Valchev, A. Pilavaki, L. Cherna, Introduction to non-formal education, EU Lifelong Learning Program, New Chance Project – training of non-formal education trainers, Sofia, 2009.
3. V. Gyurova, Andragogy, Universal Drumev, Sofia, 1998.
4. V. Bozhilova, *Annual journal of St. Kl. Ohridski University of Sofia, Faculty of pedagogy*, **105**, 203 (2012).
5. M. Eraut, *British Journal of Educational Psychology* **70**, 113 (2000).
6. D. Livingston, *NALL Working Papers* **21**, 1 (2001).
7. G. Straka, Informal learning: genealogy, concepts, antagonisms and questions, Institute Technology and Education, Bremen, 2004.
8. S. Nikolaeva, Informal education, Philosophies. Theories. Practices, Gabrovo, 2008.

# Cognitive problems for developing students' scientific literacy in their physics education

R. I. Vassileva

*Department of Physics, Faculty of Mathematics and Natural Sciences, South-West University,66, Ivan Mihailov Str., 2700 Blagoevgrad, Bulgaria*

The paper deals with one of the most topical issues related to school education – how to form and develop key competencies in natural sciences? A variety of strategies for the realization of this goal are explored and a focus is placed on the opportunities to solve context-based real-life problems. The author suggests custom-designed problems which can be used in physics education. They are in agreement with the requirements of the Program for International Student Assessment (PISA).

**Keywords:** Science education, Scientific literacy, Key competences, Context-based real-life problems, PISA

## INTRODUCTION

The acquisition of scientific literacy appears to be a main contemporary tendency in natural sciences education in the compulsory stage of school education. PISA defines scientific literacy as the ability of the student to engage conscientiously with natural sciences-related issues and thus to demonstrate:

➤ „Scientific knowledge and use of that knowledge to identify questions, acquire new knowledge, explain scientific phenomena and draw evidence-based conclusions about science-related issues.

➤ Understanding of the characteristic features of science as a form of human knowledge and enquiry.

➤ Awareness of how science and technology shape our material, intellectual and cultural environments.

➤ Willingness to engage in science-related issues, and with the ideas of science, as a reflective citizen."[1].

This definition is from 2006, when the research of PISA had put the accent on natural sciences for the first time. The concept of scientific literacy assessment was further developed and broadened in the following detailed research in 2015. Which are the main elements of scientific literacy under PISA 2015?

1. *Three basic science-related competences* accentuating the scientific approach to knowledge acquisition:
- Explaining scientifically natural processes and phenomena;
- Designing and evaluating scientific enquiry;

- Interpreting scientifically data and evidence.
2. *Context:* PISA assesses the ability of the students to apply the acquired competencies in *real-life context* using scientific and technological knowledge and skills.
3. *Attitudes:* PISA assesses students' attitudes by studying their interest in natural sciences and technologies, their understanding of the scientific approach and their responsible attitude to the environment.
4. *Knowledge:*
- *Content knowledge* (an understanding of the major facts, concepts and explanatory theories that form the basis of scientific knowledge of both the natural world and technological artefacts).

In terms of content, the knowledge assessed by PISA is grouped in three areas: physical systems (structure and properties of substances, chemical changes in substances, movement and strength, energy and energy transformation, interconnection between energy and matter); biological systems (cell, human, population, ecosystem, biosphere); Earth and Space (structure of the Earth, energy and energy resources).
- *Knowledge about science:*
- *Procedural knowledge* (knowledge of the procedures, methods and means used in the scientific research)
- *Epistemic knowledge* (understanding of the underlying rationale for these procedures and the justification for their use) [2, 3].

It is clear that what is defining for the contemporary natural sciences education is not only the subject matter that is going to be acquired in class and what the students must know, but also the skills, values and attitudes that must be formed. This is of paramount importance for the more flexible adaptation of the young people to their environment

---

* To whom all correspondence should be sent.
 E-mail: radostiv@abv.bg

and it is an essential factor for their full personal and professional realization in life. Therefore, solving the problem of the students' scientific literacy requires the use of the competence approach in organizing and putting into practice the natural sciences education.

The education practice has demonstrated a number of strategies for the development of key natural sciences competencies:

- Project-based learning
- Inquiry-based learning
- Hands-on activities
- Extracurricular activities – competitions, festivals, natural sciences olympiads, etc.
- Solving context-based real-life problems.

The present paper focuses on the last of the strategies above. A few cognitive tasks (type PISA) are offered, which have been created by the author specifically for physics education. They demand from the students to apply already acquired knowledge in new conditions – in the context of real-life situations.

## EXEMPLARY COGNITIVE TASKS IN REAL-LIFE CONTEXT

### Science example: Solar cooking
*Text 1*

According to the World Meteorological Organization, the total radiant energy received from the Sun at the upper limit of the atmosphere per unit of time per unit of area on a surface perpendicular to the Sun's rays is $1367 \, \text{W/m}^2$. It is called *solar constant* and it is the approximate average value of solar intensity for one year. Due to the movement of the Earth around the Sun in an elliptical orbit, the real solar intensity varies with $\pm 3\%$ of the value of the solar constant. Its maximal value is $1420 \, \text{W/m}^2$, when the Earth is closest to the Sun (perihelion of the Earth's orbit around the Sun), and its minimal value – $1325 \, \text{W/m}^2$, when the Earth is farthest from the Sun (aphelion).The solar constant determines the amount of direct solar radiation (DSR) that reaches the Earth's orbit. What amount of DSR will fall on a specific place of the Earth's surface, however, depends on a number of factors. One of them is the physical state of the atmosphere above the place.

*Task 1:* Point out which of the following process/es in the Earth's atmosphere cause/s weakening of the solar intensity:

o    The absorption of part of the solar radiation by the atmospheric gases.

o    The diffusing of part of the solar radiation by the air molecules and by the solid and liquid impurities (aerosols) in the air.

o    The reflecting of part of the solar radiation by clouds in the atmosphere.

o    All the processes above cause weakening of the solar intensity.

### Science example: Solar cooking
*Text 2*

The DSR reaching the Earth's surface is of practical significance for the functioning of the so-called solar cooking appliances. Fig. 1 shows a solar parabolic cooker (SPC) with a diameter of the reflector $D = 150 \, \text{cm}$.

The reflector has the form of a paraboloid and is covered with reflective foil, the purpose of which is to reflect the solar radiation falling on it with the highest possible reflection coefficient.



**Fig. 1**. Solar parabolic cooker.

The foil on the solar cookers has a normal reflection coefficient $R$ of 90%. Every SPC is actually a parabolic mirror. The solar rays parallel to the axis of the reflector reflect in it, after which they pass through the focus (Fig. 2).
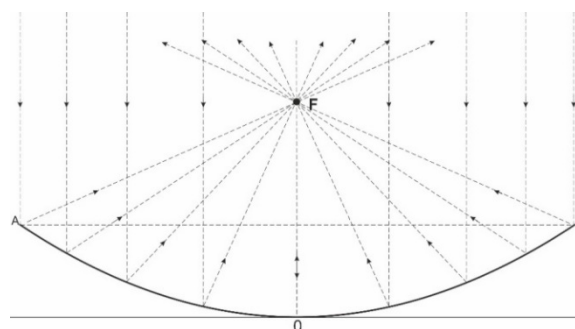


**Fig. 2**. Principle of action of the solar parabolic cooker (mirror): AB – diameter of the reflector; OF – focal distance.

Practically, the focus of SPC is a focal spot of small size, and it is not a point in the geometric sense

of the word. A metal container (a saucepan, a pan), put in the area of focus absorbs the radiant energy concentrated there, it is heated to a great degree and thus the process of cooking in the container is performed. The power of the SPC is determined by the formula

$$P = ES, \qquad (1)$$

where $E$ is the solar intensity and $S$ is the area of the mirror opening (called aperture).

*Task 2:* Calculate the heating time of $1\,\text{kg}$ of water at $20\,°C$ to $100\,°C$ with the solar cooker on Fig. 1, if you know that the solar intensity is $800\,\text{W/m}^2$ (we consider it constant for a period of time), and the container that holds the water absorbs $85\,\%$ of the radiant energy reflected in the parabolic mirror.

**Science example: Solar cooking**
*Text 3*

The maximal power of a given solar cooker for a particular location and day of the year is reached if the following three conditions are fulfilled simultaneously:

- Clear and dry weather;
- The Sun is in its climax, which is at noon;
- The mirror is positioned with its axis parallel to the coming Sun's rays.

*Task 3:* Explain the role of each of the mentioned conditions to reach to maximal power of the solar cooker.

**Science example: Solar cooking**
*Text 4*

The use of the solar cooker is most effective during those days of the year in which the Sun is highest above the horizon. In this case, the path of the Sun's rays through the atmosphere is the shortest and the weakening of the direct solar radiation is the least. The maximal height $h$ of the Sun for the day is determined by the formula:

$$h = 90° - \varphi + \delta, \qquad (2)$$

where $\varphi$ is the latitude, $\delta$ is the Sun's declination (the angle below which the Sun's rays cross the plane of the Earth's equator – Fig. 3).
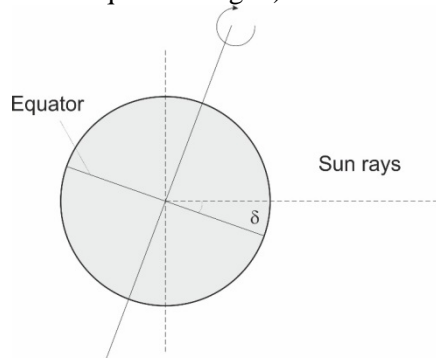


**Fig. 3**. Sun's declination.

As it is known, the values of the declination $\delta$ vary from $+23°27'$ (during the summer solstice on
74

June 22) to $-23°27'$ (during the winter solstice on December 22). The value of the declination is zero during the equinoxes.

*Task 4:* Use formula (2) and make a rough assessment of the potential possibilities of solar cooking in the following three countries: Germany, Bulgaria and Sweden considering the fact that the latitude of Germany is between 47 and 55° N, the latitude of Bulgaria – between 41 and 44° N and the latitude of Sweden – between 55 and 69° N.

**Science example: Solar cooking**

*Task 5:* Describe two advantages and two disadvantages of the SPCs.

It is important to mention that the effectiveness of using such type of tasks in the educational process can be enhanced if they are combined with elements from other strategies for forming key natural sciences competencies. In this particular case, demonstrations of cooking with the SPC from Fig. 2 were made for students from Blagoevgrad, as an extracurricular activity. Task 2 was tested experimentally. The necessary time for heating the water happened to be longer than it had been estimated theoretically. This provoked a discussion regarding the possible reasons for this result. A solar oven with a principle of action that is different from that of the SPC was also demonstrated.

CONCLUSIONS

The creation and use of real-life context tasks is not a novelty in physics education, however, such approach is particularly relevant regarding scientific literacy. The students are supposed to apply the acquired interdisciplinary knowledge and skills in real-life situations as they are searching for proof, drawing conclusions, providing arguments for their answers and making decisions. Thus they are convinced in the benefit of what is studied and develop very important skills – to find, analyze, transform and present various types of information. Therefore, the education helps the personal development of the students and this inevitably increases their motivation and interest in studying natural sciences.

REFERENCES

1. OECD, PISA 2006 Science Competencies for Tomorrow's World, Volume 1: Analysis, OECD Publishing, p. 34, 2007.
2. OECD, PISA 2015 Assessment and Analytical Framework: Science, Reading, Mathematics and Financial Literacy, OECD Publishing, Paris, 2016.
3. Ministry of Education and Science of Bulgaria, Natural sciences and technologies in school of the XXI century, Center for Control and Assessment of the Quality of School Education, Sofia, 2016.

# The role of using educational tasks in teaching chemistry

V. P. Dimitrova, M. E. Shekerliyska[*]

*South-West University Neofit Rilski, Blagoevgrad, Bulgaria*

One of the main purposes of modern education is building scientific literacy in students. Teaching chemistry provides a variety of opportunities for achieving this. An appropriate tool for acquiring literacy is the use of educational tasks. Research was conducted on implementation of such tasks in learning of chemical processes in the 10th grade. The results showed that systematic and purposeful application can lead to increased interest, development of skills for self-studying and building scientific competence.

**Keywords:** Chemistry, Education, Using educational tasks, Scientific competence.

## INTRODUCTION

An important goal of modern education is to develop and improve science literacy among students. Numerous studies of this concept and definitions proposed by Pella *et al*. [1], Miller [2, 3], AAAS [4], NRC [5], Hazen *et al*. [6], Bybee [7], DeBoer [8], OECD [9-11], Tafrova-Grigorova [12], NGSS [13], Kolarova *et al.* [14] allow us to summarize that a natural-literate person is the one who understands the scientific concepts, principles and processes, which helps in the understanding of scientific and technological achievements, as well as of the phenomena in the living and inanimate nature. A scientific literate society must be able to assess the impact of science and technology on people's lives and environment.

## EXPOSURE

Natural science literacy is undoubtedly related to the acquisition of knowledge, skills and competences that can address real life issues.

According to most authors, **competence** is *a quality of personality based on the presence of a significant amount of knowledge and skills obtained through system training and practical experience in a certain theoretical or practical field.* Educational competence is achieved thanks to the continuous efforts of the participants in the education [15].

It can be summed up that the individual competences are set in the educational targeting, and the general educational competence is manifested as a personal characteristic, "the ability to form and exercise in a unity well-structured knowledge, value engagement and effective actions, optimally and necessarily manifesting itself in a specific application through adequate skills" [15].

In this sense, the expected results in the State educational requirements for curriculum and syllabuses can be considered as elements of the overall general educational competence. The set of competences related to scientific literacy, acquired, conceived and practicable in real situations, leads to the formation of specific science competences for student 1, student 2, etc. (Fig. 1).
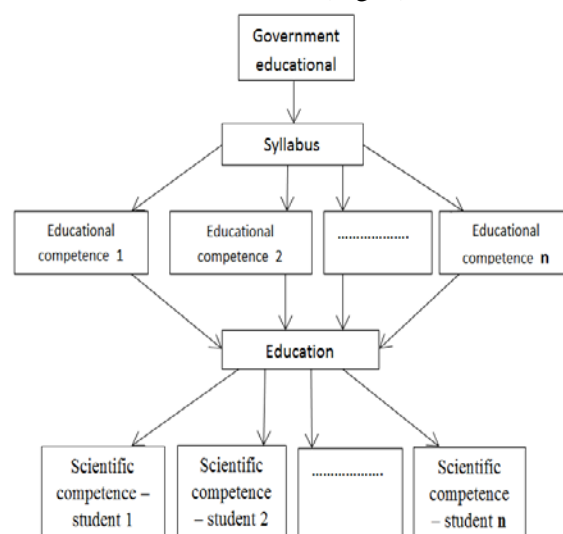


**Fig. 1.** Integration map - State Educational Requirements – Scientific Competence

A new type of specialists - symbol analysts who have basic skills: abstraction, systemic thinking, experimentation and collaboration are of particular importance to modern society. The formation of such skills is a factor that will be the basis of the success of society [16]. Unfortunately, the analysis of the results of the national and international surveys shows that Bulgarian students do not have systematic thinking, cannot extract and convert information from texts, graphics, tables and images, cannot find regularities and draw

* To whom all correspondence should be sent.
E-mail: megi.shekerliyska@hotmail.com

conclusions from given results. The lessons learned in school are forgotten for a few weeks. This is only the visible symptom of a deep illness that is rooted in the previous programs. The training in scientific disciplines is no longer suitable for the society, which citizens should be prepared for [17].

Bulgarian teachers say: "The curriculum and the syllabuses are 'overloaded' compared to the planned schooling time, which leads to a small number of hours for consolidation. As a result, pupils' knowledge, skills and competences can be limited to SER because they are superficial and chaotic" [12].

One of the possible options for overcoming this condition is the use of **active and interactive methods** in learning, which, unlike the traditional approach, saves time for teaching new learning content. It is presented through certain assignments, which the student independently attains, making the necessary comparisons, analyzes and generalizations. **Learning tasks** can be considered to be such a type of assignment. These are the tasks through which students learn new knowledge, rediscover and create scientific truths [18]. In solving them, previously acquired theoretical knowledge is applied, which stimulates and develops cognitive activity and autonomy, creates a constructivist learning environment.

According to J. Bruner, the constructivism-based learning is an active process in which learners construct new ideas and concepts based on their previous knowledge, with new cognitive structures (mental, logic constructions) providing new experience and enabling a person "to take action beyond what is available" [19].

In a survey of pupils' opinion on chemistry training at school a large number of respondents declare willingness to study in a constructivist learning environment by solving tasks and case studies based on real life situations. Half of the students share the opinion that the hours for practical tasks, including laboratory exercises, should be increased. 93% of the students say they approve of the use of additional tasks besides the content of the textbook they are taught at school. In their view, this is the way to acquire more long-lasting and in-depth knowledge [20].

All mentioned above directed our attention to studying the possibilities of applying teaching-cognitive tasks to chemistry education, the requirements for their compilation and the conditions for solving in order to improve students' learning achievements.

The aim of this paper is to highlight some opportunities for the role of learning-cognitive tasks in chemistry training for the formation and development of natural science competences.

First of all, we should highlight the expected results set in the legislative documents - State Educational Requirements for Educational Content and Syllabuses. Accordingly, the learning content is determined, which is appropriate for presentation through learning-cognitive tasks. A task specification is drawn up and only then follows its compilation with regard to Bloom's taxonomy for expected natural-science competencies. Learning tasks include elements of textbooks containing facts, concepts or laws, data in tabular or graphical form, substance or process models, apparatus diagrams, and more. The tasks are formulated clearly and unambiguously, independently of each other. Depending on the level of the expected result, the points for each assignment are determined, which allows an adequate assessment and self-assessment of the student's achievements. For example:

*Section: "Solutions and chemical reactions in aqueous solutions"*
*Topic: "Electrolyte Solutions"*

| Evaluated expected results: | Knowledge level |
|---|---|
| To explain the acidity and alkalinity of aqueous solutions with a concentration of hydrogen and hydroxide ions in them and relate them to the pH value. | Understanding Application |
| To evaluate the importance of acidity and alkalinity of aqueous solutions for the flow of life processes. | Application |
| To analyze data from a chemical experiment to determine pH of solutions. | Analysis |

*Task:*

According to the theory of electrolytic dissociation, acids are electrolytes that dissociate in aqueous solution to hydrogen cations and acidic anions.

*A. Express the electrolytic dissociation of HCl, HNO$_3$ and H$_2$SO$_4$. Which ions are their common properties due to?*

*B. Express the electrolytic dissociation of NaOH, KOH and Ca(OH)$_2$. What are the common*

*ions in the aqueous solutions of these compounds? Define the concept of bases under the theory of electrolyte dissociation.*

The number of moles of hydrogen cations which are removed from one mole of acid determines its alkalinity, and the number of moles of hydroxide anions that are removed from one mole of base determines the valence of the base.

*C. The substances are: HBr, NaCl, Ba(OH)₂, H₂SO₃, LiOH, MgCl₂. Determine which ones are acids and which are bases. Indicate one monovalent base and one dialkali acid.*

The properties of the aqueous solutions of the electrolytes are determined by the concentration of the hydrogen cations. These values are very low and it is not convenient to work with them. It is accepted that the acidity of the medium is expressed not by the concentration of hydrogen cations itself but by the negative logarithm of it, called pH indcator.

*For example:*
$c(H^+) = 10^{-4}$
$pH = -lg\ c(H^+) = 4$
At $c(H^+) = c(OH^-) = 10^{-7}$;
$pH = 7 \rightarrow$ neutral environment

*D. To one glass of clean water acid is gradually added, while to another glass of clean water base is gradually added. After each added portion, the pH value is measured. Using the experimental data shown in Fig. 2, determine which chart to which glass corresponds.*
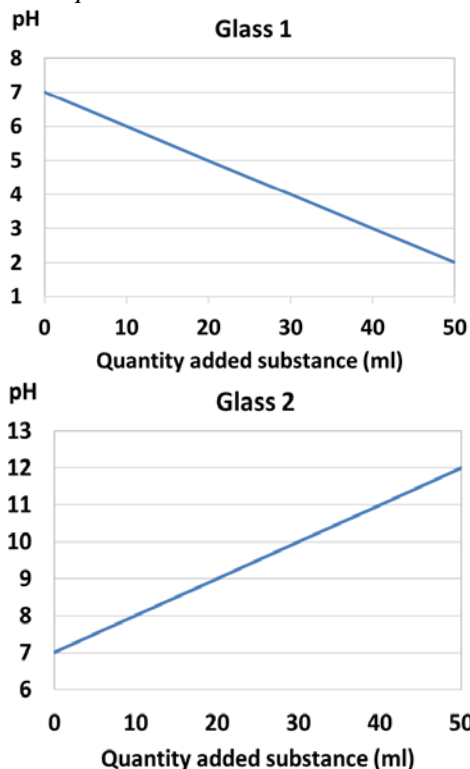


**Fig. 2.** Change in pH with addition of acid or base.

Figure 3 shows the pH values of some solutions.
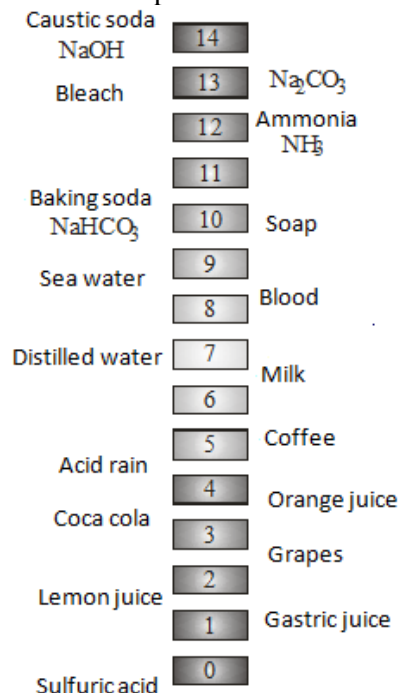


**Fig. 3.** pH values for some solutions

*E. How is the violet litmus colored in orange juice? What environment does the reported change show?*

*F. How is phenolphthalein stained in a bleach solution? What environment does the reported change show?*

*G. Which of the two substances - coca cola or baking soda solution should be taken with increased acidity of gastric juice?*

*H. The pH value for normal human skin is about 5.5. Is it convenient to use soap for its daily hygiene? Justify your answer.*

Tasks of this type are primarily designed for classroom work. Students work in pairs without the use of aids. The teacher is their mentor. Tasks requiring additional data or more time for responses are appropriate for extra-curricular work. It lacks teacher's support and teamwork, so they must be as clear as possible with precisely defined assignments. In both cases, the student actively learns, formulates knowledge and develops his / her skills to work with texts, graphics, tables, images, patterns, schemes, etc.

Searching for the answer, students teach themselves by discussing different options for reaching the decision. They clarify the relationship between the given and the sought-after and construct a plan, draw a scheme by which they reach the ultimate goal.

In the implementation of the plan the pupils pre-decode the given information. As a result, they de-

velop practical and mental activities, modelling skills are formed [21]. The transformation of the given data leads to reflexive skills as the students "go through conscious intermediate judgments" [22]. In this way, practical and mental activities are developed leading to a final result resembling real life situations.

These actions effectively lead to "embedding" the most essential information "in the value-meaning sphere of the students' consciousness and become a permanent personal knowledge" [23].

CONCLUSION

It can be summed up that the use of learning-cognitive tasks in the training allows for:
➢ Increasing the interest in natural sciences;
➢ Active and interactive learning;
➢ Application of constructivist method;
➢ Development of:
  - Reflexive skills;
  - Modelling skills;
  - Skills to deal with life problems;
  - Evaluation and self-evaluation skills.

As a result of the present study on the role of the cognitive tasks in chemistry and environmental protection to develop students' natural sciences, the following findings can be made:
✓ In order to meet the educational requirements, learning and cognitive tasks must be compiled in accordance with the normative documents.
✓ The development of pupils' scientific competence should be accomplished through gradual formation and improvement of individual educational competences.

It is appropriate to develop learning-cognitive tasks for different purposes: for part-time individual work in class; for self-employment outside the classroom; for entirely independent work in class - through worksheets, interactive boards or the use of computer presentations. Learning assignments can be used in different chapters in chemistry education and in combined science lessons.

REFERENCES

1. M. O. Pella, G. T. O'Hearn, & C. W. Gale, *J. Res. Sci. Teach.,* **4**, 199 (1966).
2. J. D. Miller, *Daedalus*, **112**(2), 29 (1983).
3. J. D. Miller, Civic scientific literacy in Europe and the United States. Annual Meeting of the World Association for Public Opinion Research, 1 (2006).
4. AAAS [American Association for the Advancement of Science] Science for all Americans: a project 2061 report on literacy goals in science, mathematics and technology, Washington: AAAS (1989).
5. NRC [National Research Council], National science education standards. Washington: National Academic Press, 1996.
6. R. M. Hazen, J. Trefil, Science matters. Achieving scientific literacy, New York, Anchor Books Doubleday, 1991.
7. R. W. Bybee, Achieving scientific literacy: from purposes to practices,Portsmouth, Heinemann, 1997.
8. G. E. DeBoer, *J. Res. Sci. Teach.*, **37**, 582 (2000).
9. OECD [Organization for Economic Co-operation and Development], Assessing scientific, reading and mathematical literacy: a framework for PISA, Paris, OECD Publishing, 2006.
10. OECD [Organization for Economic Co-operation and Development], Assessing scientific, reading and mathematical literacy: a framework for PISA Paris, OECD Publishing, 2009.
11. OECD [Organization for Economic Co-operation and Development]. PISA 2015 draft science framework, Paris, OECD Publishing, 2013.
12. Tafrova-Grigorova, M. Kirova, E. Boyadgieva. Teachers in natural sciences for scientific literacy, Himia, Sofia, Bulgaria, 2011.
13. NGSS Lead States, The next generation science standards: for states, by states. Washington: National Academic Press, 2013.
14. T. Kolarova, I. Hadjiali, M. Dokova, V. Aleksandrov, Natural science literacy of the students at the beginning of the XXI century – looking for conceptual unity, Natural Sciences in Education, Sofia, **2**(26), 2017.
15. V. Velikova, Educational competence as a result of educational activity, in: Pedagogics, **6,** Sofia, Bulgaria, 2003.
16. S. Angelova, Possibilities for the formation of skills in biology teaching, Natural Sciences in Education, Sofia, 2013.
17. Tafrova-Grigorova, Modern trends in natural science teaching of students, Natural Sciences in Education, Sofia, p. 123, 2013.
18. V. Shivacheva, Person-oriented teaching in school, EKS-Press, Bulgaria, p. 128. 2011.
19. J. Bruner, Review of the psychological theories underlying the distance learning. https://sites.google.com/site/teoriipsihologii/001-teorii-2/teorii/12-konstruktivizm-constructive-theory-j-bruner (October, 2014).
20. M. Shekerliyska, V. Dimitrova, Study of students' opinion on chemistry teaching in school, Natural Sciences in Education, Sofia, p. 560, 2015.
21. N. Tsankov, *Chemistry*, **21**(3) (2012).
22. M. Shekerliyska, Educational-cognitive tasks in chemistry and environmental protection for the formation of reflexive skills, Strategies of educational and scientific politics, Sofia, Bulgaria, p. 183, 2016.
23. J. Dimova, *Chemistry*, **11**(5), Sofia, Bulgaria, 2002.

Section

*Physics and Technical Sciences*

# Study of residual radioactivity in fish and fishery products imported into Bulgaria from China, Vietnam, Japan and Norway

L. Direkov

*South-West University "Neofit Rilski", Blagoevgrad, Bulgaria*

In the last few years - 2012 - 2014, in Bulgaria, fish and fish products are massively imported from the regions of China, Vietnam, Japan and Norway. As we know in these areas, especially in the zone 61, which is adjacent to the nuclear power plant Fukushima, where there was a global nature disaster in 2011(7 degrees on the scale of INES), there was mass infection with radioactive substances of the Pacific water, plankton, algae and fish. Contamination of the Pacific water with radioactive substances. It was extremely dangerous in the initial period after the accident, but after this as well, mainly after 2015.

**Keywords**: fish, radioactive, Fukushima, Pacific water, Strontium-90, plankton, nuclear reactors.

## INTRODUCTION

In the last few years - 2012 - 2014, in Bulgaria, mass imported fish and fish products from the regions of China, Vietnam, Japan and Norway. As we know in these areas, especially in the zone 61, which is adjacent to the nuclear power plant Fukushima, where there was a global emergency in 2011(7 degrees on the scale of INES), there was mass infection with radioactive substances of the Pacific water, plankton, algae and fish. Contamination came from the Pacific water with radioactive substances It was extremely dangerous, during the initial period after the accident, but also and after this, especially in 2015 years.
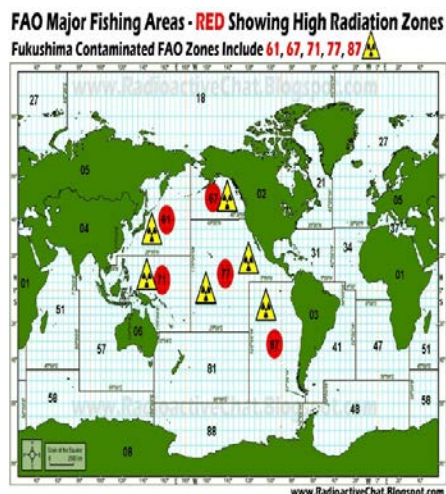


**Fig.1.**Fishing zone 61

The characteristic features of the three main species of fish that are widely imported into Bulgaria are the following:

**Scomber** (Scomber scombrus) is one of the most widely consumed fish in the world. In our country it is widespread and popular because it is at a very affordable price, especially frozen, imported from China. Mackerel is a marine fish of aerodynamic shape, the most widespread in the Atlantic Ocean and its associated seas - the Baltic Sea, the Mediterranean and others.



**Fig.2. Scomber** (Scomber scombrus)

The Black Sea mackerel spends the winter in the Sea of Marmara, and it can be seen in Bulgaria Black see in the period April- September. It is known as chirz and is back in September-January. This fish is more fed and with a higher quality. In Bulgaria, mackerel is available in any state - from freshly caught to frozen, whole, cleaned, without heads, only fillets; Smoked, salted, preserved in vegetable fat or tomato sauce "Breakfast" and "Ropotamo". Mackerel has great health benefits and beneficial properties. First of all, we must note that this type of fish contains in significant quantities the mineral substances - potassium, phosphorus, fluorine, sulfur, zinc, chlorine, sodium, as well as the whole spectrum of vitamins B, omega-3 fatty acids. The condition of the skin, the work of the heart, the brain, and the nervous system. As a powerful antioxidant, Omega-3 helps to strengthen membranes of the body's cells at the expense of neutralizing free electrons. These are radicals that can break the walls of the cells and

---

* To whom all correspondence should be sent.
 E-mail: luboad@abv.bg

disrupt their activity, resulting in a number of diseases.

**Pangasius** (Pangasius) is a silver-plated fish with a flat head and a horizontal mouth, often referred to as a silver shark. Adult specimens are quite impressive in size, reaching up to 1.5 m in length. The natural range of the species is the Indo-Kid's pools of Mekong, Chao Praia and Meklong, where this fish is a very important fishery resource.



**Fig.3. Pangasius** (Pangasius)

Since its cultivation is relatively easy, and the ever-increasing world demand for fish products makes it a major export commodity for Vietnam. Which is also the world's largest producer of pangasius with over 3500 tons a day. Production rates are steadily rising and this raises concerns about the emergence of different environmental and social problems. From a culinary point of view, the Pangasius is considered part of the so-called white fish group. It is a pronounced freshwater species that is also evident in its chemical composition - the notorious polyunsaturated omega 3 fatty acids are many times less. Otherwise, his meat is white, tender, slightly grainy and has a sweet and fine taste. Pangasius in Bulgaria and worldwide is sold exclusively in the form of frozen fillets without skin.

**Salmo** (Salmo salar) Salmon is born in freshwater, and when young salmon are big enough to cope with the salinity of the sea, they migrate. The so-called alpine salmon occupies the northern Atlantic and the rivers that flow into it.



**Fig.4. Salmo** (Salmo salar)

Different Pacific salmon live mainly in the Northern Pacific Ocean and its associated rivers. In 1960, Norway created the first marine farms, which are floating cells in the fjords. The salmon that grows here takes about 2 years. This is the time it takes to reach the market size (about 2 pounds). Since it is a carnivorous fish, salmon feeds on fishmeal and butter (50%), and contains other ingredients such as plant meals and extracts (cereals, legumes, soybeans), vitamins, mineral salts as well as astaxanthin (a natural or synthetic pigment) vital to her health, which gives her the distinctive character color. The color of salmon changes with age due to hormonal influences. Salmon grows up to a maximum length of 1.50 meters and can weigh up to 35 kg.

Salmon, which is grown in the kennels, can be known on its characteristic spine fins, which are curved, unlike the normally developed wild salmon fins. The most distinctive feature of salmon is the color of the meat, which is light red to pink. In commercial chains, the salmon fillet is sold either without head or packed in vacuum packs. Today, the main salmon producing countries in these methods are Norway, Chile, and Canada. Norway's fish catches $ 4 billion a year and is second only to oil.

Salmon is a rich source of healthy proteins. Omega-3 fatty acids are beneficial to heart health. They prevent blood clotting, irregular heart rhythm and lipid profile by increasing the level of good cholesterol and lowering blood triglycerides. Salmon is also rich in vitamin B12 and niacin. Niacin helps to lower cholesterol levels and B12 favors the work of the heart. Salmon maize is able to reduce the inflammation and pain associated with osteoporosis and arthritis.

## EXPERIMENTAL

When severe accidents occur in energy or experimental nuclear reactors, large amounts of radioactive isotopes, such as iodine - 131, cesium - 137, strontium - 90, and so on, are extremely dangerous to humans. Although iodine - 131 has a relatively short decay period (about 8 days), it accumulates significantly in algae, plankton, sea and ocean waters and their inhabitants. Strontium - 90 has a half-life of 28 years and, as an analogue of calcium, mainly accumulates in the bones of the animal organisms where it resides for a long time. Cesium - 137 has a half-life of 30 years and mainly accumulates in the blood and soft tissues of seafood and ocean occupants. The present study aims to establish the presence of radioactive substances in fish and fishery products imported in Bulgaria in excess of the limit values from the fishing and breeding areas of China, Japan, Vietnam and Norway. About six months ago, various samples of fish mackerel, pangasius, salmon and fish canned from mackerel "Breakfast."

The samples were purchased from the retail chains located in the region of Blagoevgrad and tested in the laboratory "Environmental Radiation Analyzes" y Spectrometer - 20 050



**Fig. 5**. Spectrometer radiometric analyzes 20 050.

The results of these studies are as follows:

**Table 1.** Specific activity of the samples in November 2016.

| № of the sample | Date of sampling and analysis | Type (name) of the sample | Sample activity - Bq / kg |
|---|---|---|---|
| 1. | November 2016 | Mackerel from China | 580 |
| 2. | November 2016 | Pangasius from Vietnam | 460 |
| 3. | November 2016 | Salmon from Norway | 412 |
| 4. | November 2016 | Canned "Breakfast" | 390 |
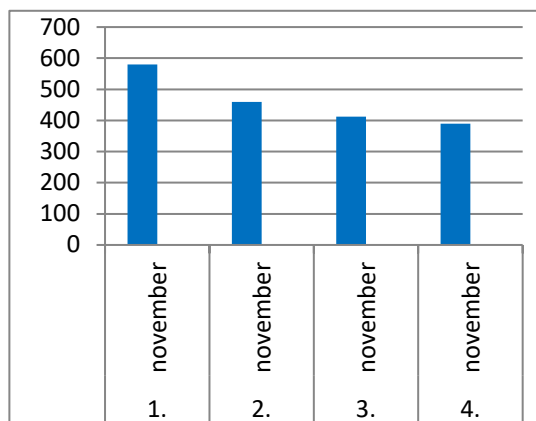


**Fig. 6.** Specific activity of the samples in November 2016.

**Table 2.** Specific activity of the samples in February 2017.

| № of the sample | Date of sampling and analysis | Type (name) of the sample | Sample activity - Bq / kg |
|---|---|---|---|
| 1. | Fvebruary 2017 | Mackerel from China | 529 |
| 2. | February 2017 | Pangasius from Vietnam | 587 |
| 3. | February 2017 | Salmon from Norway | 492 |
| 4. | February 2017 | Canned "Breakfast" | 410 |
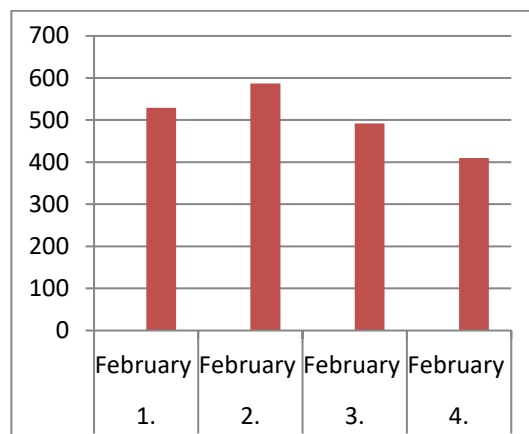


**Fig. 7.** Specific activity of the samples in February 2017.

**Table 3.** Specific activity of the samples in April 2017.

| № of the sample | Date of sampling and analysis | Type (name) of the sample | Sample activity - Bq / kg |
|---|---|---|---|
| 1. | April 2017 | Mackerel from China | 556 |
| 2. | April 2017 | Pangasius from Vietnam | 527 |
| 3. | April 2017 | Salmon from Norway | 462 |
| 4. | April 2017 | Canned "Breakfast" | 431 |
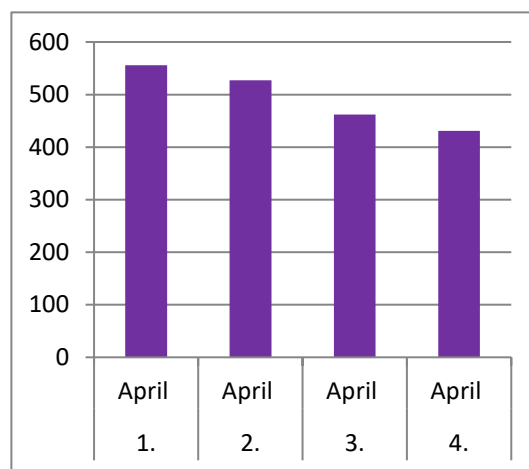


**Fig.8.** Specific activity of the samples in April 2017.

CONCLUSIONS

1. The results obtained show that in analyzed samples of fish and fishery products, none of them have activity above the limit values.

2. The activity closest to the limit values is the activity in mackerel samples taken in a fishing zone 61 close to the Japanese Fukushima nuclear power plant in which a global accident occurred in 2011.

3. Since radioactive substances with relatively longer half-lives are accumulated in the waters and underwater plants in this Pacific region, periodic radiological analyzes should be carried out after catches of fish and other ocean and seafarers.

REFERENCES

1. L. Direkov. Protection of human health and environment under extreme conditions.13-26(2005).
2. EU Council regulation (Euratom) 2016/52.
3. L. Direkov, Chemical and radiation analyzes in the environment. 107-115(1996).
4. EU Maximum permitted levels of radioactive contamination of food.(2015).
5. EU Health and Food Audits and Analysis.(2016).

# Study of residual stresses during electron beam welding of alloyed steels using neutron diffraction

P. Petrov[1], D. Kaisheva[1,*], G. Bokuchava[2], I. Papushkin[2]

[1]*Institute of Electronics of the Bulgarian Academy of Sciences, 72 Tzarigradsko Chaussee, 1784 Sofia, Bulgaria*
[2]*Frank Laboratory of Neutron Physics, Joint Institute for Nuclear Research, 6 Joliot-Curie Str., 141980 Dubna, Russia*

In this work the results from studies of residual stresses of plates of alloyed steel welded using electron beam welding technology (EBW) are presented. The chemical composition of the first and the second welded plate is respectively (wt %): 0.11% C; 0.27% Si; 1.35% Cr; 0,6% Mn; 3,25% Ni and 0.08% C; 1% Si; 2% Mn; 0.045% P; 0.03% S; 8-10.5% Ni; 18-20% Cr. EBW was carried out on the ESW300 / 15-60 welding units manufactured by Leybold-Heraeus at the Institute of Electronics – BAS. The technological parameters of the EBW process were the following: accelerating voltage $U = 60$ kV; beam current $I = 50$ mA, welding speed $V = 0.5$ cm/s; 1 cm/s; 2 cm/s, focusing lens-specimen distance $D_0 = 38$ cm. The measurement of residual stresses was carried out at the Laboratory of Neutron Physics of the Joint Institute for Nuclear Research - Dubna, Russia. The flow of neutrons obtained by pulsed fast reactor IBR-2 was used. The diffraction spectra were obtained on a Fourier stress diffractometer FSD, located on the channel №11a of the reactor. The temperature fields in EBW of both of the alloyed steels were calculated.

**Keywords:** Residual stresses, Neutron diffraction, Alloyed steels, Temperature fields

## INTRODUCTION

As a result of the local heating during welding and the non-uniform temperature distribution residual stresses and distortions occur in the welded joint. They can significantly reduce the quality and reliability of the welded components [1]. Fig. 1 presents schematically the changes in the temperature - stress diagrams for the different cross-sections of a plate when the weld is not instantly realized over the entire length [2, 3]. In the cross-section A-A before the heat source, the temperature is constant and is assumed to be zero, and there are no stresses. The cross-section B-B, just after the welding source, is the most heated one. The temperature in the weld and the heat- affected zone (HAZ) rapidly increases, inducing compressive stresses there, since the cold regions of the base metal prevent their free expansion. These stresses are relatively weak, because the metal heated to a very high temperature has a low yield stress. In accordance with the counter-balance conditions, these weak compressive stresses cause weak tensile stresses in the adjacent cold regions. Since the yield stress in the heated zone is low, compressive plastic strains are induced. Over the cross-section C-C the joint is mainly in a cooling phase. The maximal temperatures and the temperature gradients decrease. The compressive stresses turn into tensile, since the heated metal has the tendency to shrink, which is prevented by the adjacent zones. When the tensile stresses reach the yield stress for the respective temperature, tensile plastic strains form, which partly compensate the compressive plastic strains accumulated during heating. After complete cooling of the last cross-section considered, D-D, the longitudinal residual tensile stresses remain at the yield stress, and the adjacent zones of the welded joint remain compressed. The total residual longitudinal strain corresponds to a decrease in the plate length. The stress diagrams obtained are typical for metals without phase transformation during the welding process [3].

In accordance with the above, the main reason for the occurrence of the welding stress is the uniform distribution of the temperature field in the cross section of the welded samples. In the practice for the investigation of the residual stresses and distortions during welding there are two approaches: experimental and numerical modeling.

The mathematical methods allow obtaining relatively quick results of the final state and of the thermo-mechanical history. However, the precision of the results strongly depends on the exactness of the mathematical modeling of the welding process. Because the welding process and the resulting mechanical mechanism are very complex, many physical phenomena have to be taken into account. The accuracy of the numerical simulation of welding depends on the precision of the mathematical modeling of the heat input and the thermo-mechanical behaviour [2, 3].

---
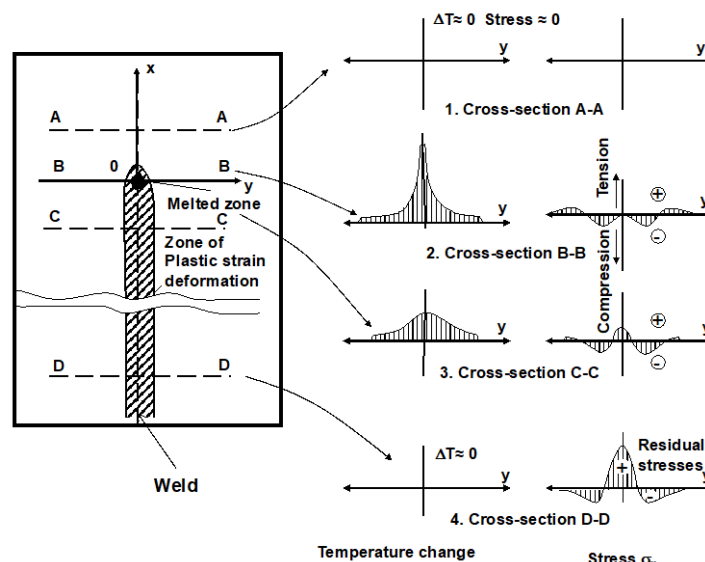
**Fig. 1.** Schematic presentation of the changes in the distribution of the temperature and longitudinal stress during welding of the plate [2]

The experimental investigations are very expensive and costly in terms of time (time-consuming). The results display only the final state without monitoring of the material behaviour during the process. The experimental methods can require a local or complete destruction of the objects. Residual stresses can be measured by various destructive or non-destructive methods [4].

The neutron diffraction method [5, 6] has a number of advantages over other methods, such as: preservation of the integrity of the studied sample, as the method is non-destructive; large depth of penetration of neutrons and a possibility for measuring to a large depth - up to 6 cm for steel and up to 10 cm for aluminum; possibility to measure macrostresses and microstresses; possibility to study samples of a random shape; high resolution of the gauge volume in the sample - up to 1 mm in any direction; possibility to determine the deformation in different directions of the crystal and to study the pattern of anisotropy of the deformation in different planes [hkl]; possibility to study the distribution of stress for each phase of multiphase material separately; high resolution of the diffractometer and possibility to measure relative deformation close to $10^{-3}$-$10^{-4}$; high accuracy for stress determination - 20-40 MPa (10 MPa - for aluminum, 30 MPa - for steel, 15 MPa - for titanium); possibility to estimate

microstresses, density of the dislocations and spot defects in the material *via* analyzing the shape and width of the diffraction maxima [7, 8].

In this work residual stresses of alloyed steels during electron beam welding were measured by the neutron diffraction method. Results from theoretical calculation of the temperature fields during electron beam welding are presented too.

EXPERIMENT AND MODELING

The welded specimens of two kinds of steel (chrome-nickel steel X5CrNi18-10 and constructive alloyed steel 12XH3A) were examined. Electron beam welding (EBW) was carried out on the ESW300/15-60 welding units manufactured by Leybold-Heraeus at the Institute of Electronics "Acad. E. Djakov", Bulgarian Academy of Sciences, Sofia, Bulgaria.

The technological parameters of the EBW process were the following: accelerating voltage $U = 60$ kV; beam current $I = 50$ mA; welding speed $V$ from 0.5 to 2 cm/s; focusing lens – specimen distance $D_0 = 38$ cm.

Table 1 contains data on the chemical composition of the studied samples. Table 2 contains data on the thermophysical parameters of the studied materials, which were used for calculation of temperature fields.

**Table 1**. Chemical composition.

|  | Element | C | Si | Cr | Mn | Ni | P | S |
|---|---|---|---|---|---|---|---|---|
| 12XH3A | w,% | 0.11 | 0.27 | 1.35 | 0.6 | 3.25 |  |  |
| X5CrNi18-10 | w,% | 0.08 | 1 | 18-20 | 2 | 8-10.5 | 0.045 | 0.03 |

**Table 2**. Thermophysical parameters.

|  | $\lambda$, W/(mm.K) | $\rho$, kg/m$^3$ | $C$, J/(kg.K) | $a$, mm$^2$/s |
|---|---|---|---|---|
| 12XH3A | 0.0270 | 7680 | 540 | 6,510 |
| X5CrNi18-10 | 0.0215 | 7920 | 550 | 4.936 |

*Experimental Residual Stresses Distributions*

Residual stresses in welded specimens were measured at the Frank Laboratory of Neutron Physics, Joint Institute for Nuclear Research, Dubna, Russia on a Fourier stress diffractometer (FSD) [7, 8] on a fast pulsed IBR-2 reactor. FSD diffractometer is dedicated for residual stress studies in bulk industrial components and new advanced materials. A fast Fourier chopper for the primary neutron beam intensity modulation and the RTOF method for data acquisition make it possible to obtain high resolution neutron diffraction spectra $\Delta d/d \approx 4\times10^{-3}$.

Internal stresses existing in a material, causing respective lattice strains, result in shifts of Bragg peaks in the diffraction spectrum. This yields direct information on changes in interplanar spacing in a gauge volume, which can be transformed into data on residual stresses, using known elastic constants of a material:

$$\frac{(d_{exp}-d_0)}{d_0} = \frac{\Delta a}{a_0} \approx \frac{\sigma}{E} \qquad (1)$$

where $d_{exp}$ is the measured interplanar spacing, $d_0$ is the same interplanar spacing in the sample without internal stresses, $\Delta a/a_0$ is the strain as the relative change in the unit cell parameter of a material, $E$ is the Young's modulus of a material, and $\sigma$ is the stress.

The principle of determining the crystal lattice strain is based on the Bragg's law, showing the condition of diffraction maximum:

$$n\lambda = 2d_{hkl}sin\theta \qquad (2)$$

where $\lambda$ is the neutron wavelength, $d_{hkl}$ is the interplanar spacing, and $\theta$ is the Bragg angle or the angle of incidence and scattered rays, $n$ is an integer.

When using TOF diffraction method at a pulsed neutron source, the strain is determined by the relative change in the neutron time of flight $\Delta t/t$. Depending on the neutron wavelength, the peak position on the time scale is defined by the condition:

$$t = \frac{L}{v} = \frac{\lambda m L}{h} = \frac{2mLd_{hkl}sin\theta}{h} \qquad (3)$$

where $L$ is the total flight distance from a neutron source to the detector, $v$ is the neutron velocity, $m$ is the neutron mass, $h$ is Planck's constant.

Hence, in case of TOF neutron diffraction the lattice strain is determined as:

$$\varepsilon_{hkl} = \frac{d_{hkl}-d_{hkl}^0}{d_{hkl}^0} = \frac{\Delta t}{t} \qquad (4)$$

where $d_{hkl}$ and $d_{hkl}^0$ are the interplanar spacings for strained and unstrained lattices, and $t$ is the neutron time of flight.

*Modeling of Temperature Fields*

During EBW the heating of the material is due to the kinetic energy being given to the metal from an electron flow with a power density above $5.10^6$ W/cm$^2$. The accelerated electrons penetrate into depth and, as a result of their interaction with the metal atoms, a melting and evaporation process starts. This forms a vapor-gas channel, called "keyhole". The power of the source $Q$ [W] is determined by the accelerating voltage $U$ [kV] and the beam current $I$ [mA]: $Q = U.I$. We assume that the power of the source is distributed between two separate moving sources. The first source is a point source that moves on the surface of the metal and its power is $Q_1 = 0.1\,Q$. The second one is a linear source and it moves inside the metal with a thickness equal to the depth of the molten pool. Its power is $Q_2 = 0.9\,Q$. According to the models of moving point and linear sources [9, 3] based on solving the thermal conductivity equation, the temperature at a certain point and a certain moment can be determined using the following equations:

$$T(x,r,\infty) - T_0 = \frac{Q_1}{2\pi\lambda r} e^{-\frac{v(x+r)}{2a}} \qquad (5)$$

$$T(x,r,\infty) - T_0 = \frac{Q_2/h}{2\pi\lambda r} e^{-\frac{vx}{2a}} K_0\left(\frac{vr}{2a}\sqrt{1+\frac{4ab}{v^2}}\right) (6)$$

where $r$ is the radius-vector, $v$ is the welding speed, $\lambda$ is the heat conductivity, $h$ is the depth of weld, $a$ is the thermal conductivity, $b$ is the coefficient of heat transfer, $K_0(u)$ is the modified Bessel function of the second kind of order zero.

RESULTS AND DISCUSSIONS

Fig. 2 shows the position of coordinate system axiss in relation to the sample for clarity. The specimen is moving along the X-axis. Because of the relative motion we can see that the electron beam moves along the surface of the sample and the displayed coordinate system moves along with the source. The residual stresses are measured along the Y-axis. The temperatures are calculated along the X-axis for different values of the Y-coordinate.
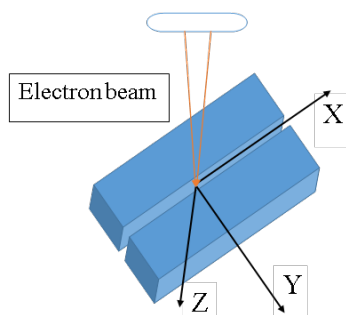
**Fig. 2.** Coordinate system associated with the moving source.

The measured diffraction spectra were processed using the Rietveld method. As a result of these analyses the lattice parameter values dependency *versus* interplanar distance $d_{hkl}$ were obtained. The residual stresses tensor components in the studied specimens were determined from the obtained lattice parameter values. The dependences of residual stresses from the X-coordinate (across the welding joint) are presented on Figs. 3 - 8.
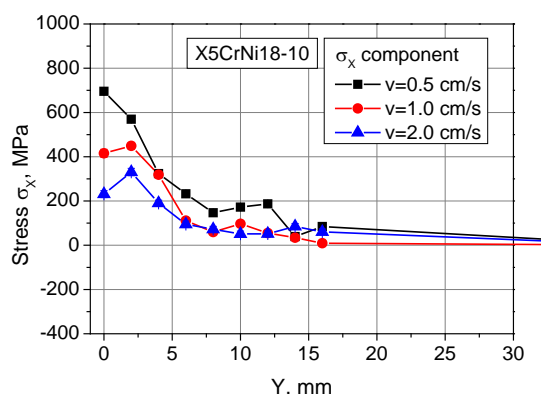


**Fig. 3.** X-components of residual stress in the studied EBW specimens from X5CrNi18-10 steel during scanning along Y-coordinate across welds for welding speeds V=0.5 cm/s, V=1 cm/s and V=2 cm/s.
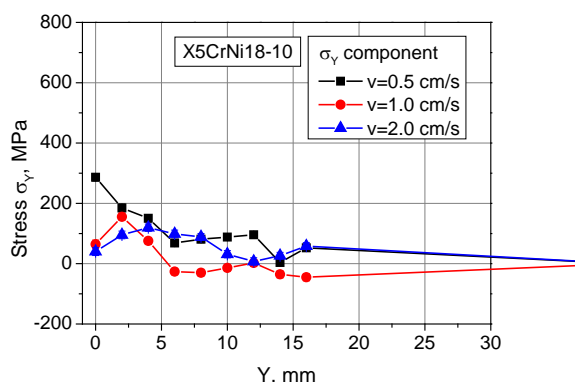


**Fig. 4**. Y-components of residual stress in the studied EBW specimens from X5CrNi18-10 steel during scanning along Y-coordinate across welds for welding speeds V=0.5 cm/s, V=1 cm/s and V=2 cm/s.
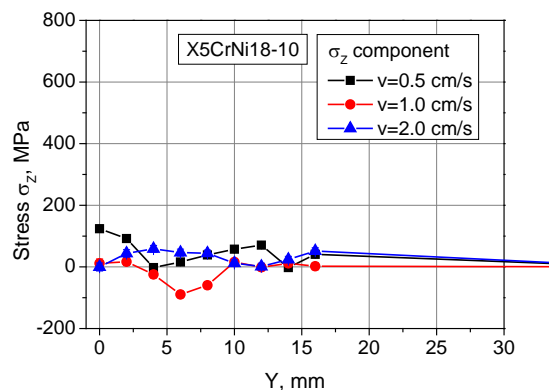


**Fig. 5.** Z-components of residual stress in the studied EBW specimens from X5CrNi18-10 steel during scanning along Y-coordinate across welds for welding speeds V=0.5 cm/s, V=1 cm/s and V=2 cm/s.
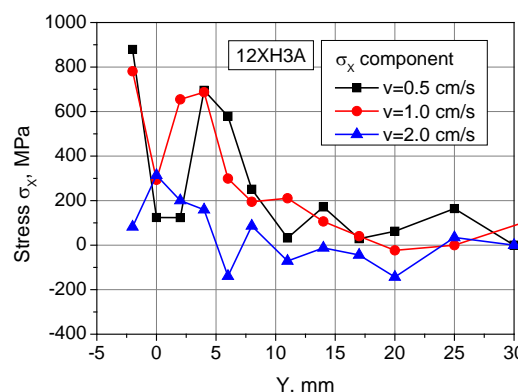


**Fig. 6**. X-components of residual stress in the studied EBW specimens from 12XH3A steel during scanning along Y-coordinate across welds for welding speeds V=0.5 cm/s, V=1 cm/s and V=2 cm/s.
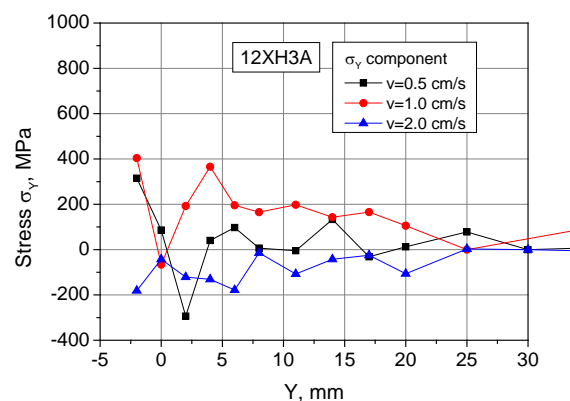


**Fig. 7**. Y-components of residual stress in the studied EBW specimens from 12XH3A steel during scanning along Y-coordinate across welds for welding speeds

V=0.5 cm/s, V=1 cm/s and V=2 cm/s.
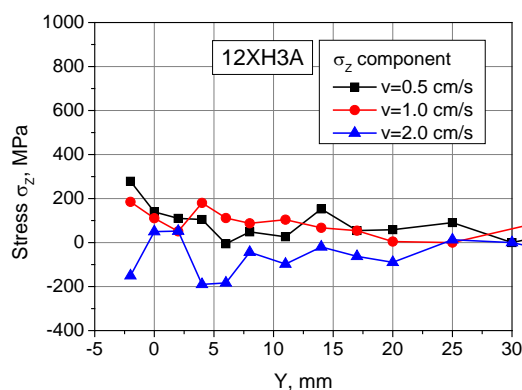


**Fig. 8**. Z-components of residual stress in the studied EBW specimens from 12XH3A steel during scanning along Y-coordinate across welds for welding speeds V=0.5 cm/s, V=1 cm/s and V=2 cm/s.

Residual stresses with alternating signs, i.e. compressive and tensile, are observed. The highest values of the stress are close to the welding seam. They are of the order of 870 MPa for the chrome-nickel steel and of 700 MPa for the constructive one. The residual stresses strongly depend on the electron beam parameters of welding (accelerating voltage, beam current, welding speed). The highest residual stress value is obtained at the lowest welding speed, because the sample receives more energy per unit time at a lower speed.

The calculated temperature cycles for the specimen from X5CrNi18-10 steel is presented on Fig. 9. It shows the change of temperature in the direction of the source movement, respectively in time. At a lower source speed, heating to higher temperature and slower cooling are observed. The closer to the weld seam certain point, the higher is the temperature. Due to imperfections of the model, the temperature at points very close to the source converges to infinity.
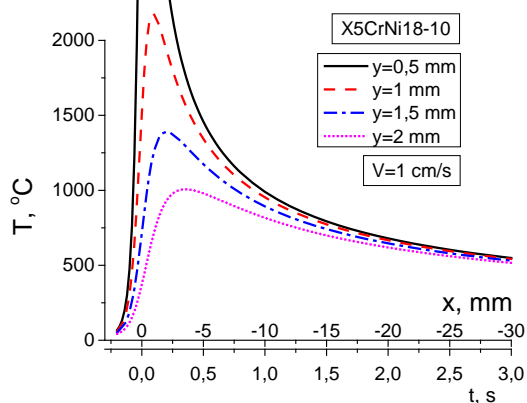


**Fig. 9.** The temperature distribution on X-axis and on time-axis for the studied EBW specimens from X5CrNi18-10 steel along X-coordinate for welding speed V=1 cm/s.

The data from the temperature cycles were used to obtain the dependence between the maximum temperature and Y-coordinate. These dependences for the specimen from X5CrNi18-10 steel for three different welding speeds are shown on Fig. 10.
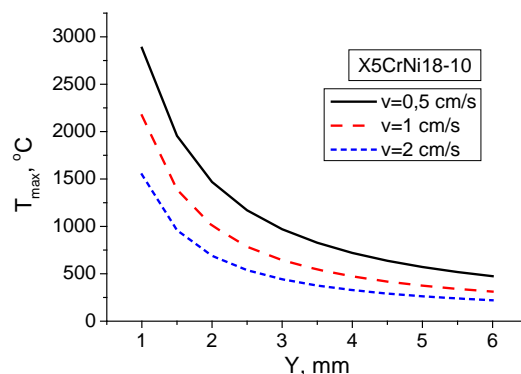


**Fig. 10**. The dependence between the maximum temperature and Y-coordinate for welding speeds V=0.5 cm/s, V=1 cm/s and V=2 cm/s.

The temperature fields for 12XH3A steel are very similar to these of X5CrNi18-10 steel. There are small differences due to different thermophysical parameters.

The calculated data of the temperature field for EBW specimens from X5CrNi18-10 steel presented on Fig. 10 show a very high temperature gradient along the coordinate axis Y. This is the main reason for the experimentally obtained stresses, which are shown on Figs. 3-5. Similar results were obtained for EBW 12XH3A steel.

CONCLUSION

The residual stress distributions in the flat plate alloyed steel specimens during electron beam welding with different welding speeds were determined using a non-destructive neutron diffraction method. The residual stress level is significantly dependent on welding speed that allows optimization of the welding process by selecting appropriate parameters. The temperature distribution during electron beam welding of alloyed steel shows high gradients which directly affect the residual stresses.

REFERENCES

1. D. Radaj, Welding Residual Stresses and Distortion: Calculation and Measurement, second ed., Elsevier, München, 2003.

2. K. Masubuchi, Analysis of welded structure, Pergamon Press, New York, 1980.
3. V. Mihailov, V. Karhin, P. Petrov, Fundamentals of welding (In English), Polytechnic University Publishing, St. Petersburg, 2016.
4. N. S. Rossini, M. Dassitsi, K. Y. Benyounis, A. G. Olabi, *Mater. Design*, **35**, 572 (2012).
5. A.J. Allen, M.T. Hutchings, C.G. Windsor, *Adv. Phys.*, **34**, 445 (1985).
6. L. Pintschovius, in: Measurement of Residual and Applied Stress Using Neutron Diffraction, M.T. Hutchings, A. D. Krawitz (eds.), NATO ASI Series E No 216, Kluwer, Dordrecht, 1992.
7. G.D. Bokuchava, V. L. Aksenov, A. M. Balagurov, E. S. Kuzmin, V. V. Zhuravlev, A. P. Bulkin, V. A. Kudryashev, V. A. Trounov, *Appl. Phys. A- Mater.*, **74** [Suppl. 1], 86 (2002).
8. G. D. Bokuchava, A. M. Balagurov, V. V. Sumin, I. V. Papushkin, *J. Surf. Invest.- X-ray*, **4**, 879 (2010).
9. D. Rosenthal, *Weld. J.*, **20 (5)**, 220 (1941).

# Improved multisoliton compressor

## L. M. Ivanov

*Department of Physics, Faculty of Mathematics and Natural Sciences, South-West University, 66 Ivan Mihailov Str., 2700 Blagoevgrad, Bulgaria and*
*Institute of Electronics, Bulgarian Academy of Sciences, 72, Tsarigradsko chaussee Blvd., 1784 Sofia, Bulgaria*

A fiber optic laser pulse compressor, consisting of two fibers, one with positive and the other with negative dispersion of group velocities for the same wavelength, was investigated. This compressor combines the positive sides of the known fiber grating compressor and multisoliton compressor and can be viewed as modified and improved variant of the multisoliton compressor. A numerical model was made to examine the parameters of the proposed compressor and determine the conditions at which the highest compression degree is obtained. The optimal length of the additionally added fiber with positive dispersion which gives maximum compression was determined. A comparative analysis was made between the classic multisoliton compressor and the proposed scheme with improvements. The proposed method is suitable for pulse compression within the spectral range $1.3 − 1.5$ μm, where fibers with positive as well as with negative dispersion can be produced using one and the same material.

## INTRODUCTION

Compression of optical pulses is one of the important areas of laser physics because the generation of super-short optical pulses allows to study the super-fast processes in chemistry, physics, biology and so on. Fiber-optical methods for laser pulse compression are one of the most powerful techniques because the optical fibers have the ability to maintain high energy densities at very long distances [1].

The compression of optical pulses in all types of compressors is done as follows. First, the pulses are spectrally broadened and then compressed to temporary lengths determined by their spectral bandwidth.

Within the spectral range of positive dispersion of the group velocity in quartz fibers the so-called fiber-grating compressor is usually used [1,2]. In this type of compressor the input pulse first passes through an optical fiber with positive group velocity dispersion where it is spectrally broadened due to the self-phase modulation [3]. After that the pulse is compressed up to the time duration determined by its spectral bandwidth in a pair of gratings which works as an optical line with negative dispersion.

Within the spectral range of negative dispersion of the group velocity the method" multisoliton compression" is used [1,4]. The compression is performed due to the mutual influence of the self-phase modulation and of the negative dispersion of the fiber. This type of compressor consists only of a piece of fiber with negative dispersion whit appropriate length. As it is well known, in this case the pulse periodically changes its shape and its duration. So if we take a fiber with an appropriate length the output pulse will be much shorter than the input pulse.

The main advantage of this method is its simplicity. The disadvantage is the appearance of a broad pedestal, where most of the energy is concentrated. The reason for this is the simultaneous flow of the processes of the spectral broadening of the pulses due to the Kerr non-linearity and the compression of the pulse due to the negative dispersion. Thus, it is impossible to obtain a linear chirp all over the optical pulse but only within its central part and as a result only a small part of the full energy remains within the compressed pulse and the other goes to the pedestal.

Such a combination of both techniques was first applied in [5] and then improved in [6,7].

Recent progress in technology and performance of fibers, especially of fibers with a shifted dispersion allows producing a fiber with positive as well as with negative dispersion at some fixed wavelength, for example for $\lambda = 1.4 \mu m$. It is possible because fibers dispersion is the sum of the material and the waveguide dispersion. On the other hand, waveguide dispersion depends on the refractive index profile. It means that the change of dispersion may be done by changing the refractive index profile of the fiber.

---

\* To whom all correspondence should be sent.
E-mail: mihovli@swu.bg

For the first time the idea to use a fiber with negative dispersion after a fiber with positive dispersion in order to compensate the dispersion pulse broadening in optical communication lines is proposed in [8]. Now it is broadly used and is known as "dispersion management".

In our previous work [9.10] we have proposed a new type of compressor which consists of successively connected fiber with positive dispersion and fiber with negative dispersion (Figure 1). In the first fiber with positive dispersion we expect a spectral broadening of the pulses due to self-phase modulation and a temporal broadening due to the positive dispersion. We also hope to improve the linearity of the frequency chirp. In this sense the first fiber is intended to help the process of multisoliton compression performed in the second fiber with negative dispersion and to improve the compression rate and the quality of the received pulses.

The present work is aimed to investigate the parameters of the proposed compressor - the length of the used fibers and the dispersion module ratio which gives the maximum increase of the compression degree.

*Numerical model*

Analysis of the nonlinear dynamics of the pulse propagation in single mode optical fibers is performed by the standard split-step Fourier method [11,12] in numerical solving of the nonlinear Schrödinger equation [1]. In the numerical model we assume that the transition between both fibers is realized without any changes of the transverse size of the radiation and the optical connector is of sufficient quality as a result of which the optical losses of the transition from one to the other fiber can be neglected. Because the lengths of the used fibers do not exceed a few tens of meters we also neglect the optical losses in both fibers.

It is taken into account that the dispersion for both fibers differs not only by the sign but by its module. As a result, we will write the equation for an evolution of temporal and of frequency pulse parameters in the first fiber:

$$i\frac{du}{d\xi} - \beta^* \frac{1}{2}\frac{d^2u}{d\tau^2} + |u^2|u = 0 \qquad (1)$$

Also for the second optical waveguide we have:

$$i\frac{du}{d\xi} + \frac{1}{2}\frac{d^2u}{d\tau^2} + |u^2|u = 0 \qquad (2)$$

Normalization is made following the standard approach and concerns the initial pulse parameters and the dispersion module of the second fiber which is with negative dispersion. There

$$u = \sqrt{\frac{\gamma\tau_0^2}{|\beta_2^-|}}A \qquad L_D = \frac{\tau_0^2}{|\beta_2^-|} \qquad \tau = \frac{t - z/v_g}{\tau_0}$$

$$\beta^* = \frac{|\beta_2^+|}{|\beta_2^=|} \qquad (3)$$

Here $A$ is the slowly varying amplitude of the pulse envelope, $\gamma$ is the coefficient of nonlinearity, $\tau_0$ is the initial pulse width, $\beta_2^+$ $\beta_2^=$ are the group velocity dispersion parameters in the first and second fiber respectively, $L_D$ is the dispersion length, $v_g$ is the group velocity.

Such manner of normalization of the equation allows easier comparison of the compression quality for one and the same pulse using either the pure multisoliton compression or the method proposed by us. The initial pulse shape is assumed to be hyperbolic secant $\sec h(\tau)$ with energy corresponding to $N$ less than 15 solitons. Such an expression of the shape allows us to compare our obtained results with those from multisoliton compression studied by other authors.



**Fig. 1**. Improved multisoliton compressor

The qualitative advantage of the studied method compared to multisoliton compression is presented

on fig. 2. This figure shows the compression dynamics for the initial pulse with energy corresponding to a 10-soliton pulse.

Curve "a" is the compression dynamics in our optical compressor with dispersion ratio $\beta^* = 1.25$. Optimal compression conditions were selected. Curve "b" is the compression dynamics in a multisoliton compressor.
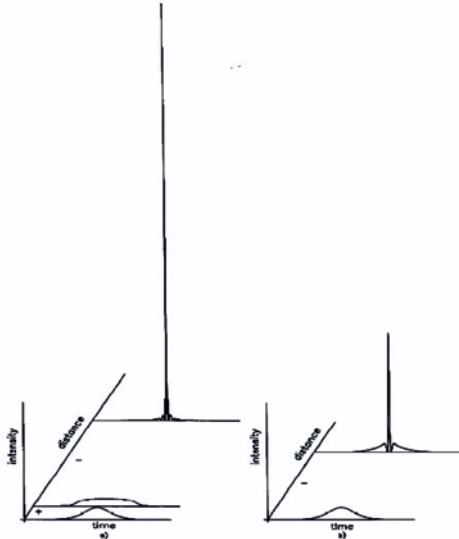


**Fig. 2.** Compression dynamics for the 10-soliton pulse following the here proposed method (a) and the pure multisoliton compression (b).

In the case of our optical compressor it is evident that the pulse in the first fiber acquires a nearly rectangular shape. This is due to the spectral broadening and to the linearization of the chirp of the whole pulse. When the chirped and spectrally broadened pulse passes through the fiber with negative dispersion, it compresses much more ion and peak power, increased nearly five times compared to the pure multisoliton compression.

## RESULTS

The quality of the compression is determined by the compression factor which is defined as a ratio between initial pulse duration and compressed pulse duration $F_c = T_o/T_{comp}$, where $T_o$ and $T_{comp}$ are the full width at half maximum (FWHM) pulse intensities of the initial and of the compressed pulse.

Several configurations of various ratios of the dispersion module of both fibers between 1.25 and 0.50 were investigated. To determine the optimal compression conditions, we proceed as follows. We fix the energy of input pulses (soliton number) and the dispersion ratio. Then we vary the length of the first fiber with positive dispersion and for each length determine the optimal length of the second

fiber with negative dispersion which gives the best compression degree. Thus, for the most suitable lengths of the two fibers we choose those that give the maximum degree of compression.

Our results show that we can approximate the optimal length of the first fiber by the expression:

$$z_{opt} = 0.46\, L_D\big/N$$

At this length of the fiber with positive dispersion and optimizing the fiber's length with negative dispersion we achieve the highest quality compression.

This result substantially differs from the optimal length of the fiber usable in the "fiber grating compressor" which can be calculated by the expression:

$$z_{opt} = 2.5\, L_D\big/N$$

Probably this is connected with the substantial difference between our proposed method and the fiber grating compressor. As a distinction of the pair diffraction gratings, the fiber of negative dispersion is an essentially nonlinear medium and there is a strong nonlinear impact on the pulse besides the compression.

The results for the dependence of the $F_c$ compression degree *versus* the soliton number and the dispersion ratio module for both pieces of fibers are given in Figure 3. The following dependence is observed for all the studied dispersion ratios $\beta^*$. Initially, the compression degree increases linearly with the energy of the input pulses (soliton number). Then, when some critical value is reached, a collapse and a sharp decrease in compression quality occur.

The occurrence of collapse is explained by the fact that in fixed $\beta^*$ and great pulse energies the phase modulation is so strong that the enrichment of the spectrum is very great. The linearity of the frequency modulation is disturbed and the negative dispersion of the second fiber cannot give qualitative compression.

The soliton number in which the collapse occurs, depending on the dispersion ratio, has a good approximation with the following formula:

$$N = 7.8 + 4.8(\beta^*)^2$$

This indicates that for high performance compression of high energy pulses it is necessary to use a compressor with a big dispersion ratio.

In the linear part, enhancement of the compression degree compared to pure multisoliton compression (curve 5) is slightly dependent on β and is more than 2 times lower. As an example for a 10-soliton pulse, the compression degree is 78 at a

dispersion ratio of 0.75 (curve 3) when the multisoliton compression gives only 38.
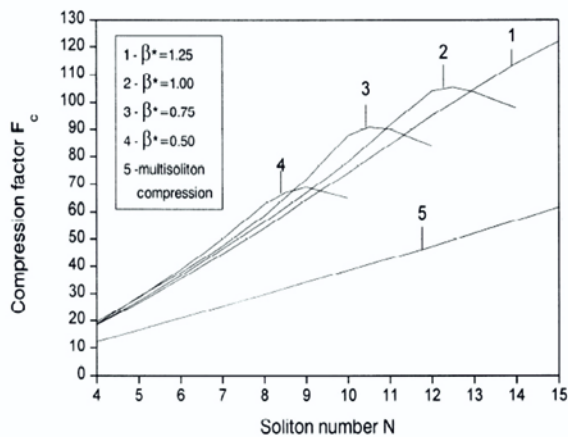


**Fig. 3.** Compression factor Fc *versus* the soliton number N.

It is interesting to note that the incensement of the compression degree is only about 2 times while, as it was mentioned, the peak energy of compressed pulses increases more than five times. This is most likely due to the decrease of the energy in the pedestal. Therefore it should be expected that simultaneously with increasing the compression degree, the quality of the compressed impulses will be improved, i.e. increasing the energy in the central part of the pulse at the expense of the energy in the pedestal. Determining the optimum conditions for this will be a goal of further research.

## CONCLUSION

A scheme of optical pulse compression based on an idea of the "dispersion management" is investigated. This idea consists of the consequent usage of a fiber with positive and fiber with negative dispersion.

This improved optical fiber compressor combines the advantages of the classic fiber-grating compressor and of multisoliton compression. Such scheme allows improving of the compression degree as well as of the quality factor. This improvement depends on the soliton number of the input pulse as well as the dispersion of the used fibers. Thus, we have obtained 2 times increase of the compression degree compared to the multisoliton compression more than 5 times growth of the peak power of the compressed pulse compared to the classic multisoliton compression. The proposed method is suitable for pulse compression within the spectral range $1.3 - 1.5 \, \mu m$ where using one and the same material we are able to produce fibers with positive as well as fibers with negative dispersion.

## REFERENCES

1. G. P Agrawal, Nonlinear fiber optics, Fourth ed., Academic press, San Diego, 2007.
2. R. L. Fork, C. H. Brito Cruz, P. C. Becker, C. V. Shank, *Opt. lett.,* **12,** 483 (1987).
3. R.H. Stolen, C. Lin, *Phys. Rev*., **A17**, 1448 (1978).
4. L.F. Mollenauer, R.H. Stolen, J.P. Gordon, W.J. Tomlinson, *Opt. Lett*., **8**, 289 (1983).
5. K. Tai, A. Tomita, *Appl. Phys. Lett*., **48**, 1033 (1986).
6. A.S. Gouveia-Neto, A. S. L. Gomes, J.P. Taylor, *Opt. Lett.* **12**, 395 (1987).
7. A.S. Gouveia-Neto, A. S. L. Gomes, J.P. Taylor, *J. Mod. Opt.,* **35**, 7 (1988).
8. K. J. Blow, N.J. Doran, B.P. Nelson, *Opt. Lett.,* **10,** 393 (1985).
9. N. I. Kaymakanova, L. M. Ivanov, P. P. Branzalov, L. I. Pavlov, *Journal of Research in Physics*, **29**, 37 (2002).
10. L.M. Ivanov, Proceedings of the Sixth International Scientific Conference – FMNS2015, **2**, 73 (2015).
11. R.A. Fisher, W.K. Bischel, *J. Appl. Phys*, **46,** 4921 (1975).
12. J.W. Cooley, J.W. Tukey, *Math. Comput.,* **19**, 297 (1965).

# Analysis of average power at simistor phase adjustment

V. Milovanski, G. Kalpachka*

*South-West University „Neofit Rilski", 66 Ivan Mihailov Str., 2700 Blagoevgrad, Bulgaria*

The systems for phase adjustment of average power depend on the type of the load. The influence of an active load on the adjustment mode is considered in the paper. When different modes of operation are changing smoothly then the change in the familiar ways is inconvenient. A criterion for delivered average power (when the visual control is missing) is the indication of the measuring instruments that are plugged in the regulated electric circuit. The analysis, that is made and presented in the article, shows a highly nonlinear variation of the average regulated power at corresponding linear amendment of the parameters of the regulating element of the delay time. This leads to complicated settings in the operating mode. Through the made research of the process and the change in the control electric circuit is reached linearization of the delivered average power to the load.

**Keywords:** Average power, Simistors, Phase adjustment.

## INTRODUCTION

From a long time the phase adjustment of the power on various consumers that are connected to the electricity network is used in various applications. Semiconductor switches with four-layer structure – thyristors and simistors are used in the simplest and most common devices as regulating element. The devices, which are manufactured on this principle, are used for phase adjustment of the power of light of incandescent electric lamps or for regulating the speed of rotation of electric motors. In both examples, the simplest way of control is the visual one. When the power of a heater appliance must be smoothly adjusted, this approach could not be used.

The research is reduced to analysis of the processes of action of an simistor regulator of active power to find the best modes of operation. For this purpose a model has been developed, relationships are derived and conclusions are formulated.

## ANALYSIS

On Fig. 1a is presented a simplified circuit of a simistor phase regulator. The main element of the circuit is an electronic key – the simistor $S$, which is connected in series to a powerful resistor $R_T$.

The principle of phase adjustment consists in change of the average power that is fed to $R_T$ [1; 2]. This is presented on Fig. 1b. After a certain delay time $\tau$, a control pulse $u_{mst}(t)$ is generated from the beginning of each half-period of the network voltage. The control pulse unlocks the simistor $S$ and through the resistor $R_T$ flows

current that forms voltage drop $u_R(t)$. As is known [3], the area enclosed by the characteristic $u_R(t)$ corresponds to the active energy that is dissipated by the load. When $\tau = 0$, maximum energy is supplied to the load. When $\tau$ increases, this energy decreases.
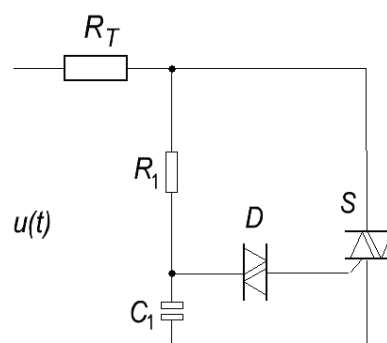


**Fig. 1a.** A simplified circuit.
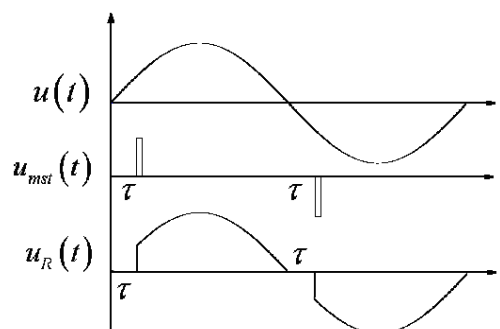


**Fig. 1b.** Instantaneous values of $u(t)$, $u_{mst}(t)$, $u_R(t)$.

The control of the simistor is reduced to formation of an impulse with certain delay time from the beginning of each half-period of the network voltage. The parameters of the electric circuit (elements $R_1$ and $C_1$) determine a value of $\tau$.

*To whom all correspondence should be sent:
E-mail: kalpachka@swu.bg

Then the analysis comes down to two modes of operation of the simistor regulator:

– researching of the relationship between the delay time $\tau$ and the average power $\overline{p} = \overline{p}(\tau)$;

– researching of the commutation circuit and selecting $R_1$ and $C_1$ so that there is matching of the changes of their parameters with the change of the average power.

*Analysis of the relationship between the switch-on time of the simistor and the average power dissipated in the load*

The parameters of the electric circuit are: an electricity network with an effective value of the voltage $U = 220\,\text{V}$ and frequency $f = 50\,\text{Hz}$. An active load $R_T$ is included in the circuit.

The instantaneous values of voltage and current are:

$$u(t) = u_m \sin(\omega t + \psi_U), \ i(t) = i_m \sin(\omega t + \psi_i).$$

Consequently, the instantaneous power is as follows:

$$p(t) = u(t)i(t) = u_m i_m \sin(\omega t + \psi_U)\sin(\omega t + \psi_i). \quad (1)$$

From the condition of an active load in the circuit, the voltage and current are in phase $|\psi_U - \psi_i| = 0$. Furthermore, the simistor from the circuit on Fig. 1a is locked at the end of each half-period, thus synchronizing the operation of the device with the beginning of each new half-period of the voltage and current. Therefore $\psi_U = \psi_i = 0$.

After substituting in (1), the instantaneous power $p(t)$ is:

$$p(t) = u_m i_m \sin^2(\omega t) = \frac{u_m^2}{R_T}\sin^2(\omega t) = i_m^2 R_T \sin^2(\omega t). \quad (2)$$

The processes that are developing in the phase regulator do not depend on the value of $R_T$. In order to simplify the mathematical relationships that describe the processes, it is assumed that $R_T = 1\,\Omega$. From here follows that:

$$p(t) = u_m^2 \sin^2(\omega t) \quad (3)$$

or

$$p(t) = \frac{u_m^2}{2}[1 - \cos(2\omega t)] \quad (4)$$

On Fig. 2 the relationships $p(t)$, $u(t)$ and $i(t)$ are presented graphically.

Due to the active nature of the load, the graphics of the $u(t)$ and $i(t)$ are same (Fig. 2). The instantaneous power $p(t)$ changes with the double frequency of the network voltage and it is entirely with positive values.
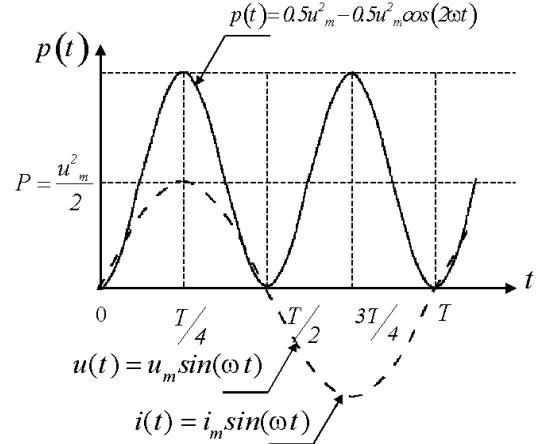


**Fig. 2.** Relationships $p(t)$, $u(t)$, $i(t)$.

The average power $\overline{p}$ for one half-period $\left(\dfrac{T}{2}\right)$ of $u(t)$ is determined by the expression [4]:

$$\overline{p} = \frac{2}{T}\int_{t_1}^{\frac{T}{2}} p(t)\,dt, \quad (5)$$

where $t_1$ is the delay time $\tau$.

As a result of short transformations and analogous relationships, the average power $\overline{p}$ and the average voltage $\overline{u}$ are determined by the following formulas:

$$\overline{p} = \frac{u_m^2}{2}\left(1 - \frac{2t_1}{T}\right) + \frac{u_m^2}{4\pi}\sin\left(\frac{4\pi t_1}{T}\right), \quad (6)$$

$$\overline{u} = \frac{u_m}{\pi}\left[1 + \cos\left(\frac{2\pi t_1}{T}\right)\right]. \quad (7)$$

On Fig. 3 is presented the relationship $\overline{\overline{p}} = \overline{\overline{p}}(t_1)$.

In Table 1 are presented the values of $\overline{u}$ and $\overline{\overline{p}}$ at four points.
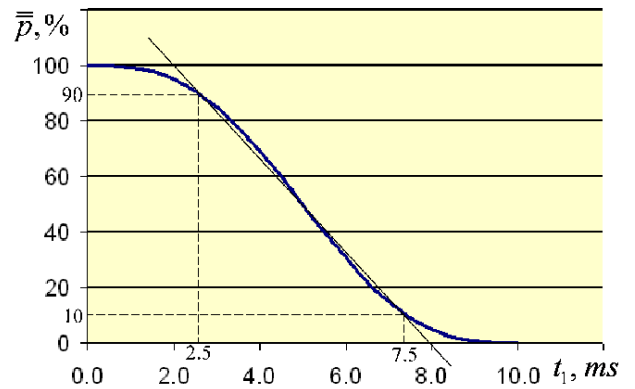


**Fig. 3.** Normalized average power value $\overline{\overline{p}}(t_1)$.

The normalized average power value $\overline{\overline{p}} = 100 \dfrac{\overline{p}(t_1)}{P}, \%$ is used instead of the average value of $\overline{p}$, where $P$ is the average power dissipated in the load for the whole half-period of the network voltage.

The graphic on Fig. 3 is built as a result of calculations. The function $\overline{\overline{p}} = \overline{p}(t_1)$ has a different character at dissimilar places. In general, it can be divided into three sectors: $0 \leq t_1 \leq 2.5 \text{ ms}$; $2.5 \text{ ms} < t_1 \leq 7.5 \text{ ms}$; $7.5 \text{ ms} < t_1 \leq 10 \text{ ms}$. For each of these sectors a different approach applies.

**Table 1.** Values of $\overline{u}$ and $\overline{\overline{p}}$ at four points.

| $t$, ms | $\overline{u}$, V | $\overline{\overline{p}}$, % |
|---------|-------------------|------------------------------|
| 0.0 | 198 | 100 |
| 3.7 | 139 | 75 |
| 5.0 | 99 | 50 |
| 6.3 | 59 | 25 |

*Analysis of the commutation circuit*

The commutation circuit consists three elements (Fig. 1a) – resistor $R_1$, capacitor $C_1$ and dinistor $D$. The formation of delay time $\tau$ is determined by the time of loading capacitor $C_1$. When the threshold value of the element $D$ is reached, the dinistor is unlocked and almost all of the stored electrical energy in $C_1$ passes through the input of $S$ and unlocks the simistor.

On Fig. 4 (without indexes) is presented an equivalent scheme of the idealized $RC$ delay circuit.
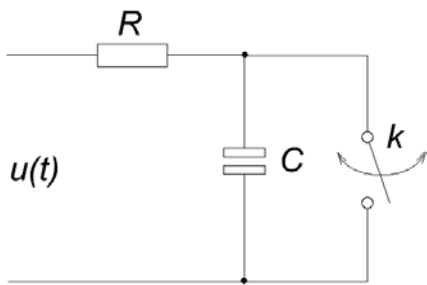


**Fig. 4.** *RC* block.

The commutator $k$ replaces the dinistor $D$ (Fig. 4). During the first commutation cycle ($k$ is open) the capacitor $C$ is loaded through $R$. During the second commutation cycle, when $k$ is closed in a very short time, the capacitor $C$ is unloading through $S$ and unlocks it.

During the first commutation $k$ the independent initial conditions of the circuit are recording:
$$t = 0, \ u(t) = 0, \ u_C(t) = 0.$$

The classical method for researching of transient processes is applied [5]. An equation compiled by Kirchhoff's second law can be written for the circuit after commutation $k$:

$$u(t) = Ri + u_C(t) = RC \frac{du_C}{dt} + u_C(t), \tag{8}$$

where $u(t) = u_m \sin(\omega t)$ and $i = C \dfrac{du_C}{dt}$.

The characteristic equation is:
$$0 = RCp + 1 \tag{9}$$

$$\Rightarrow \ p = -\frac{1}{RC} = -\frac{1}{\tau}.$$

The voltage $u_C(t)$ is determined as sum of two components – established one and free one:

$$u_C(t) = u_C(\tau << t) + Ae^{-\frac{t}{RC}}.$$

For finding the established mode of $u_C(\tau << t)$ is used an operating method for representing the sinusoidal functions of the time in complex form.

The complex impedance of the circuit is:
$$Z = ze^{j\varphi}, \tag{10}$$

where $z$ and $\varphi$ are respectively its module and argument:

$$\begin{cases} z = \sqrt{R^2 + x_C^2} \\ \varphi = arctg \dfrac{x_C}{R} \end{cases} \tag{11}$$

After the transformations that are made, the complex recording of the established voltage on the capacitor $\dot{U}_C$ is:

$$\dot{U}_C = \frac{x_C U}{z} e^{j\left(-\varphi - \frac{\pi}{2}\right)} = U_C e^{j\left(-\varphi - \frac{\pi}{2}\right)}, \tag{12}$$

where $x_C = \dfrac{1}{\omega C}$ is the resistance of the capacitor.

Conversely, in the time domain the voltage is:

$$u_C(\tau << t) = u_{Cm} \sin\left(\omega t - \varphi - \frac{\pi}{2}\right). \tag{13}$$

After determining of the integration constant and involving both components, $u_C(t)$ acquires the final form:

$$u_C(t) = u_{Cm} \sin\left(\omega t - \varphi - \frac{\pi}{2}\right) - u_{Cm} \sin\left(-\varphi - \frac{\pi}{2}\right)e^{-\frac{t}{RC}}. \tag{14}$$

SOLVING OF AN EXAMPLE CASE

From the analysis that is made in the first part of the section II (ANALYSIS) it becomes clear that the relationship $\overline{\overline{p}} = \overline{p}(t_1)$ has three sectors.

97

The third sector ( $7.5\,\text{ms} < t_1 \leq 10\,\text{ms}$ ) covers a time interval in which the average power does not exceed 10 % and in this case it can be ignored. The other two sectors are considered.

A capacitor with capacity $C = 100\,\text{nF}$ is chosen.

For the time interval $0 \leq t_1 \leq 2.5\,\text{ms}$ and by the relationship (14) the maximum value of $R = 82\,\text{k}\Omega$ is calculated. There is not such a standard value. By parallel connection of a resistor with variable resistance $R = 100\,\text{k}\Omega$ and a resistor with constant resistance $R = 470\,\text{k}\Omega$ a resistor with equivalent resistance $R_1 = 82.46\,\text{k}\Omega$ is obtained.

In a similar way for the time interval $2.5\,\text{ms} < t_1 \leq 7.5\,\text{ms}$ by parallel connection of a resistor with variable resistance $R = 500\,\text{k}\Omega$ and a resistor with constant resistance $R = 2.4\,\text{M}\Omega$ a resistor with equivalent resistance $R_2 = 414\,\text{k}\Omega$ is obtained.

One more resistor with constant resistance $R_3$ is connected in series to $R_1$ and $R_2$. Its task is to limit the maximum current through the control circuit. A resistor with resistance $R_3 = 4.7\,\text{k}\Omega$ is completely sufficient. The minimum delay in this case is $t = 0.69\,\text{ms}$, where $\overline{\overline{p}} = P = 100\,\%$ .

## CONCLUSION

There is no direct proportionality linear relationship between the average values of the voltage $\overline{u}$ and the power $\overline{p}$ .

The relationship that exists is determined by the relationships (6) and (7). The knowing of $\overline{u} = \overline{u}(p)$ (for specific values of $\overline{p}$ ) facilitates the calibration process of the adjusting elements.

The conducted laboratory experiments show minor deviations from the calculated, mainly because of the tolerances in the parameters of the used elements.

## REFERENCES

1. D. Nyurman, Power supplies, Technique, Sofia, 1999.
2. V. Milovanski, Force transformer's impulse control of the power, in: Jubilee Scientific Conference (Proc.), Stara Zagora, p. 103, 2005.
3. S. Sharma, Basics of Electrical Engineering, I. K. International Publishing House Pvt. Ltd, New Delhi, 2015.
4. M. Wang, Understandable Electric Circuits, The Institution of Engineering and Technology, London, 2010.
5. T.A. Kuznetsova, E.A. Kulyutnikova, I.B. Kuharchuk, A. A. Ryabuha, Theory of linear electric circuits, part 1, PNRPU, Perm, 2012.

# Thermodynamic properties of helium – oxygen mixtures

## A. Majchrzycka

*West Pomeranian University of Technology, Szczecin, Faculty of Mechanical Engineering and Mechatronics, Department of Thermal Engineering, 70-310 Szczecin, Piastów Av.19, Poland*

The paper reports regression functions describing thermodynamic properties of helium-oxygen mixtures covering the pressure range p=0.1-1.8 MPa, temperature T=273.15-333K and helium molar fraction $x_{He}$=0.65-0.98. Regression equations that have been derived enable to determine specific heat, specific enthalpy, density, dynamic viscosity and thermal conductivity as the function of pressure, temperature and helium molar fraction in helium-oxygen (HELIOX) breathing mixtures.

**Keywords***: Thermodynamic properties, Helium-oxygen mixtures*

## INTRODUCTION

Development of off-shore industry and submarine rescue contributed to increasing importance of underwater operations at a great depth. The diving operations where the divers are exposed to the ambient water pressure can be classified in two groups: bounce (nonsaturation) dives for short jobs and saturation diving for long ones. The saturation diving theoretically enables the divers to stay on the bottom for a long time but the divers must be supported by a hyperbaric complex on the surface, where the divers live in a dry hyperbaric environment at a pressure equal to the ambient pressure existing at their work site [1].

The tissues of a diver's body absorb the inert gases as a function of the duration of the diving operation and the type of the breathing mixture used. In long duration dives, the body tissues become saturated with the inert gases. The techniques of saturation diving make use of the fact that once the body reaches this equilibrium, it can safely remain saturated for long periods, and the diver's obligation of decompression does not increase with further exposure. Decompression is performed during return of the divers at the sea level [1,2].

Saturation diving enables improving of the effectiveness of the diving operation. Two crews of the divers rotate; one crew works on the bottom while the other one rests in the living compartment of DDC (2).

Helium causes certain problems related to dangerous cooling of the divers. This is due to the high thermal conductivity of helium, six times that of air [1-7]. One of the major tasks for the life support systems of the hyperbaric facilities is to create the environment which maintains the safe level of oxygen partial pressure, contaminants, temperature, relative humidity, velocity of the breathing gas and consequently the thermal comfort for the divers. In saturation diving, the partial pressure of oxygen should be maintained between $p_{O2}$=0.02-0.05 MPa [1-3].

The comfort temperature in the hyperbaric environment increases with the total pressure of gas and should be maintained at a level higher (t≈ 20-36℃) than that in normobaric air environment [1-3,8,9] while relative humidity should be kept within $\varphi$ = 0.4-0.7.
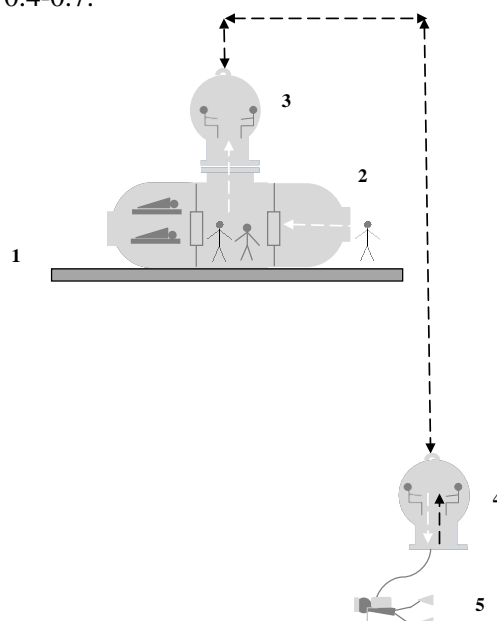


**Fig. 1.** Hyperbaric complex for saturation diving: 1 - deck of a vessel or drilling platform, 2 - deck decompression chamber (DDC), 3 - personnel transfer capsule (PTC) mated to DDC, 4 - personnel transfer capsule (PTC) in the sea, 5 - the diver performing work at the operational depth.

---

* To whom all correspondence should be sent.
E-mail: anna.majchrzycka@zut.edu.pl

It must be noted that also toxic effects of contaminants are increased in the hyperbaric environment [10]. Helium-oxygen breathing mixtures are used at depths down to 200 m [1-3]. The use of helium as an inert component of the breathing mixture enables elimination of nitrogen narcosis when diving to less than 50 m and reduces the diver's effort while breathing. The pressure and composition of the helium-oxygen (HELIOX) breathing mixture depend on the depth of bottom operation and duration of the diver's exposure. The thermodynamic properties of the breathing mixture that depend on composition, pressure and temperature are as follows: specific heat at constant pressure, specific heat at constant volume, specific enthalpy, specific volume, density, dynamic viscosity, thermal conductivity.

Thermodynamic properties of the breathing mixtures have impact on the diver and the parameters to be maintained by environmental life support systems in hyperbaric objects. As the depth of the diving operation increases, the pressure of the breathing mixture increases and it contributes to significant increase of the breathing mixture density. Increased density of the breathing mixture causes increased physical effort of the diver while breathing. It may result in improper lung ventilation, hypoxia, chest tightness, etc. [1,3]. Viscosity of the breathing mixture also has an impact on the respiratory resistance of the diver and the heat exchange during respiration.

Thermal properties of the inert gases (helium, hydrogen) cause certain problems related to dangerous cooling of the divers. This is due to the high thermal conductivity and specific heat of inert gases, however, the other thermodynamic properties also influence thermal sensations of the divers and finally the effective work.

Maintenance of the diver's thermal homeostasis requires creation of a microclimate in a hyperbaric facility of the parameters compensating heat loss from the diver's body.

The most important variables which influence the condition of thermal comfort in hyperbaric environment are as follows: composition, temperature, pressure, humidity and relative velocity of the breathing gas, mean radiant temperature, activity level and thermal resistance of the diver's clothing. Thermal comfort in the hyperbaric facilities can be achieved by many different combinations of the above mentioned variables. It should be noted that thermal sensations of the divers can be different. Microclimate parameters should provide thermal comfort to the divers who stay in the hyperbaric facility. Creation

of a hyperbaric microclimate of comfort parameters is a complex issue of great ergonomic importance.

Calculation of gas mixture thermodynamic properties as the function of gas composition, pressure and temperature is essential for solving the comfort equation for hyperbaric environment [8,9]. It makes also possible to determine contributions of heat loss to the overall diver's thermal balance in the hyperbaric environment.

Based on experimental data of oxygen and helium, gaseous components of HELIOX (helium-oxygen) breathing mixture given by Bretsznajder [4], Golubiev [5, 6] Varhaftik [7] and methods of calculation of thermodynamic properties of real gas mixtures published by Bretsznajder [4] and Sobański [11], the correlations describing thermodynamic properties of HELIOX will be derived. Specific heat at constant pressure, specific enthalpy, specific volume, density and thermal conductivity of the HELIOX mixture will be given as functions of pressure, absolute temperature and molar fraction of helium. When designing hyperbaric systems, it is required to know the thermodynamic properties of the breathing mixtures as the function of pressure, temperature and its composition. Methods of gas mixture thermodynamic properties calculation published by Bretsznajder [4] and Sobański [11] are very accurate but very laborious, as they require calculation of many auxiliary parameters. In order to simplify the further calculations, while maintaining a sufficient engineering accuracy, the regression equations for calculating the thermodynamic properties of helium-oxygen mixtures as a function of pressure, temperature and molar fraction of helium in the mixture will be derived.

## THERMODYNAMIC PROPERTIES OF HELIUM- OXYGEN MIXTURES

In order to determine the thermodynamic properties of helium-oxygen (HELIOX) mixtures experimental data of oxygen and helium thermodynamic properties published by Bretsznajder [4], Gołubiev [5] Varhaftik [7] were applied. Regression correlations describing the thermodynamic properties of oxygen and helium as the functions of pressure and absolute temperature were developed in a numerical experiment in which experimental data published in the above mentioned works were used. Regression correlations were developed with the use of Statistics software.

Specific heat of oxygen at constant pressure in the range of pressure p= 0.1-5.0 MPa, absolute

temperature T= 280-330 K is expressed by equation (1), where the correlation coefficient R=0.976:

$$c_p = 0.8858 + exp(-2.3169 + 0.1881 \cdot p - 0.0027 \cdot T) \quad (1)$$

Specific enthalpy of oxygen in the range of p = 0.1-5.0 MPa, T= 280-330 K is expressed by equation (2), where the correlation coefficient R=0.988:

$$i = 0.7239 + 0.9069 \cdot T - 7.887 \cdot p + 0.0185 \cdot p \cdot T \quad (2)$$

Specific volume of oxygen in the range of p= 0.1-5.0 MPa, T= 280-330 K is expressed by equation (3), where the correlation coefficient R=0.999:

$$v = 0.0776 \cdot p^{-1.0086} + 5.1000 \cdot 10^{-6} \cdot T \quad (3)$$

Dynamic viscosity of oxygen in the range of p = 0.1-5.0 MPa, T= 280-330 K is expressed by equation (4), where the correlation coefficient R=0.999:

$$\eta = (0.7142 \cdot p^{1.5075} + 28.4129 \cdot T^{0.4441} + \\ -149.2896) \cdot 10^{-7} \quad (4)$$

Thermal conductivity of oxygen in the range of p= 0.1- 6.0 MPa, T= 280-350 K is expressed by equation (5), where the correlation coefficient R=0.997:

$$\lambda = (0.4282 \cdot p^{1.0758} + 51.8641 \cdot T^{0.1609} + \\ -103.3646) \cdot 10^{-3} \quad (5)$$

Specific heat of helium at constant pressure in the range of p= 0.1-5.0 MPa, T= 273-323 K is expressed by equation (6), where the correlation coefficient R=0.900:

$$c_p = 1.5642 \cdot p^{6.77 \cdot 10^{-5}} + 3.6654 \cdot T^{-0.0017} + \\ +4.4 \cdot 10^{-6} \cdot p \cdot T \quad (6)$$

Specific enthalpy of helium in the range of p= 0.1-6.0 MPa, T= 273-330 K is expressed by equation (7), where the correlation coefficient R=0.999:

$$i = -1418.467 + 5.19300 \cdot T + 3.36408 \cdot p + \\ -0.00035 \cdot p \cdot T \quad (7)$$

Specific volume of helium in the range of p= 0.1-5.0 MPa, T= 273-323 K is expressed by

equation (8), where the correlation coefficient R=0.997:

$$v = 0.6259 \cdot p^{-0.9980} + 0.2167 \cdot T^{-4.8881} \quad (8)$$

Dynamic viscosity of helium in the range of p= 0.1-5.0 MPa, T= 273-473 K is expressed by equation (9), where the correlation coefficient R=0.999:

$$\eta_i = [1.8503 \cdot p^{0.0009} + A] \cdot 10^{-5} \\ where \quad (9) \\ A = 0.0086 \cdot (T - 273)^{0.8693}$$

Thermal conductivity of helium in the range of p= 0.1-5.0 MPa, T= 270-350 K is expressed by equation (10), where the correlation coefficient R=0.999:

$$\lambda = 4.273 \cdot 10^{-4} \cdot p^{1.0491} + \\ +6.2322 \cdot 10^{-3} \cdot T^{0.5593} \quad (10)$$

Thermodynamic properties of helium - oxygen mixtures were calculated from correlations published by Bretsznajder [4] and Sobański [11]. Calculations were performed at the following assumptions: pressure p = 0.1÷1.8 MPa, absolute temperature T = 273.15÷333.15 K. Oxygen partial pressure was assumed to be constant $p_{o2}$=35 kPa in the range of assumed pressure. Molar fraction of helium $x_{He}$=0.65÷0.98.

To derive regression correlations with the use of Statistics software, the obtained results of HELIOX thermodynamic properties were used as input data. Regression correlations describing the thermodynamic properties of helium-oxygen (HELIOX) mixtures in the range of p=0.1-1.8 MPa, T=273-333 K, $x_{He}$=0.65÷0.98 at constant oxygen partial pressure $p_{O2}$ =35 kPa, are as follows:

- specific heat at constant pressure, correlation coefficient R=0.999:

$$c_p = [1648.3867 + exp\,B] \cdot 10^{-3} \\ where \quad (11) \\ B = 0.002472 \cdot 10^{-3} \cdot p + \\ -1.2602 \cdot 10^{-4} \cdot T + +8.2017 \cdot x_{He}$$

- specific enthalpy, correlation coefficient R=0.978:

$$i = -161.1602 + exp\,C \\ where \\ C = 0.0124 \cdot p + 0.01153 \cdot T + 2.2312 \cdot x_{He}$$

$$(12)$$

- density, correlation coefficient R=0.950:

$$\rho = 2543.7189 + 28.1176 \cdot p + 1.5787 \cdot T + -2878.7407 \cdot x_{He}$$

$$(13)$$

- dynamic viscosity, correlation coefficient R=0.9947:

$$\eta = 9.8048 \cdot 10^{-6} - 4.5019 \cdot 10^{-7} \cdot p + 5.1973 \cdot 10^{-8} \cdot T - 4.4600 \cdot 10^{-6} \cdot x_{He}$$

$$(14)$$

- thermal conductivity, correlation coefficient R=0.9930:

$$\lambda = -0.1300 + 2.1188 \cdot 10^{-3} \cdot p + 3.1898 \cdot 10^{-4} \cdot T + 0.1849 \cdot x_{He}$$

$$(15)$$

Regression correlations describing the thermodynamic properties of oxygen, helium and helium-oxygen mixtures were elaborated with the use of Statistica Software - nonlinear and multiple regression. The selection of the nonlinear estimation function was determined by the simplicity of the regression function and the high correlation coefficient. Regression functions that have been derived are simpler to use in practical application than the analytical relationships given in the literature [4,11] because some stages of indirect calculations have been eliminated. It is possible to calculate the thermodynamic properties of helium-oxygen mixtures only as a function of pressure, temperature and molar fraction of helium.

Fig. 2 illustrates the relationship of specific heat at constant pressure of HELIOX calculated from equation (11) pressure and molar fraction of helium at absolute temperature T=273K.
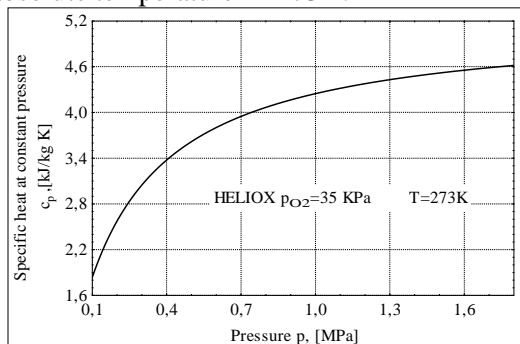


**Fig. 2.** Relationship between specific heat at constant pressure of HELIOX and pressure at absolute temperature T=273 K.

As it follows from Fig. 2 increasing pressure at constant absolute temperature contributes to a significant increase in specific heat of the oxygen-helium mixture at constant pressure.

Figure 3, based on the regression equation (13), illustrates the relationship between the density of HELIOX mixture pressure and the temperature. As it follows from Figure 3 the density of the HELIOX mixture increases with pressure. Increasing temperature at constant pressure contributes to reduce the density. At a lower pressure of HELIOX the effect of pressure and temperature on density is lower.
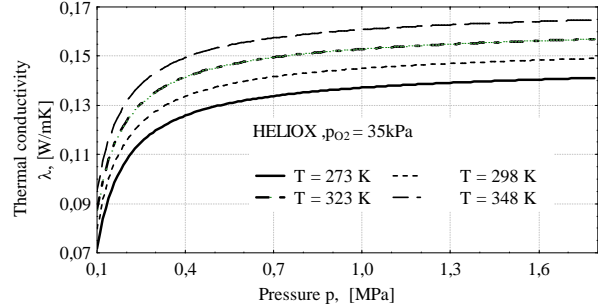


**Fig. 3.** Relationship between density of HELIOX pressure and temperature

Figure 4 illustrates the relationship between thermal conductivity of Heliox pressure and temperature. As it follows from Fig. 4 increasing pressure and temperature contribute to increase HELIOX thermal conductivity.
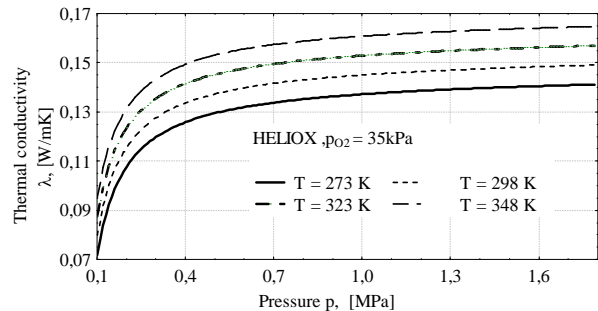


**Fig.4.** Relationship between thermal conductivity of HELIOX pressure and temperature

Figure 5 illustrates the relationship between thermal conductivity of HELIOX pressure and molar fraction of helium at absolute temperature T=303 K.
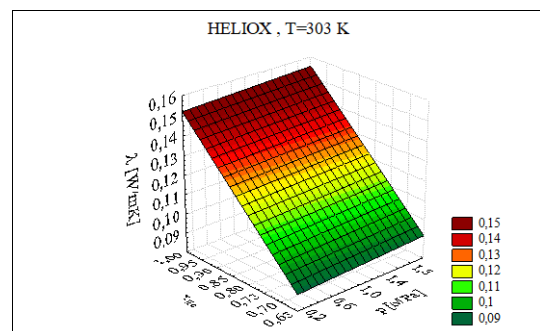
**Fig. 5.** Relationship between thermal conductivity of HELIOX pressure and molar fraction of helium at absolute temperature of T=303 K.

It is evident from Fig. 5 that increased pressure and molar fraction of helium at the absolute temperature T=303K contribute to increase HELIOX thermal conductivity. It means that at great depth heat losses from the diver's body (respiratory heat loss, heat loss by convection, conduction through the clothing) will also increase, therefore the temperature necessary to maintain the divers in thermal comfort should be increases with the depth of saturation diving.

## CONCLUSIONS

• Based on experimental data of oxygen and helium thermodynamic properties published in the literature [4,11] regression correlations describing specific heat at constant pressure, specific enthalpy, specific volume, dynamic viscosity and thermal conductivity as the functions of pressure and temperature have been derived. Correlation coefficients have shown that regression equations are well matched.

• Based on experimental data of oxygen and helium thermodynamic properties published in the literature [4,11] thermodynamic properties of helium-oxygen (HELIOX) mixtures have been calculated in the range of pressure p= 0.1-1.8 MPa, absolute temperature T = 273.15÷333.15 and helium molar fraction $x_{He} = 0.65$-$0.98$.

• Regression correlations that enable to determine specific heat at constant pressure, specific enthalpy, specific volume, dynamic viscosity and thermal conductivity of HELIOX as the functions of pressure, temperature and molar fraction of helium have been derived. Correlation coefficients have shown that regression equations are well matched.

• The regression correlations are simple in practical application and allow determining thermodynamic properties of oxygen, helium and HELIOX mixtures with satisfactory engineering accuracy. They eliminate some intermediate, time-consuming computational steps that need to be performed using analytical relationships,

• The regression correlations that have been obtained are very useful in mathematical modelling of thermal comfort in hyperbaric HELIOX atmosphere.

## NOMENCLATURE

$c_p$ – specific heat at constant pressure , kJ/kg K,
$i$ – specific enthalpy, kJ/kg,
$p$ – total pressure of the breathing mixture, MPa,
$p_{O2}$ – partial pressure of oxygen, kPa,
$R$ – correlation coefficient,
$v$ – specific volume, $m^3$/kg,
$t$ – temperature, $^\circ$C,
$T$ – absolute temperature, K,
$x_{He}$ – molar fraction of helium,
$\lambda$ – thermal conductivity, W/m K,
$\eta$ – dynamic viscosity, kg/ms
$\rho$ – density, kg/$m^3$

## REFERENCES

1. C.W. Shilling, M.F. Werts, N.R. Schandelmeier, The Underwater Handbook. A Guide to Physiology and Performance for the Engineer, Plenum Press, New York, London, 1976, ISBN 0-306-30843-6.
2. US Navy Manual, Best Publishing Company, California, 1993.
3. R.W. Hamilton Jr., Breathing mixtures, Technical Memorandum CRL-T-750, Ocean Systems and Development Laboratory, Tarrytown, New York, December, 1973.
4. S.Bretsznajder, Własności cieczy i gazów, wyd. PWN, 1965.
5. I.F. Golubiev, Viazkost' gazov i gazovych smiesiej, Wyd. Fiziko-Matematičeskoj Literatury, Moskwa 1959.
6. Handbook of compressed gases, Chapmann & Hall, New York, London, 3$^{rd}$ ed., 1990, ISBN 0-412-99211-6,
7. N.B. Varhaftik, Spravočnik po tieplofizičeskim svojstvam gazov i židkostej, Wyd. Nauka, Moskva,1972
8. A. Majchrzycka, Model of thermal comfort in the hyperbaric facility, in: Polish Maritime Research, 1(68), vol.18, p.37, 2011.
9. A. Majchrzycka, Komfort cieplny nurka w strefie saturacji mieszaninami oddechowymi o różnych właściwościach fizycznych, ISBN 978-83-7663-226-5, Szczecin, 2012.
10. R. Kłos, Mathematical modelling of the hyperbaric facilities ventilation, in: Military diving, 2001, R. Kłos (ed.) Naval University of Gdynia, ISBN 83-87280-87-9.
11. R. Sobański, Thermal properties of the breathing mixtures. Prace Naukowe Politechniki Szczecińskiej (Scientific Research Works of Technical University of Szczecin), 12-35, Technical University of Szczecin), Szczecin, 1982.

# Stress distribution in elastic isotropic semi-space with concentrated vertical force

L. B. Petrova

*Department of Mechanics, Todor Kableshkov University of Transport, Geo Milev str.158, 1574 Sofia, Bulgaria*

The distribution of stresses in elastic isotropic semi-space in horizontal and vertical direction under the effect of concentrated vertical force is investigated. A transition to line influences for stresses and their determination to arbitrary load is performed. Analysis and comparison of the results obtained is made.

## INTRODUCTION

Elastic halfplane is a disk limited only on one straightlinear end and spread to infinity on one side of this end. Such is the stress and deformation state of a disk, loaded on its contour, the dimensions of which are too big in comparison with the length of the loading part. The solution of infinite elastic halfplane at uniformly distributed load (problem of Boussinesq), with concentrated load (problem of Flammant) and at arbitrary distributed load is discussed in [1]. Expressions are derived for the stresses at an arbitrary point of the halfplane. Through limits transition of these problems the expressions for determination of stresses under the effect of concentrated forces are obtained. A similar problem is encountered in the investigation of beams of elastic foundation, long strips, fundaments, etc.

The purpose of the present work is to determine the distribution of the stresses in the elastic halfplane in horizontal and vertical direction under the effect of concentrated force, to construct the influences for the stresses and through the obtained influences to determine the stresses at arbitrary load.

## STRESSES IN THE HALFPLANE

Normal and tangential stresses are known from strength of materials. In the case of concentrated vertical force acting on the top edge, the expressions of the stresses in an arbitrary point of the halfplane are as presented in Figure1:
where

$x, y$ are the coordinates of a point at which the stresses should be determined;

$q$ is the intensity of load equivalent to the force $F$, distributed uniformly on the part with length $2a$ and symmetrically located about axis $y$;

The introduced coordinate system $xOy$ is in the middle of the distributed load (Fig.1).

As a general signification of stresses $S(x, y)$ is used.

The written expressions are applied for investigation of the elastic halfplane loaded with concentrated force, with the characteristics $a = 10\,m$; $F = 1\dfrac{kN}{m}$. The intensity of the load in the cases is to coordinate with a single value of the force.

The analysis of the distribution of stresses is made with arbitrary and different in this case and in particular, multiple of $a$, an accepted discretization step in the axe's directions of the halfplane. Calculations are made with compound programs of PC.



$$\sigma_x = -\frac{2F}{\pi}\frac{x^2 y}{\left(x^2 + y^2\right)^2},$$

$$\sigma_y = -\frac{2F}{\pi}\frac{y^3}{\left(x^2 + y^2\right)^2},$$

$$\tau_{xy} = -\frac{2F}{\pi}\frac{xy^2}{\left(x^2 + y^2\right)^2}.$$
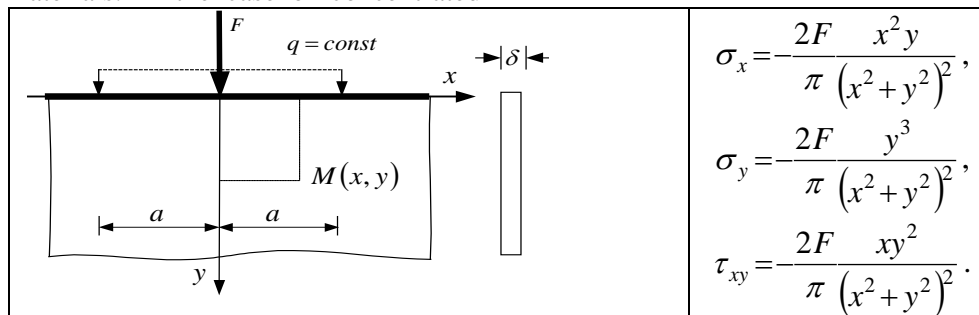
**Fig. 1.** The expressions of the stresses in an arbitrary point of the halfplane

\* To whom all correspondence should be sent.
 E-mail: lbphr@abv.bg

**Stresses distribution in vertical direction**

The solution of the stresses is made at $0 \leq y \leq 15a$ by step $\dfrac{a}{2}$. The results of the solutions are shown in Table 1.

**Table 1**. The solution of the stresses is made at 0≤y≤15a by step a/2

| y | $\sigma_x(0,y)$ | $\sigma_x\left(\frac{a}{2},y\right)$ | $\sigma_x(a,y)$ | $\sigma_y(0,y)$ | $\sigma_y\left(\frac{a}{2},y\right)$ | $\sigma_y(a,y)$ | $\tau_{xy}(0,y)$ | $\tau_{xy}\left(\frac{a}{2},y\right)$ | $\tau_{xy}(a,y)$ |
|---|---|---|---|---|---|---|---|---|---|
| 0 | -6,3649 | -2,5465e-7 | -6,3662e-8 | -6,3649e-4 | 0,0000 | 0,0000 | -0,0636 | -5,0930e-13 | -6,3662e-14 |
| 5 | -5,0930e-9 | -0,0318 | -0,0204 | -0,1273 | -0,0318 | -5,0930e-3 | -2,5465e-5 | -0,0318 | -0,0102 |
| 10 | -6,3662e-10 | -0,0102 | -0,0159 | -0,0637 | -0,0407 | -0,0159 | -6,3662e-6 | -0,0204 | -0,0159 |
| 15 | -1,8863e-10 | -3,8197e-3 | -9,0408e-3 | -0,0424 | -0,0344 | -0,0203 | -2,8294e-6 | -0,0115 | -0,0136 |
| 20 | -7,9578e-11 | 1,7623e-3 | -5,0930e-3 | -0,0318 | -0,0282 | -0,0204 | -1,5916e-6 | -7,0491e-3 | -0,0102 |
| 25 | -4,0744e-11 | -9,4175e-4 | -3,0279e-3 | -0,0255 | -0,0235 | -0,0189 | -1,0186e-6 | -4,7087e-3 | -7,5698e-3 |
| 30 | -2,3579e-11 | -5,5803e-4 | -1,9099e-3 | -0,0212 | -0,0201 | -0,0172 | -7,0736e-7 | -3,3482e-3 | -5,7296e-3 |
| 35 | -1,4848e-11 | -3,5651e-4 | -1,2692e-3 | -0,0182 | -0,0175 | -0,0155 | -5,1969e-7 | -2,4956e-3 | -4,4421e-3 |
| 40 | -9,9472e-12 | -2,4109e-4 | -8,8114e-4 | -0,0159 | -0,0154 | -0,0141 | -3,9789e-7 | -1,9287e-3 | -3,5245e-3 |
| 45 | -6,9863e-12 | -1,7042e-4 | -6,3442e-4 | -0,0141 | -0,0138 | -0,0128 | -3,1438e-7 | -1,5338e-3 | -2,8549e-3 |
| 50 | -5,0930e-12 | -1,2482e-4 | -4,7088e-4 | -0,0127 | -0,0125 | -0,0118 | -2,5465e-7 | -1,2482e-3 | -2,3544e-3 |
| 55 | -3,8264e-12 | -9,4099e-5 | -3,5855e-4 | -0,0116 | -0,0114 | -0,0108 | -2,1045e-7 | -1,0351e-3 | -1,9720e-3 |
| 60 | -2,9473e-12 | -7,2670e-5 | -2,7902e-4 | -0,0106 | -0,0105 | -0,0100 | -1,7684e-7 | -8,7204e-4 | -1,6741e-3 |
| 65 | -2,3182e-12 | -5,7274e-5 | -2,2122e-4 | -9,7942e-3 | -9,6793e-3 | -9,3465e-3 | -1,5068e-7 | -7,4456e-4 | -1,4379e-3 |
| 70 | -1,8560e-12 | -4,5931e-5 | -1,7825e-4 | -9,0946e-3 | -9,0025e-3 | -8,7344e-3 | -1,2992e-7 | -6,4304e-4 | -1,2478e-3 |
| 75 | -1,5090e-12 | -3,7393e-5 | -1,4568e-4 | -8,4883e-3 | -8,4133e-3 | -8,1943e-3 | -1,1318e-7 | -5,6089e-4 | -1,0926e-3 |
| 80 | -1,2434e-12 | -3,0844e-5 | -1,2054e-4 | -7,9578e-3 | -7,8960e-3 | -7,7148e-3 | -9,9472e-8 | -4,9350e-4 | -9,6435e-4 |
| 85 | -1,0366e-12 | -2,5737e-5 | -1,0085e-4 | -7,4897e-3 | -7,4381e-3 | -7,2866e-3 | -8,8114e-8 | -4,3754e-4 | -8,5724e-4 |
| 90 | -8,7328e-13 | -2,1698e-5 | -8,5211e-5 | 7,0736e-3 | -7,0301e-3 | -6,9021e-3 | -7,8595e-8 | -3,9056e-4 | -7,6690e-4 |
| 95 | -7,4253e-13 | -1,8461e-5 | -7,2634e-5 | -6,7013e-3 | -6,6643e-3 | -6,5552e-3 | -7,0540e-8 | -3,5075e-4 | -6,9002e-4 |
| 100 | -6,3662e-13 | -1,5836e-5 | -6,2408e-5 | -6,3662e-3 | -6,3345e-3 | -6,2408e-3 | -6,3662e-8 | -3,1673e-4 | -6,2408e-4 |
| 105 | -5,4994e-13 | -1,3686e-5 | -5,4010e-5 | -6,0631e-3 | -6,0357e-3 | -5,9545e-3 | -5,7744e-8 | -2,8741e-4 | -5,6710e-4 |
| 110 | -4,7830e-13 | -1,1908e-5 | -4,7050e-5 | -5,7875e-3 | -5,7636e-3 | -5,6930e-3 | -5,2613e-8 | -2,6198e-4 | -5,1754e-4 |
| 115 | -4,1859e-13 | -1,0425e-5 | -4,1233e-5 | -5,5358e-3 | -5,5150e-3 | -5,4531e-3 | -4,8138e-8 | -2,3978e-4 | -4,7418e-4 |
| 120 | -3,6842e-13 | -9,1785e-6 | -3,6335e-5 | -5,3052e-3 | -5,2868e-3 | -5,2323e-3 | -4,4210e-8 | -2,2028e-4 | -4,3602e-4 |
| 125 | -3,2595e-13 | -8,1228e-6 | -3,2182e-5 | -5,0930e-3 | -5,0767e-3 | -5,0284e-3 | -4,0744e-8 | -2,0307e-4 | -4,0227e-4 |
| 130 | -2,8977e-13 | -7,2229e-6 | -2,8637e-5 | -4,8971e-3 | -4,8826e-3 | -4,8396e-3 | -3,7670e-8 | -1,8779e-4 | -3,7228e-4 |
| 135 | -2,5875e-13 | -6,4511e-6 | -2,5593e-5 | -4,7157e-3 | -4,7028e-3 | -4,6644e-3 | -3,4931e-8 | -1,7418e-4 | -3,4551e-4 |
| 140 | -2,3201e-13 | -5,7854e-6 | -2,2966e-5 | -4,5473e-3 | -4,5357e-3 | -4,5012e-3 | -3,2481e-8 | -1,6199e-4 | -3,2152e-4 |
| 145 | -2,0882e-13 | -5,2082e-6 | -2,0685e-5 | -4,3905e-3 | -4,3801e-3 | -4,3490e-3 | -3,0279e-8 | -1,5104e-4 | -2,9993e-4 |
| 150 | -1,8863e-13 | -4,7053e-6 | -1,8696e-5 | -4,2441e-3 | -4,2347e-3 | -4,2067e-3 | -2,8294e-8 | -1,4116e-4 | -2,8044e-4 |



$\sigma_x(0,y)\ \sigma_x\left(\frac{a}{2},y\right)\sigma_x(a,y)$ | $\sigma_y(0,y)\ \sigma_y\left(\frac{a}{2},y\right)\sigma_y(a,y)$ | $\tau_{xy}(0,y)\ \tau_{xy}\left(\frac{a}{2},y\right)\tau_{xy}(a,y)$
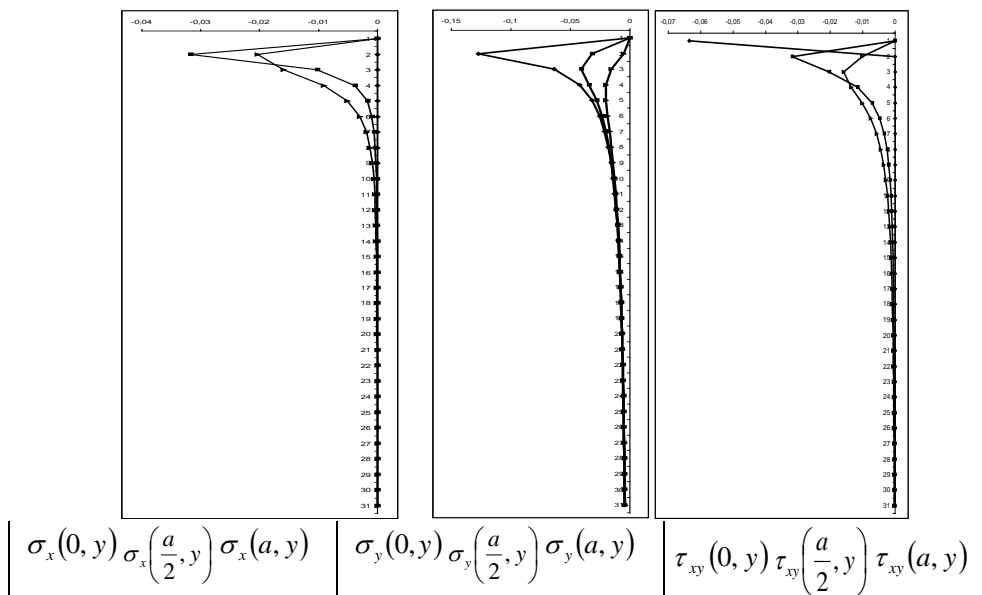
**Fig. 2.** Graphical distribution of the stresses in the elastic halfplane in vertical direction

Table 2. The ordinates and the kind of the line influences

| $x$ | $\sigma_x(x,0.01)$ | $\sigma_x\left(x,\frac{a}{2}\right)$ | $\sigma_x(x,a)$ | $\sigma_y(x,0.01)$ | $\sigma_y\left(x,\frac{a}{2}\right)$ | $\sigma_y(x,a)$ | $\tau_{xy}(x,0.01)$ | $\tau_{xy}\left(x,\frac{a}{2}\right)$ | $\tau_{xy}(x,a)$ |
|---|---|---|---|---|---|---|---|---|---|
| -60 | -1,7684e-6 | -8,7204e-4 | -1,6741e-3 | -4,9122e-14 | -6,0558e-6 | -4,6503e-5 | 2,9473e-10 | 7,2670e-5 | 2,7902e-4 |
| -55 | -2,1045e-6 | -1,0351e-3 | -1,9720e-3 | -6,9571e-14 | -8,5544e-6 | -6,5190e-5 | 3,8264e-10 | 9,4099e-5 | 3,5854e-4 |
| -50 | -2,5465e-6 | -1,2482e-3 | -2,3544e-3 | -1,0186e-13 | -1,2482e-5 | -9,4175e-5 | 5,0930e-10 | 1,2482e-4 | 4,7087e-4 |
| -45 | -3,1438e-6 | -1,5338e-3 | -2,8549e-3 | -1,5525e-13 | -1,8936e-5 | -1,4098e-4 | 6,9862e-10 | 1,7042e-4 | 6,3442e-4 |
| -40 | -3,9789e-6 | -1,9287e-3 | -3,5245e-3 | -2,4868e-13 | -3,0136e-5 | -2,2028e-4 | 9,9472e-10 | 2,4109e-4 | 8,8113e-4 |
| -35 | -5,1969e-6 | -2,4955e-3 | -4,4421e-3 | -4,2424e-13 | -5,0930e-5 | -3,6262e-4 | 1,4848e-9 | 3,5651e-4 | 1,2692e-3 |
| -30 | -7,0736e-6 | -3,3482e-3 | -5,7296e-3 | -7,8595e-13 | -9,3005e-5 | -6,3662e-4 | 2,3579e-9 | 5,5803e-4 | 1,9099e-3 |
| -25 | -1,0186e-5 | -4,7087e-3 | -7,5698e-3 | -1,6297e-12 | -1,8835e-4 | -1,2112e-3 | 4,0744e-9 | 9,4175e-4 | 3,0279e-3 |
| -20 | -1,5915e-5 | -7,0491e-3 | -0,0102 | -3,9789e-12 | -4,4057e-4 | -2,5465e-3 | 7,9577e-9 | 1,7623e-3 | 5,0930e-3 |
| -15 | -2,8294e-5 | -0,0115 | -0,0136 | -1,2575e-11 | -1,2732e-3 | -6,0272e-3 | 1,8863e-8 | 3,8197e-3 | 9,0408e-3 |
| -10 | -6,3662e-5 | -0,0204 | -0,0159 | -6,3662e-11 | -5,0930e-3 | -0,0159 | 6,3662e-8 | 0,0102 | 0,0159 |
| -5 | -2,5465e-4 | -0,0318 | -0,0102 | -1,0186e-9 | -0,0318 | -0,0407 | 5,0929e-7 | 0,0318 | 0,0204 |
| 0 | 0,0000 | 0,0000 | 0,0000 | -63,6620 | -0,1273 | -0,0637 | 0,0000 | 0,0000 | 0,0000 |
| 5 | -2,5465e-4 | -0,0318 | -0,0102 | -1,0186e-9 | -0,0318 | -0,0407 | -5,0929e-7 | -0,0318 | -0,0204 |
| 10 | -6,3662e-5 | -0,0204 | -0,0159 | -6,3662e-11 | -5,0930e-3 | -0,0159 | -6,3662e-8 | -0,0102 | -0,0159 |
| 15 | -2,8294e-5 | -0,0115 | -0,0136 | -1,2575e-11 | -1,2732e-3 | -6,0272e-3 | -1,8863e-8 | -3,8197e-3 | -9,0408e-3 |
| 20 | -1,5915e-5 | -7,0491e-3 | -0,0102 | -3,9789e-12 | -4,4057e-4 | -2,5465e-3 | -7,9577e-9 | -1,7623e-3 | -5,0930e-3 |
| 25 | -1,0186e-5 | -4,7087e-3 | -7,5698e-3 | -1,6297e-12 | -1,8835e-4 | -1,2112e-3 | -4,0744e-9 | -9,4175e-4 | -3,0279e-3 |
| 30 | -7,0736e-6 | -3,3482e-3 | -5,7296e-3 | -7,8595e-13 | -9,3005e-5 | -6,3662e-4 | -2,3579e-9 | -5,5803e-4 | -1,9099e-3 |
| 35 | -5,1969e-6 | -2,4955e-3 | -4,4421e-3 | -4,2424e-13 | -5,0930e-5 | -3,6262e-4 | -1,4848e-9 | -3,5651e-4 | -1,2692e-3 |
| 40 | -3,9789e-6 | -1,9287e-3 | -3,5245e-3 | -2,4868e-13 | -3,0136e-5 | -2,2028e-4 | -9,9472e-10 | -2,4109e-4 | -8,8113e-4 |
| 45 | -3,1438e-6 | -1,5338e-3 | -2,8549e-3 | -1,5525e-13 | -1,8936e-5 | -1,4098e-4 | -6,9862e-10 | -1,7042e-4 | -6,3442e-4 |
| 50 | -2,5465e-6 | -1,2482e-3 | -2,3544e-3 | -1,0186e-13 | -1,2482e-5 | -9,4175e-5 | -5,0930e-10 | -1,2482e-4 | -4,7087e-4 |
| 55 | -2,1045e-6 | -1,0351e-3 | -1,9720e-3 | -6,9571e-14 | -8,5544e-6 | -6,5190e-5 | -3,8264e-10 | -9,4099e-5 | -3,5854e-4 |
| 60 | -1,7684e-6 | -8,7204e-4 | -1,6741e-3 | -4,9122e-14 | -6,0558e-6 | -4,6503e-5 | -2,9473e-10 | -7,2670e-5 | -2,7902e-4 |
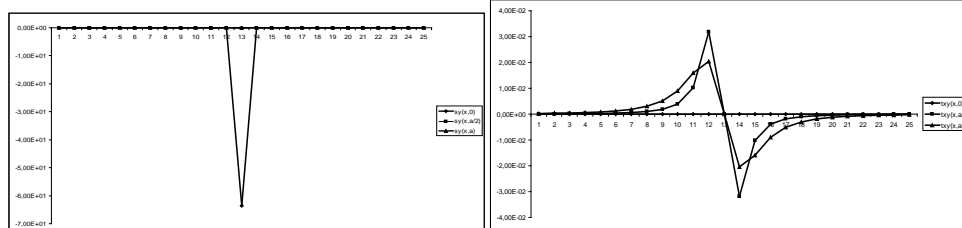


**Fig. 3.** Graphical distribution of the stresses in the axis elastic halfplane in horizontal direction

From the results obtained it is seen that the normal stresses $\sigma_x$ in vertical direction have big values in the interval $0 \le y \le 2a$. The normal stresses $\sigma_y$ in vertical direction have very big values in the interval $0 \le y \le 2a$ and then gradually decrease. The tangential stresses $\tau_{xy}$ have big values in the interval $0 \le y \le 2a$, and then gradually decrease. The biggest values of the normal and the tangential stresses in vertical direction are obtained at $y = \dfrac{a}{2}$.

The normal stresses $\sigma_x$ in horizontal direction have big values in the interval $-6a \le x \le 6a$. The normal stresses $\sigma_y$ in the horizontal directions have very big values in the interval $-a \le x \le a$, and then gradually decrease. The tangential stresses $\tau_{xy}$ have relative big values in the interval $-4a \le x \le 4a$, and then gradually decrease. The big-

gest values of the normal and the tangential stresses in horizontal direction are obtained at $x = 0$ и $y = 0$.

In vertical direction the normal stresses $\sigma_y$ are bigger in comparison with the normal stresses $\sigma_x$.

The results obtained form stresses line's state in an elastic halfplane.

From the diagrams of stress's distribution in a vertical and horizontal direction, in a selection arbitrary section of elastic halfplane, after integration – analytical of numerical can to make a verification of equilibrium of calculated stresses.

STRESSES LINE INFLUENCES

The expressions of the functions's stresses in a horizontal directions can to interpreter to construct the lines influences of the normal and tangential stresses in elastic halfplane (Fig. 4).
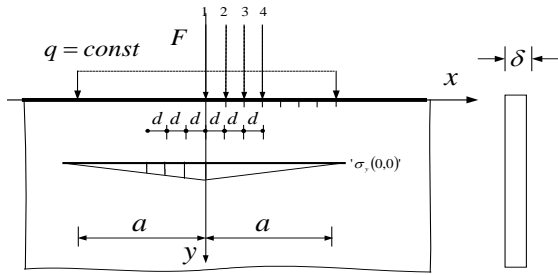
**Fig. 4.** The expressions of the functions's stresses in a horizontal directions

Here,

$d$ is the length of the discretization step in horizontal direction; $i = 1,2,3,4...$ – successive situations of the force $F = 1$ in the top edge of the elastic halfplane.

The ordinates and the kind of the line influences, for example $"\sigma_x\left(0,01;\dfrac{a}{2}\right)"$, $"\sigma_y\left(0,01;\dfrac{a}{2}\right)"$, $"\tau_{xy}(0,01;\dfrac{a}{2})"$, etc., are shown in Table 2 and Fig. 3. The ordinates of stresses influences are reports with multiplay of discratization step, suitable to the situation of the forces $F = 1$ and of the stress at the point to from which the line influence refers. For each particular case expressions are written for line influences of the stresses at the point of elastic halfplane presented through stresses line states. For example:

$$"\sigma_x\left(0;\frac{a}{2}\right)" = \sigma_x\left(x;\frac{a}{2}\right), \qquad "\sigma_y\left(\frac{a}{2};\frac{a}{2}\right)" = \sigma_y\left(x - \frac{a}{2};\frac{a}{2}\right),$$

$$"\tau_{xy}\left(-\frac{a}{2};\frac{a}{2}\right)" = \tau_{xy}\left(x + \frac{a}{2};\frac{a}{2}\right).$$

Graphical line influences of the stresses at the selected points of the elastic halfplane are shown in Fig. 5.
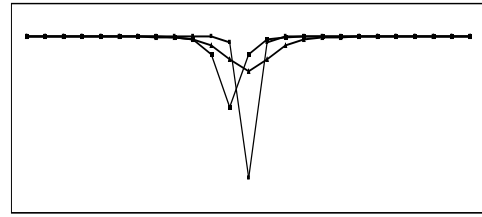


$"\sigma_x\left(-\dfrac{a}{4};\dfrac{a}{2}\right)" \ "\sigma_x\left(0;\dfrac{a}{2}\right)" \ "\sigma_x\left(\dfrac{a}{4};\dfrac{a}{4}\right)"$
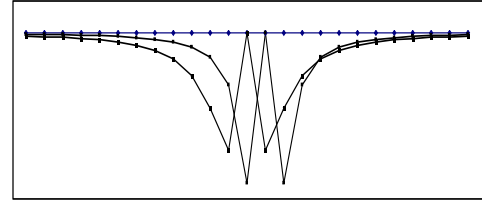
$"\sigma_y\left(-\dfrac{a}{4};\dfrac{a}{2}\right)" \ "\sigma_y\left(0;\dfrac{a}{2}\right)" \ "\sigma_y\left(\dfrac{a}{4};\dfrac{a}{4}\right)"$

$"\tau_y\left(-\dfrac{a}{4};\dfrac{a}{2}\right)" \ "\tau_y\left(0;\dfrac{a}{2}\right)" \ "\tau_y\left(\dfrac{a}{4};\dfrac{a}{4}\right)"$
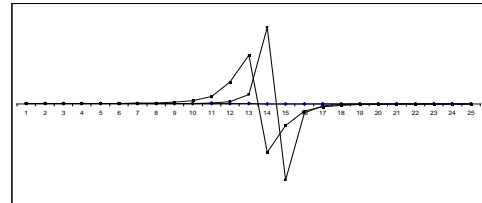
**Fig. 5.** Influences of the stresses at the selected points of the elastic halfplane

From the line influences the stresses at a unspecified point of elastic halfplane at an arbitrary load can be determined. At the load, distributed by arbitrary law, it is known that the arbitrary stress is determines with the expression: $S(x,y) = \int_{q_1}^{q_2} S(x,y) q(x) dx$ where $q_1$, $q_2$ are the limits (start, end) of the distributed load, $y$ is a previously determined level in vertical direction at the point at which the stresses are determined through line influences.

At a uniformly distributed load $q = const$ with length *2a*, symmetrically situated about axis

$$y \ \sigma_x\left(0,\frac{a}{2}\right) = \int_{-a}^{a} -\frac{2q}{\pi} x^2 \frac{\frac{a}{2}}{\left[x^2 + \left(\frac{a}{2}\right)^2\right]^2} dx = -\frac{2\left(-2 + 5a \, tg(2)\right)}{5} \frac{q}{\pi} = -0,4502q \ ;$$

$$\sigma_y\left(0,\frac{a}{2}\right) = \int_{-a}^{a} -\frac{2q}{\pi} \frac{\left(\frac{a}{2}\right)^3}{\left[x^2 + \left(\frac{a}{2}\right)^2\right]^2} dx = -\frac{2\left(2 + 5a \, tg(2)\right)}{5} \frac{q}{\pi} = -0,9595q \ ;$$

107

$$\sigma_y\left(\frac{a}{2},\frac{a}{2}\right)=\int_{-a}^{a}-\frac{2q}{\pi}\frac{\left(\frac{a}{2}\right)^3}{\left[x^2+\left(\frac{a}{2}\right)^2\right]^2}dx=-\frac{2}{5\pi}q=-0,9022q\,;$$

$$\tau_{xy}\left(0,\frac{a}{2}\right)=\int_{-a}^{a}-\frac{2q}{\pi}x\frac{\left(\frac{a}{2}\right)^2}{\left[x^2+\left(\frac{a}{2}\right)^2\right]^2}dx=0\,;\,\tau_{xy}\left(\frac{a}{2},\frac{a}{2}\right)=\int_{-a}^{a}-\frac{2q}{\pi}x\frac{\left(x+\frac{a}{2}\right)^2}{\left[(x+\frac{a}{2})^2+\left(\frac{a}{2}\right)^2\right]^2}dx=-\frac{2}{5\pi}q=-0,1273\,q\,.$$

At a load with length $a$, distributed by triangle law with zero of a triangle at the $x=0$ (Fig. 6), the stresses, determined through line influences, are of the type:
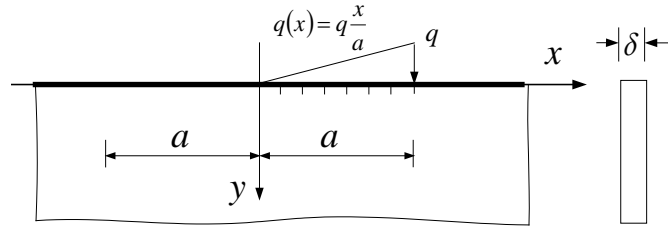


**Fig. 6.** Type of the stresses, determined through line influences

$$\sigma_x\left(0,\frac{a}{2}\right)=\int_{0}^{a}-\frac{2}{\pi}x^2\frac{\frac{a}{2}}{\left[x^2+\left(\frac{a}{2}\right)^2\right]^2}\left(\frac{qx}{a}\right)dx=\left(\frac{-(1+15\ln5)}{10\pi}+\frac{(1+2\ln5)}{2\pi}\right)q=-0,1288q\,;$$

$$\sigma_y\left(0,\frac{a}{2}\right)=\int_{0}^{a}-\frac{2}{\pi}\frac{\left(\frac{a}{2}\right)^3}{\left[x^2+\left(\frac{a}{2}\right)^2\right]^2}\left(\frac{qx}{a}\right)dx=-\frac{2}{5\pi}q=-0,1273q\,;$$

$$\sigma_y\left(\frac{a}{2},\frac{a}{2}\right)=\int_{0}^{a}-\frac{2}{\pi}\frac{\left(\frac{a}{2}\right)^3}{\left[\left(x-\frac{a}{2}\right)^2+\left(\frac{a}{2}\right)^2\right]^2}\left(\frac{qx}{a}\right)dx=-\frac{1}{8}\left(\frac{(-2+\pi)}{\pi}+1\right)q=-0,0908q\,;$$

$$\tau_{xy}\left(0,\frac{a}{2}\right)=\int_{0}^{a}-\frac{2}{\pi}x\frac{\left(\frac{a}{2}\right)^2}{\left[x^2+\left(\frac{a}{2}\right)^2\right]^2}\left(\frac{qx}{a}\right)dx=\frac{2-5arctg\,2}{10\pi}q=-0,1126q\,;$$

$$\tau_{xy}\left(\frac{a}{2},\frac{a}{2}\right)=\int_{0}^{a}-\frac{2}{\pi}\left(x-\frac{a}{2}\right)\frac{\left(\frac{a}{2}\right)^2}{\left[(x-\frac{a}{2})^2+\left(\frac{a}{2}\right)^2\right]^2}\left(\frac{qx}{a}\right)dx=\left(\frac{1}{\pi}-\frac{1}{2\pi}arctg\,2\right)q=0,1421q\,.$$

The results obtained through line influences coincide exactly with the values of the stresses in the elastic isotropic halfspace, obtained from the solution under the effect of indicated distributed loads.

## CONCLUSIONS

With more concentrated forces the diagrams of stresses are superimposed. In a similar way the stress-es at different points of an elastic isotropic semi-space with other acting loads can be determined.

## REFERENCES

1. Ch. Varbanov , *Theory of elasticity*, Technika, Sofia, 1989.
2. T. Krustev, T. Karamanski, Guidance for a solution of a problem of theory of elasticity, stability and dynamics of elastic systems, *Technika*, Sofia, 1974.

# Force line influences in a single static undetermined beam

L. B. Petrova

*Department of Mechanics, University of Transport Todor Kableshkov, Geo Milev Str. 158, 1574 Sofia, Bulgaria*

General expressions for force line influences in a single static undetermined beam – bilateral fixed and beam fixed–joint pin are investigated. The ordinates of the line influences were obtained in an arbitrary section of the beam. The beam's elements with constructed lines influences are used for finding line influences in static undetermined systems with application of the displacement method.

**Keywords:** Single static undetermined beams, Line influences, Displacement method

## SINGLE STATIC UNDETERMINED BEAMS - FORCE LINE INFLUENCES

The beams are with length $l$ and constant rigidity $EI$. The moments and the shear forces are taken for positive, when turning a cutting beam clockwise. The basic relationships in the construction of Force line influences in the beams using the Force method are written in a general kind. The sections of the beam, in which the force influences are applied, are determined with the coordinates $x_k$, $x_k^I = l - x_k$. It is known that in static undetermined systems force line influences are linear curves. The ordinates of the constructed force line influences are determined in sections $k$, arbitrary in number and situation with the coordinates $x_m$,

$x_m^I = l - x_m$.

### Bilateral fixed beam

For a basic system a beam simply supported at the ends is chosen. The basic unknowns are the moments in the supported joints.

The matrix of displacements $[D] = [\delta_{ij}]$ is:

$$[D] = \frac{L}{3EI} \begin{vmatrix} 1 & \frac{1}{2} \\ \frac{1}{2} & 1 \end{vmatrix}.$$

The corresponding matrix of the $[\beta]$ - numbers is:

$$[\beta] = [\beta_{ij}] = -[\delta_{ij}]^{-1} \qquad [\beta] = \frac{EI}{l} \begin{bmatrix} -4 & 2 \\ 2 & -4 \end{bmatrix}.$$

In the chosen basic system the matrix influences for displacements of the applied point of each basic unknown $X_i$ into its direction are presented as:

$$\{"D_f"\} = \begin{Bmatrix} "\Delta_{1f}" \\ "\Delta_{2f}" \end{Bmatrix},$$

$$\begin{vmatrix} \Delta_{1f} = \dfrac{1}{EI} \dfrac{l}{6} x_m^I (1 - \dfrac{x_m^{I\,2}}{l^2}) \\ \Delta_{2f} = \dfrac{1}{EI} \dfrac{l}{6} x_m (1 - \dfrac{x_m^2}{l^2}) \end{vmatrix},$$

where $m$ indicates the number of the beam's sections in which the ordinate from the $"\Delta_{if}"$ is determined.

The line influences for the basic unknowns are obtained according to the expressions:

$$\{"X"\} = [\beta]\{"D_f"\} \qquad \begin{vmatrix} "X_1" = \beta_{11}"\Delta_{1f}" + \beta_{12}"\Delta_{2f}" \\ "X_2" = \beta_{21}"\Delta_{1f}" + \beta_{22}"\Delta_{2f}" \end{vmatrix}$$

and after transformations:

$$\begin{vmatrix} X_1 = \dfrac{1}{3}\left[ -2x_m^I\left(1 - \dfrac{x_m^{I\,2}}{l^2}\right) + x_m\left(1 - \dfrac{x_m^2}{l^2}\right) \right] \\ X_2 = \dfrac{1}{3}\left[ x_m^I\left(1 - \dfrac{x_m^{I\,2}}{l^2}\right) - 2x_m\left(1 - \dfrac{x_m^2}{l^2}\right) \right] \end{vmatrix}.$$

The reaction's and force line influences in the beam are generally obtained according to the principle of superposition:

$$"S_m" = "S_m^o" + \sum_i S_{m_i}"X_i".$$

The significations in the written expression are known.

For the forces they are:

$$\begin{vmatrix} "M_k" = "M_k^o" + \sum_i M_{k_i}"X_i" \\ "Q_k" = "Q_k^o" + \sum_i Q_{k_i}"X_i" \end{vmatrix}$$

$$\begin{vmatrix} "M_k" = "M_k^o" + \dfrac{x_\kappa^I}{l}"X_1" + \dfrac{x_\kappa}{l}"X_2" \\ "Q_k" = "Q_k^o" - \dfrac{1}{l}"X_1" + \dfrac{1}{l}"X_2" \end{vmatrix}.$$

---

* To whom all correspondence should be sent.
E-mail: lbphr@abv.bg

In an arbitrary section of the beam, determined with the coordinate $x_k$, the analytical expressions for line influences of reactions and forces are:



**Fig. 1.**

$$M_k = \begin{vmatrix} \dfrac{x_k^I x_m}{l} + \dfrac{1}{3l}\left[ x_m\left(1-\dfrac{x_m^2}{l^2}\right)(x_k^I - 2x_k) + x_k^I\left(1-\dfrac{x_m^{I\,2}}{l^2}\right)(x_k - 2x_k^I) \right] & 0 \le x_m \le x_k \\[4mm] \dfrac{x_k x_m^I}{l} + \dfrac{1}{3l}\left[ x_m\left(1-\dfrac{x_m^2}{l^2}\right)(x_k^I - 2x_k) + x_m^I\left(1-\dfrac{x_m^{I\,2}}{l^2}\right)(x_k - 2x_k^I) \right] & x_k \le x_m \le l \end{vmatrix}$$

$$Q_k = \begin{vmatrix} -\dfrac{x_m}{l} - \dfrac{1}{l}\left[ x_m\left(1-\dfrac{x_m^2}{l^2}\right) - x_m^I\left(1-\dfrac{x_m^{I\,2}}{l^2}\right) \right] & 0 \le x_m \le x_k \\[4mm] \dfrac{x_m^I}{l} - \dfrac{1}{l}\left[ x_m\left(1-\dfrac{x_m^2}{l^2}\right) - x_m^I\left(1-\dfrac{x_m^{I\,2}}{l^2}\right) \right] & x_k \le x_m \le l \end{vmatrix},$$

where $m$ indicates the number of beam's sections in which the ordinate of line influences $"M_k", "Q_k"$ is determined.

The expressions for $"M_k", "Q_k"$ present the left and the right part of the line influences.

The ordinates of line influences for forces in a section with coordinates $x_k = 0.5l$, $x_k = 0.2l$, $x_k = 0.3l$ with $m = 10$ points of the beam are shown in Table 1.

The force line influences in the selected sections of the bilateral fixed beam are shown in Fig. 2.

### Beam fixed- joint pin

The basic system is a simply supported beam. The basic unknown is the moment at the supported joint.

The matrix of deformation $[D] = [\delta_{ij}]$ is:

$$[D] = \frac{L}{3EI}[1].$$

The corresponding $[\beta]$ - matrix is:

$$[\beta] = [\beta_{ij}] = -[\delta_{ij}]^{-1} \qquad [\beta] = \frac{3EI}{l}[1].$$

The matrix influence on the displacements of the basic unknown's applied point $X_i$ into its directions is:

$$["D_f"] = \{"\Delta_{1f}"\}, \quad \Delta_{1f} = \frac{1}{EI}\frac{l}{6}x_m^I\left(1-\frac{x_m^{I\,2}}{l^2}\right).$$

The line influences for the basic unknowns are:
$$\{"X"\} = [\beta]\{"D_f"\} \quad "X_1" = \beta_{11}"\Delta_{1f}",$$

$$X_1 = -\frac{x_m^I}{2}\left(1-\frac{x_m^{I\,2}}{l^2}\right).$$

**Table 1.** The ordinates of line influences for forces in a section with coordinates $x_k=0.5l$;, $x_k=0.2l$; $x_k=0.3l$, with $m=10$ points of the beam

| $m$ | 0 | 1 | 2 | 3 | 4 | 5 | 6 | 7 | 8 | 9 | 10 |
|---|---|---|---|---|---|---|---|---|---|---|---|
| | | | | | | $x_k = 0{,}5l$ | | | | | |
| $M_{k_m}$ | 0.0000 | 5.000e-3 | 0.0200 | 0.0450 | 0.0800 | 0.1250 | 0.0800 | 0.0450 | 0.0200 | 5.000e-3 | 0.0000 |
| $Q_{k_m}$ | 0.0000 | -0.0280 | -0.1040 | -0.2160 | -0.3520 | $\dfrac{-0.5000}{0.5000}$ | 0.3520 | 0.2160 | 0.1040 | 0.0280 | 0.0000 |
| | | | | | | $x_k = 0{,}2l$ | | | | | |
| $M_{k_m}$ | 0.0000 | 0.0134 | 0.0512 | 0.0098 | -0.0144 | -0.025 | -0.0256 | -0.0198 | -0.0112 | -0.0034 | 0.0000 |
| $Q_{k_m}$ | 0.0000 | -0.0280 | $\dfrac{-0.104}{0.8960}$ | 0.7844 | 0.648 | 0.5000 | 0,3520 | 0.2160 | 0.1040 | 0.0280 | 0.0000 |
| | | | | | | $x_k = 0{,}3l$ | | | | | |
| $M_{k_m}$ | 0.0000 | 0.0106 | 0.0408 | 0.0882 | 0.0504 | 0.0250 | 0.0096 | 0.0018 | -0.0008 | -0.0006 | 0.0000 |
| $Q_{k_m}$ | 0.0000 | -0.0280 | -0.0104 | $\dfrac{-0.216}{0.7840}$ | 0.6498 | 0.5000 | 0.352 | 0.2160 | 0.1040 | 0.0280 | 0.0000 |



$"M_k"$

$"Q_k"$
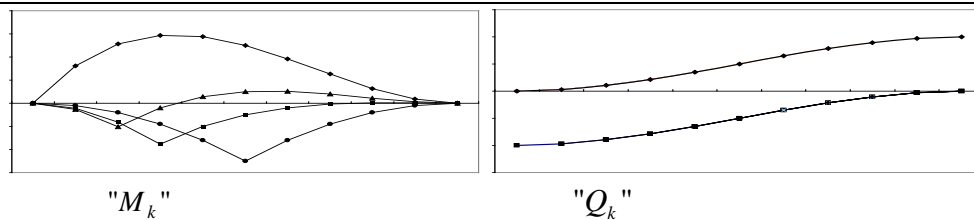
**Fig. 2.** The force line influences in the selected sections of the bilateral fixed beam

111

The force line influences in the beam are in general:

$$"S_k" = "S_k^o" + \sum_i S_{k_i} "X_i"$$

$$\left| \begin{matrix} "M_k" = "M_k^o" + \sum_i M_{k_i} "X_i" \\ "Q_k" = "Q_k^o" + \sum_i Q_{k_i} "X_i" \end{matrix} \right. .$$

Finally they become:

$$"M_k" = "M_k^o" + \frac{x_k^I}{l} "X_1" ; \quad "Q_k" = "Q_k^o" - \frac{1}{l} "X_1" .$$

In the signified sections of the beam the ordinates of force lines influences are:



**Fig. 3.**
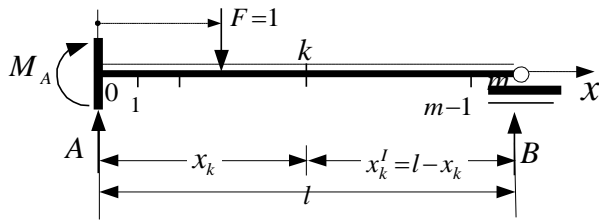
$$M_k = \left| \begin{matrix} \dfrac{x_k^I x_m}{l} + \dfrac{x_k^I x_m^I}{2l}\left(1 - \dfrac{x_m^{I\,2}}{l^2}\right) & 0 \le x_m \le x_k \\[2ex] \dfrac{x_k x_m^I}{l} + \dfrac{x_k^I x_m^I}{2l}\left(1 - \dfrac{x_m^{I\,2}}{l^2}\right) & x_k \le x_m \le l \end{matrix} \right. ,$$

$$Q_k = \left| \begin{matrix} -\dfrac{x_m}{l} - \dfrac{1}{l}\left[ x_m^I\left(1 - \dfrac{x_m^{I\,2}}{l^2}\right) - x_m\left(1 - \dfrac{x_m^2}{l^2}\right) \right] & 0 \le x_m \le x_k \\[2ex] -\dfrac{x_m^I}{l} - \dfrac{1}{l}\left[ x_m^I\left(1 - \dfrac{x_m^{I\,2}}{l^2}\right) - x_m\left(1 - \dfrac{x_m^2}{l^2}\right) \right] & x_k \le x_m \le l \end{matrix} \right.$$

where $m$ indicates the number of beam's sections in which the ordinates of lines influences $"M_k", "Q_k"$ are determined.

The expressions for $"M_k", "Q_k"$ present the left and the right part of the line influences.

The ordinates of force line influences in the section with a coordinate $x_k = 0,5l$, $x_k = 0,2l$, $x_k = 0,3l$ with $m = 10$ points of the beam are shown in Table 2.

The force line influences in selected sections of the beam fixed-joint pin are shown in Fig. 4.

*Line influences for the reactions in the beam's elements*

Reactions line influences in a beam's element can be obtained from the constructed force line influences and the investigated expressions.

*Bilateral fixed beam*

The investigated analytical expressions for the vertical reactions support are:

**Table 2**. The ordinates of line influences for forces in a section with coordinates $x_k=0.5l$;, $x_k=0.2l$; $x_k=0.3l$, with $m=10$ points of the beam

| $m$ | 0 | 1 | 2 | 3 | 4 | 5 | 6 | 7 | 8 | 9 | 10 |
|---|---|---|---|---|---|---|---|---|---|---|---|
| | | | | | | $x_k = 0,5\ell$ | | | | | |
| $M_{k_m}$ | 0.0000 | 0.0725 | 0.0280 | 0.06075 | 0.1040 | 0.15625 | 0.1160 | 0.08175 | 0.0520 | 0.02525 | 0.0000 |
| $Q_{k_m}$ | 0.0000 | -0.0145 | -0.0560 | -0.1215 | -0.2080 | $\dfrac{-0.3125}{0.6875}$ | 0.5680 | 0.4365 | 0.2960 | 0.1495 | 0.0000 |
| | | | | | | $x_k = 0,2\ell$ | | | | | |
| $M_{k_m}$ | 0.0000 | 0.0116 | 0.0448 | -0,0028 | -0,0336 | -0,0500 | -0,0544 | -0,0492 | -0,0368 | -0,0196 | 0.0000 |
| $Q_{k_m}$ | 0.0000 | -0.0145 | $\dfrac{-0.0560}{0.9440}$ | 0.8785 | 0.7920 | 0.6875 | 0.5680 | 0.4365 | 0.2960 | 0.1495 | 0.0000 |
| | | | | | | $x_k = 0,3\ell$ | | | | | |
| $M_{k_m}$ | 0.0000 | 0.01015 | 0.0392 | 0.08505 | 0.0456 | 0.01875 | 0.0024 | -0.00555 | -0.0072 | -0.00465 | 0.0000 |
| $Q_{k_m}$ | 0.0000 | -0.0145 | -0.0560 | $\dfrac{-0.1215}{0.8785}$ | 0.7920 | 0.6875 | 0.5680 | 0.4365 | 0.2960 | 0.1495 | 0.0000 |



$"M_k"$ $\qquad\qquad\qquad$ $"Q_k"$
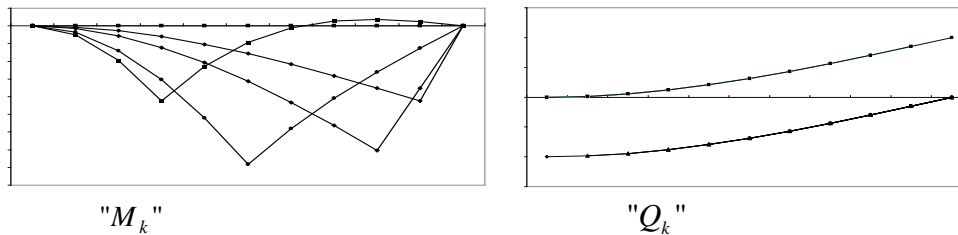
**Fig. 4.** The force line influences in selected sections of the beam fixed-joint pin

$$\left|\begin{matrix} "A_v"="A_v^0"+\sum_i A_{v_i}"X_i" \\ "B_v"="B_v^0"+\sum_i B_{v_i}"X_i" \end{matrix}\right.$$

$$\left|\begin{matrix} "A_v"="A_v^0"-\dfrac{1}{l}"X_1"+\dfrac{1}{l}"X_2" \\ "B_v"="B_v^0"+\dfrac{1}{l}"X_1"-\dfrac{1}{l}"X_2" \end{matrix}\right. .$$

After substitution the coordinates of sections support $A$ - $x_k=0, x_k^I=l$, respectively $B$ - $x_k=l, x_k^I=0$, the expressions for moments in the supports become:

$$"M_A"="X_1" \qquad "M_B"=-"X_2".$$

In the signified sections of the beam the ordinates of reaction's lines influences are:

$$A=\frac{x_m^I}{l}-\frac{x_m}{l}\left(1-\frac{x_m^2}{l^2}\right)+\frac{x_m^I}{l}\left(1-\frac{x_m^2}{l^2}\right),$$

$$B=\frac{x_m}{l}+\frac{x_m}{l}\left(1-\frac{x_m^2}{l^2}\right)-\frac{x_m^I}{l}\left(1-\frac{x_m^2}{l^2}\right);$$

$$M_A=\frac{1}{3}\left[-2x_m^I\left(1-\frac{x_m^{I\,2}}{l^2}\right)+x_m\left(1-\frac{x_m^2}{l^2}\right)\right],$$

$$M_A=\frac{1}{3}\left[-2x_m\left(1-\frac{x_m^2}{l^2}\right)+x_m^I\left(1-\frac{x_m^{I\,2}}{l^2}\right)\right].$$

The ordinates of reaction's line influences at $m=10$ points of the beam are shown in Table 3.

The ordinates of the reaction's line influences at the right end of the beam can be written mirrorly, coordinated with the accepted positive directions of the support's reactions.

*Beam fixed-joint pin*

In this case the expressions for the reactions in the beam, at the investigated analytical expressions are:

$$"M_A"="X_1" \qquad \left|\begin{matrix} "A_v"="A_v^0"+A_{v_1}"X_1" \\ "B_v"="B_v^0"+B_{v_1}"X_1" \end{matrix}\right.$$

$$\left|\begin{matrix} "A_v"="A_v^0"-\dfrac{1}{l}"X_1" \\ "B_v"="B_v^0"+\dfrac{1}{l}"X_1" \end{matrix}\right. .$$

In the beam the ordinates of the reaction's line influences are:

$$M_A=-\frac{x_m^I}{2}\left(1-\frac{x_m^{I\,2}}{l^2}\right), \quad \text{`}$$

$$A=\frac{x_m^I}{l}+\frac{x_m^I}{2l}\left(1-\frac{x_m^{I\,2}}{l^2}\right), \qquad B=\frac{x_m}{l}-\frac{x_m^I}{2l}\left(1-\frac{x_m^{I\,2}}{l^2}\right).$$

The ordinates of the reaction's line influences at $m=10$ points of the beam are shown in Table 4. Reaction's line influences in a bilateral fixed beam end in a beam fixed – joint pin have a kind shown in Fig. 4.

The solutions of the ordinates of the lines influences are made with $l=1$. The force line influences, constructed at $l=1$ with a multiplier $\frac{1}{l}$ can be converted to force line influences at $l\neq1$.

The construction of line influences is made with compound programs of PC.

**Table 3.** The ordinates of reaction's line influences at *m=10* points of the beam

| m | 0 | 1 | 2 | 3 | 4 | 5 | 6 | 7 | 8 | 9 | 10 |
|---|---|---|---|---|---|---|---|---|---|---|---|
| $A$ | 1 | 0.9720 | 0.8960 | 0.7840 | 0.6480 | 0.5000 | 0.3520 | 0.2160 | 0.1040 | 0.0280 | 0.0000 |
| $M_A$ | 0.0000 | -0.0810 | -0.1280 | -0.1470 | -0.1440 | -0.1250 | -0.0960 | -0.0630 | -0.0320 | -9.000e-3 | 0.0000 |

**Table 4**. The ordinates of the reaction's line influences at *m=10* points of the beam

| m | 0 | 1 | 2 | 3 | 4 | 5 | 6 | 7 | 8 | 9 | 10 |
|---|---|---|---|---|---|---|---|---|---|---|---|
| $M_A$ | 0.0000 | -0.0855 | -0.1440- | -0.1785 | -0.1920 | -0.1875 | -0.1680 | -0.1365 | -0.0960 | -0.0495 | 0.0000 |
| $A$ | 1.0000 | 0.9855 | 0.9440 | 0.8785 | 0.7920 | 0.6875 | 0.5680 | 0.4365 | 0.2960 | 0.1495 | 0.0000 |
| $B$ | 0.0000 | 0.0145 | 0.0560 | 0.1215 | 0.2080 | 0.3125 | 0.4320 | 0.5635 | 0.7040 | 0.8505 | 1.0000 |
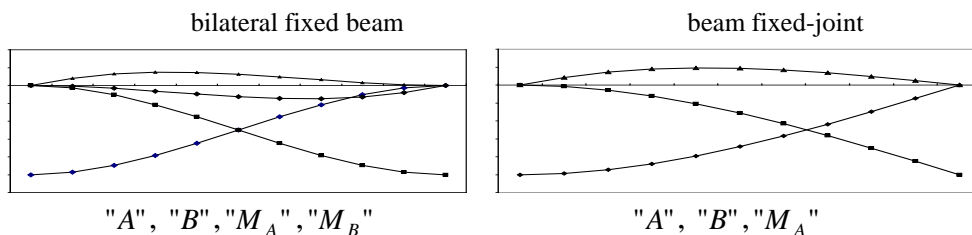
bilateral fixed beam  beam fixed-joint



"$A$", "$B$","$M_A$","$M_B$"  "$A$", "$B$","$M_A$"

**Fig. 4.** Reaction's line influences in a bilateral fixed beam end in a beam fixed – joint pin

*L. B. Petrova: Force line influences in a single static undetermined beam*

## CONCLUSIONS

With the expressions investigated the ordinates of force line influences can be obtained in arbitrary sections of beams. The expressions investigated are necessary to determine line influences in indetermined systems with application of the displacement method.

The obtained ordinates of force line influences conform with the results obtained for line influences obtained using expressions for reactions in the beam's elements – bilateral fixed and beam fixed – joint pin.

The investigated expressions can be used for generating line influences for forces and reactions in the basic beam's elements with an arbitrary number and location ordinates.

## REFERENCES

1. I. Baichev, Help tables of structural mechanics, UASEG, Sofia, 2000.
2. B. Bankov, Structural mechanics, p. I, II, UACEG, Sofia, 2001.
3. T. Karamanski, T. Ganev, T. Bobev, A. Popov, N. Kapitanov, I. Bajchev. Structural Mechanics, Sofia, "Technika" 1988, (in Bulgarian).
4. T. Karamanski T. Ganev, T. Bobev, A. Popov, N. Kapitanov, I. Bajchev, Application to book of structural mechanics, Sofia, 1987.
5. T. Karamanski, R. Rangelov, Methodical guidance for solving of problems of structural mechanics, Sofia, 1976.
6. T. Karamanski, R. Rangelov, Applications to methodical guidance for solving of problems of structural statics, Sofia, 1976.
7. S. Simeonov, Statics of building constructions, p. I, II, Technika, Sofia, 1993.

114

# Optimization algorithms for finding the shortest paths

F. I. Sapundzhi[*], M. S. Popstoilov

*South-West University Neofit Rilski, 2700 Blagoevgrad, Bulgaria*

Graph traveling problems are among the oldest problems of graph theory. The shortest path algorithms are intensively studied problems, which have a lot of applications such as: many problems of dynamic programming with discrete state and discrete time; network optimization problem-networks of roads and telecommunication networks, etc. At the present time the graphs provide simple but often useful formal representation of biological networks capturing one-to-one relationships between biological units. The aim of the present work is to evaluate the Dijkstra's algorithm, Floyd-Warshall algorithm, Bellman-Ford algorithm, and Dantzig's algorithm in solving the shortest path problem, that can be applied to very different biological systems and problems for biological system modelling. A brief overview of the different types of algorithms for finding the shortest paths is given. C# implementation of the considered algorithms are presented to show how works each of them. The results of evaluating the algorithms along with their time complexity are shown.

**Keywords:** Molecular modelling, Shortest path problem, Dijkstra's algorithm, Floyd-Warshall algorithm, Bellman-Ford algorithm, Dantzig's algorithm.

## INTRODUCTION

With the advent of computational biology, biological information is more often represented and stored in the form of biological interactions between genes, proteins, miRNAs, etc. The biological data assay has developed from understanding the function of single genes to interpreting the collective behaviour of complex biological systems, which can be modelled and analysed in the form of protein-ligand interaction networks, gene regulatory networks and others. In the fields of biology and medicine applications of network analysis include identification of drug target, determining the functions of proteins and genes, designing effective strategies for treating various diseases, providing early diagnosis of disorders, etc [1].

Networks of protein-protein interaction, biochemical networks, transcriptional regulation networks, signal transduction are the highlighted network categories in systems biology often sharing characteristics [2].

Signal transduction networks often use graphs to represent a series of interactions between proteins, chemicals or macromolecules. Databases that store information about signal transduction pathways are MiST [3], TRANSPATH [4], etc.

To operate the plenty of information, complex computational methods are needed to manage the number and size of biological networks which can be represented in the form of mathematical graphs.

Many transport, distribution tasks, tasks for selecting optimal routes or situation of service centers, tasks for making schedules, are described by the language of graphs and networks. Series of physical, chemical, economical and managing systems are successfully interpreted and examined using graph theory.

In many cases tasks are linear – target function is linear, as well as all of the constraints, which means that they can be solved using linear optimization. The real tasks (these who fully enough affect the reality) are too complex, which causes searching efficient and flexible algorithms regarding output data. Graph theory gives good opportunities for this [1,2,5,6].

The objectives of this research paper are: (a) to determine and identify the concepts of the shortest path problem; (b) to determine the representation of graphs in computer in order to solve the shortest path problem, as well as to explore and understand the different basic terms of graphs; (c) to explain the general concepts and the C# implementations of Dijkstra's algorithm, Floyd-Warshall algorithm, Bellman-Ford algorithm and Danzig's algorithm; (d) to evaluate each algorithm, and to present the evaluations' results.

## MATERIALS AND METHODS

### Graph theory and definitions

The shortest path problem is a task for finding the shortest path or route from a starting point to a final destination. In order to represent the shortest path problem we use graph theory. To introduce the basic concepts of it, we give the empirical and the mathematical description of graphs that represent networks as they are originally defined in the literature [5,6].

* To whom all correspondence should be sent.
 E-mail: sapundzhi@swu.bg

A *graph G* is a pair $(V, E)$, where $V$ is a finite set of vertices and $E$ is a set of connections (edges) between the vertices. An edge $e = (u, v)$ consists of two vertices such that $u, v \in V$.

A graph $G = (V, E)$ is *edge-weighted,* if each edge $e \in E$ *has a weight,* $W(e) \in \mathbb{R}$. Let $G = (V, E)$ denotes an edge-weighted graph with real edge weights $W(e), e \in E$. We will say that $D$ is a *metric* for $G$ if, for any three vertices $u, v, w \in V$, $D(u, v) = D(v, u) \geq 0$, with $D(u, v) = 0$ if and only if $u = v$, and $D(u, v) \leq D(u, w) + D(w, u)$. One way of defining metric distance on a weighted graph is to use the *shortest-path* metric $\delta(\dots)$ on the graph or its sub graph, i.e., $(D(u, v) = \delta(u, v))$, the shortest path distance between $u$ and $v$ for all $u, v \in V$. We will say that the edge weighted tree $T = T_G(V', E')$ is a *tree metric* for $G$, with respect to distance function $D$, if for any pair of vertices $u, v$ in $G$, the length of the unique path between them in $T$ is equal to $D(u, v)$. An *ultra-metric* is a special type of tree metric defined on rooted trees, where the distance to the root is the same for all leaves in the tree, an approximation that introduces small distortion. A metric $D$ is an ultra-metric if, for all points $x, y, z$ we have $D[x, y] \leq \max\{D[x, z], D[y, z]\}$. An ultra-metric does not satisfy all the properties of a tree metric distance. To create a general tree metric from an ultra-metric, we need to satisfy the *4-point* condition:

$$D[x, y] + D[z, w] \leq \max\{D[x, z] + D[y, w], D[x, w] + D[y, z]\}, \text{ for all } x, y, z, w.$$

A metric that satisfies the 4-point condition is called an *additive metric*.

If routes are one-way then the graph will be directed or else it will be undirected. In the literature are presented many different types of algorithms that solve the shortest path problem. Only several of the most popular conventional shortest path algorithms are going to be discussed in this paper, and they are as follows: Dijkstra's algorithm, Floyd-Warshall algorithm, Bellman-Ford algorithm and Dantzig's algorithm [8-11].

## EXPLANATION AND IMPLEMENTATION OF THE ALGORITHMS

### *Explanation and implementation of Dijkstra's algorithm*

*Explanation:*

*Step 1:* Mark the initial vertex (s). Let: $d(s) = 0$ (Constant distance label) $d(x) = \infty$ (Tentative distance label) $p = s$ ($p$ – last marked vertex).

*Step 2:* (Changing the tentative distance labels). For all unmarked vertices $x$ the numbers $d(x)$ are recalculated by Eqn.1:

$$d(x) = \min\{d(x), d(p) + c(p, x)\} \qquad (1)$$

where $d(x)$ is the minimal tentative distance from $s$ to $x$, $d(p)$ – minimal tentative distance from $s$ to $p$ and $c(p, x)$ is the edge's weight from $p$ to $x$. (Obviously we may change only those $d(x)$, for which the edge $(p, x)$ exists, the rest of the numbers remain the same).

If $d(x) = \infty$, for each unmarked vertex $x$, stop the procedure – it means that there are no paths from $s$ to all unmarked vertices. Otherwise mark the one vertex $x$ which has minimal distance label $d(x)$. Also color the edge which goes into vertex $x$, for which the minimal distance label from Eqn.1 is reached. Let $p = x$.

*Step 3:* If $p = t$, the procedure ends, the only way from $s$ to $t$, made out of marked edges, is the shortest path between $s$ and $t$. Otherwise, go back to Step 2 [9].

*Implementation:*

The following basic variables are used: $Dictionary < V, double > distances$ -stores the distances from source vertex to all vertices; $Dictionary < V, E > bestVertexEdg$ -stores an edge for every vertex that minimizes its distance label; $Dictionary < V, bool > marked$ -if some vertex is marked, its value in this dictionary is true; $List < E > markedEdges$ -list of all marked edges; $V$ $currentVertex$ - last marked vertex [7].

The algorithm of Dijkstra determines the shortest path and its length from a given vertex $s$ to a target vertex $t$. It is supposed that all edge's lengths are positive. The algorithm stops: (1) if there's no path from $s$ to $t$; (2) if one or more edges have negative weights; (3) when the target vertex $t$ is marked.

*Step 1:* A tentative distance for all vertices in the given graph that represents the minimal distance from the source vertex to all vertices and use $Dictionary < V, double > distances$ for these labels. Initially, all labels are set to big enough number to represent infinity but $s$ ($distances[s] = 0$) and ($distances[v] = inf, v \neq s$) which means that the path lengths from $s$ to the rest vertices are unknown, after that mark source vertex $s$ as visited and set it as current vertex ($currentVertex := s$).

*Step 2:* The distance labels ($distances[v]$) for each unmarked neighbor vertex $v$ where an edge exists from $currentVertex$ to $v$ are recalculated by Eqn. 2:

$$distances[v] = \min\{distances[v], distances[currentVertex] + c(currentVertex, v)\} \qquad (2)$$

where $c$ ($currentVertex, v$) is edge's weight from $currentVertex$ to $v$. Then set $currentVertex$ this

unmarked vertex $v$ which has minimal distance label and color the edge entering $v$ for which the minimal number from Eqn. 2 is reached.

*Step 3:* If current vertex is target ($currentVertex = t$) the procedure ends. The only path from $s$ to $t$, made out of marked edges, is the shortest path between $s$ and $t$. Otherwise, go back to Step 2.

*Dijkstra's algorithm using adjacency matrix:* In this case following variables are used: $double[,] adjacencyMatrix$ – graph's adjacency matrix; $Dictionary < V, int > verticesIndices$ - stores the corresponding index of every vertex in the adjacency matrix; $int verticesCount$-number of all vertices; $int sourceIndex$ - starting vertex index; $int targetIndex$ - destination vertex index; $int currentVertexInde$-last marked vertex index; $double[] distances$ – stores the distances from source vertex to all vertices. All vertices are indexed with the numbers from 0 to $verticesCount - 1; List < E > bestVertexEdg$- stores an edge for every vertex that minimizes its distance label; $bool [] marked$ – if $marked[i]$ is true then the vertex with index $i$ is marked; $List < E > markedEdges$ - list of all marked edges [7].

S*tep 1:* Convert the graph to adjacency matrix (a square matrix) with dimensions $n \times n$ ($n$ – number of vertices). The matrix elements are calculated by Eqn. 3:

$$A_{ij} = \begin{cases} \infty \text{ if there isn't an edge from } i \text{ to } j \\ \text{minimal edge's weight from } i \text{ to } j \end{cases} \quad (3)$$

where $A_{ii} = 0, \forall i$. A hash table which keeps the index of every vertex in the adjacency matrix is created, that so the path could be restored. A tentative distance label which represents the minimal current distance from vertex *s* to the rest vertices *v* is assigned for each vertex in the graph. For this purpose, an array $distances[]$ is used. The array is initialized as follows: $distances[s] = 0$, $distances[v] = $ big enough number where $v \neq s$ (*s* and *v* – array's indices). The vertex *s* was marked as visited and set it as current vertex using its index.

*Step 2:* The distance labels ($distances[v]$) are recalculated for each unmarked neighbor vertex *v* where an edge exists from $currentVertex$ to *v* by Eqn. 4:

$$distances[v] = \min \begin{cases} distances[vIndex], \\ distances[currentVertexIndex] \\ +c(currentVertexIndex, v) \end{cases} \quad (4)$$

where $vIndex$ and $currentVertexIndex$ are respectively the distances array's indices of vertices *v* and current marked vertex. Then it is appropriated $currentVertexIndex$ the index of this unmarked

vertex $v$ which has minimal distance label and colored the edge entering $v$ for which the minimal number from formula were reached (Eqn. 4).

*Step 3:* If the current vertex index equals the target vertex index ( $currentVertexIndex = targetVertexIndex$) the procedure ends. The only path from *s* to *t*, made out of marked edges, is the shortest path between *s* and *t*. Otherwise go back to Step 2.

### Explanation and implementation of Ford's algorithm

*Explanation:*

The Bellman-Ford algorithm is Dijkstra's algorithm modification in case that some edges have negative weights [9]. The Bellman-Ford algorithm's modification consists of: in Step 2 the distance labels $d(x)$ for all vertices are recalculated. If the distance label $d(x)$ of some vertex *x* can be changed, the distance is updated to the new lower value and if this vertex *x* is marked, its marking and the incident with it colored edges are ignored. The algorithm stops when all vertices are marked and after S*tep* 2 none of the distance labels $d(x)$ has changed. This algorithm is slower than Dijkstra's. As it admits edges with negative weights, a graph can contain negative length cycle. In case like this, the algorithm won't work properly.

*Implementation:*

Instead of $Dictionary < V, bool > marke$ , here $HashSet < V > markedVertices$ (set of all marked vertices) and $HashSet < V > unmarkedVertices$ (set of unmarked vertices) are used. The $distances[v]$ for every vertex in the graph (unlike Dijkstra's algorithm the labels of unmarked vertices are recalculated) are recalculated.

### Explanation and implementation of Floyd's algorithm

*Explanation:*

This algorithm finds the shortest path length between every couple of vertices. Edges can have negative weights but loops with negative length are not allowed [10].

*Step 1:* All vertices are numbered with the numbers from 1 to *n*. Matrix $D^0 = (d_{ij}^0)_{nxn}$ is determined. Element $(i, j)$ is the shortest edge's length (with least weight) between *i* and *j*. $d_{ij}^0 = \infty$ if $(i, j)$ edge is missing and $d_{ii}^0 = 0, \forall i$.

*Step 2:* For each $m \in [1, n]$ are determined the matrix elements $D^m = (d_{ij}^m)_{nxn}$ by the matrix elements $D^{m-1} = (d_{ij}^{m-1})_{nxn}$ using Eqn. 5:

$$d_{ij}^m = min\{d_{ij}^{m-1}, d_{im}^{m-1} + d_{mj}^{m-1}\} \quad (5)$$

Every element $(i,j)$ in the matrix $D^n$ is the shortest path's length from $i$ to $j$.

*Implementation:*

*Step 1:* Convert the graph to adjacency matrix (a square matrix) with dimensions $n$ x $n$ (n – number of vertices). The matrix' elements are calculated by Eqn. 6:

$$d_{ij}^0 = \begin{cases} \infty \; if \; there \; isn't \; an \; edge \; from \; i \; to \; j \\ minimal \; edge's \; weight \; from \; i \; to \; j \end{cases} \quad (6)$$

where $d_{ii}^0 = 0, \forall i$. A hash table which keeps the index of every vertex in the adjacency matrix is created, so the path could be restored [7].

*Step 2:* Three nested for-loops are used to represent Eqn.5:

$$Dm[i,j] = Math.Min(prevD[i,j], prevD[i,m-1] + prevD[m-1,j])$$

*Explanation and implementation of Danzig's algorithm*

*Explanation:*

*Step 1:* All vertices are numbered with the numbers from 1 to *n*. Matrix $D^0 = (d_{ij}^0)_{nxn}$ is determined. The element $(i,j)$ is the shortest edge's length (with least weight) between $i$ and $j$ [11]. The elements $d_{ij}^0 = \infty$ if $(i,j)$ edge is missing and $d_{ii}^0 = 0$ for every $i$.

*Step 2:* The matrix $D^m$ for each $m = 1, 2, ..., n$ using $D^{m-1}$ and $D^0$ are determined by the following equations:

$$d_{ii}^m = 0 \; for \; each \; i \; and \; each \; m \quad (7)$$
$$d_{ij}^m = \min\{d_{ij}^{m-1}, d_{im}^m + d_{mj}^m\}, when \; i, j$$
$$= 1, 2, ..., m-1 \quad (8)$$
$$d_{im}^m = \underset{j=1,2,...,m-1}{min}\{d_{ij}^{m-1} + d_{jm}^0\}, when \; i$$
$$= 1, 2, ..., m-1 \quad (9)$$

$$d_{mj}^m = \underset{i=1,2,...,m-1}{min}\{d_{mi}^0 + d_{ij}^{m-1}\}, when \; j$$
$$= 1, 2, ..., m-1 \quad (10)$$

This algorithm performs the same operations as Floyd's algorithm but in other order. In this case the matrix $D^m$ ($m \geq 1$) has dimensions $m \times m$.

*Implementation:*

For this algorithm following variables are used: $double[,] adjacencyMatrix$ -stores the adjacency matrix which elements are described below; $Dictionary < V, int > verticesIndices$ - stores the corresponding index of every vertex in the adjacency matrix; $int \; verticesCount$ - number of all vertices in the graph; $double[,] D0$ - matrix $D^0$; $double[,] Dm$ -current matrix $D^m$ ($m = 1 ... n$); $double[,] prevDm$ -represents matrix $D^{m-1}$.

*Step 1:* Convert the graph to adjacency matrix (a square matrix) with dimensions $n \times n$ (n -number of vertices) [7]. The matrix elements are

$$d^0_{ij} = \begin{cases} \infty, \; if \; there \; isn't \; an \; edge \; from \; i \; to \; j \\ minimal \; edge's \; weight \; from \; i \; to \; j \end{cases} \quad (11)$$

$d^0_{ii} = 0, \forall i$. We also create a hash table which keeps the index of every vertex in the adjacency matrix so we can restore the path.

*Step 2:* The matrix $D^m$ for each $m = 1 ... n$ is determined by the equations for $Dm[i, m-1]$ and $Dm[m-1, j]$ ($i, j = 0 ... m-2$):

$$Dm[i, m-1] = Math.Min(Dm[i, m-1], prevDm[i,j] + D0[j, m-1]) \quad (12)$$

$$Dm[m-1, j] = Math.Min \quad (13)$$

The elements of $Dm[i,j]$ ($i, j = 0 ... m-2$) depend on the upper ones $Dm[i,j] = Math.Min(prevDm[i,j], Dm[i, m-1] + Dm[m-1, j])$.

**Table 1.** The values of execution time and different number of vertices for shortest path algorithms (Dijkstra, Ford, Floyd, Dantzig).

| № | Vertices | Edges | Dijkstra's algorithm | Dijkstra's algorithm by adjacency matrix | Ford's algorithm | Floyd's algorithm | Dantzig's algorithm |
|---|---|---|---|---|---|---|---|
| 1 | 100 | 10 000 | 0.142 | 0.066 | 0.042 | 0.341 | 0.387 |
| 2 | 500 | 50 000 | 1.165 | 0.504 | 0.584 | 32.123 | 35.229 |
| 3 | 500 | 100 000 | 1.036 | 0.769 | 0.755 | 34.307 | 36.981 |
| 4 | 500 | 1 000 000 | 3.03 | 5.209 | 2.707 | 37.406 | 45.805 |
| 5 | 1 000 | 100 000 | 1.468 | 0.64 | 3.238 | 266.92 | 324.216 |
| 6 | 2 500 | 1 000 000 | 15.764 | 9.753 | 14.622 | 993.166 | 1985.166 |
| 7 | 5 000 | 500 000 | 24.813 | 5.958 | 61.076 | - | - |
| 8 | 5 000 | 1 000 000 | 48.685 | 4.987 | 17.488 | ~13620 | - |
| 9 | 5 000 | 1 000 000 | 35.545 | 12.706 | 69.894 | - | - |
| 10 | 10 000 | 100 000 | 68.81 | 19.942 | 75.975 | - | - |
| 11 | 10 000 | 1 000 000 | 84.742 | 17.783 | 80.715 | - | - |
| 12 | 25 000 | 5 000 000 | 506.299 | - | - | - | - |
| 13 | 25 000 | 5 000 000 | 2259 | - | - | - | - |
| 14 | 25 000 | 5 000 000 | - | - | 757.885 | - | - |
| 15 | 25 000 | 5 000 000 | - | - | 1232.543 | - | - |

RESULTS AND DISCUSSION

The algorithms of Dijkstra [8], Floyd-Warshall [9], Bellman-Ford [10] and Dantzig [11] for finding the shortest path were tested using Visual Studio Community 2015, Intel® Pentium® Processor N3710, 1.6 GHz (4 CPUs), 4096 MB RAM [7,13]. The values of execution time and different number of vertices for shortest path algorithms (Dijkstra, Ford, Floyd, Dantzig) are presented in Table 1The experimental results are shown in Table 2. Time complexity of the shortest path algorithms depends on the number of vertices, number of edges and edge length. As can be seen, the time complexity of the Dijkstra's algorithm depends on the number of vertices and is inversely proportional to the number of vertices. The time complexity was higher for Bellman-Ford algorithm than Dijkstra's algorithm. For higher number of nodes, the Dijkstra's algorithm is better and efficient (Table 3) [14-17].
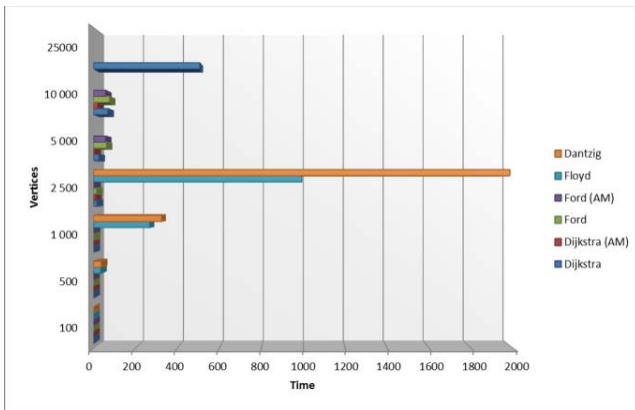


**Fig. 1.** Execution time and different number of vertices for the shortest path algorithms - Dijkstra, Ford, Floyd and Dantzig.

As it can be seen from the results in Table 2, the Dijkstra's algorithm and its implementation for adjacency matrix in C # representation of graphs provide better performance in the cost of memory. The time complexity for the matrix representation is $O(V^2)$.

The algorithms for finding the shortest paths – Dijkstra's, Ford's, Floyd's and Dantzig's were examined and analyzed. The best results for the values of execution time and different number of vertices are obtained by Dijkstra's algorithm (Table 2 and Figure 2). This algorithm is also implemented through a adjacency matrix. As can be seen in Figure 2, better results are obtained when using an adjacency matrix for the same input parameters.

A C# implementation for drawing the shortest path for Dijkstra's algorithm was developed. The software draws and marks the nodes and edges of the finding shortest path by coloring them in red. The algorithm of Dijkstra is implemented and visually demonstrated in Visual Studio Community 2015 [7,13]. Figure 3 shows C # implementation of some examples of Dijkstra's algorithm. Graphic representation is going to be implemented for the rest algorithms for finding the shortest paths.

**Table 3.** Dijkstra's algorithm execution time in seconds.

| Number of vertices | Dijkstra's algorithm | Dijkstra's algorithm by adjacency matrix |
|---|---|---|
| 50 | 0.173 | 0.297 |
| 100 | 0.322 | 0.329 |
| 250 | 0.327 | 0.491 |
| 500 | 0.334 | 0.4 |
| 750 | 0.507 | 0.61 |
| 1000 | 1.3 | 0.494 |
| 2500 | 13.425 | 2.223 |
| 5000 | 16.682 | 2.959 |
| 7500 | 34.61 | 6.198 |
| 10 000 | 81.373 | 24.103 |
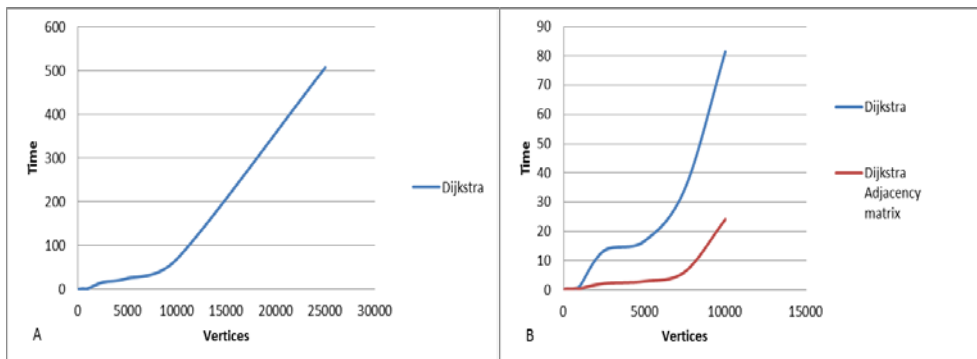


**Fig. 2.** Relationship between the number of vertices and execution time for Dijkstra's algorithm and its implementation: A) without adjacency matrix in C #; B - with adjacency matrix in C #.
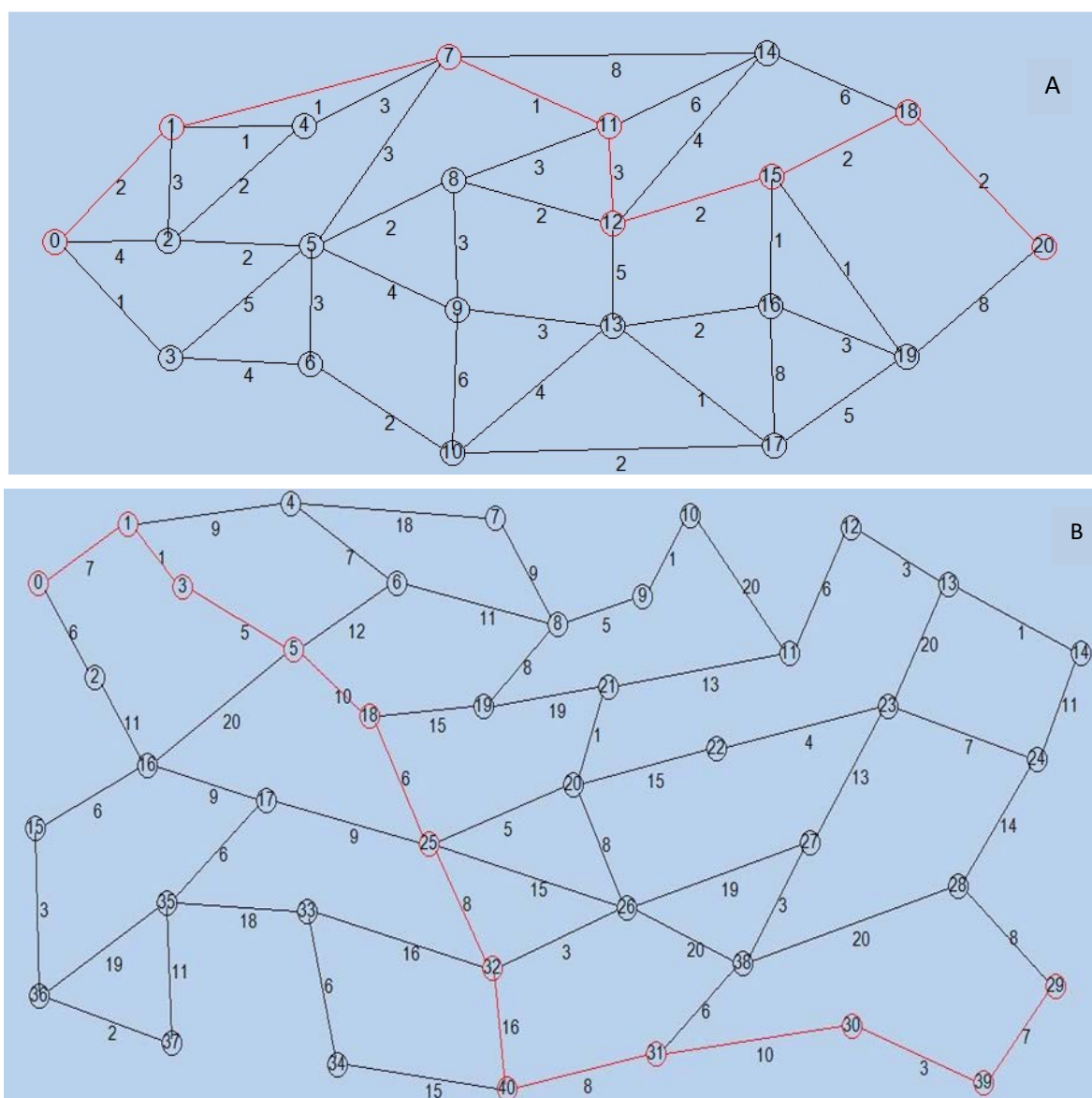
**Fig. 3.** Illustration of Dijkstra's algorithm search for finding shortest path from a start node to a goal node: A) n = 21, m= 41, B) n = 41, m = 60. The found shortest path is coloured in red.

In conclusion, we can say that the calculation of shortest paths in interaction graphs is an important method for network analysis in computational biology. This report draws attention to the important computational problem and provides a number of new algorithms, partially specifically tailored for biological interaction graphs.

REFERENCES

1. K. Magzhan, H. Jani, *IJSTR*, **2** (6), 100 (2013).
2. G. Pavlopoulos, M.Secrier, C.Moschopoulos, T. Soldatos, S. Kossida, J. Aerts, R.Schneider, P. Bagos *BioData Mining,* **4**(10), 1 (2011).
3. L. Ulrich, *Nucleic Acids Res.,* **35**, 386 (2007).
4. M. Krull, N. Voss, C.Choi, S. Pistor, A. Potapov, E. Wingender, *Nucleic Acids Res.*, **31**(1), 97 (2003).
5. T. Cormen, Ch. Leiserson, R. Rivest, C.Stein, Cambridge, Massachusetts 02142, *The MIT Press,* (2009).

6. W. Huber, V. Carey, L. Long, S. Falcon, R. Gentleman, *BMC Bioinformatics*, **8,** S8 (2007).
7. M. Negnevitsky, *Artificial Intelligence: A Guide to Intelligent Systems*, Third ed., Addison-Wesley, (2011).
8. J. Edmonds, *Lectures in Applied Mathematics*, **2,** 346 (1968).
9. E. Dijkstra, *Numer. Math.,* **1**, 269 (1955).
10. L. Ford, *Raud Corporation Report*, P-923 (1946).
11. R. Floyd, *Comm. ACM*, **5**, 345 (1962)
12. G. Dantzig, International Symposium, Rome, Gordon and Breach, 91, 1966.
13. B. Johnson, *Professional Visual Studio* (2015).
14. V. Vladimirov, F. Sapundzhi, R. Kraleva, V. Kralev, *Biomath Communications*, **3** (1), P71, (2016).
15. F. Sapundzhi, T.Dzimbova, N.Pencheva,P.Milanov, *Journal of Computational Methods in Molecular Design*, **5**, 98 (2015).
16. V. Kralev, *IJASEIT,* **7** (5), 1685 (2017).
17. V. Kralev, R. Kraleva, *IJACR,* **7** (28), 1 (2017).

*Workshop*

*Recent Progress in Bio-electrochemical systems*

# Sulfide and nitrate driven fuel cell. Chemical and biochemical denitrification

S. Stefanov*, E. Razkazova-Velkova, M. Martinov, Ts. Parvanova-Mancheva, V. Beschkov

*Institute of Chemical Engineering, Bulgarian Academy of Sciences, Acad. G. Bonchev, Str. Bldg.103, 1113 Sofia, Bulgaria*

A fuel cell is constructed for simultaneous sulfide oxidation and nitrate reduction. The results for biological and chemical denitrification in the cathode compartment are compared. The influence of different concentrations of sulfides and nitrates on the electrical power output of the fuel cell is examined, as well as their simultaneous neutralization. The electrodes used in the anode compartment are graphite rods and pyrolyzed paddling. The biological reduction of the nitrates is carried out by *Pseudomonas denitrificans* which increases the rate of nitrate depletion compared to the chemical fuel cell.

**Keywords**: Fuel cell, Sulfide oxidation, Denitrification, *Pseudomonas denitrificans*

## INTRODUCTION

Wastewater is polluted with a variety of harmful substances, but we focused our efforts on hydrogen sulfide and nitrate pollution because of their high toxicity and detrimental environmental impact as a major prerequisite for acid rain. The sources of pollutants can be divided generally to natural and anthropogenic. Specifically for hydrogen sulfide the natural sources are volcanoes, thermal springs, closed deep water basins. The anthropogenic ones are associated with the petroleum, leather, pulp and textile industries, as well as sewage systems and wastewater treatment plants. The main processes for its neutralization are adsorption or absorption that can be combined with oxidation with strong oxidants [1-6], precipitation with metals [7] or biological oxidation [8]. Methods for thermal and electrical decomposition are also developed [9-11]. A classical method for hydrogen sulfide treatment is the Claus process but it requires high temperatures and specific and expensive catalysts [12]. Nitrate ion content in natural waters can be due to the excessive use of nitrogen composts or insufficient purification of wastewaters from households, industry and agriculture. After their reduction the nitrites produced are much more harmful for the animals' and humans' health. There are several established processes for treatment and neutralization of nitrate-containing waters, which can be generally divided as physicochemical and biological ones. Some of the main physicochemical methods are reverse osmosis, ion exchange, electrodialysis, distillation and activated carbon absorption [13-16]. Physicochemical methods are usually very expensive, especially when large

quantities of wastewaters have to be treated and most result in high nitrate concentrated waters that can lead to additional problems concerning their follow up treatment. Biological denitrification is regarded as a very perspective and efficient method [16, 17]. The conclusion that can be derived from this is that most of the techniques for elimination of these pollutants are energy consuming and expensive as they need large capital investment and have high exploitation cost. The aim of the present study is to utilize the energy of oxidation of sulfides and reduction of nitrates in a fuel cell harvesting electrical power simultaneously with wastewater treatment.

## MATERIALS AND METHODS

The principle scheme of the fuel cell and the scheme of the experimental installation are shown in Fig. 1.
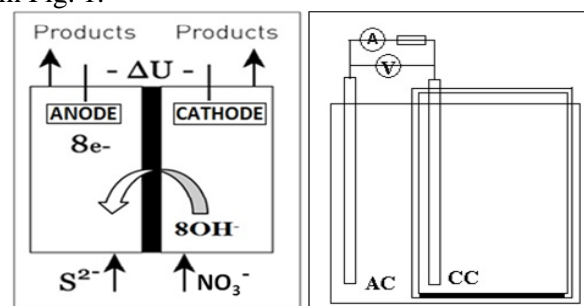


**Fig. 1.** Principle scheme of the fuel cell and the experimental installation

It consists of two concentrically situated compartments with effective volume of 300 ml each. The membrane (Celgard® 3501, S = 0.002 m², Table 1) is placed on the bottom of the inner one. The outer volume is the anode compartment (AC) and the inner one is the cathode one (CC). The electrodes used in the anode compartment are five standard cylindrical graphite rods (d=0.006 m,

* To whom all correspondence should be sent.
 E-mail: mitovmario@swu.bg

**Table 1.** Characteristics of the membrane Celgard® 3501

| Membrane | Type | Material | Thickness | Resist.($\Omega.cm^2$) | Purpose |
|---|---|---|---|---|---|
| CelGard® 3501 | Anion | Polypropylene | 25 μm | 2.55 | Alkaline battery separator |
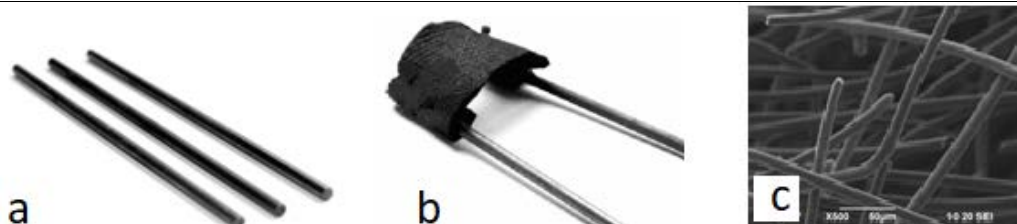


**Fig. 2.** Electrodes used in the fuel cell: a) Graphite rods, b) Paddling of activated carbon; c) SEM of a paddling of activated carbon.

L = 0.02 m, S=0.003 m$^2$) with total working surface of 0.015 m$^2$ (5 x 0.003 m$^2$) or pyrolyzed paddling of activated carbon with the same geometrical surface.

The pyrolyzation with simultaneous activation of the paddling is done by a patented technology [18] A photograph of the electrodes and SEM images of the paddling are presented in Fig. 2.

In some of the experiments 120 g (300 ml) of activated carbon (Fujikasau®, Japan, 680 m$^2$.g$^{-1}$.) were added in the cathode compartment in order to increase the electrode surface.

The feeding solutions were prepared by dissolving technical grade of $Na_2S \times 9\ H_2O$ and $KNO_3$.

The concentration of the sulfide solution was determined photometrically by converting the sulfide ion to methylene blue by addition of N,N-p-phenylenediamine [19], and the concentration of nitrates – by UV photometry by the method of Goldman & Jacobs [20].

The assumed reactions are as follows:

Anode:
$$S^{2-} + 6\ OH^- \rightarrow SO_3^{2-} + 3\ H_2O + 6\ e^-$$
$$SO_3^{2-} + 2\ OH^- \rightarrow SO_4^{2-} + H_2O + 2\ e^-$$
Total:
$$S^{2-} + 8\ OH^- \rightarrow SO_4^{2-} + 4\ H_2O + 8\ e^-$$
Cathode:
$$2\ NO_3^- + 2\ H_2O + 4\ e^- \rightarrow 2\ NO_2^- + 4\ OH^-$$
$$2\ NO_2^- + 4\ H_2O + 6\ e^- \rightarrow N_2 + 8\ OH^-$$
Total:
$$2\ NO_3^- + 6\ H_2O + 10\ e^- \rightarrow N_2 + 12\ OH^-$$
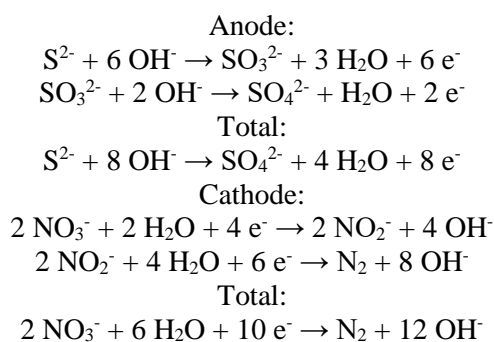
The intermediates of both reactions (sulfites and nitrites) and the product of the anode reaction (sulfates) are monitored qualitatively. By adding $BaCl_2$ to the anode solution in the presence of sulfite and sulfate ions opalescence appears due to formation of precipitates of $BaSO_3$ and $BaSO_4$. By adding 2M HCl the $BaSO_3$ dissolves and any residual opalescence is due to the presence of sulfate ($SO_4^{2-}$) ions. In the presence of nitrites the

addition of KI or KMnO$_4$ in an acid media gives ъ colorful reaction for the former or decolorizes the latter.

The strain *Pseudomonas denitrificans* (NBIMCC 1625) was chosen to perform the microbial denitrification. This strain is facultative anaerobic, autotrophic and electrical stimulation enhances its metabolism [21]. In biological denitrification, the bacteria use nitrates as electron acceptor in their breathing process in the absence of oxygen. Denitrifying bacteria reduce inorganic nitrogen compounds, such as nitrates and nitrites, into harmless nitrogen gas. Nitrates are reduced to nitrogen, passing sequentially through nitrites and nitrogen oxides in accordance with the following reaction scheme:

$$NO_3^- \rightarrow NO_2^- \rightarrow NO \rightarrow NO_2 \rightarrow N_2$$

The sequential reduction of nitrogen compounds takes place under the action of the catalytic enzymatic activity of *Pseudomonas denitrificans* under anaerobic conditions in the presence of a suitable electron donor [22, 23]

Studies were conducted with free and immobilized cells. The growth of the culture was monitored by using UV-spectrophotometry at $\lambda = 660$ nm. The growth curve is presented in Fig. 3. After a long period of lag-phase an exponential part of growth is observed that matches the denitrification phase.
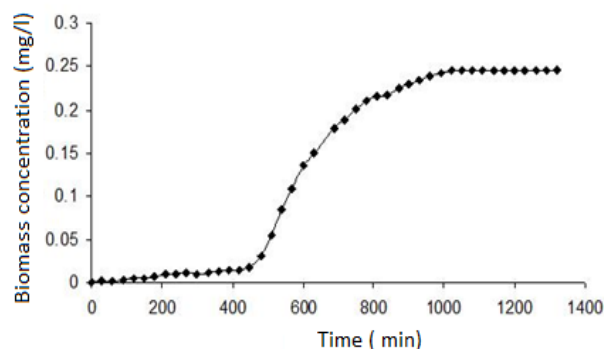


**Fig. 3.** Growth curve of *Pseudomonas denitrificans*
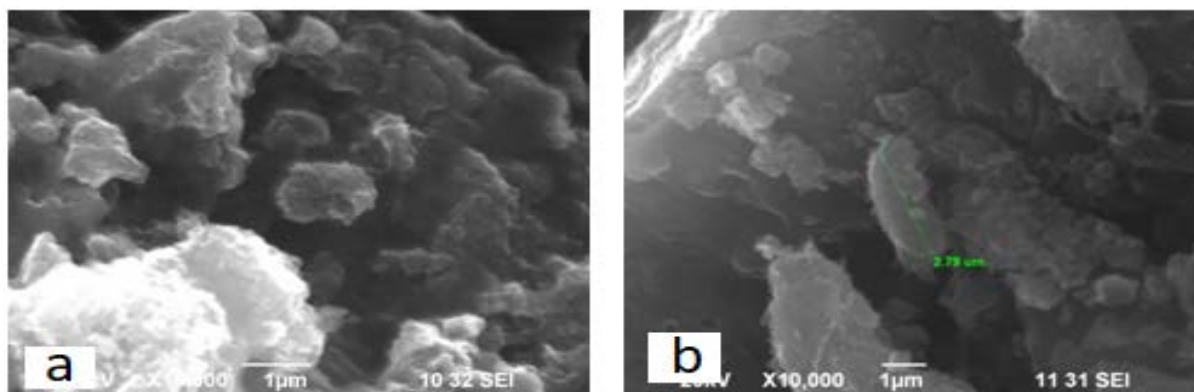
**Fig. 4.** SEM of a) Activated carbon (Fujikasui, Japan), b) Immobilized *P. denitrificans* on activated carbon (Fujikasui, Japan)

The activated granular carbon (Fujikasui®, Japan, 680 $m^2.g^{-1}$) was chosen as a support for immobilization due to the fact that microbial cells are easily attached to its surface. It has the added benefit to absorb toxic components, decreasing their concentration to tolerable values for microorganisms so that substrate and product inhibition is avoided, allowing the cell to operate at higher pollutant concentrations [24]. Additionally it has good electrical conductivity and very high specific surface area, making it an excellent electrode. The immobilized cells compose 2% of the mass of the activated carbon. SEM images of the activated carbon with and without immobilized cells are given in Fig. 4.

## RESULTS AND DISCUSSION

### *Influence of type of electrodes in anode compartment*

Previous studies by our team on a fuel cell for sulfide oxidation [25-28] show that optimal electrical and chemical results are obtained by using activated carbon as an electrode in the cathode compartment due to the large specific surface area the material provides. The effects of activated carbon as an electrode in the anode compartment are negligible compared to standard graphite rods hence an alternative was developed in

the form of pyrolyzed paddling (Figs. 2a and 2b). This configuration of electrodes was tested for the newly designed fuel cell for simultaneous oxidation of sulfides and reduction of nitrates with the results shown in Fig. 5. As the figure shows, using pyrolyzed paddling yields about 40% higher power for the first 2 hours and about 30% for the first 6 hours. The explanation for this, as well as the initial low electrical results, is that the paddling is an adsorbent and initially the two processes compete, resulting in reduction of the local concentration around the electrode and respectively the power. After the initial adsorption both the incoming and the already adsorbed sulfide ions participate in the process increasing the power output of the cell.
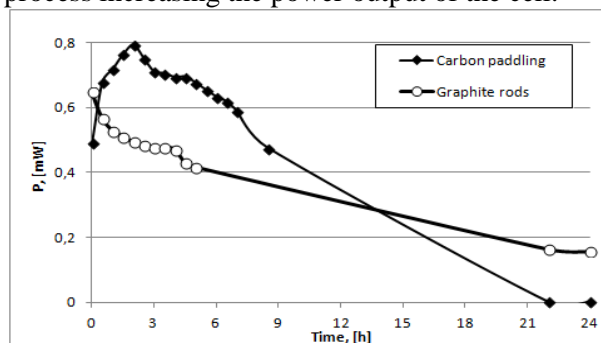


**Fig. 5.** Power in time for the tested electrodes
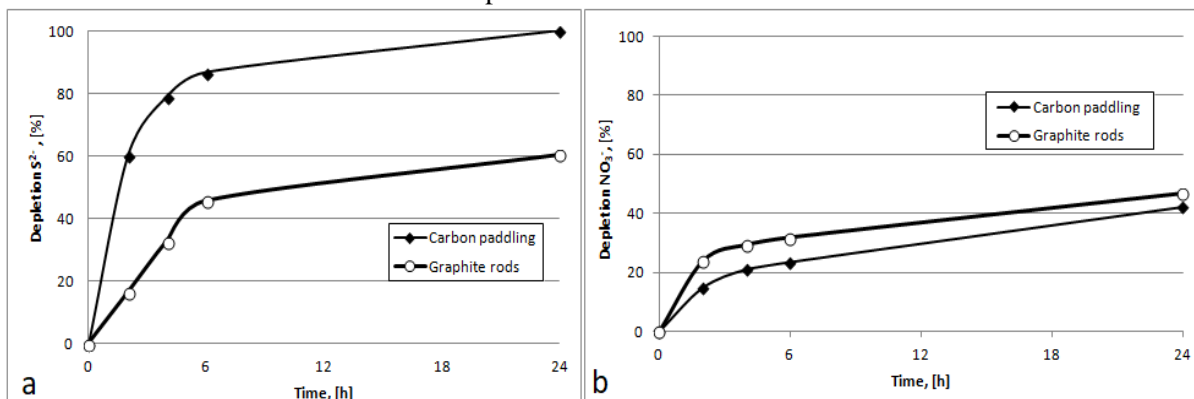


**Fig. 6.** Depletion in time of sulfides ( a) and nitrates (b)

This is also confirmed by the sulfide depletion data shown in Fig. 6a. As can be seen, the paddling rapidly adsorbs about 40% of the sulfide and accordingly intensifies the oxidation process thus increasing the power and reaching total depletion of sulfide ions for 24 hours, which is not observed in the experiment with graphite rods. This higher process intensity also provides more electrons to the cathode compartment, which intensifies the nitrate reduction process as shown in Fig. 6b.

### Influence of initial concentration

The effect of the initial concentration was studied as well. Experiments were conducted with two sets of totally different initial concentrations in the two compartments: $C (S^{2-}) = 150$ mg.l$^{-1}$ and $C (NO_3^-) = 200$ mg.l$^{-1}$ for the first experiment and $C (S^{2-}) = 500$ mg.l$^{-1}$ $C (NO_3^-) = 500$ mg.l$^{-1}$ for the second one. As can be seen from Fig. 7, the higher initial concentration provides higher power values.
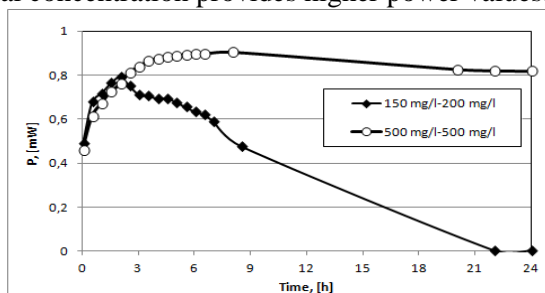


**Fig. 7.** Power in time for the tested initial concentrations

However, the capacity for oxidation of the fuel cell for sulfide ions (mg $S^{2-}$.h$^{-1}$) is limited. This is evident from the comparable power values for the first 2 hours. The "fuel" in the experiment with higher concentration is more, but the cell doesn't use it up fast enough to output more power. When the power of the lower concentration experiment decreases due to the depletion of the sulfide ions, the power in the other experiment is retained to values above the maximum for the other experiment. This is once again due to the constructive limitations for oxidation of large quantities of $S^{2-}$ ions. This is also verified by the sulfide depletion data (Fig. 8a).

On the 24$^{th}$ hour mark the sulfide concentration in the second experiment is higher than the initial one for the first experiment. By calculating the amount of processed sulfides for 24 hours we can summarize that the fuel cell oxidizes 45 mg $S^{2-}$ for 24 hours (from 45 mg total $S^{2-}$, 100% conversion) and 75 mg $S^{2-}$ for 24 hours (from 150 mg total $S^{2-}$, 50% conversion). By applying similar calculations for the reduced nitrates shown in Fig. 8b we can summarize that the fuel cell reduces 25 mg $NO_3^-$ for both experiments (from 60 mg total $NO_3^-$, ~40%, and 150 mg total $NO_3^-$, ~17%).

This allows us to assume that the maximum capacity for processing sulfides and nitrates for 24 hours of this fuel cell size using this size and type of electrodes is 75 mg of sulfides and 25 mg of nitrates.

### Fuel cell with free culture and different electrodes

One of the most promising and cheap ways for intensifying the process is the use of microorganisms. So far we have had difficulties with the use of microorganisms that promote sulfide oxidation, but we have successfully used nitrate-reducing bacterial culture – *Pseudomonas denitrificans* (strain NBIMCC 1625).

Experiments are conducted with free microorganism culture in the cathode compartment. Graphite rods are used as electrodes in contrast to the chemical cell. This is due to the impossibility to use bulk activated carbon or pyrolyzed paddling as the free culture would be immobilized on them. As such limitations are not present for the anode compartment graphite rods and pyrolyzed paddling are used as electrode as in previous experiments. The results are shown in Fig. 9.
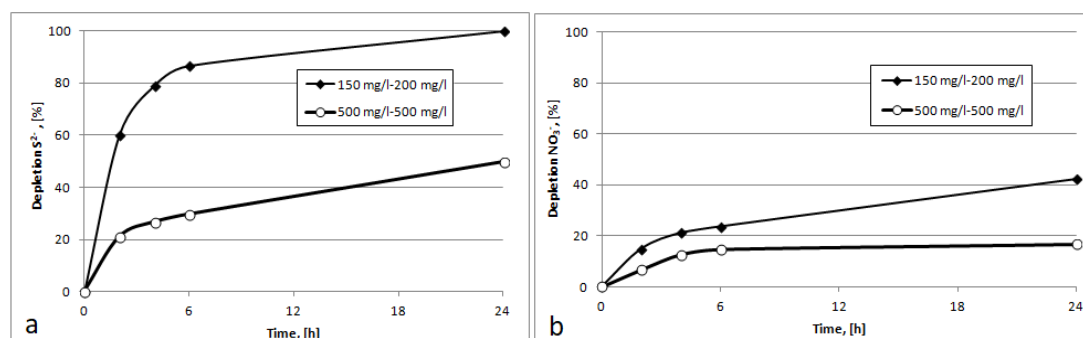


**Fig. 8.** Depletion in time of sulfides (a) end nitrates (b)
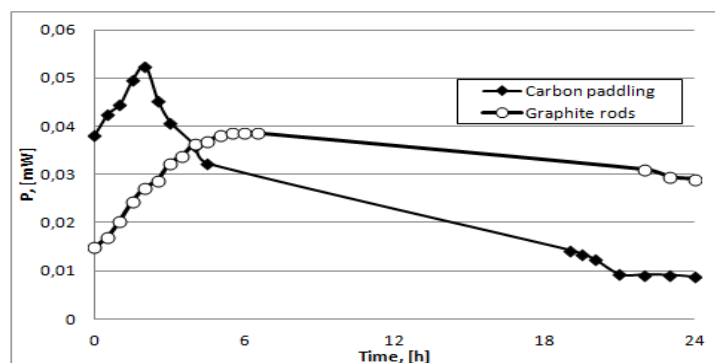
**Fig. 9.** Power in time for the tested electrodes
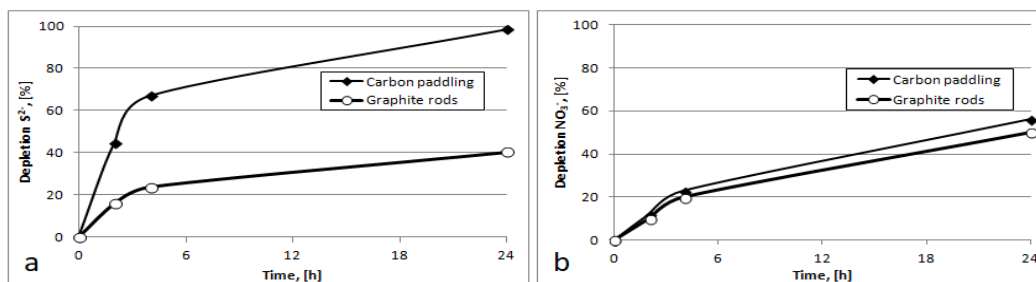


**Fig. 10.** Depletion in time of sulfides ( a) end nitrates (b)

As can be seen, the course of the curves is similar to those obtained by the chemical cell, but due to the use of electrodes with much smaller effective surface area in the cathode compartment the power obtained is by one order of magnitude lower. The rate of depletion of sulfides (Fig. 10a) is faster when the more efficient pyrolyzed paddling electrodes are used. The depletion of nitrates is increased by 10-15% (Fig. 10b) compared with the chemical cell as a result of the action of bioculture. Even though the results are better our expectations were higher in regard to the nitrate oxidation and that is the reason we worked on improving the performance of the microorganisms by immobilizing them. According to the literature [21] the immobilized culture is more resistant to concentration fluctuations and reduces more nitrates per unit of
time compared to the free one.

*Fuel cell with immobilized cells.*

The most commonly used method of intensifying the work of biocultures is to immobilize them on a suitable support. One of the most conventionally used supports is activated carbon due to the combination of chemical and physical properties of the surface, improving the fixing on the bed and promoting the development of the culture as well as its low cost. For us it has the added benefit of high electrical conductivity so the activated carbon can be used as an electrode with which we have already achieved excellent results. Data on experiments with the immobilized bioculture on the activated carbon used for the electrode in the cathode compartment and the pyrolyzed paddling in the anode compartment for two totally different initial concentrations of sulfides and nitrates are given in Fig. 11. The fuel cell shows very good power output for both initial concentrations. The rate of depletion of $S^{2-}$ (Fig. 12a) is also high, 100% for the lower initial concentration and 40% for the higher one. The reason for the poorer oxidizing performance in spite of the high power output is that the constructive limits of the capacity for oxidizing are reached in the second experiment.

The performance of bioculture in nitrate depletion (Fig. 12b) is excellent and within 90-95% for both concentrations. This is an inherent advantage of microorganisms – when there is more "food" they develop exponentially until the resource is depleted.
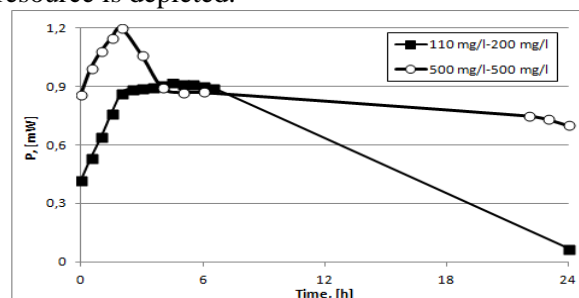


**Fig. 11.** Power in time for immobilized cells in the tested initial concentrations
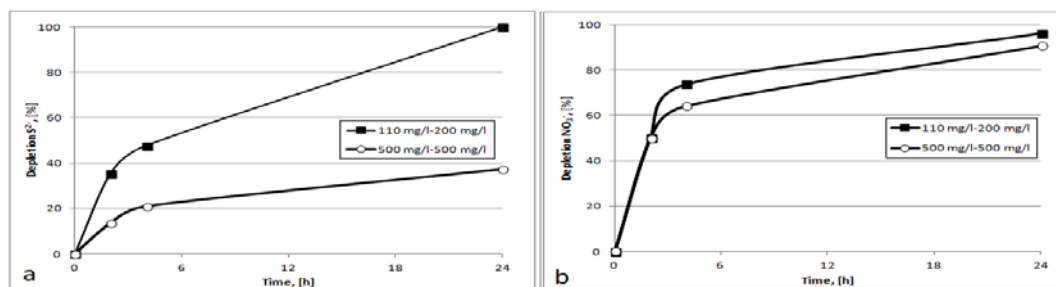
**Fig. 12.** Depletion in time of sulfides (a) end nitrates (b)

*Comparison of biological and chemical denitrification*

Experiments were carried out to compare the chemical and biological (with microorganisms in the cathode compartment) fuel cells of the same design, electrodes and high initial concentrations that are challenging for neutralizing them to harmless components. As shown in Fig. 13, the electrical power is high, with both cells delivering about 0.9 mW.h$^{1-}$(about 20 mW for 24 h). Regarding the purification of sulfides (Fig. 14a), the chemical cell performs better with 50% S$^{2-}$ depletion for 24 hours, while for the biological cell the depletion is 37% (75 mg oxidized S$^{2-}$ for the former compared to 55 mg S$^{2-}$ for the latter (from 150 mg total)). Regarding the depletion of nitrates (Fig. 14b) the fuel cell with immobilized culture has drastic advantage with 90% to 17% for the chemical cell (135 mg reduced NO$_3^-$ for the former compared to 25 mg NO$_3^-$ for the latter (from 150 mg total)).

CONCLUSIONS

The co-treatment of wastewater contaminated with sulfides and nitrates with simultaneous generation of electric energy is feasible with a fuel cell of our own design.

The energy obtained in both types of fuel cells (chemical and biological) is stable and is within the range of 0.9 mW.h$^{-1}$ for the duration of the experiment.

With regard to the purification of sulfides, both cells operate similarly but have constructive limitations and can deal with contamination up to 75 mg / 24 h.

In terms of nitrate purification, the biological cell is reducing 5 times more pollutant than the chemical one – 135 mg / 24 h for the former compared to 25 mg / 24 h for the latter.

The comparison between chemical and biological fuel cell shows that one of the promising ways to intensify the purification process is the use of microorganisms.
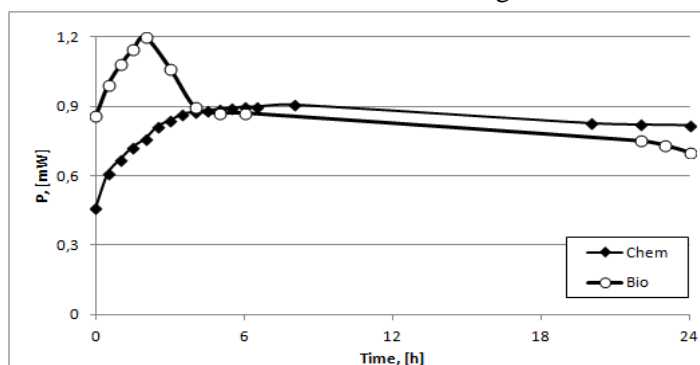


**Fig. 13.** Power in time for the tested different type fuel cell
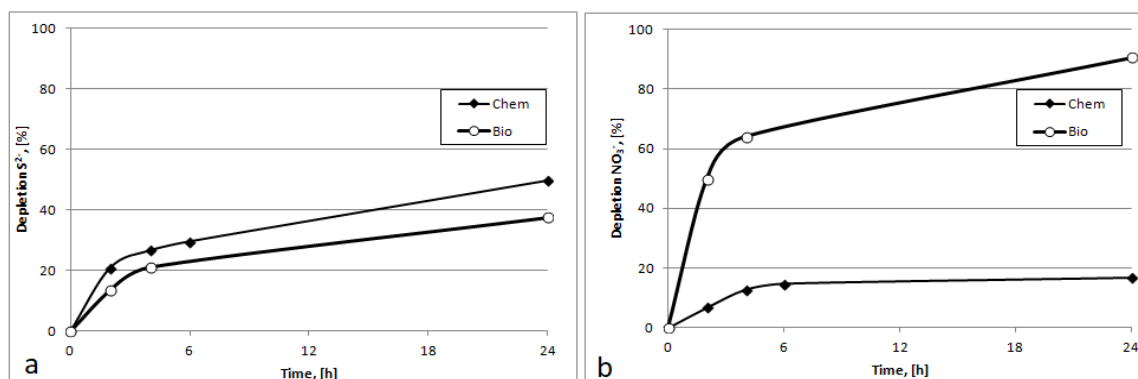


**Fig. 14.** Depletion in time of sulfides ( a) end nitrates (b)

REFERENCES:

1. R. Cotrino, A.D. Levine, P. Amitzoglou, J. S. Perone, *Florida Water Resourses Journal*, pp. **22-25**, (2007).

2. M. Seredych, T.J. Bandosz, *Chem. Eng. J.*, 12859, (2007).

3. R.Wang, *Sep. Purif. Technol.* **31,** 111, (2003).

4. S. Yasyerli, I. Ar, G. Dogu, T. Dogu, *Chem. Eng. Process.,* **41 (9)**, 785 (2002).

5. A. T. Lemley, J. J. Schwartz, L. P. Wagenet, *Fact Sheet* **7**, Water treatments note, January 1999.

6. M. Tomar, T.H.A. Abdullah, *Water Res.,* **28**, 2545 (1994).

7. M. Henze, P. Harremoe, J. la Cour Jansen, E. Arvin, Wastewater Treatment – Biological and Chemical Processes, editors, second ed. Springer, Berlin, 1997.

8. Y. Kodama, Y. Watanabe, *Appl. Environ. Microbiol.,* **69**, 107 (2003).

9. G. Özgül, A.S. Koparal, Ü.B. Öğütveren, *Separation and Purification Technology,* **62**, 656 (2008).

10. J. Zaman, A. Chakma, *Fuel Processing Technology,* **41**, 159 (1995).

11. Y. Wang, Y. Heqing, W. Efeng, *Journal of Electroanalytical Chemistry,* **497**, 163 (2001).

12. M. Capone, in: J.K. Kroschwitz, M. HoweGrant (eds.), *Encyclopedia of Chemical Technology*, vol. **23**, Wiley, New York, p. 432, 1997.

13. A. Mautner, T. Kobkeatthawin, A. Bismarck, *Resource-Efficient Technologies,* **3,** 22 (2017).

14. A. Bhatnagar, E. Kumar, M. Sillanpää, *Chem. Eng. J.,* **163**, 317 (2010).

15. A. Bhatnagar, M. Sillanpää, *Chem. Eng. J.,* **168**, 493 (2011).

16. M. Shrimali, K.P. Singh, *Environmental Pollution,* **112**, 351 (2001).

17. S. Xia, F. Zhong, Y. Zhang, H. Li, X. Yang, *Journal of Environmental Sciences*, **22 (2),** 257 (2010).

18. L. Ljutzkanov., A. Atanasov, BG patent № 63594 /26.06.2002.

19. T.D. Rees, A.B. Gyllenpetz, A.C. Dochery, *Analyst*, **96**, 201 (1971).

20. E. Goldman, R. Jacobs, *J. Am. Water Works Assoc.*, **53**, 187 (1961).

21. Ts. Parvanova-Mancheva, Ph. D Thesis, 2009.

22. L. Foglar, F. Briski, L. Sipos, M. Vukovic, *Bioresource Technol.*, **96**, 879 (2005).

23. J.-H. Wang, B.C. Baltzis, G.A. Lewandowski, *Biotechnol. Bioeng.*, **47**, 26 (1995).

24. V. Beschkov, Biocatalysis Research Progress, editors Francesco H.R., Andrea R., *Published by Nova Science Publishers, Inc.*, Chapter XII, p. 281-305, (2008).

25. E. Razkazova-Velkova, M. Martinov, S. Stefanov, V. Beschkov, *Proceedings of the Georgian National Academy of Sciences, Chemical Series*, **42 (3)**, 258, 2016, ISSN:0132-6074.

26. M. Martinov, E. Razkazova-Velkova, S. Stefanov, *Journal of International Scientific Publications: Ecology & Safety*, **10**, 246 (2016), ISSN:1314-7234.

27. M. Martinov, E. Razkazova-Velkova, V. Beschkov, *Scientific Works of University of Food Technologies - Plovdiv*, LX, **1**, UFT Academic Publishing House, Plovdiv, p. 1046, 2013, ISSN:1314-7102.

28. E. Razkazova-Velkova, M. Martinov, L. Ljutzkanov, N. Dermendzhieva, V. Beschkov, *Scientific Works of University of Food Technologies - Plovdiv*, LX, **1**, UFT Academic Publishing House, Plovdiv, p. 1091, 2013, ISSN:1314-7102.

# Improved operational stability of a laccase-based electrode applicable in biofuel cells

N. Dimcheva*, E. Horozova

*Department of Physical Chemistry, University of Plovdiv "P. Hilendarski", Plovdiv, Bulgaria*

To ensure high electrocatalytic activity and operational stability of immobilized laccase enzyme (isolated from the basidiomycetes *Trametes pubescens*), different immobilization protocols on various electrode materials (graphite, gold and glassy carbon) were studied. The physical methods of immobilization – physisorption or entrapment of the enzyme in a composite layer, did not yield bioelectrodes with long lasting activity, whilst the immobilization approach based on covalent attachment of the enzyme to the electrode surface was found to produce a bioelectrode with extended operational stability. The basic electrode material was found to play an important role in bioelectrode's performance. The comparative studies carried out with two different electrode materials – polycrystalline gold and glassy carbon, modified with electrodeposited gold nanoparticles, with identically immobilized laccase on them showed much higher current density for the second type of enzyme electrode. An extended operational stability of ca. 3 weeks was achieved for the laccase immobilized on gold-nanoparticles modified glassy carbon electrode. The value of the open circuit voltage (over 450 mV *vs.* Ag/AgCl, 3M KCl at pH = 4.5) of the laccase based electrode suggests that it is a good candidate for cathode when engineering biofuel cells.

**Keywords:** Laccase, Immobilization, Self-assembled monolayers, Biocathode.

## INTRODUCTION

There are two multicopper oxidases – the enzymes laccase and bilirubin oxidase, that are capable of performing the oxygen reduction even more efficiently than platinum and, hence, they are often used for the development of cathodes for biofuel cells applications [1-4]. Type of laccase immobilization is of key importance in the latter case because it has to guarantee that the enzyme is electrochemically active [5, 6], i.e. capable of exchanging electrons with the underlying electrode surface, and possesses long-lasting operational stability [7] which is one of the most important electrode characteristics when constructing biofuel cells.

One of the main drawbacks of the laccase-based bioelectrodes is the extremely short lifetime of the immobilized enzyme – depending on the immobilization type it does not exceed 24-48 hours. In this connection, the objective of the present work is to find a suitable immobilization approach, which ensures an extended lifetime of the immobilized laccase together with high electrochemical activity of the immobilized enzyme.

## EXPERIMENTAL

### Materials

Laccase (Lac) (E.C. 1.10.3.2) from *Trametes pubescens* (kindly provided by Dr R. Ludwig, BOKU University, Vienna, Austria) was with homogeneous activity of 46 U mg$^{-1}$ (1 U oxidises 1.0 µmole of ABTS per min at pH 4.5 at 25 °C).

Cysteamine (Acros), chitosan (Acros), glutaric aldehyde (Fisher), ABTS-2,2'-azino-bis(3-ethylbenzothiazoline-6-sulphonic acid (Acros), citric acid monohydrate and sodium citrate (Fluka); $HAuCl_4.H_2O$ (Acros) were of analytical grade and used as received.

The working electrodes were discs from polycrystalline gold (d = 1.0 mm, CHI, USA), glassy carbon (d = 3.0 mm, CHI, USA) or graphite (d = 3.0 mm, RWO, Germany).

Buffer solutions (0.05 M) were made of citric acid and sodium citrate dissolved in double distilled water with pHs 4.5, and 4.0, adjusted with a pH meter pH 211 (Hanna Instruments, USA). To increase the ionic strength of the buffer solutions, $NaClO_4$ was added to the buffer to 0.1 M concentration.

### Apparatus and measurements

All electrochemical experiments were performed in a conventional three-electrode cell (working volume 25 ml). Ag/AgCl (3M KCl) was used as a reference electrode, graphite, glassy carbon or polycrystaline gold as working electrode, and a platinum wire as an auxiliary electrode, connected to a computer-controlled electrochemical workstation PalmSens (Palm Instruments BV, The Netherlands).

The biocatalytic activity of the immobilized laccase was tested by constant-potential amperometry, by adding aliquots of 1 mM aqueous solutions of ABTS (freshly prepared before measurements) to 10 ml of buffer (pH=4.0 or

* To whom all correspondence should be sent.
E-mail: nina.dimcheva@uni-plovdiv.net

pH=4.5) with simultaneous registration of the current at a constant potential of -0.1 V. The solution was stirred at 460 rpm during the measurements with a magnetic stirrer (IkaMag RCT, Ika, Germany). Cyclic voltammetry (CV) at scan rates from 5 to 50 mV s$^{-1}$; differential pulse voltammetry (DPV) at a scan rate of 7 mV s$^{-1}$ with 30 mV amplitude and square wave voltammetry (SWV) with an amplitude of 25 mV, at a frequency of 2-5 Hz, were also used in the studies. When necessary, the solutions were purged with either Ar gas or air.

Five different immobilization protocols were tested for laccase immobilization: i) Physical adsorption from laccase solution (16 mg mL$^{-1}$) on graphite; ii) Sorption of Lac onto graphite modified with electrodeposited gold; iii) Entrapment of laccases in chitosan layer, deposited on graphite; iv) Immobilisation of laccases onto graphite modified with chitosan- gold particles composite; v) Covalent binding of laccase to cysteamine moieties self-assembled on gold using a bifunctional reagent (glutaric aldehyde).

Covalent immobilization was done on both smooth polycrystalline gold electrode and a glassy carbon electrode with electrodeposited thin gold layer (up to 100 nm thick). Before modification both gold and glassy carbon electrodes were polished with 0.3 and 0.05 μm alumina slurry on a polishing cloth (LECO, USA), water-rinsed and cleaned by ultrasonication in water for 2-3 min.

The working surface of the cleaned and polished glassy carbon electrodes was modified through direct electrodeposition of gold. The metal particles were grown onto the electrode surface by electroreduction of tetrachloroaurate ion from electrolyte containing 2% HAuCl$_4$, dissolved in 0.1 M HCl, by applying a constant potential of -155 mV (*vs*. Ag/AgCl, 3M KCl) for 5 s.

Prior to the enzyme immobilization both electrode types – smooth gold and gold-modified GC electrodes were cleaned electrochemically in 0.5 M H$_2$SO$_4$ by cyclic voltammetry (CV, scan rate 0.1 V s$^{-1}$) over the potential range from 0 to 1.7 V (*vs*. Ag/AgCl, 3 M KCl) for at least 10 cycles, then thoroughly rinsed with double distilled water. The self-assembly of cysteamine was carried out under static conditions by immersing the electrodes in solutions containing 20 mg ml$^{-1}$ cysteamine dissolved in distilled water. The duration of the adsorption process was varied from 1 to 24 h. After completing the chemisorption the loosely bound cysteamine was removed from the surface by soaking the electrode in water for ca. 0.5 h at room temperature and then rinsed thoroughly. Then a 9 μL drop of laccase solution (16 mg mL$^{-1}$) was cast on

the electrode surface and 3 μL of glutaric aldehyde (45 mM aqueous solution) was mixed with it and allowed to react for 30 min at ambient temperature. So prepared enzyme electrode was stored in 0.05 M sodium citrate buffer of pH=5.6 in a refrigerator at a temperature of 4 °C until measurements.

## RESULTS AND DISCUSSION

Several protocols for laccase (Lac) attachment to the electrode surface, using physical methods for immobilization (physisorption, entrapment in composite layer and sorption on porous surface) were explored in order to choose the optimal one guaranteeing high electrocatalytic activity, resp. high current density, low noise level, and extended operational stability.

The ability of laccase to perform mediated electron transfer in the presence of substituted aromatic compounds was used as a tool for measuring the apparent enzymatic activity of the immobilized enzyme. Since 2,2'-azino-bis (3-ethylbenzthiazoline-6-sulfonic acid, also known as ABTS, is routinely used to determine the homogeneous catalytic activity of laccase enzyme, it was chosen as the redox mediator (electron shuttle) in these studies for optimization of the experimental conditions and as a basis to compare the electrocatalytic activity of differently immobilized laccases.

Chronoamperometric records of the electrode response (Fig. 1A) to ABTS at a constant potential of – 100 mV (*vs*. Ag|AgCl, 3 M KCl) and under oxygenated conditions suggest that the maximum current variation upon addition of the substrate is achieved with the electrode prepared by usual physical adsorption of the enzyme onto the graphite surface. This electrode preparation shows also the lowest noise level and the widest dynamic range, which motivated us to choose this immobilization protocol for further studies. On Fig.1 B are compared the CVs of electrodes with laccase immobilized by methods 1, 2 and 4 at pH = 4.0; v = 10 mV s$^{-1}$; 25 °C. These curves differ in the values of the capacitive current, suggesting big alterations in the electrochemically accessible surface area of so modified electrodes. The graphite electrode with adsorbed laccase is characterized with the smallest surface area producing in the same time the largest response in ABTS present. From these findings it could be deduced that the electrode with physisorbed laccase ensures the highest activity of the immobilized enzyme, thus further studies shall be continued with this type of electrode fabrication.
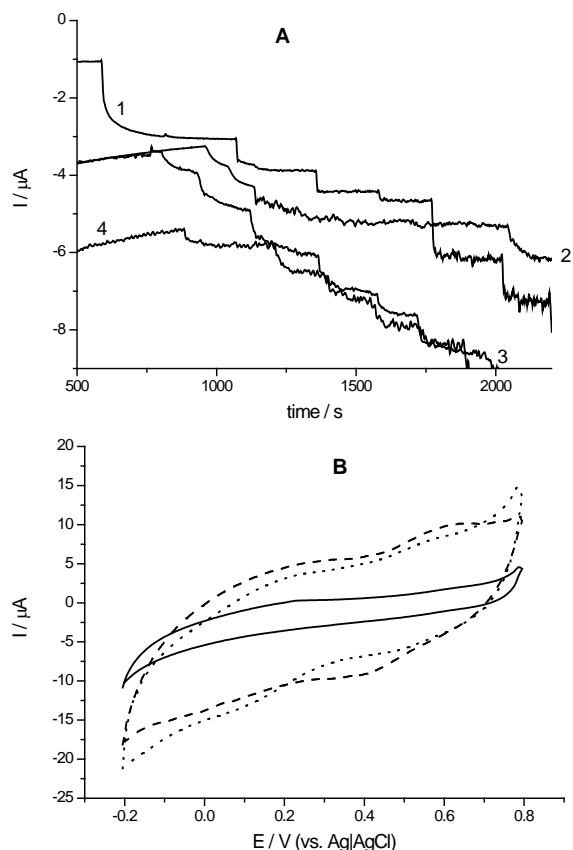
**Fig. 1**. A) Chronoamperometric record of the laccase electrode response to ABTS in presence of oxygen. Laccase enzyme immobilized through: physisorption (1); Lac adsorbed on chitosan-gold particles composite (2); laccase entrapped in a chitosan layer (3) and sorption on gold- modified graphite (4); pH = 4.0; E = -100 mV; 25 $^0$C; B) CVs of TP laccase electrodes with the enzyme immobilized through physisorption (solid); sorption on gold-modified graphite (dotted) and laccase adsorbed on chitosan-gold particles composite (dashed); pH = 4.0; v = 10 mV s$^{-1}$; 25 $^0$C.

The CVs of graphite electrodes with adsorbed laccase in buffer solution differ considerably from the CV of the bare graphite electrode (not shown). The possibility to record reproducible voltammograms upon continuous cycling of the laccase electrodes suggests that the enzyme adheres firmly to the graphite surface.

In order to evaluate the effect of the buffer composition on laccase electrocatalytic activity, the dependences of the electrode response on the mediator concentration were recorded in 0.05 M citrate and 0.05 M acetate buffer solutions, at E = -100 mV, over the pH range of 4.0 – 5.0). To maintain a constant ionic strength, sodium perchlorate was added to both buffer solutions to a concentration of 0.1 M. On the next figure (Fig. 2A) the calibration plots for ABTS on a laccase electrode are compared in the two buffer solutions. The bioelectrocatalytic activity of the laccase was found a bit higher in the citrate than in the acetate buffer solution. In all cases,

the reaction kinetics obeys the mechanism of Michaelis – Menten. As it could be seen from Fig. 2B the current variation upon addition of an aliquot of ABTS is much more distinct at pH 4.5 than at pH 4.0, which motivated us to perform all further studies at the former pH.
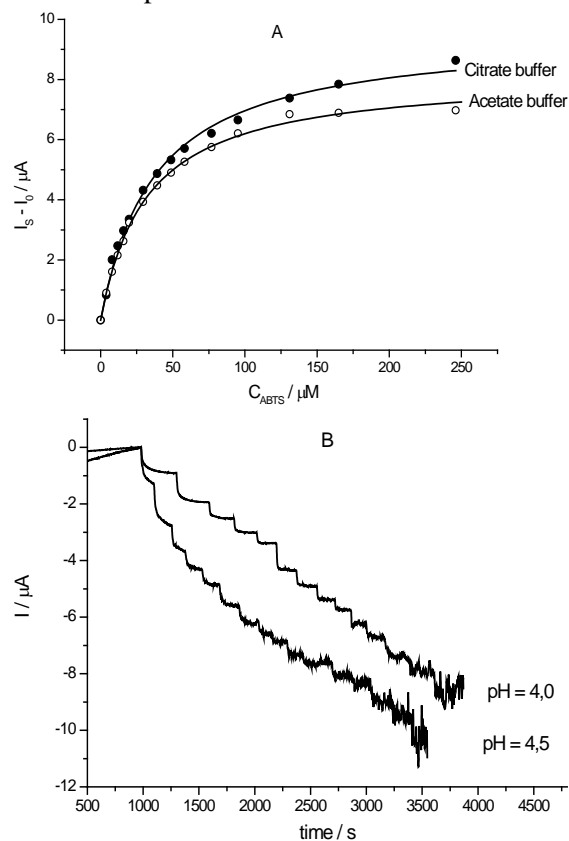


**Fig. 2.** A) Dependence of the electrode response on ABTS concentration at a constant potential E = -100 mV, pH = 4.0; in citrate buffer and in acetate buffer. B) Chronoamperometric record of the electrode response (with adsorbed laccase) to aliquots of 2 mM ABTS stock solution; air-saturated 0.05 M citrate buffer, pH = 4.0 and pH = 4.5; E = -100 mV; 25 $^0$C.
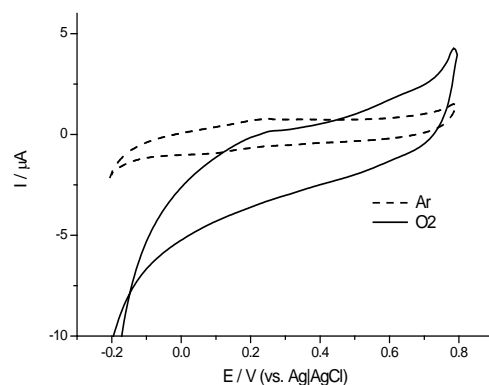


**Fig. 3.** CVs of a laccase (*Trametes pubescens)* electrode in de-aerated with Ar (dashed) and oxygenated (solid) 0.05 M citrate buffer, containing 0.1 M NaClO$_4$ , pH = 4.5; v = 10 mV s$^{-1}$; 25 $^0$C.
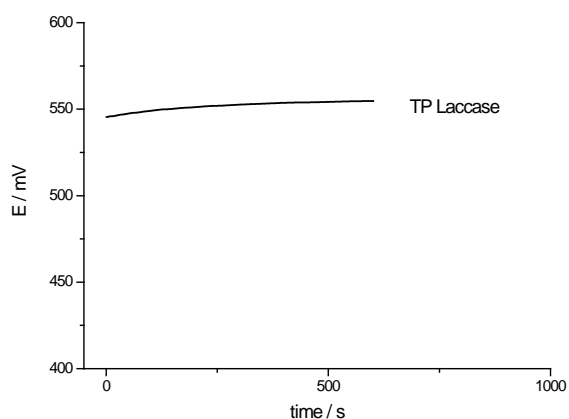
**Fig. 4.** Open circuit potential of the laccase electrode under oxygenated conditions (0.05 M citrate buffer + 0.1 M NaClO$_4$), pH 4.5.

The voltammograms presented on Fig. 3 recorded in de-oxygenated and air-saturated buffer testify that Lac is very efficient in the direct bioelectrocatalytic reduction of O$_2$. In addition, the open circuit potential (OCP, Fig. 4.) of the latter electrode measured under oxygenated conditions at pH 4.5 was found to be ca. 540 mV, i.e., Lac is a promising electrocatalyst for oxygen reduction.

Unfortunately, the stability of so obtained enzyme electrodes was found fragile – all the attempts to repeatedly use the enzyme electrodes failed. This could be due to the electrode fouling with the products from side reactions, e.g. from mediator oxidation when testing its biocatalytic activity, but could be also a result of rapid enzyme desorption from the graphite surface. Therefore, our further studies were directed towards stabilization of the enzyme layer through covalent attachment of the laccase to electrode surface. For that purpose two types of electrode materials were tested: smooth gold electrode (SGE) and glassy carbon electrode (GCE), modified with thin (below 100 nm thick) electrodeposited gold layer. The availability of gold on the electrode surface is of key importance for the immobilization procedure as its surface can be easily functionalized with sulfur-containing organics [8] using the so-called gold-thiol chemistry, (Scheme 1).
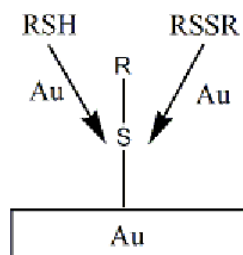


**Scheme 1.** Surface functionalization of gold surface with sulfur-containing organic compounds – thiols or disulfides.

The formation of cysteamine self-assembled monolayer onto the gold surface plays a double function in this particular immobilization protocol: i) it serves as a tool for spatial orientation of the enzyme upon immobilization: its terminal amino groups are positively charged at the working pH and hence they will attract electrostatically the negatively charged enzyme active site; and ii) it is an anchor to which the enzyme is linked *via* bi-functional reagent (glutaric aldehyde, Scheme 2.).
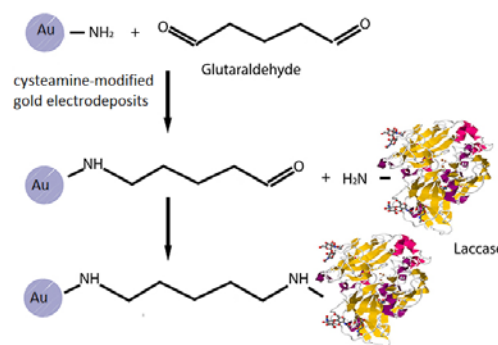


**Scheme 2.** Covalent binding of laccase to cysteamine self-assembled on gold using glutaric aldehyde.

Following the already discussed experimental procedure for testing the biocatalytic activity, the responses to ABTS for both types of enzyme electrodes (SGE and gold-modified GCE with covalently attached laccase) were examined. Chronoamperometric records of the response to ABTS at a constant potential of –100 mV (*vs.* Ag|AgCl, 3 M KCl) for the enzyme-bearing SGE under oxygenated conditions show much smaller current variation upon addition of the substrate than for the equivalently prepared laccase electrode based on gold-modified GCE (Fig. 5A).

Comparison of the CVs of the two electrode types (Fig. 5B) reveals that the electrochemically accessible surface area of the SGE is about twice as low as the surface of the gold-modified GCE with covalently immobilized enzyme, whilst in the same time the catalytic current differs more than 10 times (being bigger for the latter electrode type). The obtained much bigger current density with the second electrode type suggesting considerable activity of the immobilized enzyme motivated all further studies to be implemented with this particular type of electrode fabrication.

The record of the open circuit potential with time done in both de-oxygenated and air-saturated buffer, presented on Fig. 6, suggests that covalently immobilized laccase is still an efficient biocatalyst of the direct bioelectrocatalytic reduction of O$_2$.
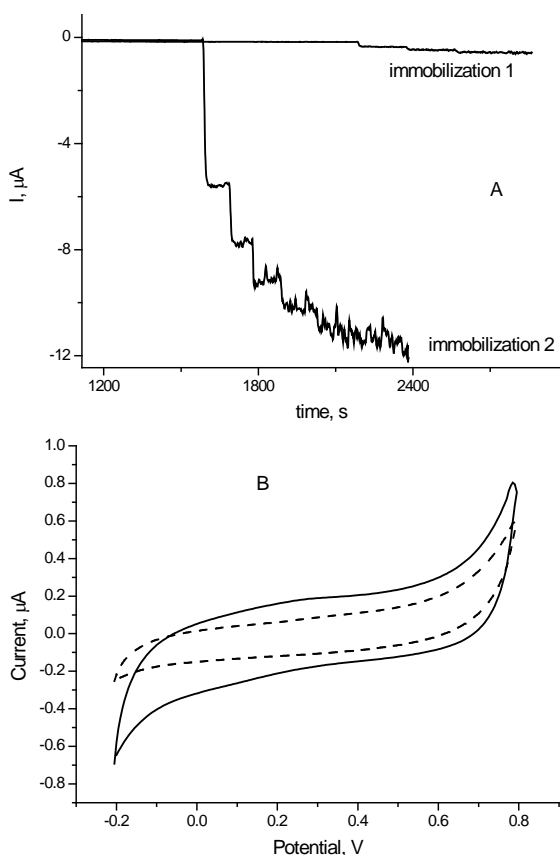
**Fig. 5**. A) Chronoamperometric record of the laccase electrode response to ABTS in presence of oxygen. Laccase enzyme immobilized covalently on gold (curve 1) and gold-thin film -modified glassy carbon (curve 2); pH = 4.5; E = -100 mV
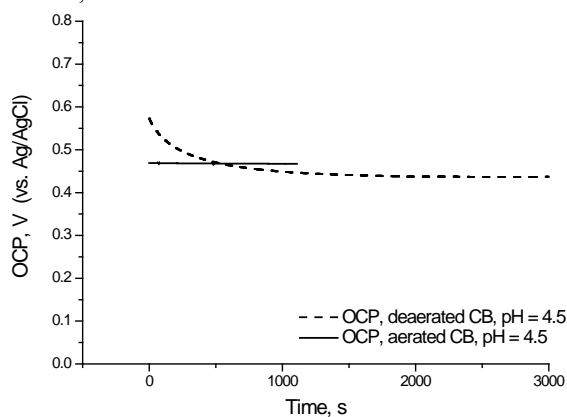


**Fig. 6.** Open circuit potential of the laccase electrode in oxygenated buffer solution (0.05 M citrate buffer + 0.1 M NaClO$_4$), pH 4.5; partly deaerated buffer (dashed line); continuously aerated buffer (solid line).

Its open circuit potential at pH 4.5 and under oxygenated conditions exceeds 460 mV. The slight decrease in OCP as compared with the value measured with laccase physisorbed on graphite electrode can be assigned to a lesser conformational "comfort" of the enzyme due to the covalent immobilization accompanied by crosslinking with the glutaric aldehyde.

DPVs of laccase electrode prepared freshly and used continuously over 1 week period indicate a gradual decrease in the intensity of the current maximum representing the rate of the electron exchange between the enzyme active site and the electrode surface (not shown). However, the activity of the immobilized Lac remains high enough to ensure proper functioning of the bioelectrode. As depicted in Fig. 7, the normalized *versus* the initial response electrode activity decreases gradually to ca. 30% of the initial one after 21 days (3 weeks) that is more than 21 times increase in operational stability of the immobilized enzyme.
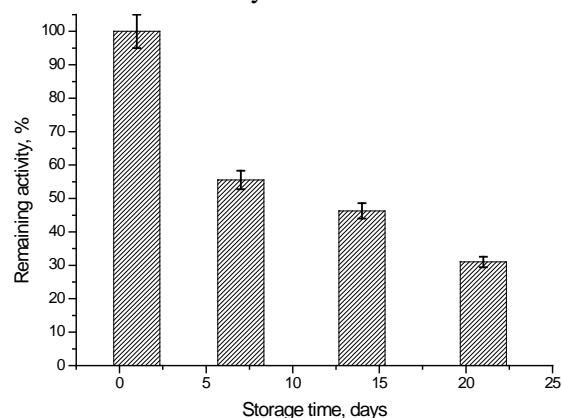


**Fig. 7.** Remaining activity of the laccase electrode as a function of storage time (days). The remaining activity was normalized *vs.* the response of the freshly prepared electrode.

Summarizing, the present studies show that physical adsorption of laccase on graphite electrodes provides high electrochemical activity of the immobilized enzyme, however, the lifespan of such a bioelectrode is rather short. Alternatively, when covalently immobilized, the enzyme exhibits more than 20 times higher operational stability, manifesting in the same time high enough electrochemical activity. Prospects are to test the so produced biocathode together with a microbial anode operating in a less acidic pH medium and to fully characterize the so constructed biofuel cell.

## REFERENCES

1. A. Le Goff, M. Holzinger and S. Cosnier, *Cellular and Molecular Life Sciences*, **72**, 941 (2015).
2. N. Mano, *Applied Microbiology and Biotechnology*, **96**, 301 (2012).
3. N. Mano and L. Edembe, *Biosensors and Bioelectronics*, **50**, 478 (2013).
4. S. D. Minteer, *Biochimica et Biophysica Acta - Bioenergetics*, **1857**, 621 (2016).
5. V. V. Kharton, *Solid State Electrochemistry II: Electrodes, Interfaces and Ceramic Membranes*, Wiley (2012).
6. D. M. Ivnitski, C. Khripin, H. R. Luckarift, G. R. Johnson and P. Atanassov, *Electrochimica Acta*, **55**, 7385 (2010).
7. S. C. Barton, J. Gallaway and P. Atanassov, *Chemical Reviews*, **104**, 4867 (2004).
8. E. Katz and I. Willner, *Angewandte Chemie International Edition*, **43**, 6042 (2004).

# Copper recovery combined with wastewater treatment in a microbial fuel cell

M. Y. Mitov[1,2*], I. O. Bardarov[2], E. Y. Chorbadzhiyska[2], Y. V. Hubenova[3,4]

[1]*Innovative Center for Eco Energy Technologies, South-West University Neofit Rilski, Blagoevgrad, Bulgaria*
[2]*Department of Chemistry, South-West University Neofit Rilski, Blagoevgrad, Bulgaria*
[3]*Department of Electrocatalysis and Electrocrystallization, Institute of Electrochemistry and Energy Systems - BAS, Sofia, Bulgaria*
[3]*Department of Biochemistry and Microbiology, Plovdiv University Paisii Hilendarski, Bulgaria*

A novel type of microbial fuel cell (MFC), called metallurgical MFC, is an attractive alternative for metal recovery with simultaneous wastewater purification. Valuable metals can be recovered at the cathode by using electricity generated from microbial-assisted oxidation of organic matter at the anode. In this study, the possibility for copper recovery combined with wastewater treatment in double-chamber MFC was examined. $CuSO_4$ solutions with different concentrations were used as a catholyte and synthetic wastewater inoculated with activated sludge from municipality WWTP-Blagoevgrad was applied as an anolyte. Current generation resulting in a decrease of copper ions concentration in the catholyte and deposition of copper on the cathode was documented. It was established that the use of more diluted $Cu^{2+}$ solutions enhances the degree of copper recovery. The decreased COD in the anolyte at the end of experiments proves the concept for simultaneous copper recovery and wastewater treatment by means of MFC technology.

**Keywords**: Metallurgical microbial fuel cell; Copper recovery; Wastewater treatment; Electricity generation.

## INTRODUCTION

As a result of the rapid industrialization and continually expanding production activities, huge quantities of waste containing various metals are generated. Without responsible waste management, metal-contaminated wastewater can cause serious environmental and health problems because most metals are toxic, non-biodegradable and accumulate in plant, animal and human organisms. On the other hand, the natural resources of metals are limited, which in the long-term perspective requires that their mining be reasonably controlled. For the storage of the metal pool and the prevention of negative ecological consequences, along with effective corrosion protection and recycling of solid metal waste, it is necessary to regenerate the metals mainly from industrial wastewaters. Various technologies based on physical, chemical and biological processes have been developed in this direction, with the greatest efforts being directed to the effective regeneration of precious metals [1]. The main problem with the application of the developed technologies is that in most wastewaters the concentration of metals is relatively low (in the range of µg/l to mg/l), which requires additional energy and raw materials to be pre-concentrated by large volumes of water.

Bioelectrochemical systems that combine the biocatalyzed anodic oxidation of biodegradable organic products with the reduction of diverse electron acceptors offer a new alternative for the recovery of metals from wastewaters without the need to pre-concentrate them. They can be particularly effective for regenerating noble and other metals that have a more positive potential than that of the bioanode. In this case, the available metal ions can be directly reduced on the microbial fuel cell cathode, with simultaneous generation of electric current.

Despite the obvious thermodynamic possibility of implementing such a process, the concept of the so-called metallurgical microbial fuel cell (MMFC) was demonstrated a few years ago [2, 3]. After proof of principle, the number of publications related to the recovery of different metals in MMFC continuously grows. Along with studies, in which a high degree of recovery of metal ions as Ag (I), Au (III), Cu (II) and Hg (II) has been achieved [4-10], simultaneous reduction of several metals in MMFC has been also reported [11].

Copper is one of the four structural metals whose high electrical and thermal conductivity, corrosion resistance, ductility and extensibility define a very wide range of applications in various industries. The biggest sources of copper pollution are mining, metallurgical and semiconductor industries, as well as various galvanic industries. Although it is an essential microelement, at higher concentrations copper is toxic to living organisms, which imposes strict measures to remove it from industrial wastewaters before discharging into natural water bodies. The applied technologies for copper removal from industrial wastewaters are mainly based on

---

* To whom all correspondence should be sent.
E-mail: mitovmario@swu.bg

methods such as precipitation, adsorption and chemical reduction. An attractive alternative to the methods used, based on the positive $Cu^{2+}/Cu$ standard redox potential (+0.34 V *vs.* SHE), is the spontaneous electrochemical reduction of $Cu^{2+}$ ions to elemental copper on the microbial fuel cell cathode. Depending on the type and concentration of the substrate used, which determine the value of the anode potential, the theoretical electromotive force of MFCs, combining $Cu^{2+}$ cathode reduction and bio-catalyzed anode oxidation of acetate or glucose as an electron donor, reaches 0.49 to 0.69 V [12].

In one of the first studies on copper recovery by MFC, Ter Heijne *et al.* [10] use a two-chamber fuel cell with flat graphite electrodes, a bipolar membrane separating the cathode and anode compartments, and acetate as an electron donor. At continuous mode of MFC operation, almost complete removal of $Cu^{2+}$ ions (1 g/l) in the catholyte to levels below the allowable drinking water standards (<1.3 mg/l) and deposition of elemental copper on the cathode was achieved within 7 days. In addition, it has been found that the process proceeds with equal efficiency both at anaerobic and aerobic conditions in the cathode chamber. High efficiency with respect to copper regeneration under different experimental conditions in MFC is also reported by other authors. Tao *et al.* [6] investigated the copper regeneration of $CuSO_4$ solutions with different concentrations in two-chamber MFCs and achieved almost complete copper removal (> 99%) from a solution of 196 mg/l Cu (II). The same research team has achieved 97% copper recovery using an ash leachate extract from the incineration of municipal solid waste as a catholyte in MFC [13].

The aim of this paper is to prove the principal possibility for development of MFC technology for simultaneous electricity generation, copper recovery and wastewater treatment by using activated sludge from a municipal wastewater treatment plant (WWTP) as a biocatalyst.

## EXPERIMENTAL

The experiments were carried out in two-chamber MFCs with a working volume of 0.1 L of each chamber. Carbon felt (SPC-7011, 30 g/m², Weißgerber GmbH & Co. KG) with a geometric area of 4.5 cm² was used as an anode and electrolytic copper foil of the same size as a cathode. Synthetic wastewater with a composition 5.00 g/l glucose, 1.00 g/l NaCl, 3.00 g/l $NaHCO_3$, 0.40 g/l $NH_4Cl$, 0.33 g/l $MgCl_2.7H_2O$, 0.28 g/l $CaCl_2$ mixed in a volume ratio 9:1 with activated sludge from the municipal WWTP – Blagoevgrad was used as an anolyte. $CuSO_4$ solutions with different initial concentrations (0.1M,

0.01M, 0.005M) were used as a catholyte. In each individual experiment, two MFCs (K1 and K2) operating under identical conditions and one abiotic (K3) without activated sludge in the anolyte as a control were examined. After an open circuit acclimation period, the fuel cells were tested at a constant load (1 kΩ) with different concentrations of copper in the catholyte for 6 to 9 days. The cell voltage across the load resistor, as well as the anodic potential (*vs.* Ag/AgCl, 3M KCl) were recorded in 5 min intervals by using a multichannel digital multimeter Keithley DMM 2700. The generated current at each measured point was calculated by using Ohm's law.

The efficiency of copper recovery was evaluated by the degree of copper regeneration, $\eta_{Cu}$, calculated as the mass ratio of copper deposited on the cathode, $m_{deposit}$, to the mass of copper in the stock solution, $m_{initial}$:

$$\eta_{Cu} (\%) = (m_{deposit}/ m_{initial}).100, \qquad (1)$$

while the percent reduction of COD in the anolyte, determined by the standardized permanganate Kübel's method, served as a wastewater treatment measure:

$$\eta_{COD} (\%) = (COD_{initial} - COD_{final}).100 / COD_{initial} \qquad (2)$$

## RESULTS AND DISCUSSION

After the start-up of MFCs, when a load resistor was connected in the external electric circuit, the anode potential maintained relatively high values, but after a certain period it began steeply shifting in a negative direction, reaching stationary values over 500 mV more negative than the initial ones in most cases (Fig. 1). It was found that the observed anode potential shift starts faster with the increase of copper ions concentration in the catholyte.

During the different periods of MFC operation, using mixed cultures as a biocatalyst, the most adaptive types of microorganisms to the certain conditions of the biofuel cell are developed [14]. Positive anode potential at startup of fuel cells favors the development of facultative anaerobic and aerobic microorganisms. As the process progresses, a biofilm is gradually formed on the anode surface, as a result of which the anode potential begins to shift in a negative direction.

The positioning of the potential at steady-state negative values testifies to the formation of a mature biofilm with optimal thickness (Fig. 2), providing access for the entire microbial community to the available substrate [15].

In the presence of exoelectrogenic bacteria in the consortium, the formed anode biofilm is

electroactive and when the circuit is closed, the system generates electrical current. Direct proof of the formation of an electroactive biofilm and its key role in the overall behavior of the system is the change of the generated current over time, which in all experiments carried out strictly follows the changes of the anode potential (Fig. 3). In the absence of a biocatalyst, respectively anode biofilm, the electric current generated by the abiotic fuel cell (K3) is negligible and does not change over time.
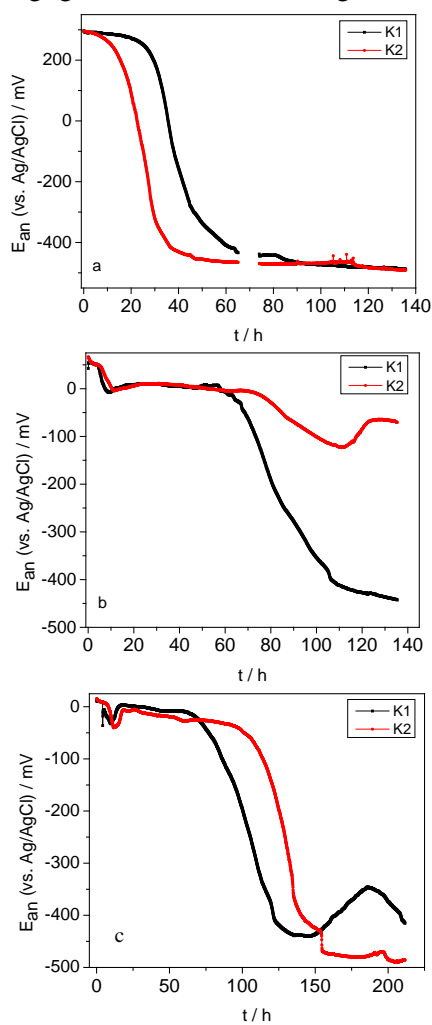


**Fig. 1**. Changes of the anode potential of microbial fuel cells over time with the use of: a) 0.1 M CuSO4; b) 0.01 M CuSO4; c) 0.005 M CuSO4 as a catholyte.



**Fig. 2.** Anodic biofilm formed during prolonged operation of MFC (K1) under load (1 kΩ).
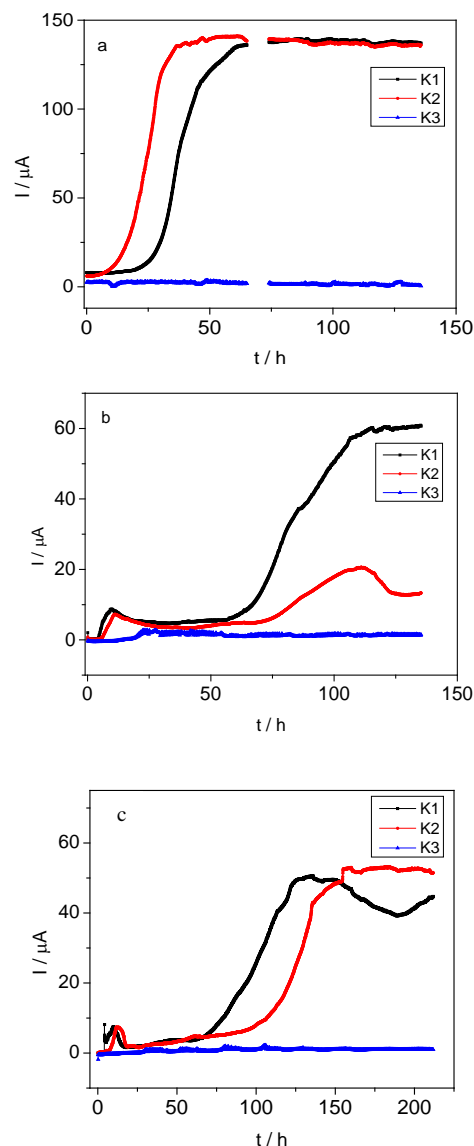


**Fig. 3.** Generation of electric current from microbial fuel cells over time using: a) 0.1 M CuSO4; b) 0.01 M CuSO4; c) 0.005 M CuSO4 as a catholyte.

As a result of the generated electric current, copper is deposited on the cathodes of the investigated fuel cells (Fig. 4), the amount of which is determined by weight analysis after each experiment (Table 1).



**Fig. 4.** Deposition of copper on cathodes after operation of microbial fuel cells at constant load (1 kΩ).

**Table 1.** Amounts of recovered copper using CuSO4 solutions of varying concentrations.

| MFC | m(Cu) / g | | |
| --- | --- | --- | --- |
| | 0.1 M CuSO4 | 0.01 M CuSO4 | 0.005 M CuSO4 |
| K1 | 0.0198 | 0.0128 | 0.0138 |
| K2 | 0.0193 | 0.0096 | 0.0096 |

The influence of $Cu^{2+}$ ions as a final electron acceptor on the overall performance of the studied MFCs is more considerable when using the most concentrated catholyte (0.1 M CuSO4). In addition to generating a larger quantity of electricity (Fig. 5) and a larger amount of deposited copper on the cathode, the higher current accelerates the formation of the anode biofilm, resulting in a more stable and reproducible behavior of the system over time.

Despite the higher amounts of deposited copper, however, its degree of recovery from the most concentrated catholyte (0.1M CuSO4) is the lowest, whereas at 20-fold dilution of the stock solution $\eta_{Cu}$ increases over 10 times - Table 2. Similar results, reported by Tao et al. [6], reveal the possibility for development of MFC-based technology for copper recovery from industrial wastewater without need of pre-concentration by applying other methods.

On the other hand, the permanganometric analysis of the anolyte showed that in most experiments the COD decreased in half (Table 3). There is no correlation between this indicator and the electrical characteristics or the $Cu^{2+}$ concentration in the catholyte, which can be explained by the existing competition between the exoelectrogenic and the other bacteria in the consortium for the available substrates.
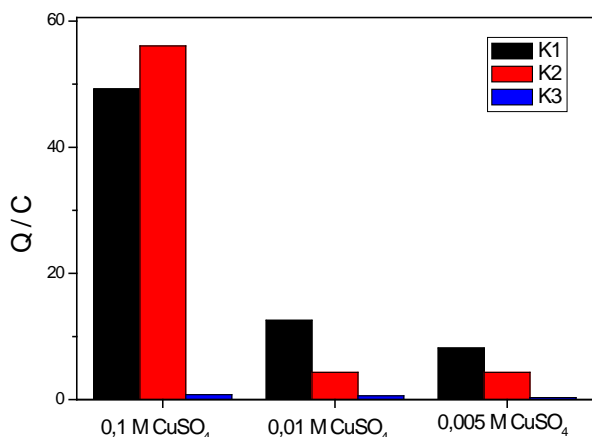


**Fig. 5.** Quantity of generated electricity (Q, C) of the investigated fuel cells at different concentrations of the catholyte.

**Table 2.** Degree of copper recovery using CuSO4 solutions of varying concentrations as a catholyte in MFC.

| MFC | $\eta_{Cu}$ / % | | |
| --- | --- | --- | --- |
| | 0.1 M CuSO4 | 0.01 M CuSO4 | 0.005 M CuSO4 |
| K1 | 3.1 | 20.2 | 43.4 |
| K2 | 3.0 | 15.1 | 30.2 |

Considering the fact that the experiments in this study were conducted in a batch system, where the available microorganisms produce and excrete various secondary metabolites in the anolyte, it could be expected that the wastewater treatment efficiency with respect to biodegradable organics will increase at operation of MFC in a flow mode.

**Table 3.** Percent reduction of COD in the anolyte using CuSO4 solutions of varying concentrations as a catholyte in MFC.

| MFC | $\eta_{COD}$ / % | | |
| --- | --- | --- | --- |
| | 0.1 M CuSO4 | 0.01 M CuSO4 | 0.005 M CuSO4 |
| K1 | 49.5 | 47.7 | 65.5 |
| K2 | 33.5 | 56.6 | 49.8 |

CONCLUSIONS

This study confirms the possibility for development of MFC-based technology for simultaneous copper recovery and purification of biodegradable organic products from wastewater, which additionally generates electricity. However, to achieve indicators with practical relevance further in-depth research is needed in the following directions:

- optimization of the MFC design and construction in order to reduce internal resistance and increase electrical outputs;
- optimization of conditions for formation of electrochemically active anode biofilm;
- development of a flow system providing more efficient copper recovery and treatment of the available organics in wastewater;
- investigations with real wastewater from different sources.

Future research in this area will also be directed towards regeneration of other valuable and/or toxic metals (Ag, Au, Hg, etc.) through MFC technology. A perspective approach is the combination of microbial fuel cell and microbial electrolysis cell, which would allow simultaneous regeneration of several metals present in the treated wastewater.

REFERENCES

1. H. Wang, Z. J. Ren, *Water Res.*, **66**, 219 (2014).
2. Z. J. Li, X. W. Zhang, L. C. Lei, *Process. Biochem.*, **43**, 1352 (2008).
3. G. Wang, L. Huang, Y. Zhang, *Biotechnol. Lett.*, **30**, 1959 (2008).
4. Z. Wang, B. Lim, H. Lu, J. Fan, C. Choi, *Bull. Korean Chem. Soc.*, **31**, 2025 (2010).
5. Z. Wang, B. Lim, H. Lu, J. Fan, C. Choi, *Bioresour. Technol.*, **102**, 6304 (2011).
6. H. Tao, M. Liang, W. Li, L. Zhang, J. Ni, W. Wu, *J. Hazard Mater.*, **189**, 186 (2011).
7. H. Tao, Z. Gao, H. Ding, N. Xu, W. Wu, *Bioresour. Technol.*, **111**, 92 (2012).
8. C. Choi, Y. Cui, *Bioresour. Technol.*, **107**, 522 (2012).
9. C. Choi, N. Hu, *Bioresour. Technol.*, **133**, 589 (2013).
10. A. ter Heijne, F. Liu, R. V. Weijden, J. Weijma, C. J. Buisman, H. V. Hamelers, *Environ. Sci. Technol.*, **44**, 4376 (2010).
11. B. Zhang, C. Feng, J. Ni, J. Zhang, W. Huang, *J. Power Sources*, **204**, 34 (2012).
12. Y. V. Nancharaiah, S. Venkata Mohan, P. N. L. Lens, *Bioresour. Technol.*, **195**, 102 (2015).
13. H.-C. Tao, T. Lei, G. Shi, X.-N. Sun, X.-Y. Wei, L.-J. Zhang, W.-M. Wu, *J. Hazard. Mater.*, **264**, 1 (2014).
14. S. Oh, B. Logan, *Water Res.*, **39**, 4673 (2005).
15. E.Y. Chorbadzhiyska, M.Y. Mitov, Y.V. Hubenova, *Bulg. Chem. Commun.*, **45A**, 205 (2013).

# Photo-induced charge transfer between *Lemna minor* and anode of photosynthesizing plant fuel cell

Y. Hubenova[1,2*], G. Ivanov[2], E. Hubenova[3], M. Mitov[4]

*¹Institute of Electrochemistry and Energy Systems, Bulgarian Academy of Sciences, Sofia, Bulgaria*
*²University of Plovdiv Paisii Hilendarski, Plovdiv, Bulgaria*
*³ Department of General Pediatrics, Center for Pediatrics, University Clinics, University of Bonn, Bonn, Germany*
*⁴Innovative Center for Eco Energy Technologies, South-West University Neofit Rilski, Blagoevgrad, Bulgaria*

The photosynthesizing plant fuel cells (PPFC) are bioelectrochemical devices, in which aquatic plants are grown as biocatalysts in fuel cell. Recently, it was proved that higher electrical current is generated by duckweed-PPFC during daytime. In this study a new experimental set-up is developed, so that the *Lemna minor* duckweeds grown in the PPFC can be irradiated with polarized monochromatic light with precise wavelength, 650 nm (red) and 450 nm (blue-violet), while the electrical current generated is monitored. The higher current values during photoperiod show that photo-induced charge transfer between duckweed and fuel cell anode takes place. The results from both chronopotentiometric and electrochemical impedance spectroscopy analyses reveal the contribution of duckweed` light absorbing photosystems (PS I and PS II) and ETC in the thylakoid membranes to a direct electron transfer to the anode.

**Keywords**: Charge transfer; Duckweeds; Electricity generation; Monochromatic light; Photosynthesizing plant fuel cell.

## INTRODUCTION

Microbial fuel cells (MFC) are bioelectrochemical devices operating on the principles of the galvanic cells. They convert chemical energy into electrical one. Instead of chemical catalysts, however, their specific feature is the utilization of living cells as biocatalysts. During the last decade, a huge diversity of MFCs has been developed. Depending on the used biocatalysts, the MFCs are referred to as bacterial fuel cells, yeast-based biofuel cells, sediment microbial fuel cells, plant fuel cells, etc. shortly biofuel cells, famous as X-MFC [1]. Among the advantages of the technology is that the biofuel cells have the potential for different applications – wastewater treatment, autonomous electricity generation, bioremediation and even biosynthesis. Bringing the MFC-technology to higher technological readiness level (TRL) is possible by improving the devices toward higher electrical outputs, finding new exoelectrogenic organisms and better understanding the intra- and extracellular processes contributing to enhanced extracellular electron transfer, having in mind that the electrical current is proportional to the cellular electrons reached the anode [2].

One of the newest types of X-MFCs - the plant microbial fuel cell (P-MFC) has been developed recently by using *Oryza sativa*, *Spartina angelica*, *Arundinella anomala* and *Glyceria maxima* as producers of organic matter by photosynthesis [3-8].

The P-MFCs operate based on the mutualism between plants and the soil microorganisms in the rhizosphere that feed on rhizodeposition and the proteins and sugars released by roots [9]. By positioning of an anode in the rhizosphere [10], a part of the chemical energy of plant-derived organics, oxidized by bacteria and fungi, is transformed in electrical current, which could even supply low-power consumers [11].

In our previous studies [12, 13], we reported that higher aquatic plants - *Lemna minuta* and *Lemna valdiviana* duckweeds, can be used as biocatalysts in a Direct Photosynthesizing Plant Fuel Cell (DPPFC) without the participation of electrogenic bacteria. High power density ($380\pm19$ mW/m$^2$), corresponding to $119.83\pm5.99$ GJ/ ha year [8, 14], were achieved during DPPFC operation under natural sunlight illumination. It was established that abiotic factors as temperature, humidity and light intensity, as well as the day/night cycle influence the generation of the current. At permanently connected resistance higher values of electrical parameters were achieved during daytime than through the nights, indicating the contribution of light-dependent photosynthetic processes. The twice higher duckweeds` biomass and the increased content of monosaccharides (44 %), proteins (47 %) together with the decreased inorganic phosphates reveal that the metabolic processes in the duckweed are intensified when grown under fuel cell polarization. We proved that the quantity of the reserve carbohydrate in form of starch was increased with ca. 30 % at these conditions, while the amylase activity was slightly decreased. Enhanced oxidative

* To whom all correspondence should be sent.
 E-mail: jolinahubenova@yahoo.com

phosphorylation processes have been suggested due to the doubly increased phytase activity delivering phosphate groups by phytate hydrolysis in the lack of inorganic phosphate in the medium. The polarization also up-regulates a secondary metabolic pathway and the secretion of electrochemically active metabolite, supposed to play a role of a plant endogenous mediator, shuttling electrons extracellularly to the anode.

The aim of the present study is to verify whether the plant photosystems, absorbing light and transferring energy and electrons in the chloroplasts, contribute to the higher current density of the PPFCs. For this purpose, a special experimental set-up for growing the duckweed in fuel cells under controlled light access and constant temperature was developed. Monochromatic red and blue-violet polarized light were applied for periodical irradiation and the electrical parameters were compared with those obtained when visible light was used.

## MATERIALS AND METHODS

### *Plant material and construction of the PPFC*

Duckweed (*Lemna minor*), collected from river Maritza, near the town of Plovdiv, Bulgaria, was used in the experiments. Each plant was washed twice with clean water and grown under autotrophic conditions (in potable water without additives) prior to experiments. 1 g of wet biomass *Lemna minor*, equal to ca. 100 plants, was put onto the anode surface of each P-MFC. The used Photosynthesizing Plant Fuel Cell (PPFC) construction is identical with the DPPFC previously described [12]. The anode (carbon felt) is fixed in such a way that the plant roots are covered by water, while the fronds are on the water surface. Potable water in a volume of 40 ml plays a role of anolyte. Five identical fuel cells differing in irradiation conditions (Table 1) were operated simultaneously. After two days of acclimatization period toward polarization by load resistor (1 kΩ), the samples were explored on varying the irradiation.

### *Development of the experimental set-up*

A lamp with illuminance of 60 kLx was used as a coherent light source. Light was transmitted through 12 optical fibers of 60 cm length, 3 of which illuminate a single PPFC. A filter for polychromatic or monochromatic light (wavelengths 450 nm and 650 nm) was put at the end of the fiber after a polaroid (PPFC1, 2, 3). The light filter was fastened so that the light illuminated the entire surface of the anode covered with plants. PPFC4 was a control irradiated by light, which is emitted in all directions (isotropically). The fuel cells bodies were wrapped with black non-transparent foil. The imitation of night conditions was achieved by using a black, light-tight lid.

### *Electrochemical analyses*

The voltage of the fuel cells was monitored continuously by using a multiplexer connected to PalmSens 3 potentiostat in chronopotentiometric mode. The current was calculated by the Ohm's law. In the graphs, it is presented as a current density in respect to the anodic geometric area. The open circuit voltage (OCV) was measured at the beginning and the end of the experimental window after recovery of the PPFCs.

At the 10th day after the start-up, electrochemical impedance spectroscopy (EIS) was applied during the irradiation. The EIS was carried out in a three electrode mode, in the frequency range from 50 kHz to 7 mHz with an applied ac signal with an amplitude 10 mV and $E_{dc}$ equal to -0.1V. The bioanode was connected as a working electrode, Pt-wire – as a counter, and Ag/AgCl (3 M KCl) - as a reference electrode. Cyclic voltammetry (CV) in the potential range from +0.6 to -0.6 V (*vs*. Ag/AgCl) with a scan rate of 10 mV/s were also performed by PalmSens 3 handheld potentiostat.

## RESULTS AND DISCUSSION

Representatives of Lemna duckweeds – *L. minuta* and *L. valdiviana,* have been shown to be capable of extracellular electron transferring (EET) when cultivated in a fuel cell [12, 13].

**Table 1**. Photosynthesizing Plant Fuel Cells irradiated with monochromatic polarized light: red (PPFC1), blue-violet (PPFC2); polarized visible light (PPFC3); non-polarized visible light (PPFC4). The duckweeds in the PPFC5 were grown as a control in laboratory conditions. The light irradiation characteristics of each PPFC are presented.

| PPFC | Irradiation with | Measured illuminance on PPFC / Lx | Irradiance / (W/m$^2$) | Characteristics: wavelength, frequency, photon energy |
|---|---|---|---|---|
| 1 | Monochromatic red light | 40±5 | 0.059±0.007 | 650 nm, 400THz, 1.65eV |
| 2 | Monochromatic blue-violet light | 500±100 | 0.732±0.146 | 450 nm, 668 THz, 2.75eV |
| 3 | Polarized visible light | 280±60 | 0.410±0.088 | 390 to 700 nm |
| 4 | Non-polarized visible light | 1050±300 | 1.537±0.439 | Random mixture of waves |
| 5 | Light in the lab | 1870±200 | 2.738±0.293 | Mixed - natural and artificial |

Depending on the illumination intensity and the period of cultivation, their response to fuel cell polarization has been related to the membrane potential of the fronds/roots, as well as to the secretion of plant endogenous mediator. The higher generated current during daytime showed a possible contribution of the light-phase of photosynthesis to the anodic reaction. Until now, however, no report has been published about the capabilities of direct electron transfer between a photosynthesizing plant biocatalyst and the anode of a PPFC.

In the present study, we used *L. minor* as a biocatalyst in a PPFC and developed a new experimental set-up (Scheme 1), by which it is possible to measure important electrochemical parameters, while the duckweeds are grown under controlled light conditions.
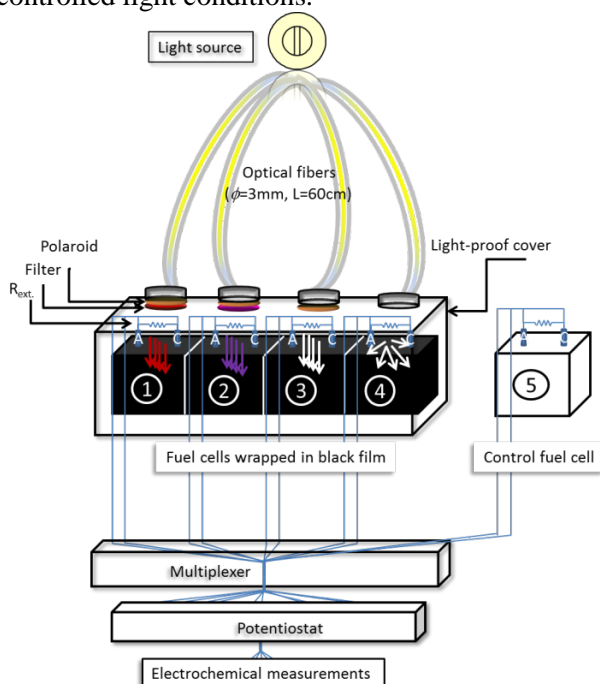


**Scheme 1**. Schematic presentation of the developed experimental set-up for controlled irradiation of photosynthesizing plant fuel cells.

To assess the influence of different light wavelengths on the electrical current generated by the PPFC, filters for polychromatic or monochromatic light with wavelength 450 nm and 650 nm were assembled with a polarizing filter (PPFC1, 2, 3) and used for temporary irradiation of the plants. Right after the irradiation of the plants in the fuel cell with polarized red or blue-violet light, the generated current increases and with small oscillations is stable up to 3 h (Fig. 1a). The periodic irradiation with red light leads to the highest values of the current densities. The wavelengths of 650 and 450 nm are near to those reported for the characteristic absorption peaks of chlorophyll a and

b, which are the most essential pigments in the light-harvesting system of green plants.
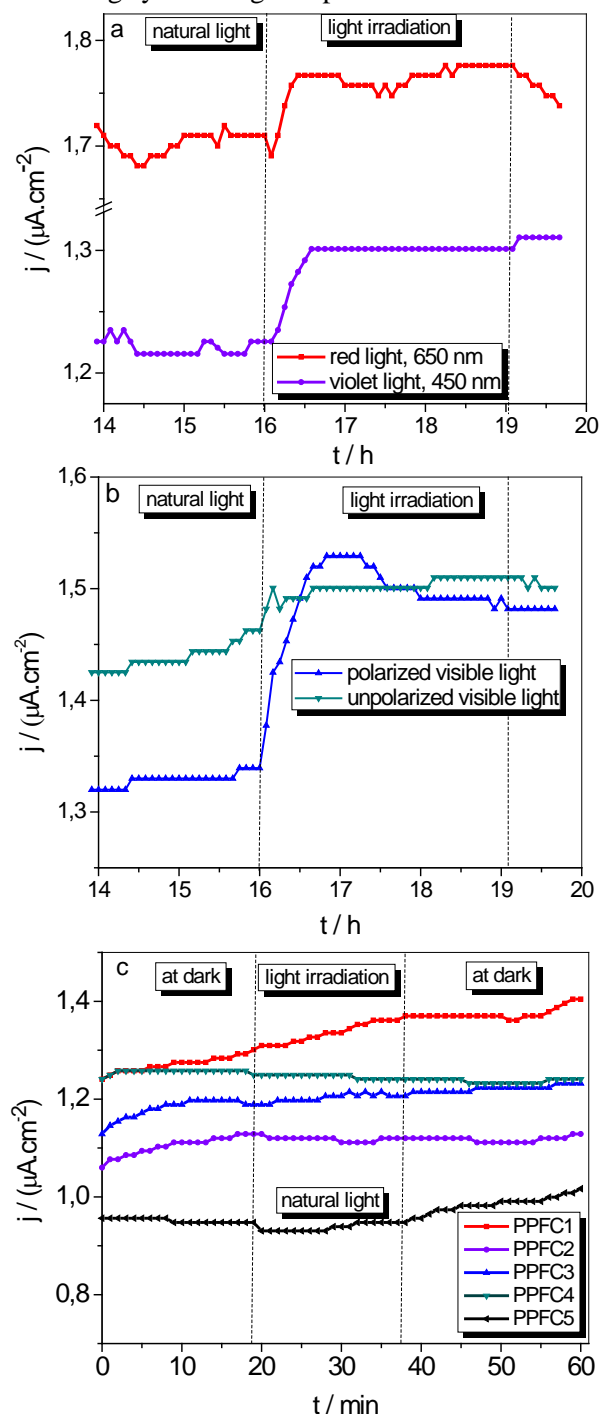


**Fig. 1.** Current density measured at the time of irradiation with: a) Red and blue-violet light introduced after the PPFCs have been incubated at natural lab light: b) polarized visible and non-polarized visible light; c) the irradiation is applied after dark incubation of the samples.

In this way, the contribution of chlorophyll a and chlorophyll b to the current generation by PPFC is supposed. The differences in current generation by PPFC3 and PPFC4 overlapped fast after applying irradiation, showing that the duckweed is capable of absorbing polarized visible light (Fig. 1b).

The participation of photosensitive complexes in the current generation could be deduced also by the results from the experiment, in which the duckweeds were incubated at dark and after that irradiated (Fig. 1c). In this case none of the PPFCs except PPFC1 responded to the irradiation, which indicates that the energy of the absorbed red light by duckweeds contributes not only to the photosynthetic processes, but also to an enhanced EET. The lowest current was achieved with the control fuel cell (PPFC5), where the irradiation was carried out naturally. After removal of the artificial light sources and exposure to the lab light illumination, the current of all fuel cells tends to equalize (Fig. 2), which is an additional evidence for the sensitivity of the duckweeds' response to the different sources of irradiation.
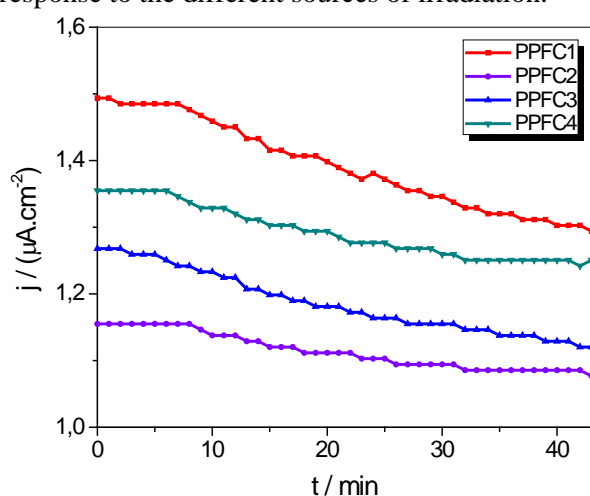


**Fig. 2.** PPFC current generation after removal of artificial light sources and incubation at lab light.

For all samples except PPFC3 the open circuit voltage (OCV) values decreased with several tenths of millivolts after 6 days of polarization with external load (Fig. 3).

The smallest OCV, comparable with that of the control, is registered for the PPFC2, which directs to possible damages of reaction centres of the photosystems by the blue-violet light irradiation, possessing the highest photon energy (Table 1). It was assumed that the reaction centres consisting of enzymes that use light to reduce molecules providing them with electrons or their surrounding by light-harvesting complexes could contribute to the

membrane potential changes of the cells and therefore the fuel cell performance. The maximal OCV was observed for PPFC3.
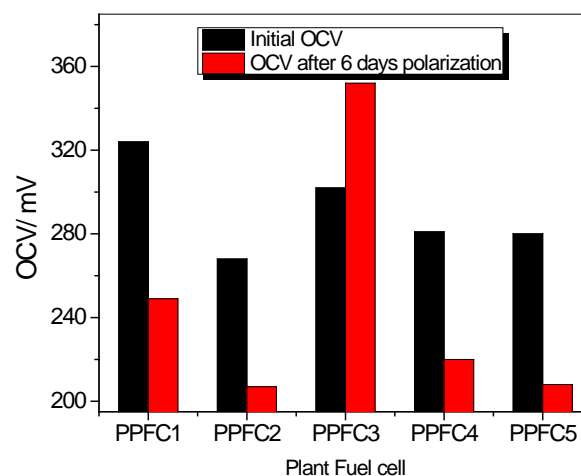


**Fig. 3.** The change of the open circuit voltage after 6 days of fuel cell polarization.

On the 10th day of the fuel cell polarization, electrochemical impedance spectroscopy analyses were implemented for establishment of the charge transfer mechanism during irradiation. The obtained impedance spectra, presented as Niquist and Bode plots on Fig. 4, show that the system responds in a different way depending on the applied irradiation. While the spectra of PPFC1 (monochromatic red light) and PPFC4 (non-polarized visible light) are well-fitted to a simplified one-time constant Randels model (Fig. 4a), those of PPFC2 (blue-violet light) and PPFC3 (polarized visible light) are consistent with an equivalent circuit model consisting of two successive RC time constants (Fig. 4b)

The values extracted from the fitted spectra of the resistances and capacitances, included in the corresponding equivalent circuit models, are summarized in Table 2.

Following the approach proposed by Jung [15] it may be assumed that the two-time constant model represents the impedance of the intracellular (second bigger semi-arc) and extracellular (smaller semi-arc) charge transfer processes. Considering the use of photosynthetic plants as a biocatalyst in our system, the intracellular charge transfer processes in this case should be assigned to the transport of photo excited electrons and protons across the thylakoid membranes.

**Table 2.** Values of resistances and capacitances, derived from the fitted EIS.

| Parameter/FC | PPFC1 | PPFC2 | PPFC3 | PPFC4 |
|---|---|---|---|---|
| $R_s$ /(k$\Omega$.cm$^2$) | 0.8 | - | 0.8 | 0.8 |
| $R_{ex}$ / (k$\Omega$.cm$^2$) | 12.2 | 1.3 | 2.0 | 2.0 |
| $R_{in}$ / (k$\Omega$.cm$^2$) | - | 21.5 | 70.0 | - |
| $C_{ex}$ ($\mu$F.cm$^2$) | 1.9 | 14.7 | 14.6 | 3.5 |
| $C_{in}$ (mF.cm$^2$) | - | 54.5 | 48.0 | - |

The intracellular charge transfer resistances ($R_{in}$) of PPFC2 and PPFC3 are respectively 16.5 and 35 times larger than the corresponding extracellular charge transfer resistances ($R_{ex}$), indicating that the intracellular charge transfer processes are the rate-limiting step when the system is irradiated by blue-violet or polarized visible light.

At the same time, the 3-fold higher intracellular capacitance ($C_{in}$) in both cases shows that almost all electrical charges generated through the photosynthetic processes reside in the intracellular reaction step [15].
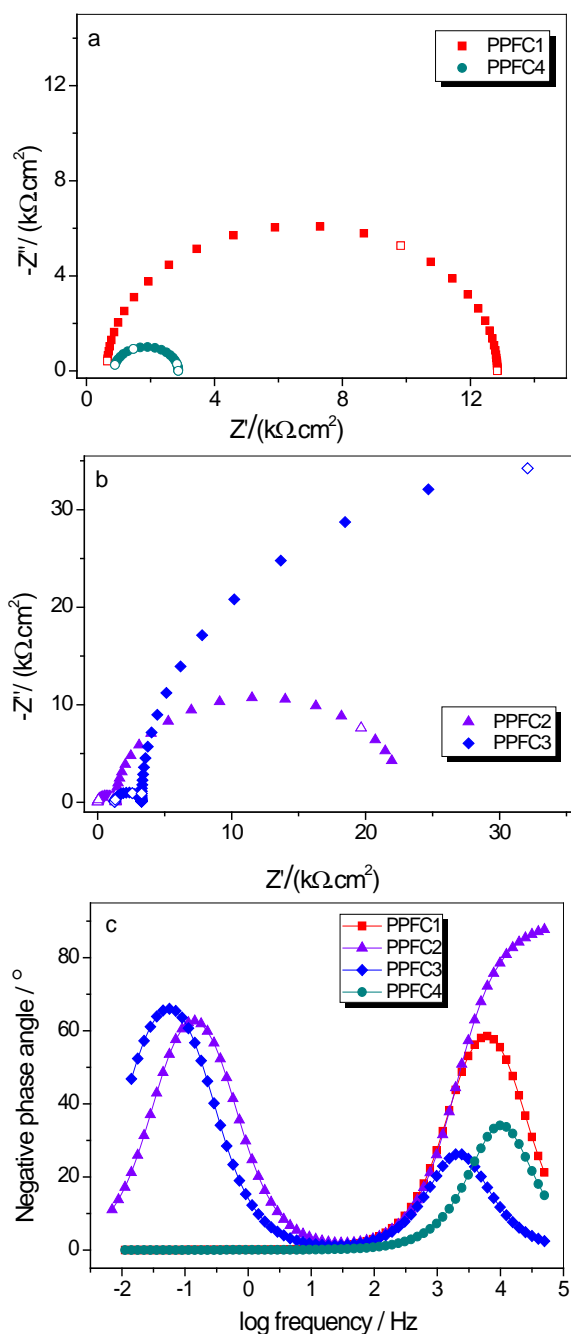
On the other hand, the existence of only one, non-ideal semi-arc in the spectra (Fig. 4a) of the samples, irradiated by monochromatic red (PPFC1) and non-polarized visible light (PPFC4), can be explained supposing that the intracellular charge transfer processes are facilitated and there is no such huge accumulation of electric charges inside the plant cells in these cases. In other words, the values of the intracellular and extracellular resistances and capacitances are of the same order of magnitude and the total charge transfer process from the duckweeds to the anode is represented as a "pseudo" one-time constant reaction.

Based on the similarity of EIS obtained with PPFC1 and PPFC4, we speculate that complexes of the plants' photosystems, capable of absorbing red light, could contribute to a direct electron transfer from duckweeds' fronds/roots to the fuel cell anode. Although the plants' chlorophyll *a* absorption maximum is at about 450 nm (blue-violet light), red light is more effective because both photosystems (PS I and PS II) absorb light of wavelengths in the red region. When PS II absorbs light, electrons in the chlorophyll reaction-center are excited to a higher energy level. Photo-excited electrons travel through the cytochrome b6f complex to photosystem I *via* an electron transport chain set in the thylakoid membrane [16]. This energy fall is harnessed to transport protons through the membrane. Having in mind that cytochrome *c* type molecules are responsible for EET in the MFCs, it may be assumed that plant cytochromes could also participate in the EET processes in the PPFC. The two oxidation peaks on the CV (Fig. 5), recorded during PPFC irradiation, support this hypothesis.



**Fig. 4.** EIS of bioanodes during irradiation, presented as: a) Niquist plot of PPFC1 (squares) and PPFC4 (circles); b) Niquist plot of PPFC2 (triangles) and PPFC3 (diamonds); c) Bode plots of all PPFCs.
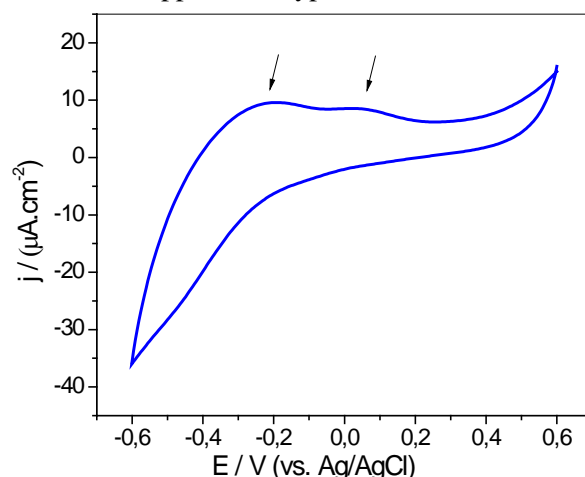


**Fig. 5**. CV of PPFC3 during irradiation with polarized light of visible spectrum.

## CONCLUSIONS

Photo-induced charge transfer across solid-solid (anode and plants) or solid-liquid interfaces in PPFC is studied for first time. The processes of light-dependent phase of photosynthesis, responsible to photon energy absorption, are related with direct transferring of the harvested electrons to the anode of the plant fuel cell, which explains the previously established higher electrical current generated by PPFC during light periods of the day/night cycle. The results obtained by EIS suggest that the irradiation with high-energy blue-violet light, as well as polarized visible light leads to a huge accumulation of electrical charges within the plant cells, while the natural non-polarized visible light facilitates in highest extent the electron transfer from duckweeds to the PPFC anode. These findings are a prerequisite for implementation of further analyses, aiming at elucidation of the plant redox complexes contribution to extracellular electron transfer in a plant fuel cell.

## REFERENCES

1. M. Mitov, Y. Hubenova, *Chemistry: Bulg. J. Sci. Edu.*, **24**, 404 (2015).
2. Y.V. Hubenova, in: Encyclopedia of Interfacial Chemistry: Surface Science and Electrochemistry, Klaus Wandelt (ed), Elsevier, 2018, p. 537.
3. D.P.B.T.B. Strik, H.V.M. Hamelers, J.F.H. Snel, C.J.N. Buisman, *Int. J. Energy Res.*, **32**, 870 (2008).
4. N. Kaku, N. Yonezawa, Y. Kodama, K. Watanabe, *Appl. Microbiol. Biotechnol.*, **79**, 43 (2008).
5. M. Helder, D.P.B.T.B. Strik, H.V.M. Hamelers, A.J. Kuhn, C. Blok, C.J.N. Buisman, *Bioresour. Technol.*, **10**, 3541 (2010).
6. R.A. Timmers, D.P.B.T.B. Strik, H.V.M. Hamelers, C.J.N. Buisman, *Appl. Microbiol. Biotechnol.*, **86**, (2010).
7. R.A. Timmers, M. Rothballer, D.P.B.T.B. Strik, M.E.S. Schulz, M. Schloter, A. Hartmann, B. Hamelers, C. Buisman, *Appl. Microbiol. Biotechnol.*, **94**, 537 (2012).
8. P. Bombelli, D.M.R. Iyer, S. Covshoff, A.J. McCormick, K. Yunus, J.M. Hibberd, A.C. Fisher, C.J. Howe, *Appl. Microbiol. Biotechnol.*, **97**, 429 (2013).
9. A.J. McCormick, P. Bombelli, R.W. Bradley, R. Thorne, T. Wenzele, C.J. Howe, *Energy Environ. Sci.*, **8**, 1092 (2015).
10. L. De Schamphelaire, L. Van den Bossche, H.S. Dang, M. Höfte, N. Boon, K. Rabaey, W. Verstraete, *Environ. Sci. Technol.*, **42**, 3053 (2008).
11. P. Bombelli, D. Ross, F. Felder, M. Cooper, D.M.R. Iyer, J. Royles, S.T.L. Harrison, A.G. Smith, C.J. Harrison, C.J. Howe, R. Soc. Open Sci., 3, 160249 (2016).
12. Y. Hubenova, M. Mitov, *Bioelectrochemistry*, **87**, 185 (2012).
13. Y. Hubenova, M. Mitov, *Bioelectrochemistry*, **106**, 226 (2015).
14. S. Liu, H. Song, X. Li, F. Yang, *Int. J. Photoenergy*, 2013, Article ID 172010 (2013).
15. S. Jung, *Int. J. Electrochem. Sci.*, **7**, 11091 (2012).
16. K.J. Appenroth, K. Krech, Á. Keresztes, W. Fischer, H. Koloczek, *Chemosphere*, **78**, 216 (2010).

# Identification of bacterial community in a sediment microbial fuel cell

S. Hristoskova[1], I. Bardarov[2], D. Yankov[1*], S. Danova[3], Y. Hubenova[4], M. Mitov[1]

*[1] Institute of Chemical Engineering – BAS, Sofia, Bulgaria*
*[2] Department of Chemistry, South-West University "Neofit Rilsky", Blagoevgrad, Bulgaria*
*[3] The Stefan Angeloff Institute of Microbiology – BAS, Sofia, Bulgaria*
*[4] Institute of Electrochemistry and Energy Systems "Acad. Evgeni Budevski" – BAS, Sofia, Bulgaria*

The aim of the present study was to investigate the bacterial community structure in a single-chamber sediment fuel cell (SMFC). The SMFC was prepared with sediment and water from Struma River and was functioned more than three years before analysis. Samples were taken from different places from cathode and anode compartments as well as from both electrodes. A protocol for microbes' isolation and characterisation has been adapted, using classical microbiological methods and different selective media. The genomic DNA was isolated from pure microbial cultures, obtained from selected single colonies and cultivated twice for biomass accumulation. The obtained DNA samples were analyzed by 1% v/v agarose gel electrophoresis and the concentration and purity were checked. The DNA was used as a target in the PCR assay and following 16 rDNA sequencing analysis. The obtained sequences were analyzed with BLAST analyses, and species identification of the strains were performed .

Keywords: sediment microbial fuel cell, bacterial community, PCR analysis, identification.

## INTRODUCTION

In the present days our society facing the threat of exhausting fossil fuels. According to predictions of British Petroleum [1] global proved oil reserves would be sufficient to meet 50.6 years of global production at 2016 levels. In view to decrease the dependence of contemporary economic from petrol and other fossil fuels, the researchers are focused on alternative energy sources. Still solar, wind, biomass-based and other systems for alternative energy generation are not enough economically effective because of their low effectiveness [2]. Nevertheless, the hopes for overcoming greenhouse gas and $CO_2$ emissions problems are put on alternative energy. A promising source of alternative energy represents fuel cells and there is abundant literature on it [2-6].

Microbial fuel cells (MFC) are kind of fuel cells in which biological redox ability of the microorganisms are combined with electrochemical reactions with the purpose of electricity production. An advantage of MFC is the possibility to combine the electricity production with waste water treatment or utilization of various waste biomass as substrate. The problems and progress in MFC utilization are discussed elsewhere [7-10].

Sediment microbial fuel cells (SMFC), also known as benthic MFC, are a kind of MFC, attracting much attention recently because of their unique properties. First of all is a very simple construction and exploitation due to lack of membrane. Another specific trait is that SMFCs work exclusive under anoxic conditions. Production of electricity in SMFC is usually coupled with environmental protecting processes as soil bioremediation from heavy metals [11, 12], hydrocarbons [13, 14] or other organic pollutants [15, 16].

The conversion of the chemical energy stored in an organic substrate to electro-energy can be realized by the aid of electrochemically active microorganisms (EAM). Assimilating the substrate (electron donor) the EAM produce electrons, which are transferred to the anode and by an external electrical circuit are leaded to the cathode where the process of oxidizing of an electron acceptor take part.

There are two main mechanisms for electron transport – direct electron transfer (DET) and indirect (mediated) electron transfer (MET) [9]. For realization of DET it is necessary that EAM have direct contact to the anode surface – either by the cytochrome *c* proteins of the outer cell's membrane or by bacteria's pili. Having in mind that EAM are prone to form a bacterial film on the anode it has to be the preferential choice. MET is characterized with presence in the system of a redox mediator, synthesized by the microorganisms or artificially added. Especially for SMFC, it is impossible to distinguish the type of electron transport mechanism due to the great variety of microorganisms present in the biofilm.

For the effective operation of an SMFC it is of great importance microbial diversity in the electrode's biofilms to be known, so the researcher

---

to concentrate his efforts towards the EAM process conditions optimization. Knowledge of the type of microorganisms present in the biofilm will give the possibility to construct an MFC with a pure culture of a single microorganism or to work with a consortium of well-defined EAM.

In a review paper on the fundamentals of benthic MFC Girgius *et al*. [17] summarized among others the data for microbial ecology in sediment MFC. The authors pointed out that in general, two major phylogenetic groups from the anode biofilm have implicated the power production: the δ- and γ-*Proteobacteria*. δ-*Proteobacteria* are ubiquitous in marine sediments, and are involved in sulfate reduction via the oxidation of organic matter or hydrogen. On the genus level the identified microorganisms were predominantly allied to the genus *Desulfuromonas*. The studies of biofilm formation on cathode revealed high representation of γ-*Proteobacteria* allied to *Pseudomonas flourescens*, capable of electron transfer via quinones.

García-Muñoz *et al*. [18] constructed an SMFC with water and sediment from Rio Tinto River. Studying the microorganisms presented in this acidic ecosystem the authors identified and quantified the acidophilic microorganisms that had colonized the anode and cathode surfaces. The dominant species on the anode surface belonged to the *Acidiphilium* genus. Minor quantities of *A. ferrooxidans* and *Leptospirillum* spp. were detected on the anode. These aerobic iron oxidizers were detected mainly on the cathode surface.

Abbas *at al*. [12] observed that after 120 days of operation the biofilms on graphite cathode and anode of an aerated and a nonaerated cathode SMFC were dominated mostly by *Pseudomonas* spp. The SEM observation revealed the difference in size of anode and cathode biofilms. The aerated SMFC gave higher power generation and toxic metal removal than nonaerated one. Majdumner *et al*. [19] studied a sediment microbial fuel cell with an air-cathode system with cotton clot electrodes. The biofilm of the anode of the SMFC was governed by γ-*Proteobacteria*.

Piscotta *et al.* [20] used SMFC for enriching graphite fiber brush anodes using two different marine sediments (from Chesapeake Bay, Annapolis and from steel piling in the Baltimore Inner Harbor). After establishment of electroactive biofilms on the anodes, they were electrically inverted to function as cathodes in two-chamber bioelectrochemical systems. Bacterial colonies were isolated from electron-accepting brushes and were analyzed. There were substantial differences

in the microbial consortia on the two biocathodes with the highest current densities. The Harbor biocathode film primarily consisted of bacteria most similar to *Eubacterium limosum*, *Desulfovibrio* sp., and *Gemmata obscuriglobus,* while the Chesapeake Bay cathode film is dominated by *G. obscuriglobus (*also identified on the Harbor cathode), and members of three different genera, *Mesorhizobium*, *Rhodococcus*, and *Azospirillum*.

Sacco *et al*. [21] have studied the performance of SMFCs constructed with sediment from Río de La Plata River. Graphite disks and rods were used as electrodes. Three different types of SMFCs were made: non-current control SMFCs, SMFCs amended with sodium acetate and SMFCs made without exogenous addition. Bacterial community analysis showed that anodic biofilms of SMFCs fed with sodium acetate were dominated by *Shewanella* sp., *Pantoea* sp. and *Pseudoalteromonas* sp., while these of SMFCs without exogenous addition were dominated by different species of the *Bacillus* genera.

In the work of Erable et al. [22] the authors studied an SMFC with marine sediment and a carbon (bioanode) and a stainless still (biocathode) electrodes. The microbial diversity of biofilms formed reveled that *α-Proteobacteria* and *δ-Proteobacter*ia were predominant in the biofilm collected from the biocathode, while *α-Proteobacteria* and *Bacteroidetes* were mainly present inside the biofilm from the bioanode. On the genus level *Sulfitobacter* sp. (*α-Proteobacteria*) were found in both anodic and cathodic biofilms.The representatives of the same genus are presented also in the sediment but there are representatives of genus *Clostridium, Bacillus* and *Sporosarcina*.

From the short literature review above, it is evident that the microbial community structure depends on the origin of sediment used, type of the electrodes, electron donors and operation time.

The aim of the present study was to identify the microbial community in a river sediment MFC after stable work for more than three years.

## MATERIALS AND METHODS

*Construction of single-chamber sediment fuel cell.*

The fuel cell was constructed using cylindrical plastic vessel. Nearly a half of the vessel was filled with sediment (collected from the basin of Struma River near Blagoevgrad (GPS coordinates: 42.051209, 23.076744). The anode (Graphite disk, 6 cm diameter, 1 cm thickness; GES Co., apparent

density 1.68 g/cm³, porosity 24%, electrical resistance 6.0 μΩ.m) was placed into the sediment (at approximately 3 cm from the bottom). The sediment was covered with water (around one third of its volume) taken from the same place. The cathode, identical as the anode, was placed nearly to the sediment/water boundary. Samples were collected from a sediment fuel cell, working for more than three years without any additions of nutrients, except water for recovering the losses caused by evaporation.

*Samples' collection*

Samples were taken from the anode and cathode space as well as from both electrodes. From the anode space 3 samples of different heights were taken - from the surface, at a depth of 5 cm (near the anode) and from the bottom (see Fig.1). Each soil sample (about 50 g) was placed on a sterile cannula and homogenized in a sterile box, then an average sample of 5 g was removed by quartering. Each sample was divided into five 1 g portions. Samples of the sediment element were poured with 9 ml of sterile saline and homogenized well to extract the maximum amount of microorganisms. After sedimentation of the soil particles, the supernatant was transferred in sterile test tubes. From the cathode space two samples were taken - near the surface and the phase boundary. Samples were taken with sterile pipettes and placed in sterile vials for further processing. Separate samples were taken from the surface of the anode and the cathode. The electrodes are carefully rinsed with sterile deionized water and the biofilm was carefully transferred in a sterile bottles using a sterile scalpel. A total of 12 samples were taken

from different parts of the two surfaces of the electrodes, each with an area of about 3 cm². Biofilm samples from both electrodes were placed in sterile saline and homogenized.

*Microorganisms, Media and Culture conditions*

1 ml of the collected samples were seeded in 9 ml of the below-mentioned media to grow the various microorganisms.

Heterotrophic saprophytic bacteria – in Meat Pepton Buiilon (MPB, BulBio) at 22 °C for 72 h and at 37 °C for 48 h;

Spore-forming bacteria – in MPB at 37 °C for 48 h after a pre-luminary step of sample's heating at 80 °C for 10 min;

*Mycromycetes* – in Czapek's medium 22 °C for 72 h;

*Actinomycetes* – in Starch-ammonia medium at 22 °C for 72 h;

Thermophilic bacteria – in MPB at 60 °C for 48 h.

Serial dilutions were made from each collected culture, after cultivation at different temperature, then were plated on Petri dishes containing selective agar medium, under the same culture conditions. The single colonies, with different morphotypes were selected, described and re-inoculated into a liquid medium and cultivated at the same conditions. All isolates were stored at -20°C in broth medium supplemented with 20% (v/v) glycerol.

For DNA isolation the biomasses of 10 ml exponential pure microbial cultures were harvested by centrifugation (5000 rpm, 5 min, Hermle centrifuge) and was frozen at -20 °C.
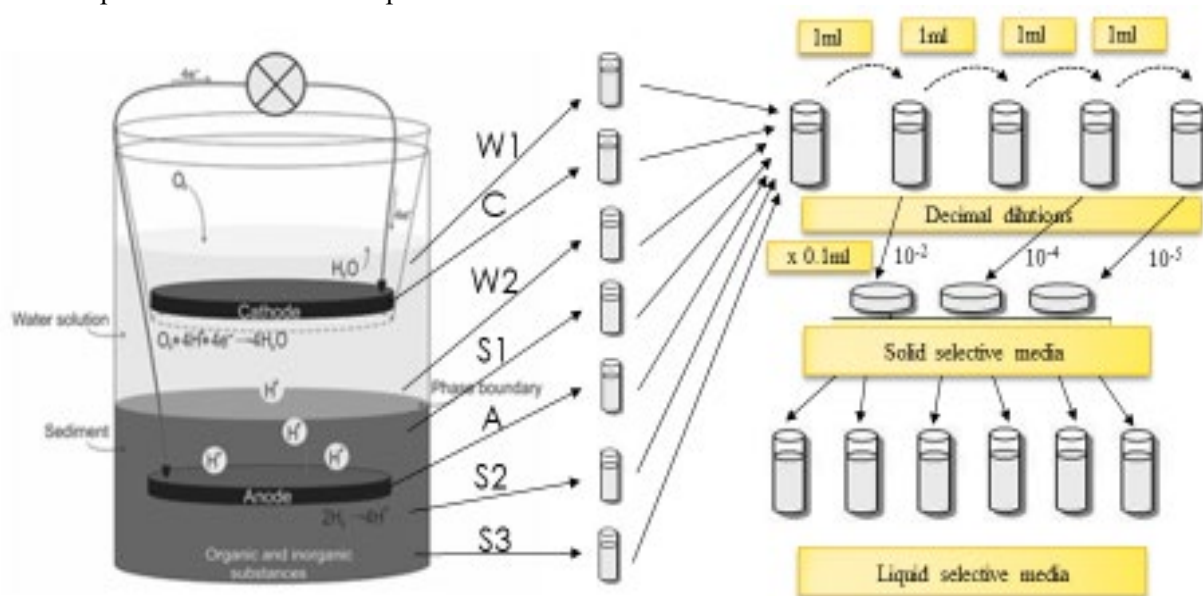


**Fig. 1.** Scheme of sediment fuel cell and samples' preparation.

*Microbial community analysis*

Total DNA from investigated isolates was extracted with ISOLATE II Genomic DNA Kit (Bioline) according the manufacturer's instructions. The amount and purity of the extracted DNA were determined by measuring the absorbance at different wavelengths by UV-Vis spectrophotometry.

The DNA concentration was determined at $\lambda = 260$ nm using the formula

$$1.0 \ A_{260} \ \text{unit} = 50 \ \mu g \ / \ \text{ml DNA.}$$

The purity of the extracted DNA was determined by measuring the absorbance at 230, 260 and 280 nm. Pure, unpolluted protein-labeled DNA has an $A_{260} / A_{280}$ ratio equal to, or greater than 1.8 and an $A_{260} / A_{230}$ ratio of at least 2.0.

The species identity of newly isolated microorganisms was determined by PCR amplification of the 16S rRNA gene and sequencing. All PCR reactions were done in a Progene cycler (Techne, UK) in 25 µl volume, using Ready To Go™ PCR beads (Amersham Biosciences).

Universal primers pair: forward fD1 (5`-AGAGTTTGATCCTGGCTCAG-3`) and reverse rD1 (5`-TAAGGAGGTGATCCAGGC - 3`) were used.

The PCR conditions were: initial denaturation for 5 min at 94 °C followed by 35 cycles of denaturation at 94 °C for 1 min, annealing at 56.5 °C for 1,15 min and elongation at 72 °C for 1,15 min; and a final elongation at 72 °C for 5 min.

Obtained PCR products were visualized on 1% (w/v) agarose gel (Sigma). A DNA ladder molecular marker 100 bp is used as a standard for the visualization of the amplified fragments. The PCR products were purified and by Macrogen Inc., (Amsterdam) and compared with the nucleotide sequence in the Gene Bank database (http://www.ncbi.nlm.nih.gov).

RESULTS AND DISCUSSION

Following the above described procedure totally 55 colonies were selected and further investigated. They possess different morphological characteristics and were isolated from selective/elective for different group of bacteria or *Micromycetes* agar plate media (Fig. 2).

A microscopic control was applied to verify the purity of all selected microbes. The domination of bacterial isolates v/s fungal ones into the group of selected 55 colonies have to be pointed.
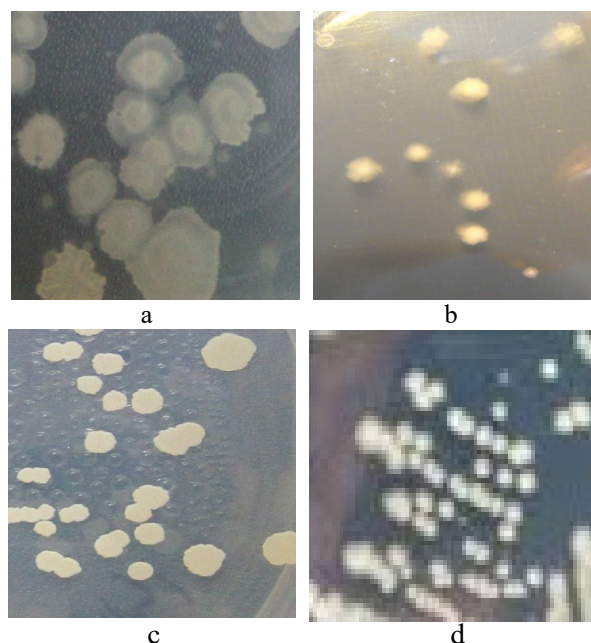
**Fig. 2.** Morphological characteristics of single colonies obtained on agar plates media, after cultiation of serial dilutions of the samples from SMFC.

The isolates were ccharacterised as
a) *Lysinibacillis* sp., b) *Clostridium* sp.,
c) *Paenibacillus* sp., d) *Pseudomonas* sp.

The species identification of bacterial strains was obtained by combining classical phenotypic and molecular methods. Isolated total DNA (Fig. 3) was used as template for PCR amplification of the 16S rRNA gene (Fig. 4), using universal primers.

**Fig.3.** Visualization of some preparations of total DNA isolates. Gel electrophoresis (1% w/v Agarose Sigma); 10 min at 100 mV and 15 min at 90 mV; 20 min in ethidium bromide and 30 min in distilled water.

Starts: 1: MAA ; 2: MAA1; *3*: MAA2; 4: MA12; 5: MA13; 6: MA22; 7: MK11; 8: MK12; 9: MK13; 10: MK21; 11: MK22; 12: MK41; 13: MC14; 14: MC13; 15: MC21; 16: MC31.
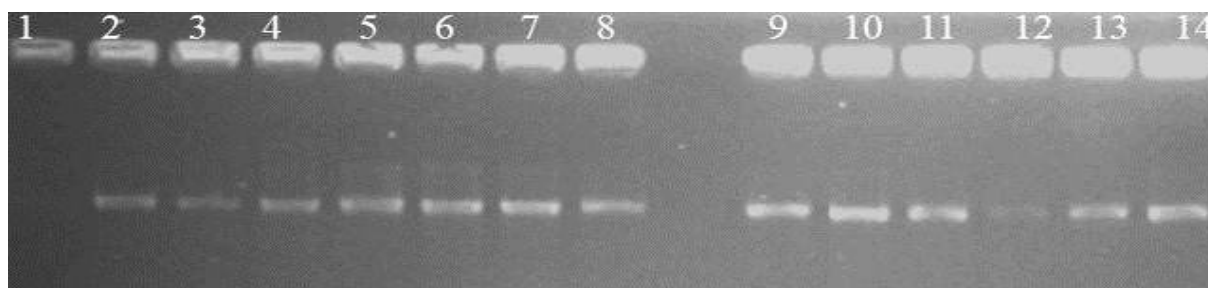
**Fig.4.** Visualization of the PCR products, obtained with universal primers for 16S rDNA analysis of isolates, in agarose gel electrophoresis (1 % w/v Agarose Sigma) after Ethidium bromide staining.

Starts: <u>1</u>: MC31; <u>2</u>: MC21; <u>3</u>: MC14; <u>4</u>: MC13; <u>5</u>: MA22; <u>6</u>: MA13; <u>7</u>: MAA2; <u>8</u>: MAA1; <u>9</u>: MAA; <u>10</u>: MA12; <u>11</u>: MK11; <u>12</u>: MK22; <u>13</u>: MK14; <u>14</u>: MC32 .

Obtained PCR products (~1550 bp) were visualized in 1 % (w/v) agarose gel (Sigma) and were sequenced in Macrogen, Inc Amsterdam.

The resulting sequences were further processed with the program *Chromas 2.3* (www.technelysium.com.au/chromas.html) and compared with the available nucleotide database from GenBank (http://www.ncbi.nlm.nih.gov) using the BLAST program).

From the selected 55 isolatees, 21 were identified – 3 on cathode, 7 on anode and 11 from sediment samples (Table 1). The majority of them (18) belongs to the phylum *Firmicutes* and three to the phylum γ-*Proteobacteria* (see Table 2). The representatives of the phylum γ-*Proteobacteria* were identified on the cathode

- *Pseudomonas oryzihabitans* strain h-2 and in the upper part of the sediment - *Pseudomonas koreensis* strain MLS-6-4 and *Pseudomonas putida* strain LCR80.

The other microorganisms on the cathode belong to the genus *Lysinibacillus*. The identified on the anode microorganisms are representative of the genus *Paenibacillus* and *Lysinibacillus*.

**Table 1**. Number of the isolated colonies and identified microorganisms.

| Position | Isolated colonies | Identified microorganisms |
|---|---|---|
| W1 | None | - |
| W2 | 8 colonies | 0 |
| K | 9 colonies | 3 |
| A | 12 colonies | 7 |
| S1 | 11 colonies | 3 |
| S2 | 7 colonies | 3 |
| S3 | 8 colonies | 5 |

**Table 2**. List of identified microorganisms.

| № | Sample | Species affiliation | Similarity | Position and medium |
|---|---|---|---|---|
| 1 | MK11 | *Pseudomonas oryzihabitans* | 85% | Cathode – MPA*; 37 ºC |
| 2 | MK22 | *Lysinibacillus fusiformis* | 85% | Cathode - MPA; 22 ºC |
| 3 | MK41 | *Lysinibacillus boronitolerans* | 86% | Cathode - MPA; 37 ºC |
| 4 | MAA | *Lysinibacillus sphaericus* | 87% | Anode – MPA; 37 ºC |
| 5 | MAA1 | *Lysinibacillus boronitolerans* | 83% | Anode – MPA; 37 $^0$C |
| 6 | MAA2 | *Lysinibacillus fusiformis* | 88% | Anode – MPA; 37 ºC |
| 7 | MA12 | *Paenibacillus dendritiformis* | 85% | Anode – MPA; 37 ºC |
| 8 | MA13 | *Paenibacillus apiarius* | 90% | Anode – MPA; 37 ºC |
| 9 | MA22 | *Paenibacillus apiarius* | 89% | Anode – MPA; 37 ºC |
| 10 | MA11 | *Paenibacillus apiarius* | 99% | Anode – MPA; 37 ºC |
| 11 | CC1 | *Pseudomonas koreensis* | 100% | S1 – Chapek's medium; 22 ºC |
| 12 | CC3 | *Pseudomonas putida* | 96% | S1 – Chapek's medium; 22 ºC |
| 13 | MC12 | *Bacillus cereus* . | 98% | S1 – MPA; 37$^0$C |
| 14 | HC2 | *Paenibacillus odorifer* | 98% | S2 – SAA**; 22 ºC |
| 15 | HC3 | *Paenibacillus caespitis* | 99% | S2 –SAA; 22 ºC |
| 16 | MC23 | *Bacillus cereus* | 100% | S2 – MPA; 22$^0$C |
| 17 | MC3A | *Clostridium mangenotii* | 98% | S3 – MPA; 22$^0$C |
| 18 | MC35 | *Lysinibacillus macroides* | 97% | S3 – MPA; 22$^0$C |
| 19 | MC36 | *Lysinibacillus macroides* . | 98% | S3 – MPA; 22$^0$C |
| 20 | MC3 | *Lysinibacillus sphaericus* . | 94% | S3 – MPA; 22$^0$C |
| 21 | MC31 | *Sporosarcina luteola* .. | 87% | S3 –MPA; 37 ºC |

*MPA-Meat Peptone agar, **SAA – Starch - ammonia agar.

Our results are in accordance with some recently published data.

In the paper of Jung *et al*. [23] the results of anode bacterial communities' studies of SMFCs with different anodes were presented. Four different anodes were used - a magnesium electrode, a magnesium electrode supplied with chitin particles, a graphite electrode, and a graphite electrode supplied with chitin particles. The reported results showed distinct difference in the anodic biofilms.

In a phylum level the magnesium anodes were dominated by *Proteobacteria* and *Firmicutes* in nearly equal proportions, while the graphite anodes were dominated solely by *Proteobacteria*. In a class level, anode bacterial communities were very different among the four anodes. Bacterial community of magnesium anode was most diverse and was comprised of *δ-Proteobacteria*, *Bacilli*, *Clostridia* and *γ-Proteobacteria*, whereas an anode bacterial community of magnesium/chitin anode was dominated by *Bacilli* and *α-Proteobacteria*. Anode bacterial communities of both graphite anodes were dominated by *δ-Proteobacteria*. The differences in bacterial communities between four anodes were most distinctive in species-level. In general bacterial communities of the chitin-absent anodes had larger richness and diversity than those of the chitin-supplemented anodes.

D. Khater *et al*. [24] have studied the performance of an air–cathode single-chamber mediator-less microbial fuel cell with electrodes made from carbon paper. MFC was seeded with mixed culture of aerobic activated sludge obtained from a municipal wastewater treatment plant. The analysis of microbial diversity on the electrode showed that the dominant phyla in the anodic biofilm are *Firmicutes, γ-Proteobacteria, α-Proteobacteria and Actinobacteria*.

Q. Zhao et al. [25] investigated SMFC with multiple anodes. The sediment was from lake origin. The microbial community structure in the sediment and anode biofilms were analyzed and it was found that the microbiota is dominated by the representatives of the phyla *Firmicutes, Proteobacteria* and *Euryarchaeota*.

Ueno and Katajima [26] analyzed an SMFC with a sediment created by mixing freshwater sediment from a fish breeding facility with andosol, zeolite and sand. While the initial sediment is dominated on the genus level by the representatives of *Thiobacillus*, microbial community analysis on the surface of the buried electrodes showed that the genus *Geobacter* had drastically propagated in a sample from the reactor where the electrodes were buried. Archaeal population had decreased to approximately 1/6 of its original level.

This study confirms the findings of other authors for the bacterial community in SMFC. The enrichment of the community with representatives of limited amount of species has also been previously reported.

CONCLUSIONS

The microbial community of investigated SMFC was dominated by the phylum *Firmicutes* with some representatives of the phylum *γ-Proteobacteria*. The most propagated are *Lysinibacillus* strains found on the cathode, the anode and in the sediment. *Paenibacillus* strains were isolated from sediment and from anode.

Anode bacterial communities of the graphite anodes were dominated by a few species - three strains of *Lysinibacillus* and two of *Paenibacillus*.

Future studies are planned to explore the possibility of using of isolated pure cultures as sole culture in SMFC.

REFERENCES

1. BP Statistical Review of World Energy June 2017
2. V. Das, S. Padmanabanb, K. Venkitusamya, R. Selvamuthukumaran, F. Blaabjerg, *Renewable and Sustainable Energy Reviews* **73**, 1 (2017).
3. B.C. Ong, S.K. Kamarudina, S. Basri, *International journal of hydrogen energy*, **42,** 10142 (2017).
4. T. Sadhasivam, K. Dhanabalan, S.-H. Roh, T.-H. Kim, K.-W. Park, S. Jung, M. D. Kurkuri, H.-Y. Jung, *International Journal of Hydrogen Energy*, **42**(7) 4415 (2017).
5. R.K.A. Rasheed, Q. Liao, Zh. Caizhi, S.H. Chan, *International journal of hydrogen energy*, **42**, 3142 (2017).
6. Sh. Hossain, A.M. Abdalla, S.N.B. Jamain, J.H. Zaini, A.K. Azad, *Renewable and Sustainable Energy Reviews*, **79,** 750 (2017).
7. V.B. Oliveira, M. Simxes, L.F. Melo, A.M.F.R. Pinto, *Biochemical Engineering Journal*, **3**, 53 (2013).
8. M. Rahimnejad, A. Adhami, S. Darvari, A. Zirepour, S.-E. Oh, *Alexandria Engineering Journal*, **54**, 745 (2015).
9. C. Santoro, C. Arbizzani, B. Erable, I. Ieropoulos, *Journal of Power Sources*, **356**, 225 (2017).
10. V.G. Gude, *Journal of Cleaner Production*, **122**, 287 (2016)
11. S.Z. Abbas, M. Rafatullah, N. Ismail, M.I. Syakir, *Int. J. Energy Res.*, **41**, 1242 (2017).
12. S. Z. Abbas, M. Rafatullah, N. Ismail, R.A. Nastro, *Int J Energy Res*, **41**, 2345 (2017).

13. M. Sherafatmand, H.Y. Ng, *Bioresource Technology*, **195**, 122, (2015).
14. X. Xu, Q. Zhao, M. Wu, J. Ding, W. Zhang, *Bioresource Technology*, **225**, 402, (2017).
15. G. Mohanakrishna, I.M. Abu-Reesh, S. Kondaveeti, R.I. Al-Raoush, Zh. He, *Bioresource Technology*, **253**, 16 (2018).
16. X. Xu, Q. Zhao, M. Wu, J Ding, W. Zhang, *Bioresource Technology*, **225**, 402 (2017).
17. P.R. Girguis, M.E. Nielsen, C.E. Reimers. "Fundamentals of Benthic Microbial Fuel Cells: Theory, Development, and Applications." In: Bioelectrochemical systems. First edition. Springer Verlag Press, 2010.
18. J. García-Muñoz, R. Amils, V.M. Fernández, A. L. De Lacey, M. Malki, *Int Microbiol*, **14**(2), 73 (2011)**.**
19. D. Majumder, J.P. Maity, Ch.-Y. Chen, Ch.-Ch. Chen, T.-Ch. Yang, Y.-F. Chang, D.-W. Hsu, H.-R. Chen, *International journal of hydrogen energy*, **39**, 21215 (2014).
20. J.M. Pisciotta, Z. Zaybak, D.F. Call, J.-Y. Nam, B.E. Logan, *Appl. Environ. Microb.* **78**(15). 5212 (2012).
21. N.J. Sacco, E.L.M. Figuerola, G. Pataccini, M.C. Bonetto, L. Erijman, E. Cortón, *Bioresource Technology*, **126**, 328 (2012).
22. B. Erable, N. Byrne, L. Etcheverry, W. Achouak, A. Bergel, *International journal of hydrogen energy*, **42**, 6059 (2017).
23. S.P. Jung, M.-H. Yoon, S.-M. Lee, S.E. Oh, H. Kang, J.-K. Yang, *Int. J. Electrochem. Sci.,* **9**, 315 (2014).
24. D.Z. Khater, K.M. El-Khatib, H. M. Hassan, *J. Gen. Engn Biotechn.*, **15**, 127 (2017).
25. Q. Zhao, M. Ji, R. Li, Zh. J. Ren, *Bioresource Technology*, **237**, 178 (2017).
26. Y. Ueno, Y. Kitajima, *Advances in Microbiology*, **4**, 252 (2014).

# BULGARIAN CHEMICAL COMMUNICATIONS

## Instructions about Preparation of Manuscripts

**General remarks:** Manuscripts are submitted in English by e-mail or by mail (in duplicate). The text must be typed double-spaced, on A4 format paper using Times New Roman font size 12, normal character spacing. The manuscript should not exceed 15 pages (about 3500 words), including photographs, tables, drawings, formulae, etc. Authors are requested to use margins of 3 cm on all sides. For mail submission hard copies, made by a clearly legible duplication process, are requested. Manuscripts should be subdivided into labelled sections, e.g. **Introduction, Experimental, Results and Discussion**, *etc*.

**The title page** comprises headline, author's names and affiliations, abstract and key words.

Attention is drawn to the following:

a) **The title** of the manuscript should reflect concisely the purpose and findings of the work. Abbreviations, symbols, chemical formulas, references and footnotes should be avoided. If indispensable, abbreviations and formulas should be given in parentheses immediately after the respective full form.

b) **The author**'s first and middle name initials, and family name in full should be given, followed by the address (or addresses) of the contributing laboratory (laboratories). **The affiliation** of the author(s) should be listed in detail (no abbreviations!). The author to whom correspondence and/or inquiries should be sent should be indicated by asterisk (*).

**The abstract** should be self-explanatory and intelligible without any references to the text and containing not more than 250 words. It should be followed by key words (not more than six).

**References** should be numbered sequentially in the order, in which they are cited in the text. The numbers in the text should be enclosed in brackets [2], [5, 6], [9–12], etc., set on the text line. References, typed with double spacing, are to be listed in numerical order on a separate sheet. All references are to be given in Latin letters. The names of the authors are given without inversion. Titles of journals must be abbreviated according to Chemical Abstracts and given in italics, the volume is typed in bold, the initial page is given and the year in parentheses. Attention is drawn to the following conventions:

a) The names of all authors of a certain publications should be given. The use of "*et al.*" in the list of references is not acceptable.

b) Only the initials of the first and middle names should be given.

In the manuscripts, the reference to author(s) of cited works should be made without giving initials, e.g. "Bush and Smith [7] pioneered...". If the reference carries the names of three or more authors it should be quoted as "Bush *et al*. [7]", if Bush is the first author, or as "Bush and co-workers [7]", if Bush is the senior author.

**Footnotes** should be reduced to a minimum. Each footnote should be typed double-spaced at the bottom of the page, on which its subject is first mentioned.

**Tables** are numbered with Arabic numerals on the left-hand top. Each table should be referred to in the text. Column headings should be as short as possible but they must define units unambiguously. The units are to be separated from the preceding symbols by a comma or brackets.

Note: The following format should be used when figures, equations, *etc*. are referred to the text (followed by the respective numbers): Fig., Eqns., Table, Scheme.

**Schemes and figures**. Each manuscript (hard copy) should contain or be accompanied by the respective illustrative material as well as by the respective figure captions in a separate file (sheet). As far as presentation of units is concerned, SI units are to be used. However, some non-SI units are also acceptable, such as °C, ml, l, etc.

The author(s) name(s), the title of the manuscript, the number of drawings, photographs, diagrams, etc., should be written in black pencil on the back of the illustrative material (hard copies) in accordance with the list enclosed. Avoid using more than 6 (12 for reviews, respectively) figures in the manuscript. Since most of the illustrative materials are to be presented as 8-cm wide pictures, attention should be paid that all axis titles, numerals, legend(s) and texts are legible.

The authors are asked to submit **the final text** (after the manuscript has been accepted for publication) in electronic form either by e-mail or mail on a 3.5'' diskette (CD) using a PC Word-processor. The main text, list of references, tables and figure captions should be saved in separate files (as *.rtf or *.doc) with clearly identifiable file names. It is essential that the name and version of

the word-processing program and the format of the text files is clearly indicated. It is recommended that the pictures are presented in \*.tif, \*.jpg, \*.cdr or \*.bmp format, the equations are written using "Equation Editor" and chemical reaction schemes are written using ISIS Draw or ChemDraw programme.

The authors are required to submit the final text with a list of three individuals and their e-mail addresses that can be considered by the Editors as potential reviewers. Please, note that the reviewers should be outside the authors' own institution or organization. The Editorial Board of the journal is not obliged to accept these proposals.

## EXAMPLES FOR PRESENTATION OF REFERENCES

### REFERENCES

1. D. S. Newsome, *Catal. Rev.–Sci. Eng.*, **21**, 275 (1980).
2. C.-H. Lin, C.-Y. Hsu, *J. Chem. Soc. Chem. Commun.*, 1479 (1992).
3. R. G. Parr, W. Yang, Density Functional Theory of Atoms and Molecules, Oxford Univ. Press, New York, 1989.
4. V. Ponec, G. C. Bond, Catalysis by Metals and Alloys (Stud. Surf. Sci. Catal., vol. 95), Elsevier, Amsterdam, 1995.
5. G. Kadinov, S. Todorova, A. Palazov, in: New Frontiers in Catalysis (Proc. 10th Int. Congr. Catal., Budapest, 1992), L. Guczi, F. Solymosi, P. Tetenyi (eds.), Akademiai Kiado, Budapest, 1993, Part C, p. 2817.
6. G. L. C. Maire, F. Garin, in: Catalysis. Science and Technology, J. R. Anderson, M. Boudart (eds), vol. 6, Springer-Verlag, Berlin, 1984, p. 161.
7. D. Pocknell, *GB Patent* 2 207 355 (1949).
8. G. Angelov, PhD Thesis, UCTM, Sofia, 2001.
9. JCPDS International Center for Diffraction Data, Power Diffraction File, Swarthmore, PA, 1991.
10. CA **127**, 184 762q (1998).
11. P. Hou, H. Wise, *J. Catal.*, in press.
12. M. Sinev, private communication.
13. http://www.chemweb.com/alchem/articles/1051611477211.html.

Selected papers presented on the Seventh International Conference
"Modern Trends in Science" - FMNS-2017, 4 - 18.06.2017, Blagoevgrad, Bulgaria

## CONTENTS